

# **Conducting Polymers and Polymer Electrolytes**



ACS SYMPOSIUM SERIES **832**

# **Conducting Polymers and Polymer Electrolytes**

## **From Biology to Photovoltaics**

**Judith F. Rubinson, Editor**  
*Georgetown University*

**Harry B. Mark, Jr., Editor**  
*University of Cincinnati*



American Chemical Society, Washington, DC

## Conducting polymers and polymer electrolytes

### Library of Congress Cataloging-in-Publication Data

Conducting polymers and polymer electrolytes : from biology to photovoltaics / Judith F. Rubinson, editor, Harry B. Mark, Jr., editor.

p. cm.—(ACS symposium series ; 832)

Developed from a symposium sponsored by the Division of Colloid and Surface Chemistry at the 219<sup>th</sup> National Meeting of the American Chemical Society, San Francisco, California, March 26–30, 2000.”

Includes bibliographical references and index.

ISBN 0–8412–3770–0

1. Conducting polymers—Congresses. 2. Polyelectrolytes—Congresses.

I. Rubinson, Judith F. II. Mark, Harry B. III. American Chemical Society. Division of Colloid and Surface Chemistry. IV. American Chemical Society. Meeting ( 219<sup>th</sup> : 2000 : San Francisco, Calif.) V. Series.

QD382 C653 2002  
647.70457—dc21

2002071718

The paper used in this publication meets the minimum requirements of American National Standard for Information Sciences—Permanence of Paper for Printed Library Materials, ANSI Z39.48–1984.

Copyright © 2003 American Chemical Society

Distributed by Oxford University Press

All Rights Reserved. Reprographic copying beyond that permitted by Sections 107 or 108 of the U.S. Copyright Act is allowed for internal use only, provided that a per-chapter fee of \$22.50 plus \$0.75 per page is paid to the Copyright Clearance Center, Inc., 222 Rosewood Drive, Danvers, MA 01923, USA. Reproduction or reproduction for sale of pages in this book is permitted only under license from ACS. Direct these and other permission requests to ACS Copyright Office, Publications Division, 1155 16th St., N.W., Washington, DC 20036.

The citation of trade names and/or names of manufacturers in this publication is not to be construed as an endorsement or as approval by ACS of the commercial products or services referenced herein; nor should the mere reference herein to any drawing, specification, chemical process, or other data be regarded as a license or as a conveyance of any right or permission to the holder, reader, or any other person or corporation, to manufacture, reproduce, use, or sell any patented invention or copyrighted work that may in any way be related thereto. Registered names, trademarks, etc., used in this publication, even without specific indication thereof, are not to be considered unprotected by law.

PRINTED IN THE UNITED STATES OF AMERICA

**American Chemical Society**  
**Library**  
**1155 16th St., N.W.**  
**Washington, D.C. 20036**

In Conducting Polymers and Polymer Electrolytes; Rubinson, J., et al.;  
ACS Symposium Series; American Chemical Society: Washington, DC, 2002.

# Foreword

The ACS Symposium Series was first published in 1974 to provide a mechanism for publishing symposia quickly in book form. The purpose of the series is to publish timely, comprehensive books developed from ACS sponsored symposia based on current scientific research. Occasionally, books are developed from symposia sponsored by other organizations when the topic is of keen interest to the chemistry audience.

Before agreeing to publish a book, the proposed table of contents is reviewed for appropriate and comprehensive coverage and for interest to the audience. Some papers may be excluded to better focus the book; others may be added to provide comprehensiveness. When appropriate, overview or introductory chapters are added. Drafts of chapters are peer-reviewed prior to final acceptance or rejection, and manuscripts are prepared in camera-ready format.

As a rule, only original research papers and original review papers are included in the volumes. Verbatim reproductions of previously published papers are not accepted.

**ACS Books Department**

# Preface

This volume contains, with a few exceptions, the text of presentations from the symposium “Electrified Polymer/Solution Interfaces” held at the San Francisco, California, American Chemical Society (ACS) National Meeting, March 25–31, 2000. In addition, two additional manuscripts from Christine Schmidt and Peter Pickup round out the coverage. Contributions span a number of fields of interest that are concerned with charged polymer–solution interfaces. Topics include not only synthesis and characterization but also applications in such diverse areas as electrochemiluminescence, electrocatalysis, sensor design, biomaterials, fuel cell design, and corrosion prevention. This symposium provided a unique opportunity for interaction and exchange of ideas, as it involved contributions from an international array of investigators, working in seemingly disparate areas, but all having their bases in the field of conducting polymers.

Acknowledgment is made to the Donors of The Petroleum Research Fund, administered by the ACS, for partial support of this symposium. In addition, we acknowledge the support of Solartron, Inc., the Five Oaks Research Institute, the ACS Division of Colloid and Surface Chemistry, and a private donor, who wished to remain anonymous.

Our thanks also go out to the authors for their insightful contributions, as well as those in the greater scientific community for their contributions to the symposium and their invaluable assistance in the critical evaluation of the manuscripts. Finally, we express our appreciation to Professor Andrzej Wieckowski for inviting us to arrange the symposium and for encouraging us to prepare this symposium volume.

## **Judith F. Rubinson**

Department of Chemistry  
Georgetown University  
37<sup>th</sup> and O Streets, NW  
Washington, DC 20057–1227

## **Harry B. Mark, Jr.**

Department of Chemistry  
University of Cincinnati  
Cincinnati, OH 45221–0172

## Chapter 1

# From Biology to Engineering: The Present Status of Conducting Polymers

Judith F. Rubinson

Department of Chemistry, Georgetown University,  
Washington, DC 20057-1227

Although the papers in this volume indicate the variety of areas in which conducting polymers have been utilized, the growth of the field in the period since has benefitted from a growing interest in their application, especially for sensing, anticorrosion and investigation of biologically important processes. This interest has, in turn, spurred improvements in synthesis and processing, the introduction of heteropolymer systems, and modification of the polymer to include functional groups tailored for specific applications. A summary of recent trends with references to specific examples is provided here.

Over the past twenty five years, conducting polymers have gone from being regarded as a curiosity to serving as the basis for a number of different new technologies (1,2). As evidenced by the work described in this volume scientists working in areas ranging from photovoltaic design to electrocatalysis to sensors to biomaterials have begun to make use of their unique advantages. Even in the period since the presentations in this volume were made, the field has ground by leaps and bounds, especially in the areas of corrosion protection, sensor design and applications in biology and medicine.

## Synthesis and Characterization

One of the considerations which has driven the search for new synthetic parameters for the production of conducting polymer films is the need for a medium that will dissolve both the monomer to be used and polar molecules or ionic species to be incorporated into the polymer. In the case of protein incorporation, it is also important that the conditions for polymer production not denature the protein.

A number of approaches have been proven effective. In some cases, a judicious choice of electrolyte or current density is sufficient. For example, within a limited current density window, it is possible to electropolymerize aniline in neutral aqueous solution (3). Poly-3-methylthiophene can be deposited from highly acidic aqueous solution if a stable suspension is achieved before electropolymerization (4), or as described in chapter 3 of this volume, from sodium dodecyl sulfate micelles in a less harsh medium. Micelles have also proven useful where addition of non-ionic surfactants to the monomer solution have been employed in the preparation of poly(3,4-ethylene dioxythiophene) (PEDOT) from aqueous perchlorate solutions (5).

When the oxidation of monomer takes place at potentials not compatible with trapping of biomolecules, these are often incorporated after the fact. These can be "wired" to the electrode through covalent attachment to pendant groups on the polymer or through hydrogen bonding between polar groups on the polymer and the molecule to be immobilized (6). Electropolymerization of N-alkylated (ethylene)- or (propylene) dioxypyrrroles result in a PEDOT analog which contains pendant groups for further functionalization for ion or molecule recognition (7).

The morphology of the polymer has, at times, a profound effect on its conductivity or electron-transfer characteristics. When a uniform layer with a small grain size is desired, pretreatment of the electrode surface with acid before electropolymerization has been proven to be effective in the deposition of polypyrrole(*p*-toluene sulfonate) on mild steel (8), while the aqueous method for production of poly-3-methylthiophene from acidic aqueous solution mentioned above also has the benefit of producing very uniform (3-4  $\mu\text{m}$ ) particles (4). Uniformity in grain size is also a function of the deposition method. For both 3-methyl thiophene and for polypyrrole, use of a brief potential step in the presence of small anionic species for production of the polymer has resulted in a production of a dense, uniform film (9, 10). A very thin uniform layer of polymer with an poly (N-phenylpyrrole) surface has been obtained by electropolymerization of 4-



aminothiophenol on gold (11). On the other hand, a porous polymer with a large surface area is ideal for some applications. For example, recent interest in the use of conducting polymers in supercapacitor applications has led to production of polypyrrole in the network of a PEDOT-polystyrene sulfonate hydrogel (12).

Adhesion of the polymer to a substrate is often enhanced by first electrodepositing a layer of some other polymer. This “priming” of the surface can be carried out to obtain a conductive layer with better adhesion properties – as is the case in electropolymerization of a mixture of 1,5- diaminonaphthalene (1,5-DAN) and polyaniline (13). In this case the 1,5-DAN preferentially deposits first, then this layer is followed by codeposition of the two polymers. A thin nonconductive layer can also serve to produce better adhesion (14).

Finally, the conductivity of the polymer can also be altered. This can be accomplished by post-polymerization processing. For example, commercial polyaniline, doped with p-toluenesulfonic acid, when dispersed using a solvent free, melt processing in polymethyl methacrylate, has been found to much more conductive (15). Higher conductivities for PEDOT doped with polystyrene sulfonate (PSS) have been achieved crosslinking PEDOT (PSS) using multivalent cations. Such a crosslinking to form a porous network can be used in polymer blends with an insulating polymer to achieve high conductivity with low density (16)

A multitude of techniques continue to be used to characterize conducting polymers systems, including spectroscopic techniques such as UV-vis (17), Raman FT-IR (18, 19) and photoelectron spectroscopy (20), scanning probe microscopy (10), electrochemical techniques such as cyclic voltammetry (21, *Chapter 4 of this volume*), and hybrid techniques such as spectroelectrochemistry (21), electrochemical quartz crystal microbalance studies (19, 22), and photocurrent spectroscopy (22). Electrochemical impedance spectroscopy has proven to be an extremely useful technique, not only for investigation of the properties of the polymers themselves, but in the area of corrosion protection to monitor their utility (23-26, *Chapters 2 and 5 of this volume*). In addition, grazing emission X-ray fluorescence has recently been added to the variety of techniques employed (27).

## Applications

Recent advances in optimization of conductivity, ease of processing and functionalization have led to a wide variety of studies exploring the applications covered in this volume as well as a number of new ones.

### Electrocatalysis

These materials have been shown to exhibit significant advantages in the area of electrocatalysis (28). In particular, these materials have an advantage over the usual bare metal or carbon electrodes in that the surface is often resistant to fouling

or poisoning by reaction products. Polythiophene and its derivatives have been shown to catalyze oxidation reactions, such as the conversion of formic acid to carbon dioxide (29, Chapter 6 of this volume), as well as reduction reactions such as the conversion of oxygen to water (4), of acetylene to ethylene (30), and carbon dioxide to formic acid (*Chapter 11 of this volume*). Electrocatalysis of redox processes important for fuel cell design and fabrication of sensors are covered in those sections below.

## Electronics and photovoltaics

Photovoltaic devices involving conducting polymers have, for the most part, been designed based on polymerization of substituted thiophenes or poly(phenylenevinylene) (PPV). Fabrication of a porphyrin-substituted polythiophene photoelectrochemical cell has resulted in an open circuit voltage of 139 mV and short circuit current of  $123.4 \mu\text{A cm}^{-1}$ . This corresponds to an energy conversion efficiency of 0.02%. A Schottky device based on polyterthiophene resulted in an open circuit voltage of 0.5 V and  $I_{sc}$  of  $0.98 \mu\text{A cm}^{-1}$ . (17) Thiophenes substituted with alkenyl groups have constituted a major advance in the field due to their enhanced processibility, stability in air, and low bandgap energies. (20, 31, 32, *Chapters 8 and 9 of this volume*). Short circuit conversion efficiencies up to 50% have been reported, with the highest efficiency involving a PPV- $C_{60}$  interpenetrating network (32).

Light-emitting diodes based on polyphenylvinylene conducting polymers have benefitted from layer-by-layer production of charge-injection layers. This allows a variety of gradients or steps to be tested for efficiency (33). Finally, a polymer of nitrosylterthiophene has been found to yield a significant enhancement of charge separation, an important variable in the optimization of these devices (34).

A polyaniline nanojunction switch has been fabricated by creating a bridge across gaps between nanometer scale polyaniline electrodes. When bridging is indicated by a short circuit, the junction can be characterized as a function of applied potential. Abrupt switching from insulator to conductor is seen at about 0.15 V vs Ag/AgCl that is explained on the bases of fast changes in domains of strands (35).

Capacitors based on polyaniline, during 20000 cycle trials, have been shown to experience about a 33% loss in charge/discharge capacity even in the absence of a deterioration in electroactivity. This can be explained as a result of compaction of the polymer over the life of the capacitor (36).

## Anticorrosion

Elimination of chromate treatment of metal surfaces has spurred the investigation of conducting polymer surface protection. Electrochemical polymerization as well as chemical polymerization (37) and a solvent free process

(38) have all been used for preparation of anticorrosion coatings. Polyaniline has been extensively investigated for treatment of metal surfaces to prevent corrosion (23-26,37-40,Chapter 10 of this volume), both alone and in combination with polypyrrole (39). In the case of its combination with polypyrrole for protection of mild steel, the polyaniline layer behaves much like it does on platinum, showing that the polyaniline does not go through to the steel (39). For protection of aluminum alloys, which often contain copper which accelerates corrosion, the action is proposed to be based on extraction of the aluminum by the polyaniline (40). The polymer in this case is fairly porous, but in most cases it is advantageous to produce smooth, nonporous polymer layers.

### Fuel cell design

A thorough review of the use of polymeric conductors as supports for fuel cell catalysts is provided along with recent results in Chapter 13 of this volume. However, there have been a few other recent developments that are of interest. For example, a novel polyvinylidene fluoride gel electrolyte membrane has been studied for use in lithium batteries. Its breakdown voltage has been found to approach 5 V and it exhibits a conductivity on the order of  $0.1 \text{ mS cm}^{-1}$  (41).

In terms of catalysts to be used in the fuel cell, a novel metal complex between cobalt and dibenzotetraaza[14]annulene, polymerized on a carbon electrode, has recently been shown to produce less peroxide than the carbon electrode itself under the same conditions. The polymer is very promising due to its stability in acid; however, efforts are underway to produce a complex of the same type that incorporates two cobalt atoms and thus might function in a four-electron process to take the reaction all the way to water (42).

Conducting polymers with pendant carboxyl groups for attachment active groups are promising as catalysts for biofuel cells. since they provide a site for hydride transfer and facile delocalization of charge. Substituted polyaniline doped with polyacrylate, polystyrene sulfonate or polyvinylsulfonate show particularly good properties since NADH can be incorporated in the film in near neutral solutions. NADH redox chemistry is the first step in a number of biological processes (43).

### Sensors and detection

Conducting polymer electrodes provide a multitude of advantages in the design of sensors, especially for biological molecules (44). In addition to the fact that they provide a surface that is more resistant to fouling and less likely to denature biomolecules, there is often a significant reduction in the overpotential for oxidation or reduction. The possibility of preparation of these polymers with pendant groups to improve selectivity also makes them ideal candidates for sensor design both for biomolecules and for ion selective electrodes or gas sensing electrodes.

Nitric oxide has been found to be an important species in signalling between cells, and thus monitoring of NO concentrations in the presence of other molecules such as ascorbate and dopamine is important in medical applications. A sensor based on polycarbazole has been found to discriminate against both of these possible interferents (45).

Monitoring of CO<sub>2</sub> and humidity levels at a conducting-insulating polymer composite, important in the area of greenhouse gases, is reported in Chapter 7 of this volume.

Detection in flowing streams continues to be an area of interest. A universal detector based on low potential amperometric detection at a polypyrrole electrode has been employed for detection of polynucleotides. This detector relies on adsorptive-desorptive processes involving the polymer and the polynucleotide, not on its electroactivity, so detection is not restricted to sequences containing purines (46).

It is also desirable to be able to measure the content of various compounds *in vivo* for assessment of brain function. These include glucose, lactate, pyruvate, and glutamate as well as a number of other neurotransmitters. A number of conducting polymer electrode materials show promise in this area (2, 47, Chapter 6 of this volume).

A calcium-selective sensor has been fabricated based on a functionalized polyaniline which exhibits a Nernstian response and selectivity coefficients on the order of 10<sup>-4</sup> (48). These electrodes show little or no effect from redox or pH, problems which have limited the utility of a number of conducting polymers in ion sensors.

### **Immobilization of enzymes, polynucleotide, and antibodies for sensing or catalysis**

The most widely investigated systems in terms of sensor design are the detection of glucose, molecular recognition based on polynucleotides, and antigen/antibody interactions. Table I provides a summary of the type of immobilization, the conducting polymer used, and the parameter measured for a number of the analytical tools that have been developed over the last few years.

Perhaps the most important points with regard to the glucose oxidase-based sensors that investigation of the "wired enzyme" electrodes has shown in some instances that there are no significant changes in the  $K_m^{app}$  values for the immobilized enzyme although the overall activity might be seen to decrease (49).

With regard to the oligonucleotide and immunosensors it is worth mentioning that although some of the sensors do not rely on an electrochemical measurement for quantitation, the ability to define the response of each element of an array by constructing each element or group of elements electrochemically still provides for very complex multivariable assays to be carried out in a minimum of time. It is also worth noting that the majority of these sensors depend on the electropolymerization

Table I. Examples of Immobilization for Sensor Applications

Immobilized Species	Polymer Matrix	Type Immobilization	Measurement	Reference
Oligonucleotide (ODN)	polypyrrole	copolymerization pyrrole and ODN-pyrrole	quartz crystal microbalance	22
Oligonucleotide (ODN)	polypyrrole	copolymerization pyrrole and ODN-pyrrole	photocurrent spectroscopy	22
Oligonucleotide (ODN)	polypyrrole	covalent grafting of ODN onto functionalized pyrrole	shift in cyclic voltammetric potentials	66
Biotinylated Hepatitis C probe - polypyrrole	polypyrrole	copolymerization biotinylated Hepatitis C probe - polypyrrole with polypyrrole	fluorescence due to binding of avidin conjugates	67,68
Oligonucleotide	polypyrrole	copolymerization of ODN-pyrrole and pyrrole on polypyrrole	Fluorescence	47,69
Triazine or diaminopyridine	bithiophene	copolymerization triazine or diaminopyridine functionalized bithiophene with bithiophene	integrated current from cyclic voltammogram	21

Oligodinucleotide	carboxylated polypyrrole	chemical grafting	current amplitude from CV	70
Anti human serum albumin	polypyrrole	entrapment	shift in cyclic voltammetric potentials	71
IgG	N-substituted polypyrrole with pendant CN	hydrogen bonding (CN-OH)	impedance	21
Horseshoe peroxidase (HPR)	poly(Ferrocenyl-o-phenylenediamine)	covalent attachment of HPR to C substrate / electropolymerization ferrocenyl-o-phenylenediamine	amperometric	72
	poly(Ferrocenyl-phenylenediamine)	same as above, then electropolymerization of a mixture of ferrocenylphenylenediamine, resorcinol and glucose oxidase	amperometric	72
Glucose oxidase	aminonaphthalene with carboxyl group	covalent grafting	amperometric	73

*Continued on next page.*

Table I. Examples of Immobilization for Sensor Applications (cont)

Immobilized Species	Polymer Matrix	Type Immobilization	Measurement	Reference
Platinum alloy	polypyrrole	electrodeposition into film	peak current, cyclic voltammetry	74
Glucose oxidase	polypyrrole/poly( <i>o</i> -phenylenediamine) bilayer	glucose oxidase trapped in polypyrrole layer, second layer of electropolymerized <i>o</i> -phenylenediamine	amperometric	75
Glucose oxidase	polypyrrole	biotinylated polypyrrole / avidin/biotinylated glucose oxidase	amperometric	49
GOD-polyanion	polypyrrole	glucose oxidase-polyanion is the dopant for the polypyrrole	amperometric	76
Glucose oxidase	polyaniline/isoprene	entrapment by electrostatics	amperometric	77
Glucose oxidase	polymer of pyrrole functionalized with osmium complex	entrapment	amperometric (based on redox of Os complex)	78

of pyrroles. This is due to the low electrochemical potential required for oxidative electropolymerization.

Although early on it was feared that incorporation of enzymes or attachment to a conducting polymer might result in inactive enzyme or poor contact between the enzyme, the electrode, and the substrate, the number of instances for glucose oxidase or horseradish peroxidase immobilization where minimal effects have been found are encouraging for the use of conducting polymer electrodes in other instances. Enhanced electron transfer rates have been found for entrapped quinoxaline-protein alcohol dehydrogenase (50). This is explained on the basis of the heme active site always being in close proximity to the polypyrrole strands.

Amphiphilic pyrroles modified with biotin have been used to attach a number of biotinylated oxidases and flavins to electrode surfaces by means of an avidin/biotin interaction. This approach not only avoids use of large amounts of enzyme but also results in a polymer with excellent swelling properties and thus improved mass transport in the polymer film (51).

## **Biomedical applications**

### *Entrapment and Release of Bioactive Substances*

Dopamine has been successfully entrapped in polyaminonaphthoquinone from dopamine-HCl solution. Under the conditions tested, release took place over a period of approximately 30 minutes (52).

Polypyrrole can be used to trap ATP for later release by either electrochemical or chemical (hydrazine or hydroxide trigger). Data suggests that the release rate and profile can be manipulated by means of film thickness and compactness, concentration of chemical release reagent or electrochemical potential (depending on trigger chosen), or through use of an outer polymer membrane of a given thickness or porosity (53).

Uptake and release of oligonucleotides has also been accomplished using PEDOT as the polymer matrix. Enhanced uptake was noted upon inclusion of water soluble neutral polymers to the polymerization mixture (54).

### *Neuroscience and cell culture applications*

There has also been a great deal of interest in the use of conducting polymers, in conjunction with substances known to enhance growth of neurons. A number of groups, including that of Christine Schmidt (*Chapter 12 of this volume*) have demonstrated enhanced length of neural processes and less branching when cells are cultured on polypyrrole at low current and voltage levels (55-57).

The enhanced cell growth for neurons has also sparked interest in the use of these electrodes for culture of endothelial tissue and bone growth as well as increases in angiogenesis (55-59). Endothelial cells have been grown in the past on fabric supports. The enhanced growth on a polypyrrole-coated polyester fabric has shown that there is an optimal range in conductivity of the fabric for growth on such media (59).



### *In vivo applications*

Electrodes based on polypyrrole doped with polystyrene sulfonate have been seen to produce acceptable signal/ noise ratios when used for short term *in vivo* measurement of neural signals (60). Both the low impedance of this polymer and the surface roughness promise to result in an enhanced signal/noise ratio on optimization. (47, 60).

### **Environmental monitoring and remediation**

Chromate reduction at polypyrrole takes place at a significantly less negative potentials than at bare metal electrodes. This observation has implications for both environmental monitoring and for remediation. Conversion of chromate to the chromium (III) form not only renders it less toxic, but also allows for precipitation with hydroxide to obtain decreased volume of waste. A repetitive cycling approach has been shown to be almost 100% effective in removal of chromate from solutions containing 10 ppm chromate (61). The lower reduction potential also has implications for chromate analysis in the presence of species that would normally interfere with its detection (62).

Arsenic analysis at polymer electrodes has also been the subject of investigation. Uptake into a polypyrrole film can be used for preconcentration of arsenic species and subsequent analysis by HPLC/ICP/MS (63).

### **Solid-state reference electrodes**

Although all solid state reference electrodes based on conducting polymers have been tested, they are still in the testing phase. The most promising systems appear to be bilayers with different ion-exchanger properties such as glassy carbon/polypyrrole in conjunction with a polypyrrole(polystyrene sulfonate) layer (64,65).

## **References**

1. Diaz, A.F.; Rubinson, J.F.; Mark, H.B., Jr., "Electrochemistry and Electrode Applications of Electroactive/Electroconductive Polymers," *Adv. Polymer Sci.* **1987**, *84*, 113.
2. Rubinson, J.F.; Mark, H.B., Jr. in *Interfacial Electrochemistry: Principles and Applications*, A. Wieckowski, ed., Marcel Dekker, 2000; p. 689.
3. Nguyen, T. Dung; Camalet, J-L; Lacroix, J-C; Aeiyaich, S; Pham, M.C.; Lacaze, P-C. *Synthetic Metals* **1999**, *102*, 1388.
4. Giacomini, M.T.; Ticianelli, E.A.; McBreen, J.; Balasubramanian, M. *J. Electrochem. Soc.* **2001**, *148*, A323.
5. Efimov, I.; Winkels, S.; Schultze, J.W. *J. Electroanal. Chem.* **2001**, *499*, 169.
6. Ouerghi, O.; Senillou, A.; Jaffrezic-Renault, N.; Martelet, C.; Ben Ouada, H.; Cosnier, S. *J. Electroanal. Chem.* **2001**, *501*, 62.

- 7 Zong, K.; Reynolds, J.R. *J. Org. Chem.* **2001** *66*, 6873.
- 8 Reut, J.; Öpik, A.; Idla, K. *Synthetic Metals* **1999**, *102*, 1392.
- 9 Zhang, H., Lunsford, S.K., Marawi, I., Rubinson, J.F., and Mark, H.B., Jr., *J. Electroanal. Chem.* **1997** *424*, 101.
- 10 Hernández-Pérez, T; Morales, M; Batina, N; Salmón, M *J. Electrochem. Soc* **2001**, *148* C369.
- 11 Dahlgren, G.; Smith, A.; Wurm, D.B. *Synthetic Metals* **2000** *113* 289
- 12 Ghosh, S.; Inganäs, O. *J. Electrochem Soc* **2000** *147* 1872.
- 13 Meneguzzi, A; Pham, MC; Ferreira, C.A; Lacroix, J.C.; Aeiyaich, S; Lacaze, PC, *Synthetic Metals* **1999**, *102*, 1390.
- 14 Jérôme, C; Geskin, V; Lazzaroni, R; Brédas, JL; Thibaut, A; Calburg, C; Bodart, I; Mertens, M; Martinot, L; Rodrigue, D; Riga, J; Jérôme, R *Chem. Mater* **2001** *13*, 1656.
- 15 Wessling, B *Synthetic Metals* **1999**, *102*, 1396.
- 16 Ghosh, S; Inganäs, O *Synthetic Metals* **1999** *101*, 413.
- 17 Too, C.O.; Wallace, G.G.; Burrell, A.K.; Collis, G.E.; Officer, D.L.; Boge, E.W.; Brodie, S.G.; Evans, E.J. *Synthetic Metals* **2001** *123*, 53.
- 18 Ballarin, B.; Seeber, R.; Tassi, L.; Tonelli., D. *Synthetic Metals* **2000** *114*, 279.
- 19 Damlin, P.; Kvarnström, C.; Neugebauer, H.; Ivaska, A. *Synthetic Metals* **2001** *123*, 141.
- 20 Greczynski, G.H.; Kugler, Th.; Keil, M.; Osikowicz, W.; Fahlman, M., Salaneck, W.R. *J. Electron Spec Rel Phenom* **2001**, *121*, 1.
- 21 Emge, A.; Bäuerle, P. *Synthetic Metals* **1999**, *102*, 1370.
- 22 Lassalle, N.; Mailley, P.; Vieil, E.; Livache, T.; Roget, A.; Correia, J.P., Abrantes, L.M. *J. Electroanal Chem* **2001** *509*, 48.
- 23 Kulszewics-Bajer, J.; Zagórska, M.; Bany, A.; Kwiatkowski, L. *Synthetic Metals* **1999**, *102*, 138.
- 24 Tallman, D.E, Spinks, G., Dominis, A., Wallace, G.G. *J. Solid State Electrochem* **2002** *6*, 73.
- 25 Spinks, G.E., Dominis, A. Wallace, G.G., Tallman, D.E. *J. Solid State Electrochem* **2002** *6*, 385.
- 26 Tallman, D.E, Vang, C., Wallace, G.G., Bierwagen, G.P. *J. Electrochem. Soc.* **2002**, *149*, 173.
- 27 Blockhuys, F.; Claes, M.; Van Grieken, R., Geise, H.J. *Anal. Chem* **2000** *72*, 3366.
- 28 Malinauskas, A. *Synthetic Metals* **1999** *107*, 75.
- 29 Ocón, P.; Herrasti, P.; Rojas, S. *Polymer* **2001** *42*, 2439.
- 30 Rubinson, J.F.; Mark, H.B, Jr., Krotine, J., Vaughn, M., Goldschmidt, M. *Electrochimica Acta*, **2000** *45*, 4309.
- 31 Ding, L.; Jonforsen, M.; Roman, L.S.; Andersson, M.R.; Inganäs, O. *Synthetic Metals* **2000** *110*, 133.
- 32 Gratzel, M. *Nature* **2001** *414*, 338.
- 33 Ho, P.K.H.; Kim, J.-S.; Burroughes, J.H.; Becker, H.; Li, S.F.Y.; Brown, T.M.; Cacialli, F.; Friend, R.H. *Nature* **2000** *404*, 481.
- 34 Cutler, C.A.; Burrell, A.K.; Collis, G.E.; Dastoor, P.C.; Officer, D.L.; Too, C.O.; Wallace, G.G. *Synthetic Metals* **2001** *123*, 225.
- 35 He, H.; Zhu, J.; Tao, N.J; Nagahara, L.A.; Amlani, I.; Tsui, R. *J. Am. Chem. Soc* **2001** *123*, 7730.
- 36 Bélanger, D.; Ren, X.; Davey, J.; Uribe, F.; Gottesfeld, S. *J. Electrochem. Soc* **2000** *147*, 2923.

37. Bernard, M.-C.; Deslouis, C.; El Moustafid, T.; Hugot-LeGoff, A.; Joiret, S.; Tribollet, B. *Synthetic Metals* **1999**, *102*, 1381.
38. Epstein A.J.; Smallfieles, J.A.O.; Guan, H.; Fahlman, M. *Synthetic Metals* **1999**, *102*, 1374.
39. Camalet, J.-L.; LaCroix, J.-C.; Aeiyaeh, S.; Chane-Ching, K.I.; Lacaze, P.-C. *Synthetic Metals* **1999**, *102*, 1386.
40. Wang, X.-H.; Li, J.; Zhang, J.-Y.; Sun, Z.-C.; Yu, L.; Jing, X.-B.; Wang, F.-S.; Sun, Z.-X.; Ye, Z.-J. *Synthetic Metals* **1999**, *102*, 1377.
41. Appetecchi, G.B.; Croce, F.; De Paolis, A.; Scrosati, B. *J. Electroanal Chem* **1999** *463*, 248.
42. Miry, C.; Le Brun, D.; Kerbaol, J.-M.; L'Her, M. *J. Electroanal. Chem* **2000** *494*, 53.
43. Bartlett, P.N.; Simon, E. *Phys. Chem. Chem. Phys.* **2000** *2*, 2599.
44. Habermüller, K.; Mosbach M.; Schuhmann, W. *Fresenius J. Anal. Chem* **2000** *366* 560.
45. Prakash, R.; Srivastava, R.C.; Seth, P.K. *Polymer Bulletin* **2001** *46*, 487.
46. Wang, J.; Jiang, M.; Mukherjee, B. *Anal. Chem.* **1999** *71*, 4095.
47. Georganopoulou, D.G.; Carley, R.; Jones, D.A.; Boutelle, M.G. *Faraday Disc* **2000** *116* 291.
48. Lindfors, T.; Ivaska, A. *Anal. Chim Acta* **2001** *437* 171
49. Cosnier, S.; Stoytcheva, M.; Senillou, A.; Perrot, H.; Furriel, R.P.M.; Leone, F.A. *Anal. Chem* **1999** *71*, 3692.
50. Ramanavicius, A.; Habermüller, K.; Csöregi, E.; Laurinavicius, V.; Schuhmann, W. *Anal. Chem.* **1999** *71*, 3581.
51. Cosnier, S.; Gondran, C.; Senilou, A. *Synthetic Metals* **1999**, *102*, 1366.
52. Piro, B.; Nguyen, T.A.; Tanguy, J.; Pham, M.C. *J. Electroanal Chem* **2001** *499*, 103.
53. Pernaut, J.-M.; Reynolds, J.R. *J. Phys. Chem B* **2000** *104*, 4080.
54. Piro, B.; Pham, M.-C.; Ledoan, T. *J. Biomed. Mat. Res* **1999** *46*, 566.
55. Cui, X.; Lee, V.A.; Raphael, Y.; Wiler, J.A.; Hetke, J.F.; Anderson, D.J.; Martin, D.C. *J. Biomed. Mat. Res.* **2001** *56*, 261.
56. Garner, B.; Georgevich, A.; Hodgson, A.J.; Liu, L.; Wallace, G.G. *J. Biomed. Mat. Res* **1999** *44*, 121.
57. Kotwal, A.; Schmidt, C.E. *Biomaterials* **2001** *22*, 1055.
58. Collier, J.H.; Camp, J.P.; Hudson, T.W.; Schmidt, C.E. *J. Biomed. Mat. Res.* **2000** *50*, 574.
59. Jakubiec, B.; Marois, Y.; Zhang, Z.; Roy, R.; Sigot-Luizard, M.-F. Dugré, F.J.; King, M.W.; Dao, L.; Laroche, G.; Guidoin, R. *J. Biomed Mat. Res.* **1998** *41*, 519.
60. Cui, X.; Hetke, J.F.; Wiler, J.A.; Anderson, D.J., Martin, D.C. *Sensors and Actuators A* **2001** *93*, 8.
61. Rodríguez, F.J.; Gutiérrez, S.; Ibanez, J.G.; Bravo, J.L.; Batina, N. *Environ. Sci. Technol.* **2000** *34*, 2018  
Yang, Y.-J.; Huang, H.-J. *Anal. Chem.* **2001** *73*, 1377.  
Gbatu, T., Ceylan, O., Sutton, K.L., Rubinson, J.F, Galal, A., Mark, H.B. Jr., Caruso, J.A., *Analytical Communications* **1999** *36*, 203.

- 64 Mangold, K.M.; Schafer, S.; Juttner, K. *Fresenius J. Anal. Chem* **2000** 367, 340.
- 65 Mangold, K.-M.; Schafer, S.; Juttner, K. *Synthetic Metals* **2001** 119, 345.
- 66 Korri-Youssoufi, H.; Yassar, A. *Biomacromolecules* **2001** 2, 58.
- 67 Bidan, G.; Billon, M.; Livache, T.; Mathis, G.; Roget, A.; Torres-Rodriguez, L.M. *Synthetic Metals* **1999** 102, 1363..
- 68 Bidan, G.; Billon, M.; Galasso, K.; Livache, T.; Mathis, G.; Roget, A.; Torres-Rodriguez, L.M.; Vieil, E. *Applied Biochem. Biotech.* **2000** 89, 183.
- 69 Livache, T.; Fouque, B.; Roget, A.; Marchand, J.; Bidan, G.; Téoule, R.; Mathis, G. *Analyt. Biochem.* **1998** 255, 188.
- 70 Garnier, F.; Korri-Youssoufi, H.; Srivastava, P.; Mandrand, B.; Delair, T. *Synthetic Metals* **1999** 100, 89.
- 71 Sargent, A.; Loi, T.; Gal, S.; Sadik O.A. *J. Electroanal. Chem* **1999** 470, 144.
- 72 Mulchandani, A.; Pan, S. *Analyt. Biochem* **1999** 267, 141.
- 73 Piro, B.; Do, V.-A.; Le, L.A.; Hedayatullah, M.; Pham, M.C. *J. Electroanal Chem* **2000** 486, 133.
- 74 Bercerik, I., Kadirgan, F. *Synthetic Metals* **2001** 124, 379.
- 75 Vidal, J.-C.; Garcia, E.; Mendez, S.; Yarnoz, P.; Castillo, J.-R. *Analyst* **1999** 124, 319.
- 76 Sun, W.J.; Bae, Y.H. *Anal. Chem.* **2000** 72, 2177.
- 77 Xue, H.; Shen, Z.; Li, Y. *Synthetic Metals* **2001** 124, 345.
- 78 Reiter, S., Habermüller, K., Schuhmann, W. *Sensors and Actuators B* **2001** 79, 150.

## Chapter 2

# Electrochemistry of Ion-Selective Conducting Poly(3-methylthiophene): The Polymer, the Charge, and the Interface

Ahmed Galal

Department of Chemistry, College of Science, University of Cairo,  
Giza, Egypt

Conducting poly(3-methylthiophene) films were electrochemically deposited onto a platinum substrate. The resulting polymer film electrode was tested in different electrolytes and solvents using electrochemical impedance spectroscopy (EIS). The effect of exposure of the polymer film to iodine was also studied. From the impedance measurements, the values of parameters such as double layer capacitance, charge transfer resistance and diffusion coefficients were obtained. For the capacitance associated with the polymer, relatively large values have been found which vary as a function of the film potential and the electrolyte/solvent used. The capacitive component of the current was separated from the faradaic one during the charging/discharging process for films exposed to iodine. The results were used to interpret the selective nature of the polymer film towards ion recognition.

Until the mid-seventies electrical conduction had been observed only in inorganic polymers and molecular crystals. In 1977, however, a group of scientists led by Heeger, Shirakawa and MacDiarmid (2) reported that an organic polymer, polyacetylene, could be made conducting by the addition of

appropriate “dopant.” Since then, conducting polymers have attracted the interest of many scientists because of their many technological applications such as electronic and optical devices (3), electrochromic displays (4), drain-source junctions in MOSFET-like devices (5), rechargeable batteries (6) and double layer capacitors (7). Conducting polymer films offer a wide variety of prospects for analyte recognition with specific as well as nonspecific interactions that translate into transducible responses. A recent review by Swager et al. (8) described conducting polymers in sensory applications in a comprehensive fashion. On the other hand, studies of the electrochemical behavior of electrodes modified with polymeric materials have been one of the most rapidly growing and advancing areas of modern electrochemistry for the last three decades. Thus, the behavior of electrodes made of poly(3-methylthiophene) films have also been of great interest (9). Poly(thiophene) films showed remarkably high electrochemical stability and exhibited selective response towards dissolved ions. The later property resulted from the “unique” advantage of the electrochemical synthesis of the polymer films that leads to a direct film deposition onto the metal substrate and a “self-doped” film that incorporates supporting electrolyte ions into the polymeric film (10). The selective potentiometric response for chloride (11a) and perchlorate (11b) ions using poly(pyrrole), and for iodide ion based on poly(N,N-dimethylaniline/poly(*o*-chloroaniline) (11c) and poly(3-methylthiophene) (11d) are among the several studies in the literature on the application of conducting polymers in potentiometry.

Electrochemical impedance spectroscopy (EIS) is a valuable technique for determining important characteristics of electrochemically active polymeric materials (12). For example, Komura and his co-workers (13) studied the charge transport at poly(*o*-phenylenediamine) electrodes. The authors showed there existed a relationship between the capacitance, the Warburg coefficient and the formal potential of the polymer electrode. Moreover, the analysis of the impedance data suggested that electron transport was via interchain electron hopping. On the other hand, the degradation processes of poly(*o*-toluidine) and poly(*o*-aminophenol) were followed by EIS measurements (14). The results revealed a noticeable change in the Nyquist plot that was illustrated by the appearance of a semicircle and increase in the polymer film resistance after degradation. The effect of electrolyte concentration on the charge transport at poly(pyrrole) film electrode was studied (15). The polymer electrode studied in aqueous electrolyte, in this case, showed apparent swelling that, resulted in migration of background electrolyte into the bulk of the film. EIS data revealed a resultant increase in the activity of polarons that brought about a small Warburg coefficient and a small limiting diffusion resistance.

In this work, we have used the EIS technique to examine different factors that affect the ion-selective response of conducting polymer electrodes. In previous studies (11d,16) we investigated the application of poly(3-

methylthiophene) electrodes in the selective determination of iodide in aqueous solutions. The effect of various pre- and post-conditioning parameters on the electrode performance and lifetime were examined and compared in the study (16). The nature of the response of the conducting polymer ion selective electrode was attributed to the oxidation of iodide at the polymer film surface that resulted in the incorporation of various iodine species within the film matrix. Other studies suggested similar rationalization(17)]. In spite of the extensive studies published to date on conducting polymer-based ion selective electrodes, and to the best knowledge of the author, the relation between the polymer electrode performance and the various electrochemical/electrical characteristics of the film is not yet investigated.

## Experimental

### *Sample preparation*

The polymer films were grown by electrochemical polymerization (18) of 3-methylthiophene on platinum electrodes of 3 mm diameter by application of constant potential of 1.65 V – 1.75 V (vs. Ag/AgCl), as indicated. The synthesis background electrolyte consisted of 0.05 M 3-methylthiophene and 0.10 M tetrabutyl ammonium hexafluorophosphate (TBAHFP) dissolved in dry acetonitrile. The thickness of the film was controlled by the control of the charge passing through the electrolyte according to the relation (19):

$$d \approx 2Q_g \quad (1)$$

where,  $d$  is the thickness in nm and  $Q_g$  is the charge passing during the electropolymerization in  $\text{mC cm}^2$ .

Impedance measurements were carried out using a PC3/750 Potentiostat /Galvanostat/ZRA equipped with an A/D converter from Gamry Instruments, Inc. (PA, USA). The Gamry's CMS300 Electrochemical Impedance Spectroscopy System/Framework was used to run the EIS experiments and, with the help of a personal computer connected to the cell (20), to analyze the data. A series of complex impedance measurements was carried out over a large frequency range ( $1 \times 10^{-2} - 5 \times 10^3$  Hz). Experiments were performed at a fixed applied potential and a small sinusoidal perturbation of 10 mV generated by the PC. The linearity of the system was verified automatically using internal standards. All measurements were normalized to an electrode area of  $1.0 \text{ cm}^2$ .

A one-compartment electrochemical cell was used for electrosynthesis and EIS measurements. A large area, Pt gauze counter electrode ( $2.5 \times 3.0 \text{ cm}^2$ , AESAR) and a saturated Ag/AgCl reference electrode were used. TBAHFP(Aldrich) was used without further purification and dried in vacuum at  $100 \text{ }^\circ\text{C}$  for ca. 24 h prior to use. 3-Methylthiophene (Aldrich) was distilled in an

inert atmosphere and stored over argon. Acetonitrile (HPCL grade, Aldrich) was used as received and kept over molecular sieves. Solutions were purged with argon prior to electrochemical measurements.

## Results and Discussion

The first set of results is represented in the form of a Nyquist diagram, plotting the imaginary component ( $Z''$ ) as a function of the real component ( $Z'$ ) of the impedance, cf. Figure 1. The data illustrate the results obtained for a polymer film formed under constant applied potential of 1.7 V for 25 s with an estimated thickness of 100 nm according to equation 1. Curves a - e depict the data obtained for the polymer film taken at +1.2 V, +0.5 V, 0.0 V, -0.2 V, and -0.5 V, respectively. In this case, the applied potential at the polymer film was increased gradually from the reduced state to the oxidation state. It could be seen that in the oxidized state a vertical line is obtained, as shown in curve (a). This could be explained in terms of the capacitive effect that is predominant for polymeric films in the oxidized state (21). The linearity decreased gradually as the reduction potential increases, as shown in curves (b-e). Moreover, the non-linear part of the curves was amplified at lower frequencies. At relatively low applied potential (for example -0.5 V) an almost straight line is observed that does not correspond to 45°. Similar complex behavior due to the superimposition of the low frequency transport phenomenon was also observed earlier in a similar study (21). The internal capacitance,  $C_p$ , of the polymer film could be estimated from the vertical part of the curve of the Nyquist plot. The internal capacitance of the film is associated with an internal resistance,  $R_f$ . The later can be deduced from the relation:

$$R_t = R_s + R_i + R_f \quad (2)$$

Where  $R_t$  is the total resistance,  $R_s$  is the solution resistance, and  $R_i$  is the intrinsic polymer resistance due to charge transfer (or  $R_{ct}$ ).

The Bode- $|Z|$  diagrams obtained at different applied potentials for 100 nm-thick poly(3-methylthiophene) films in 0.1 M TBAHFP/AcN are given in Figure 2. As is evident in Figure 2, at a given potential the impedance,  $Z$ , values gradually decrease as the applied potential increases. This trend was observed for all films with different thicknesses tested. Thus, running the same experiment at constant potential, a progressive decrease in  $Z$  was noticed when the film thickness increases. Faradaic type impedance represented several types of conducting polymers including poly(aniline), poly(pyrrole), poly(3-methylthiophene), and poly(acetylene) (21-24). In this study several equivalent circuits were tested in an attempt to fit the experimental data obtained for the



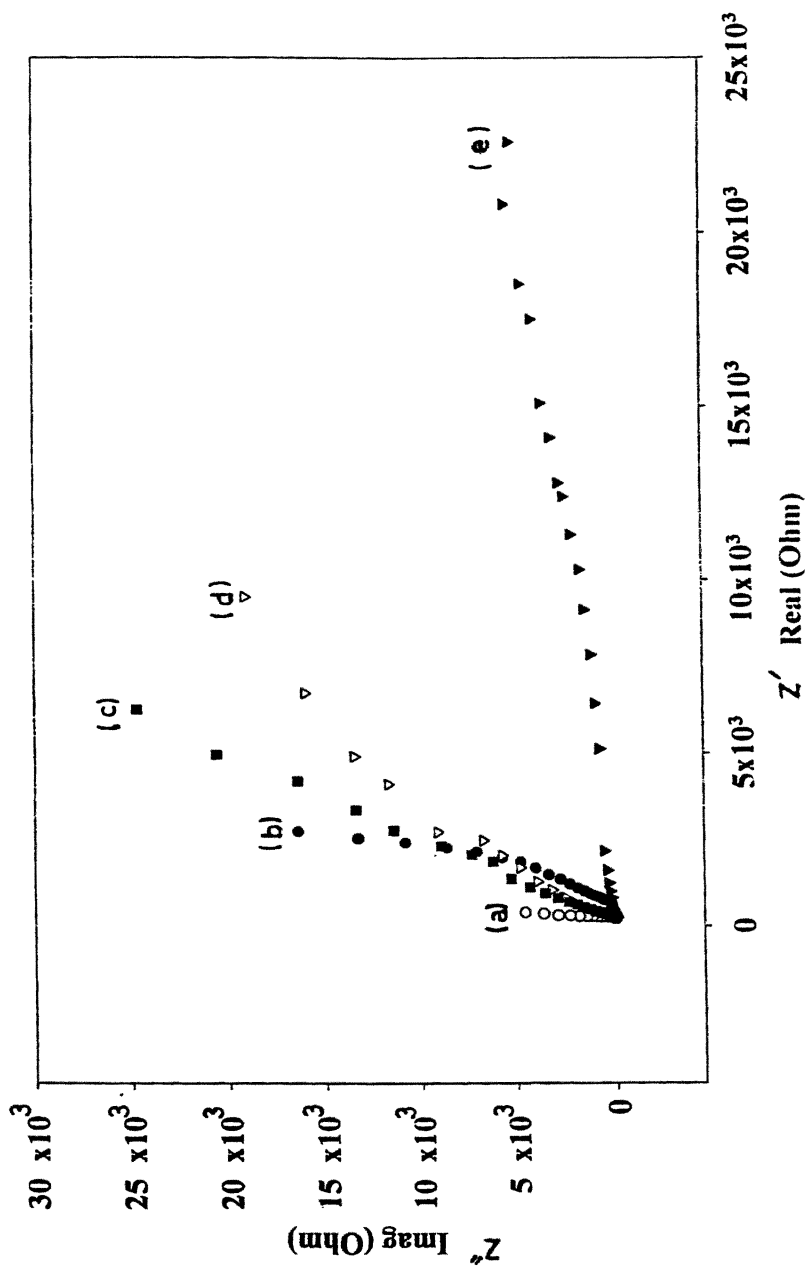


Figure 1. Nyquist diagrams of a 100 nm polymer film taken at different potentials: 1.2 V (a), 0.5 V (b), 0.0 V (c), -0.2 V (d) -0.5 V (e)

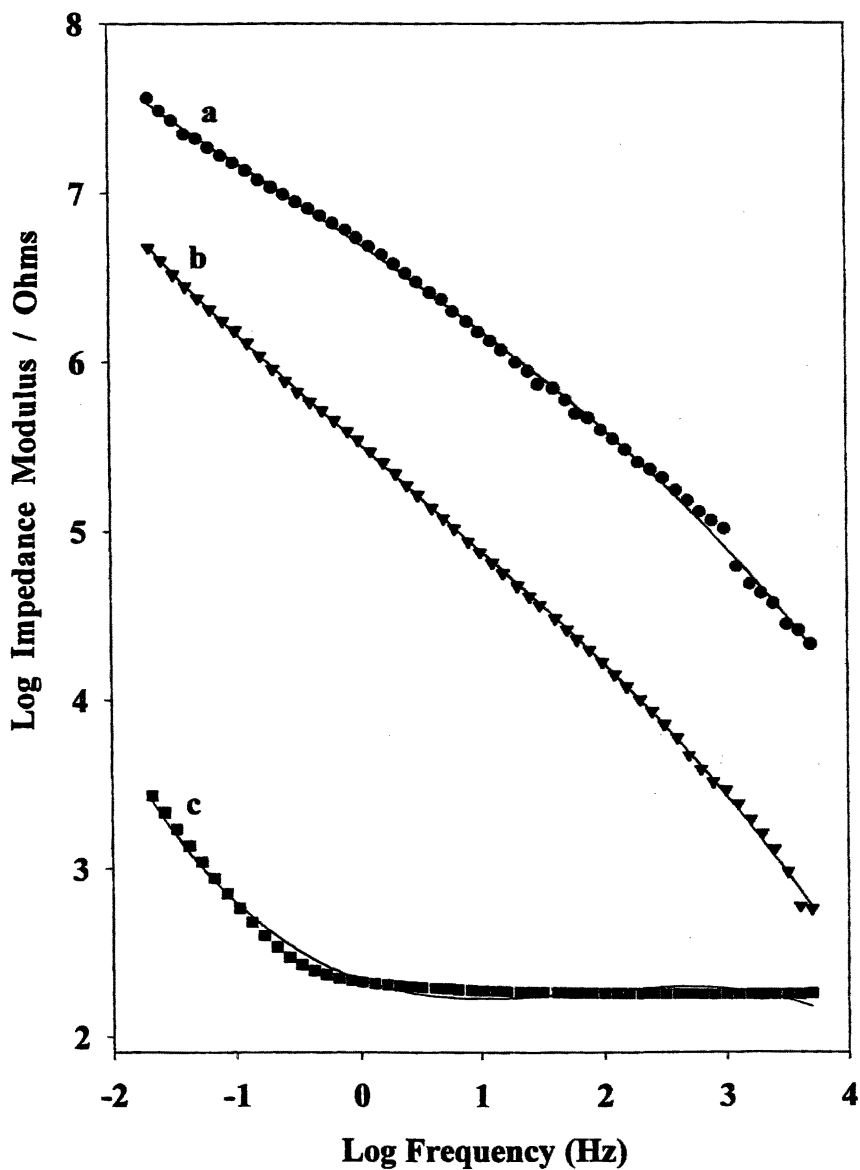


Figure 2. EIS curves for 100 nm-thick poly(3-methylthiophene) film in 0.1 M TBAHFP/AcN at different applied potentials, -0.5 V (a), 0.0 V (b), +1.2 V (c).

oxidized and reduced forms of the polymer film, respectively. We came to the conclusion that the circuits depicted in Figure 3 best describe the behavior of the polymer films in the doped and undoped states. Although the Bode- $|Z|$  plots shown in Figure 2 appear to be relatively simple, significant differences were found in the corresponding Bode/phase angle data when exposing the polymer film formed under similar preparative conditions to an aqueous solution of 0.2 M  $\text{LiClO}_4$ , (Figures 4 and 5). The phase angle-frequency diagram (Figure 5) exhibited phase angle values over  $60^\circ$  in the low frequency region and much lower values in the relatively high frequency region. At intermediate and relatively low frequencies and at a given frequency value, the region of the highest phase angle values shifted to a lower value when the polymer is oxidized. We observed similar trend when the thickness of the film was increased. It is worth mentioning that the Nyquist diagrams shown in Figure 1 exhibited a semicircular shape for all potentials applied in the relatively high frequency of the region studied. Moreover, the relatively low frequency region showed a second semicircular shape for low applied potential when the polymer is in the undoped/reduced state. The second semicircular region becomes ill defined as the applied potential to the polymer film increases, bringing it gradually towards the oxidized state. This is an indication of the existence of different processes in the polymer film related to more than one complex element in the equivalent circuit.

In summary, two processes should be considered as indicated above when the polymer is reduced and can be represented by the equivalent circuit of Figure 3a. In this diagram,  $R_s$  represents the solution resistance,  $C_{dl}$  refers to the double layer capacitance,  $R_i$  is the intrinsic resistance due to charge transfer of the redox process within the polymer film,  $W$  is the equivalent to the ionic diffusion at the film/electrolyte interphase,  $C_f$  is the film capacitance, and  $R_f$  is the film resistance. In all cases, an electronic resistance component of the polymer film is considered to be connected in series with the solution resistance. Similar equivalent circuits were described in the literature for poly(2,5-di-(2-thienyl)-thiophene) films earlier in the literature (25). The value of the electrical resistance of the polymer film varies considerably according to the applied potential to the polymer film, the film thickness and the electrolytic medium in which the measurement is taking place (26). Polymer film parameters are summarized in Table 1 for both oxidized and reduced states, respectively.

A second major goal of this study is to compare the AC impedance characteristics of the polymer film in aqueous to non-aqueous media and to investigate the effect of iodine doping of the polymer that led to the possible application of the polymer film for iodide ion selective determination (11d,16). In this work, one of the major setbacks for the selective nature of the polymer electrode towards iodide was the necessary pretreatment step in an iodine containing-environment and the short lifetime of the probe. However, controlled

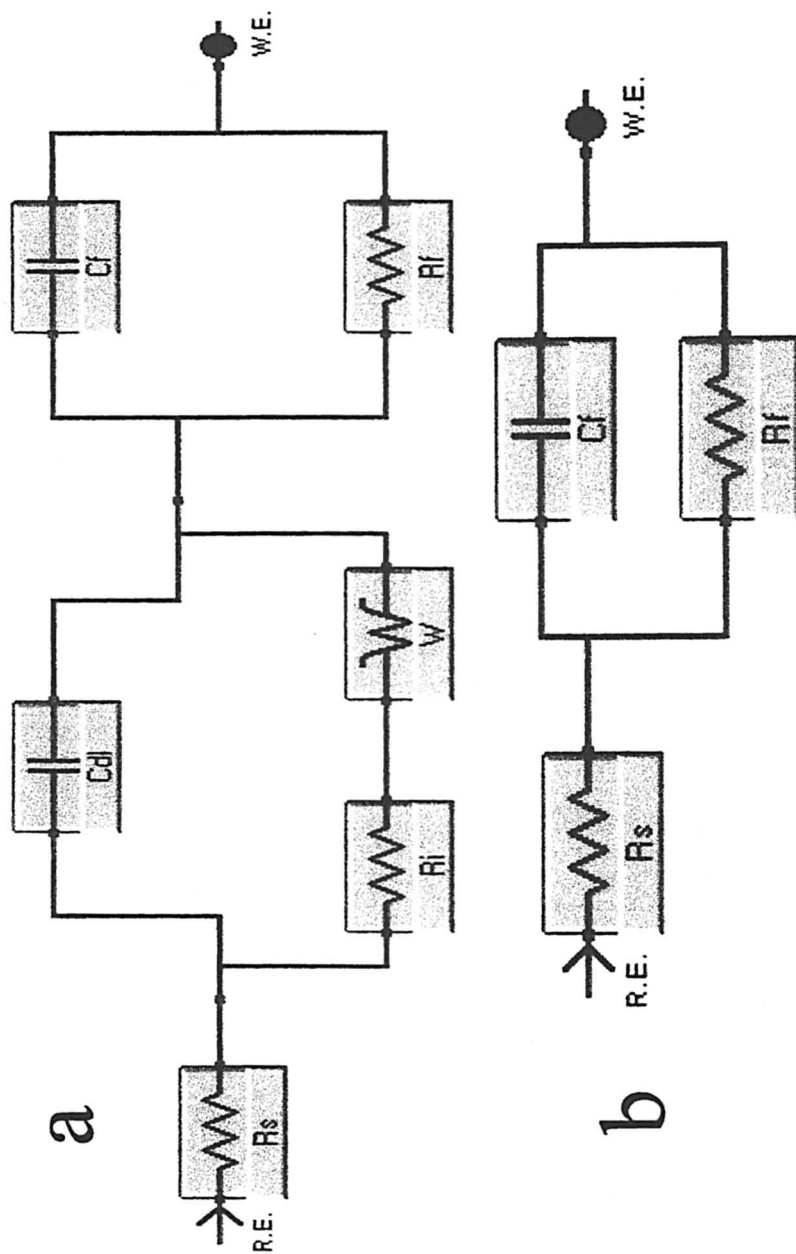


Figure 3. Equivalent circuit for poly(3-methylthiophene) in doped (a) and undoped (b) states.

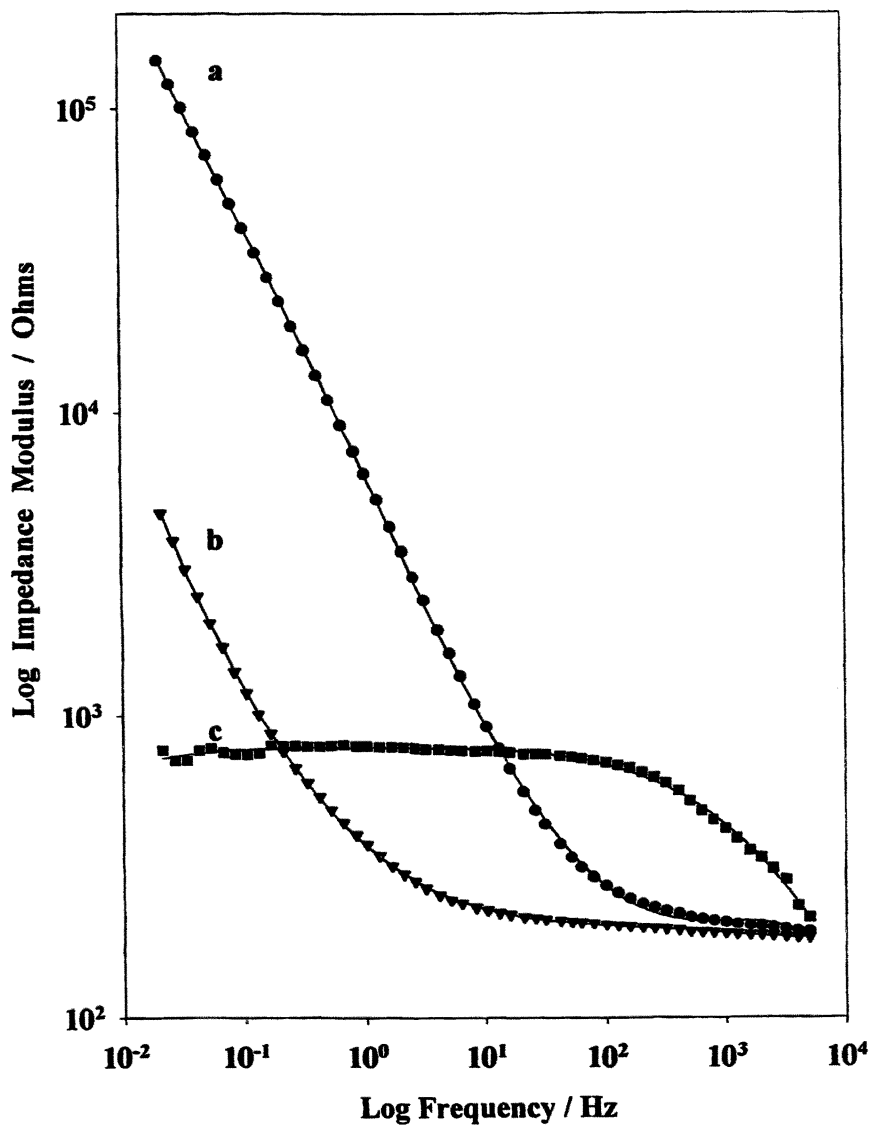
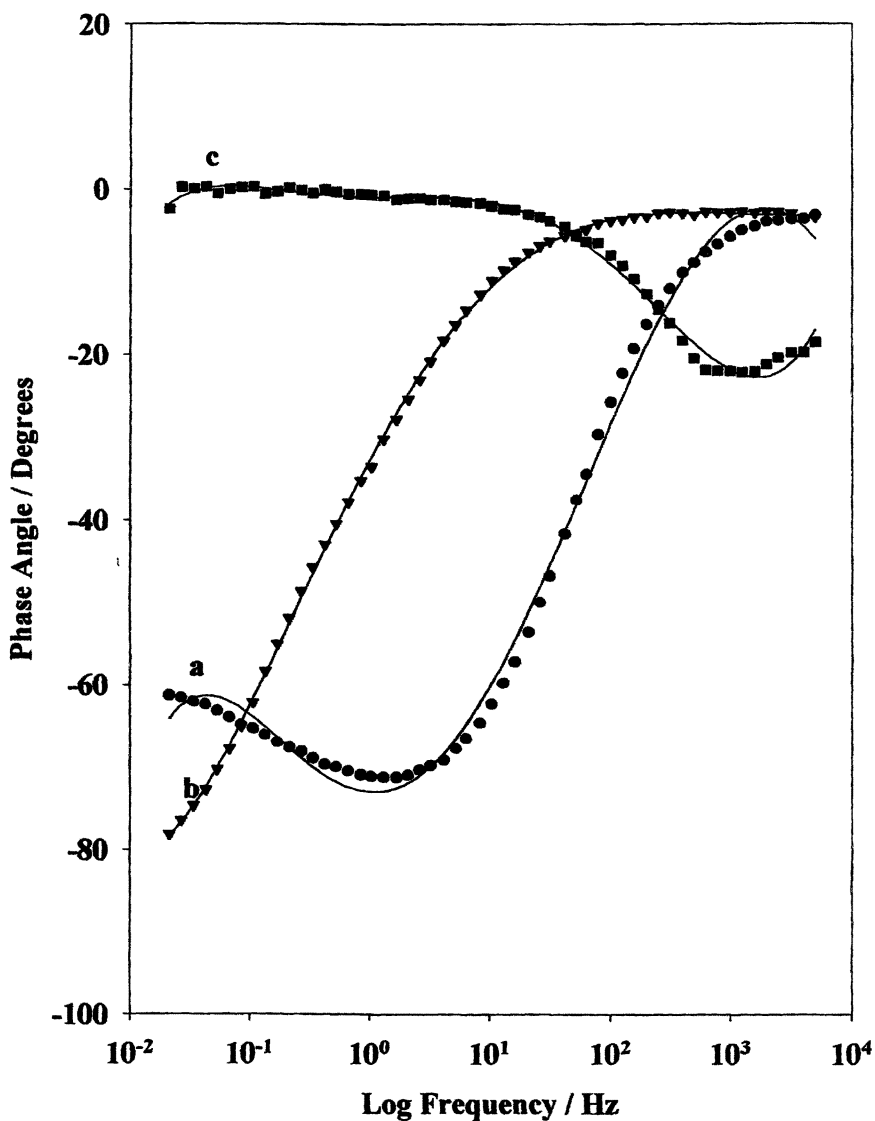


Figure 4. EIS curves for 100 nm-thick poly(3-methylthiophene) film in 0.1 M  $\text{LiClO}_4$  at different applied potentials, -0.5 V (a), 0.0 V (b), +1.2 V (c).



*Figure 5. EIS curves showing phase angle change with frequency for 100 nm-thick poly(3-methylthiophene) film in 0.1 M LiClO<sub>4</sub> at different applied potentials, -0.5 V (a), 0.0 V (b), +1.2 V (c).*

**Table I. Values of parameters derived from the fits of the impedance data for 100 nm-thick poly(3-methylthiophene) film in 0.1 M TBAHFP.**

<i>Polymer</i>	$C_f$ ( $\mu F$ )	$C_{dl}$ ( $mF$ )	$C_L$ ( $mF$ )	$R_f$ ( $\Omega$ )	$D$ ( $cm^2 s^{-1}$ )
P3-MT Oxidized	14.1	2.8	4.7	72	$2.7 \times 10^{-12}$
P3-MT Reduced	8.9	1.1	2.3	102	$1.3 \times 10^{-12}$

Note:  $C_L$  is the limiting capacitance

exposure of the polymer film to iodine extended the performance of the probe to several months (16). At this stage no clarification was available to the reason why the performance of the electrode differed considerably upon exposure to iodine. The effect of exposure of the polymer film to iodine for 10 minutes followed by testing the electrode in 0.1 M TBAHFP and 0.1 M LiClO<sub>4</sub> is depicted in Figures 6A and 6B, respectively. Thus, exposing the polymer film to iodine resulted in a relative increase in the impedance as the applied potential increases as depicted in the Bode- $|Z|$  plot in 0.1 M TBAHFP/ACN of Figure 6A. However, at an applied potential value of 0.0 V, around the neutral undoped state of the polymer, the impedance value exhibited the lowest value when compared to the other potential values. On the other hand, the Bode- $|Z|$  plot in 0.1 M LiClO<sub>4</sub> showed a complicated behavior once again as the impedance value showed the lowest value at the polymer oxidation potential value of +1.2 V, cf. Figure 6B. The conductivity of the polymer film is expected to increase as the iodine adsorbed within the polymer film reduces, resulting in free ionic iodide within the polymer matrix and a relative decrease in the impedance value. The opposite trend is obviously taking place when the polymer film is tested in 0.1 M TBAHFP/ACN, thus explaining a poorer response of the polymer film in non-aqueous medium toward the detection of iodide. Figure 7 shows the effect of exposing a 100 nm-thick polymer film to iodine for 10 minutes as a Bode- $|Z|$  plot. This experiment showed that the polymer film doped with iodine exhibited better conductance when compared to that unexposed to iodine. The explanation given in previous publications (11d, 16) for the specific response of the polymer was attributed to the doping of the film with iodide/iodine/tri-iodide species to the film. This could be also confirmed by the fact proven in this study from the apparent decrease in the impedance of the polymer film upon its

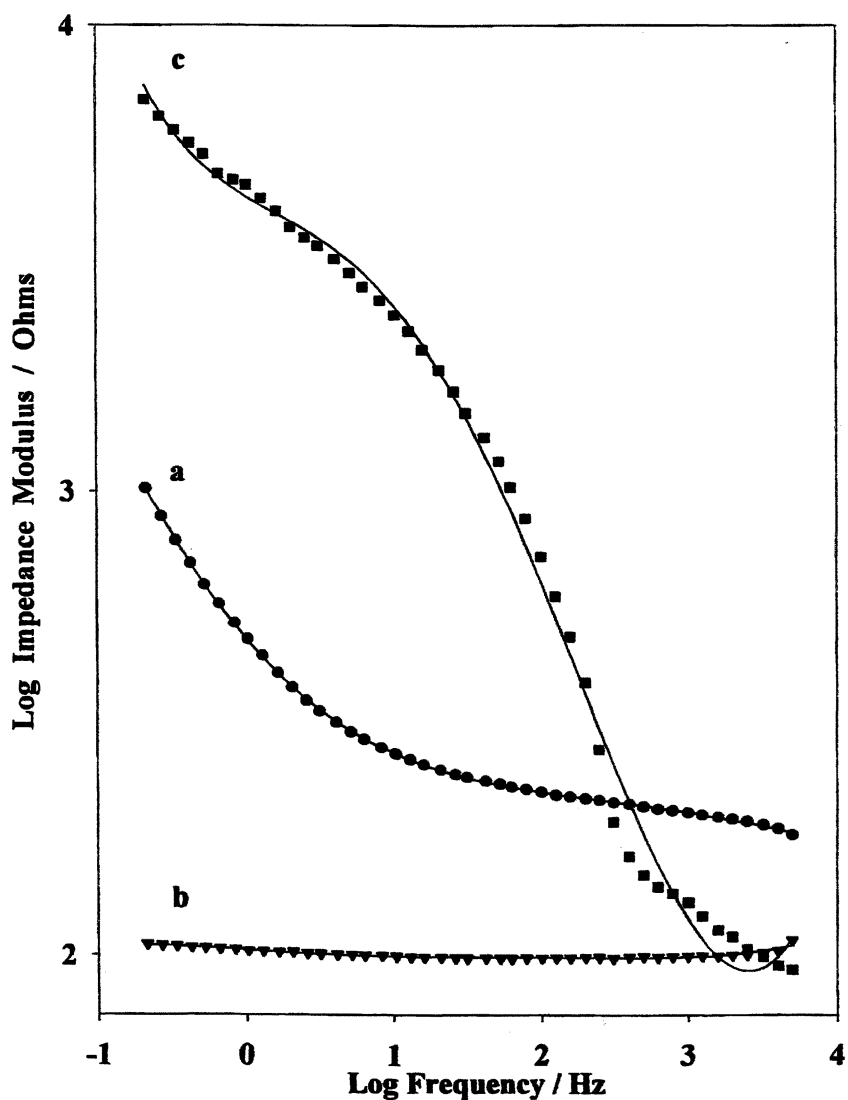


*Figure 6A. EIS curves for 100 nm-thick poly(3-methylthiophene) film in 0.1 M TBAHFP/AcN at different applied potentials, -0.5 V (a), 0.0 V (b), +1.2 V (c) after exposure to iodine for 10 minutes.*



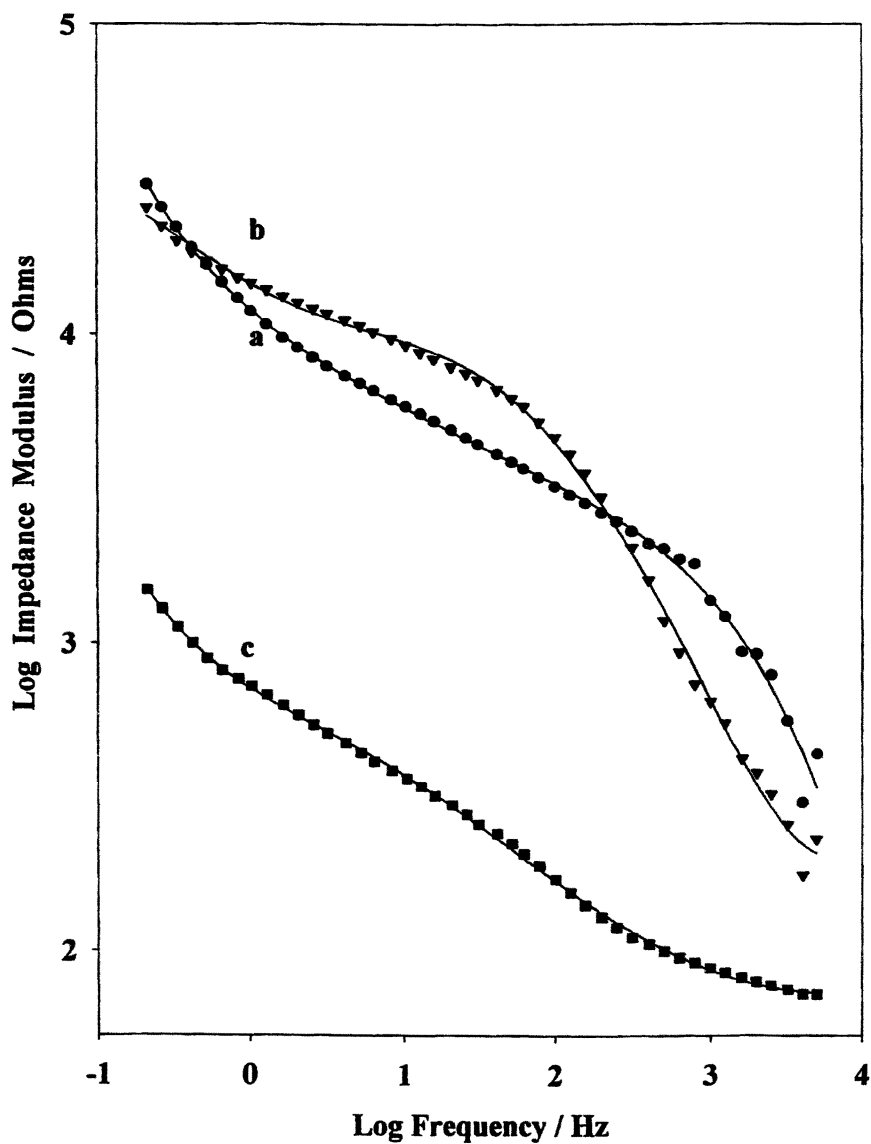
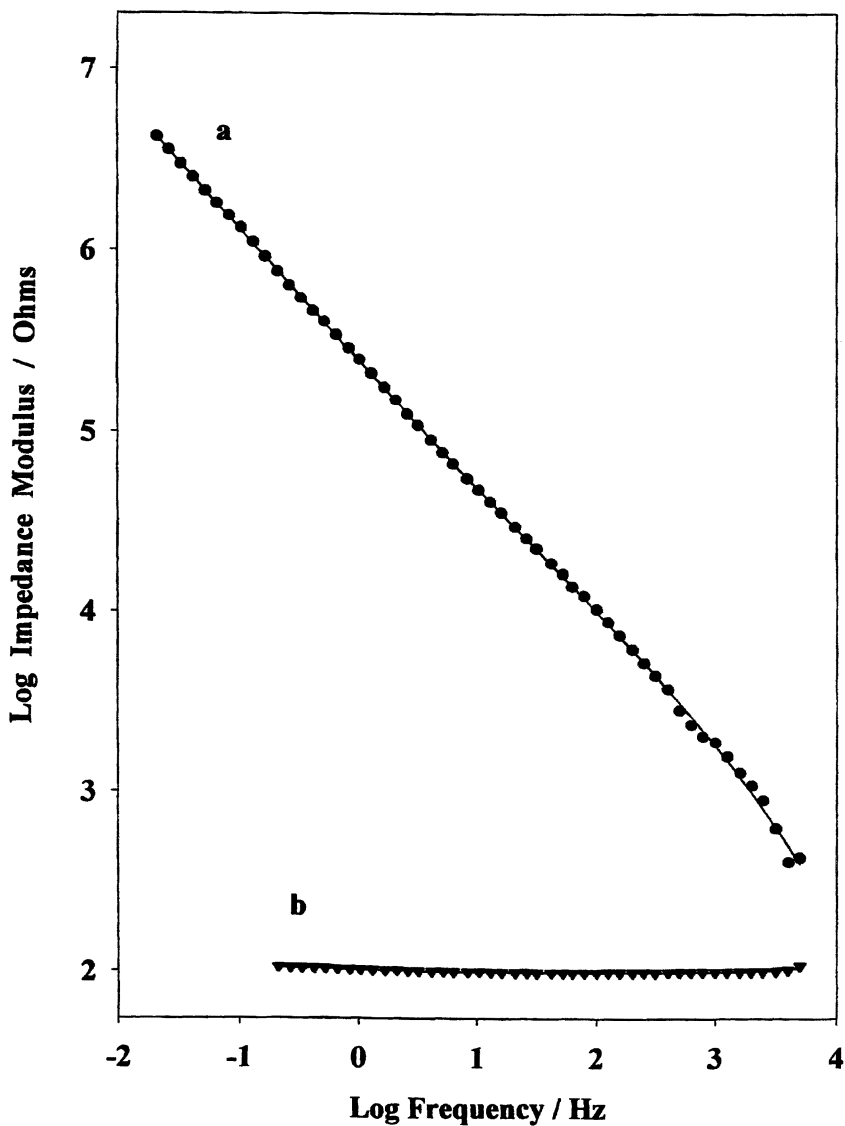


Figure 6B. EIS curves for 100 nm-thick poly(3-methylthiophene) film in 0.1 M  $\text{LiClO}_4$  at different applied potentials, -0.5 V (a), 0.0 V (b), +1.2 V (c) after exposure to iodine for 10 minutes.



*Figure 7. EIS curves for 100 nm-thick poly(3-methylthiophene) film in 0.1 M TBAHFP/AcN at different applied potentials, not exposed to iodine (a), and after exposure to iodine for 10 minutes (b).*

exposure to iodine. However, this was not satisfactory for reasonable explanation of the noticed deterioration of the response of the polymer film to iodide when leaving the electrode exposed to air for extend periods of time. Moreover, the change in the selective response of the sensor was not interpreted in terms of the electrical properties of the film. In this respect, it was necessary to carry out some experiments in order to reveal the relation between the change in the electrical properties and the sensor behavior of the polymer. Thus, experiments were conducted on a 100 nm-thick polymer film in 0.1 M TBAHFP and in 0.1 M LiClO<sub>4</sub> between -0.5 V and +1.2 V as depicted in Figures 8A and 8B, respectively. The following conclusions could be withdrawn from the data:

1. In both cases, the impedance of the film decreases with increase in the applied frequency.
2. The film passes through a transition from high impedance to lower values as the applied potential shifts towards the oxidation of the film.
3. For all potential values, the impedance values of the film in aqueous solution are relatively lower than those exhibited by the film in AcN.
4. The effect of time on the impedance values of the polymer film is given in Figure 8C. As can be noticed, the impedance value shows no change in the impedance values in the potential range of -0.2 V to 1.2 V in day two after synthesis. It could be concluded that the switching ability of the polymer film between the doped and undoped states cannot be realized in this case. The retain of the film to this property is apparently affecting its response with time as selective sensor for iodide ion.

In conclusion, we investigated the AC electrochemical behavior of polymer films in aqueous and non-aqueous media and compared their behavior upon doping with iodine. The polymer film exhibited normal behavior in non-aqueous media as mentioned previously in the literature. More complex behavior was found in aqueous electrolytes, which was attributed to the physical nature of the polymer. Doping of the polymer film with iodine affected its behavior differently when tested in aqueous and non-aqueous electrolytes. The time of exposure of the film affected its electrical properties considerably and consequently was given as an explanation for the poor response of the electrode when used as a selective sensor. The change in film thickness proved to decrease the impedance and change the interfacial response of the film towards charge transfer. Film impedance shows two distinct regions, the first of relatively high impedance for the fully reduced (doped) form of the polymer and the second showed gradual decrease in the impedance value as the polymer is oxidized (doped). The physical nature of the polymer film, namely the

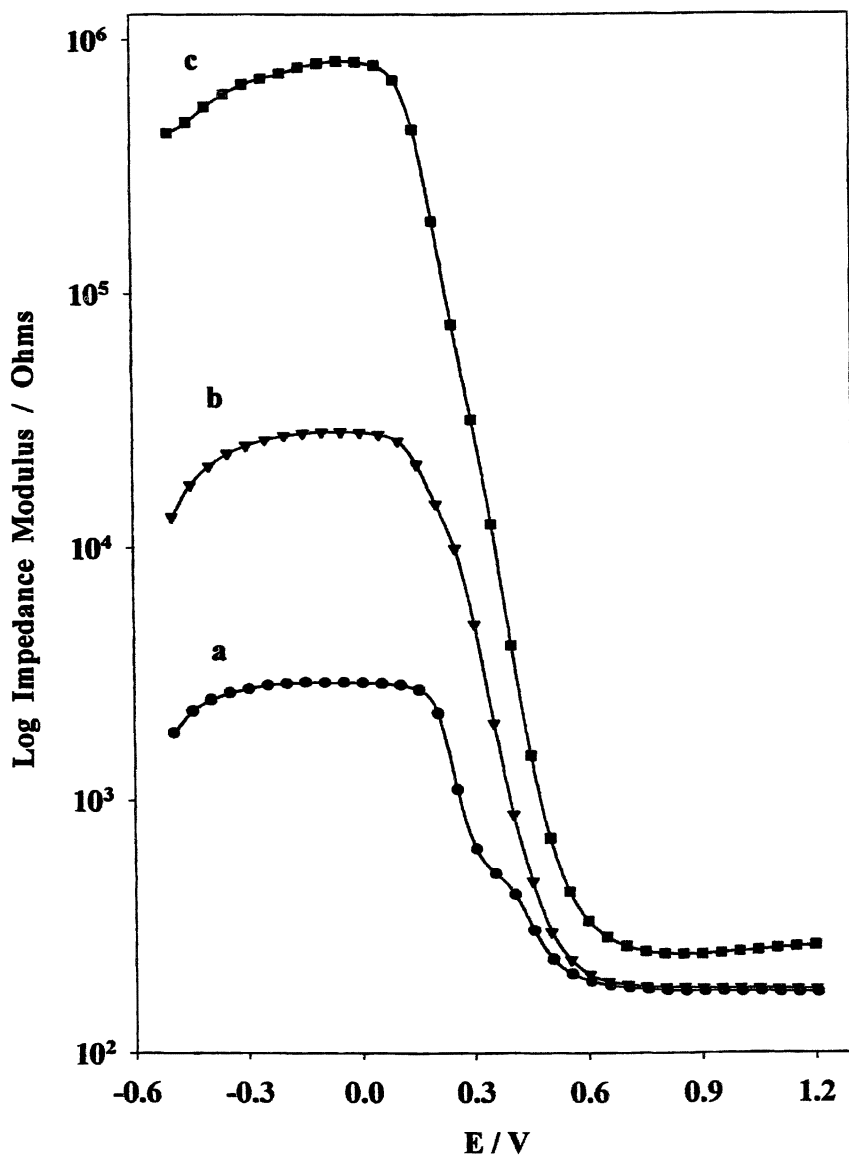


Figure 8A. Phase angle / frequency plots for 100 nm-thick poly(3-methylthiophene) film in 0.1 M TBAHFP/AcN at different applied frequencies, 5000 Hz (a), 100 Hz (b) and 0.2 Hz (c).

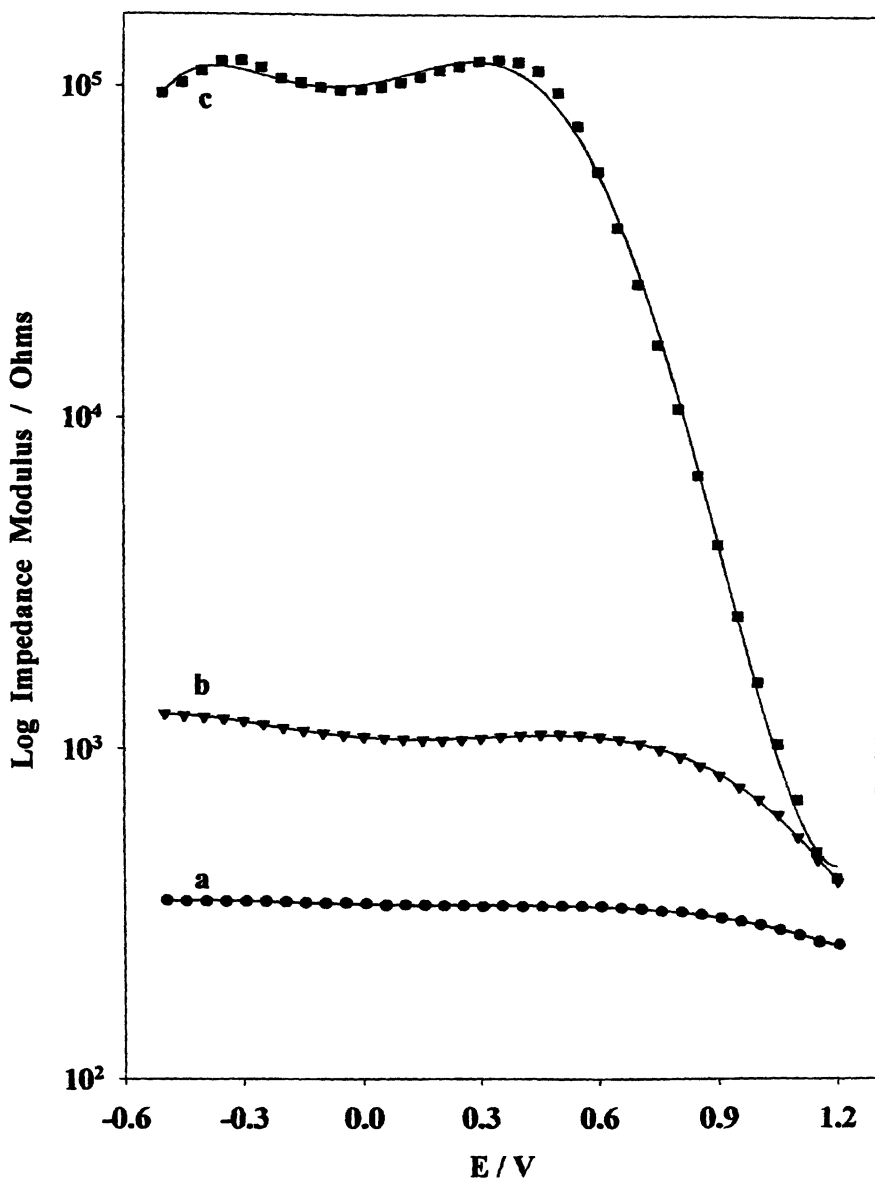


Figure 8b. Mott Schottky plots for 100 nm-thick poly(3-methylthiophene) film in 0.1 M LiClO<sub>4</sub> at different applied frequencies, 5000 Hz (a), 100 Hz (b) and 0.2 Hz (c).

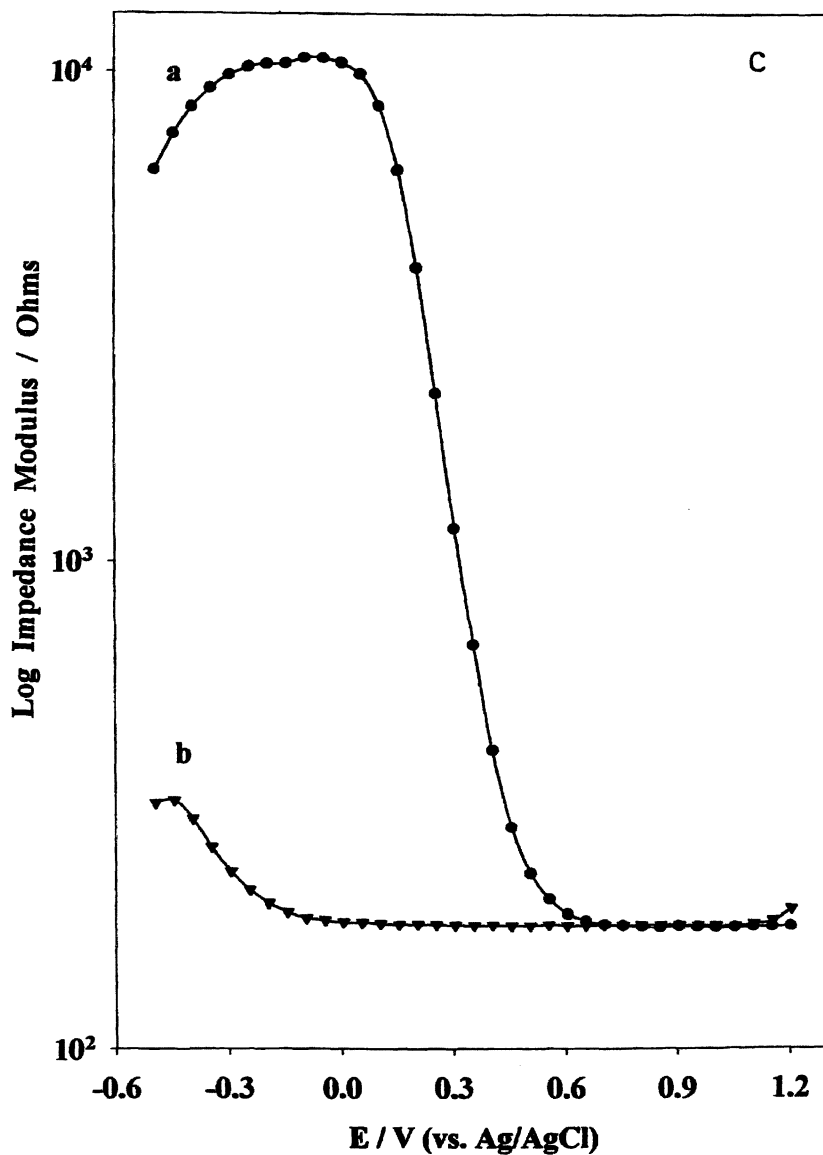


Figure 8C. Mott Schottky plots for 100 nm-thick poly(3-methylthiophene) film in 0.1 M LiClO<sub>4</sub> showing the effect of time at 5000 Hz, day one (a), day two (b).

hydrophobicity, is a possible reason for the distinct difference in the impedance values in aqueous and non-aqueous electrolytes.

## Acknowledgement

The author would like to thank Prof. Harry B. Mark, Jr. of the University of Cincinnati for his constructive comments and guidance throughout this work. We are indebted to the Research Council of the United Arab Emirates University for partial financial support for this work.

## References

1. On leave at: Department of Chemistry, College of Science, United Arab Emirates University, P.O. Box 17551, Al-Ain, United Arab Emirates. e-mail: [ahmed.helmy@uaeu.ac.ae](mailto:ahmed.helmy@uaeu.ac.ae), Fax: (971)3-7671291.
2. Chiang, C. K.; Fincher, Jr. C. R.; Park, Y. W.; Heeger, A. J.; Shirakawa, H.; Louis, E. J.; Gau, S. C.; MacDiarmid, A. G., *J. Chem. Soc. Chem. Commun.*, 1977, 16, 578.
3. Stubb, H.; Punkla, E.; Paloheimo, J., *Materials. Science and Engineering*, 1993, 10, 85.
4. Kobayashi, T.; Yoneyama, H.; Tamura, H., *J. Electroanal. Chem.*, 1984, 161, 419.
5. Paul, E. W.; Ricco, A. J.; Wrighton, M. S., *J. Phys. Chem.*, 1985, 89, 1441.
6. Nagatomo, T.; Ichikawa, C.; Omoto, O., *Synthetic Metals*, 1987, 18, 649.
7. Nishino, N., *Natn. Tech. Rep.*, 1985, 31, 22.
8. McQuade, D. T.; Pullen, A. E.; Swager, T. M., *Chem. Rev.*, 2000, 100, 2537.
9. (a) Wang, J.; Li, R., *Anal. Chem.*, 1989, 61, 2809, (b) Atta, N.; Galal, A.; Karagözler, A. E.; Russell, G. C.; Zimmer, H.; Mark, Jr. H. B., *Biosensors and Bioelectronics*, 1991, 6, 333, (c) Josowicz, M.; Janata, J.; Ashely, K.; Pons, S., *Anal. Chem.*, 1987, 59, 253, (d) Imisides, M. D.; Wallace, G. G.; Wilke, E. A., *Trends Anal. Chem.*, 1988, 7, 143.
10. (a) MacDiarmid, A. G.; Heeger, A. J., in *Molecular Metals*, Hatfield, W. E., Ed., Plenum, New York, N.Y., 1979, (b) Diaz, A. F.; Kanazawa, K. K.; Gardini, G. P., *J. Chem. Soc. Chem. Commun.*, 21, 635.
11. (a) Dong, S.; Sun, Z.; Lu, Z., *Analyst*, 1988, 113, 1525, (b) Lu, Z.; Sun, Z.; Dong, S., *Electroanalysis*, 1989, 1, 271, (c) Camperella, L.; Ferri, T.; Majone, M.; Mihic, T.; Russo, M. V.; Salvi, A. M., in *Recent Developments in Ion Exchange*, Williams, P. A.; Hudson, M. J. (eds.), Amsterdam, 1987, pp 315-321, (d) Karagözler, A. E.; Ataman, O. Y.; Galal, A.; Xue, Z.; Zimmer, H.; Mark, Jr. H. B., *Anal. Chim. Act.*, 1991, 248, 163.

12. (a) Deslouis, C.; Musiani, M. M.; Tribollet, B., *J. Phys. Chem.*, **1996**, *100*, 8994, (b) Rubinson, J. F.; Mark, Jr. H. B., in *Interfacial Electrochemistry, Theory, Experiment, and Applications*, Wieckowski, A., Ed., Marcel Dekker, Inc., New York, N.Y., **1999**, pp. 689-705.
13. Komura, T.; Yamaguti, T.; Takashi, K., *Electrochim. Act.*, **1996**, *41*, 2865.
14. Rodriguez Nieto, J. F.; Tucceri, R. I.; Posadas, D., *J. Electroanal. Chem.*, **1996**, *403*, 241.
15. Komura, T.; Usui, T.; Takashi, K., *Bull. Chem. Soc. Jpn.*, **1995**, *68*, 3391.
16. Galal, A.; Wang, Z.; Karagözler, A. E.; Zimmer, H.; Mark, Jr. H. B.; Bishop, P. L., *Anal. Chim. Act.*, **1994**, *299*, 145.
17. (a) Atta, N. F.; Galal, A.; Mark, Jr. H. B.; Yu, T.; Bishop, P. L., *Talanta*, **1998**, *47*, 987, (b) Hutchins, R. S.; Bachas, L. G., *Anal. Chem.*, **1995**, *34*, 1654.
18. Tourillon, G.; Garnier, F., *J. Electroanal. Chem.*, **1982**, *135*, 173.
19. Roncali, J.; Garnier, F., *Macromolecule*, **1989**, *22*, 804.
20. "CMS300 Electrochemical Impedance Spectroscopy System," Operator's Manual, Revision 2.1, **1994**, Gamry Instruments, Inc., Pa., USA.
21. Tanguy J.; Baudoin J. L.; Chao, F.; Costa, M.; *Electrochim. Act.*, **1992**, *37*(8), 1417.
22. Jow, T. R.; Shaclette, L. W., *J. Electrochem. Soc.*, **1988**, *129*, 1009.
23. Otero, T. F.; Angulo, E., *Synth. Met.*, **1992**, *51*, 87.
24. Genz, O.; Lohrengel, M. M.; Schultze, J. W., *Electrochem. Acta*, **1994**, *39*, 179.
25. Brillas, E.; Cabot, P. L.; Garrido, J. A.; Montilla, M.; Rodríguez, R. M.; Carrasco, J., *J. Electroanal. Chem.*, **1997**, *430*, 133.
26. Abdo, A., *Ph.D. Thesis*, **1992**, University of Cincinnati, Oh., USA.



## Chapter 3

# Thin Polyheteroaromatic Films Synthesized in Organized Media: Structures and Properties

S. Aeiyaeh, J. J. Aaron, M. Jouini, K. I. Chane-Ching, J. C. Lacroix,  
J. Tanguy, and P. C. Lacaze

Institut de Topologie et de Dynamique des Systèmes de l'Université Paris 7-  
Denis Diderot, Associé au CNRS (UPRES-A 7086), 1 rue Guy de la Brosse,  
75005 Paris, France

Two novel approaches have been developed for the electrochemical polymerization of thiophene derivatives in aqueous solution. The first one is based on the host (thiophene derivatives)-guest (cyclodextrins-CDs) inclusion complexes. Polymer films obtained from electrochemical oxidation of bithiophene- $\beta$ CD complex have long conjugated chains partially encapsulated by the CDs. Electropolymerization of the terthiophene- $\beta$ CD complex leads to polymer films with short conjugated chains and high structural order (sexithiophene). The second approach is based on the electropolymerization of thiophene derivatives in micelles. In aqueous sodium dodecylsulfate (SDS) solutions, polymer films prepared from EDOT and MOT have well-defined structures, good chain organization on the electrode surface and interesting physical and chemical properties.

## Introduction

Of all the conducting polymers polyheteroaromatics, particularly polythiophene (PT) and its derivatives, have attracted a great deal of attention for both fundamental and applied standpoints (1-2). The electrochemical oxidation of thiophene or its derivatives in anhydrous organic (3) or highly acidic ( $\text{pH} \leq 0$ ) media (4) leads generally to the formation of polymer film with good physicochemical properties. On the other hand, the electropolymerization of these monomers in moist organic or neutral aqueous media (1-4) did not yield any polymer film. The main factors which hinder this polymerization process are (i) the very low water-solubility of thiophene monomers; (ii) the potential of polymer film electrosynthesis being higher than that of water decomposition and (iii) the relatively high reactivity of water molecules with thienyl radical-cations formed from the oxidation of thienyl monomers.

Polymerization in organized systems in water such as micelles, microemulsions, vesicles and host-guest inclusion complexes has recently become an important research field (5). Using these systems to synthesize polymer films makes it possible to control their architecture and physicochemical properties. It has been shown that the electropolymerization of benzene in emulsions using anionic surfactants enhances the structural organization and improves the crystalline structure of the resulting polyparaphenylene films (6). Moreover, the electropolymerization of pyrrole (7) or thiophene derivatives in anionic micelles in water leads to the formation of polymer films having a columnar structure (8). The electropolymerization of [2]-pseudorotaxanes based on the inclusion of thiophene derivative guests inside cyclodextrins (CD) hosts leads to the formation of polymer films exhibiting well-ordered structures (9-10).

The aim of this paper was to study the electropolymerization of thiophene derivatives such as bithiophene (BT), terthiophene (3T), 3,4-ethylenedioxythiophene (EDOT) and 3-methoxythiophene (MOT) in aqueous solution. Two different strategies have been used. In the first one, polymer films are synthesized in constrained aqueous media based on host-guest inclusion complexes between CDs and thiophene derivatives. The second strategy consists in electrosynthesizing polythiophene films in micellar solutions, using anionic surfactants.

## Experimental

EDOT (Bayer), BT and 3T (purity  $\geq 99\%$ , Acros), MOT (purity  $\geq 98\%$ , Aldrich),  $\beta$ -cyclodextrin (CD) and hydroxypropyl- $\beta$ -cyclodextrin (HP $\beta$ CD)

(Aldrich) SDS (purity  $\geq 99\%$ , Fluka or Sigma) and  $\text{LiClO}_4$  (purity  $\geq 99\%$ , Fluka or Acros) were used without further purification. All aqueous solutions were prepared with distilled water further purified with a Millipore purification system. Electrochemical experiments and spectroscopic techniques such as Raman, FTIR, XPS, UV-Vis, MALDI-TOF and AFM have been described elsewhere (8-10)

## Results and Discussion

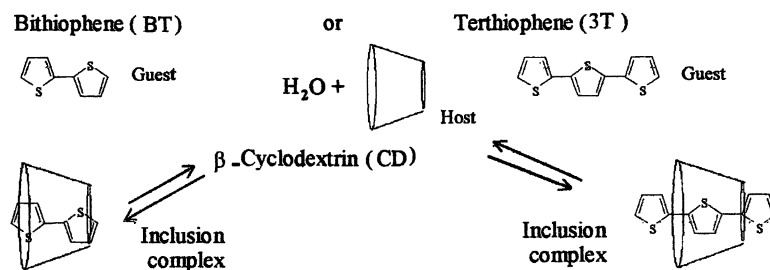
### Electropolymerization of Host-Guest Complexes (Thiophene derivatives - Cyclodextrins) in Aqueous Solutions

The self-assembly of supramolecular structures such as host-guest inclusion complexes has recently been the focus of a number of research efforts. This approach allows the design and building of nanoscale molecular devices. It constitutes a convenient route to realizing the polymerization of hydrophobic molecules (guests) such as thiophene derivatives in aqueous solution by using CDs (hosts) and to customizing the polymer architectures (9-11).

CDs are macrocyclic oligosaccharides made up of 6-12 glucopyranose units linked by glycosidic  $\alpha$ -1,4 bonds. Among these oligosaccharides, only  $\alpha$ ,  $\beta$  and  $\gamma$ -CD, which consist of six, seven and eight glucose units, respectively, have been widely used. Their cylindrical structures (toroid shape) with hydrophobic cavities, about 0.7 nm deep and 0.5 - 0.8 nm inside diameter, and hydrophilic outer side yield various unique properties. In particular, CDs have the ability to form stable host-guest inclusion complexes through non-covalent interactions with guest molecules that fit into the cavity in aqueous solutions (12-13). Because of these particular properties, CDs are some of the most widely studied water-soluble molecular receptors (hosts) and are used in a variety of fields, particularly in electrochemistry (13). CDs are not electroactive and can be used to form inclusion complexes with suitable redox-active guests. Much work has been devoted to studying the electrochemical behavior of the CDs with many different redox-active molecules (13). However, until now little attention has been paid to the electropolymerization of host-guest (CD-redox-active molecule) inclusion complexes and to the effect of CDs on the structure of polymer films. In this study, electrochemical polymerization of two thiophene derivatives, BT and 3T, with  $\beta$ -CD is performed in aqueous solution. It is hoped that the use of CDs will induce self-assembly properties allowing to electrosynthesize PT films with a well-ordered polypseudorotaxane - like structure (molecular wires encapsulated by CDs).

### Host-Guest Inclusion Complexes Formation.

The formation of inclusion complexes between  $\beta$ CD or its derivatives (HP $\beta$ CD) and BT or 3T was carried out in aqueous solutions.  $\beta$ CD should be able to encapsulate these monomers since the size of its cavity fits well the size of BT and 3T molecules. BT and 3T are highly hydrophobic organic molecules with solubilities in water of about  $2 \cdot 10^{-5}$  and  $10^{-7}$  M, respectively. These solubilities are markedly increased when  $\beta$ CD or its derivatives are added to aqueous solutions. For example, the solubility of BT in water reaches  $5 \cdot 10^{-3}$  and  $5 \cdot 10^{-2}$  M in the presence of  $\beta$ CD and HP $\beta$ CD, respectively, while that of 3T in water with HP $\beta$ CD is  $10^{-3}$  and  $5 \cdot 10^{-3}$  M at 25°C and 40°C, respectively. This large increase in solubility suggests that inclusion complexes are formed between CDs and BT or 3T (guest) due to hydrophobic forces, which are able to drive a guest into the CD cavity (Schema 1).



*Scheme 1. Inclusion complexes formed by  $\beta$ CD or HP $\beta$ CD with bithiophene and terthiophene in aqueous solution.*

Host-guest inclusion complexes can be precipitated from aqueous solutions of  $\beta$ CD and BT or 3T (Scheme 1). Elementary analysis shows that stable complexes with 1:1 stoichiometry are obtained. In order to confirm the complex formation, fluorescence spectroscopy was used. The inclusion of a guest inside a cyclodextrin cavity produces a change in the electronic environment of the guest. As a result, differences in the fluorescence spectra of free and CD-complexed monomer are expected. Fluorescence spectroscopy provides generally important information on the stoichiometry and equilibrium constants of inclusion

complexes. Fluorescence studies of BT ( $5.10^{-5}$  M) and 3T ( $3.10^{-6}$  M) were performed in aqueous solutions containing increasing HP $\beta$ CD concentrations at 25°C and 40°C, respectively. The fluorescence intensities of BT- HP $\beta$ CD (Figure 1) are decreased, while those of 3T- HP $\beta$ CD solutions are enhanced, upon increasing the HP $\beta$ CD concentrations. This behavior is characteristic of inclusion phenomena. Fluorescence data have been employed to determine the complex binding constant by using a non linear regression approach.

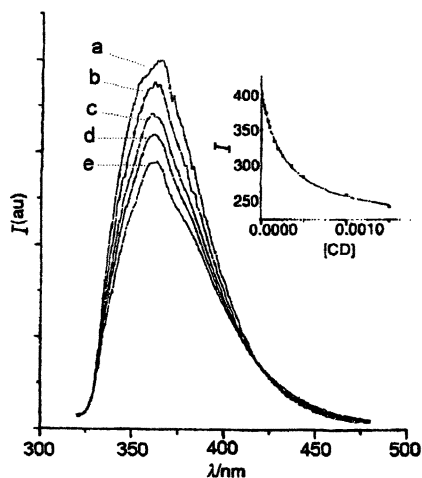
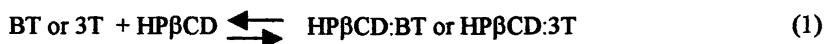


Figure 1. Fluorescence spectra of BT ( $5.10^{-3}$  M) with increasing HP $\beta$ -CD concentration: a) 0 M, b)  $5.10^{-5}$  M, c)  $1.5.10^{-4}$  M, d)  $2.5.10^{-4}$  M e)  $5.10^{-4}$  M. Inset: plot of fully corrected emission of BT at 365 nm at various HP $\beta$ -CD concentrations (•) experimental data (—) fit based on eqn. (2). (Reproduced from reference 10 by permission of The Royal Society of Chemistry).

Assuming the formation of a 1:1 complex (eqn. 1), the binding constant  $K_1$  was determined from equation 2, where  $I_0$ ,  $I$  and  $I_\infty$  denote the fluorescence intensity of BT or 3T in water without HP $\beta$ CD, at a given intermediate HP $\beta$ CD concentration and in the fully complexed form, respectively.



$$I = \frac{I_0 + I_\infty K_1 [HP\beta CD]_T}{1 + K_1 [HP\beta CD]_T} \quad (2)$$

The values of  $K_1$  are  $3570 \pm 90 \text{ M}^{-1}$  at  $25^\circ\text{C}$  and  $3300 \pm 70 \text{ M}^{-1}$  at  $40^\circ\text{C}$  for BT and 3T, respectively. These rather large values suggest that HP $\beta$ CD forms a 1:1 complex with BT and 3T. These values are in good agreement with those reported for the same type of complex (14).

### *Host-Guest Polymerization*

The electropolymerization of 0.02 M BT was performed in aqueous solutions containing 0.1 M HP $\beta$ CD and 0.1 M LiClO<sub>4</sub> at a Pt or ITO electrode, using cyclic voltammetry and the galvanostatic technique. In general, the growth of polymer films depends on the polarization potential. The anodic polymerization of HP $\beta$ CD-BT solution by cyclic voltammetry using switching potentials of - 0.3 and 1.1 V ( $v = 0.1 \text{ V s}^{-1}$ ) leads to the formation of thin, electroactive, homogenous and adherent polybithiophene (PBT) films at Pt electrodes. In addition, anodic and cathodic peaks increase with the number of successive cycles; electrochromic behavior was also observed during the growth of PBT films, which turn from red in the reduced state to green in the oxidized state. This phenomenon indicates that the HP $\beta$ CD-PBT prepared are electroactive whereas acetonitrile-PBT films do not exhibit any electroactivity in aqueous solution. These results suggest that PBT films electrosynthesized in aqueous solution using the host/guest strategy are structurally different from those prepared in organic media. The former may allow the partial penetration of water molecules and counter-ions, whereas the latter are highly hydrophobic and may inhibit this penetration (9-10).

PBT films can also be generated in aqueous solution at constant current densities of 0.05, 0.1 and 0.2 mA cm<sup>-2</sup>. For  $j = 0.1 \text{ mA cm}^{-2}$ , we observed two steps in the PBT film growth. In the first one, the potential varies from 0.98 to 0.96 V. In the second step, a deposition regime occurs in which the potential starts to rise sharply from 1V, indicating that the polymer initially generated is conductive and that its conductivity changes during electropolymerization. This implies that the structure of the polymer film upper layers is different from that of the inner layers (10).

Thin, homogenous polyterthiophene (P3T) can also be synthesized in an aqueous solutions containing 0.005 M 3T 0.1 M HP $\beta$ CD and 0.1 M LiClO<sub>4</sub> at a Pt or ITO electrode, using cyclic voltammetry and the galvanostatic technique. The resulting films are soluble in the usual organic solvents (11).

*PBT and P3T Structures*

The structures of PBT and P3T films prepared in aqueous solutions have been investigated by Raman, UV-Vis, FTIR, XPS and MALDI-TOF techniques. Analysis of PBT films by Raman spectroscopy ( $\lambda_{\text{ex}} = 514.5 \text{ nm}$ ) shows that their structures are similar to those of PBT films prepared in organic media. Raman spectra of PBT films exhibit an intense band at  $1455 \text{ cm}^{-1}$  and a weaker band at  $1495\text{--}1492 \text{ cm}^{-1}$ , which are assigned to the symmetric stretching mode and antisymmetric stretching vibration ( $\nu_{\text{as}}$ ) of the aromatic C=C band ( $\nu_s$ ), respectively. The wavenumber and the intensity of the latter band, generally, decrease monotonically as the average conjugation length increases (15). The  $\nu_{\text{as}}$  values for BT, 3T, quaterthiophene and sexithiophene are 1556, 1530, 1519 and  $1507 \text{ cm}^{-1}$ , respectively. However,  $\nu_{\text{as}}$  for polythiophene films is below  $1500 \text{ cm}^{-1}$  (15). Thus, it seems very probable that the PBT chains generated from aqueous HP $\beta$ CD solutions have an average conjugation length longer than sexithiophene (10).

UV-Vis absorption spectra were recorded for fully reduced PBT films deposited on ITO electrodes in aqueous HP $\beta$ CD solutions. The spectra are similar to those reported for PBT films prepared in organic media under the same electrochemical conditions. They display an absorption maximum around  $\lambda_{\text{max}} = 480 \text{ nm}$ , which corresponds to long conjugated polymer chains of about 16 thiophene units (10). This result is supported by data for long thiophene oligomers (16) and by the above Raman spectral data.

On the other hand, UV-Vis spectra of P3T films electrosynthesized from aqueous 3T-HP $\beta$ CD solutions on ITO electrodes show an absorption band at  $\lambda_{\text{max}} = 400 \text{ nm}$  corresponding to sexithiophene (17). This result indicates that the P3T chains consist mainly of dimers (sexithiophene), which is confirmed by mass spectrometry analysis. Moreover, UV-Vis spectra exhibit a vibronic structure corresponding to vibrational coupling of the electronic states (17). The absence of such structure in P3T films generated in organic media suggests that HP $\beta$ CD induces a well-ordered structure in the polymer films. The FTIR spectra of PBT prepared in aqueous BT-HP $\beta$ CD solutions exhibit features similar to those obtained in organic media except for the presence of strong HP $\beta$ CD bands at  $3400$ ,  $2960$  and  $2930 \text{ cm}^{-1}$ . This suggests that PBT film chains may be threaded into the HP $\beta$ CD cavity during the electropolymerization process. Furthermore, the FTIR data make it possible to estimate that the degree of polymerization (DP) is 24 thiophene units for PBT films, which is very close to the value obtained for PBT prepared in acetonitrile.

In order to elucidate the insertion of PBT in HP $\beta$ CD during film growth, we used the electrochemical quartz crystal microbalance technique (EQCM). EQCM is also appropriate to provide possible information about the influence of the electrochemical conditions on this phenomenon. EQCM results indicate that

no mass excess due to HP $\beta$ CD is observed during the polymer growth (galvanostatic conditions). However, under cyclic voltammetric or double potential step protocols a large amount of HP $\beta$ CD can be inserted in the film during the polymer reduction, depending on the experimental conditions. For example on the first potential step in Fig. 2 (part a) there is no polymer insertion during reduction. But on the second and the third potential steps a large frequency change is observed during reduction indicating that a large amount of HP $\beta$ CD is deposited on the electrode. The number of HP $\beta$ CD molecules is high enough to make the polymer surface completely insulating. Since polymerization continues and since the oxidation current does not decrease during the successive scans it seems likely that HP $\beta$ CD molecules diffuse quickly into the polymer. When the polymer layer is too thick the cell admittance  $Y$  falls dramatically (part c) indicating that the polymer is no longer rigid and the EQCM measurement is not valid. It is probable that the insertion process continues but it cannot be measured by EQCM.

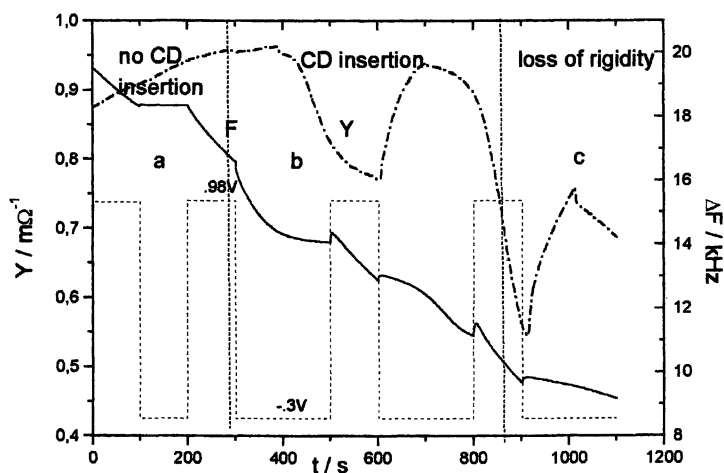


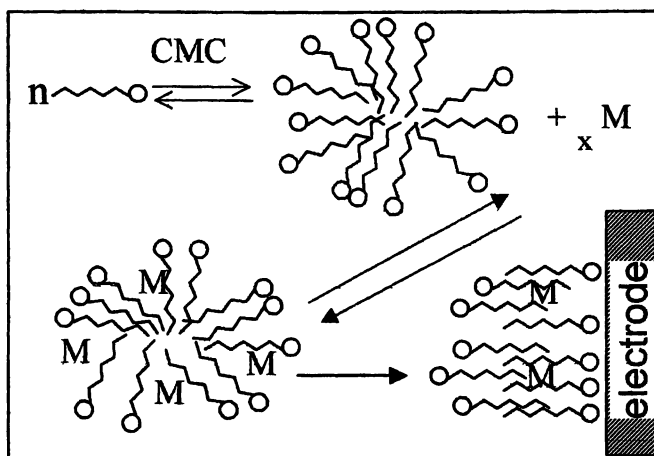
**Figure 2.** Frequency ( $F$ ) and admittance ( $Y$ ) changes observed under double potential steps ( $+0.98\text{ V}$  and  $-0.3\text{ V}$ ). a) no insertion in thin polymer layer, b) large insertion in moderately thick polymer, c) no insertion measured. (Reprinted from *J. Electroanal. Chem.*, 476, Lagrost, Tanguy, Aeiyaeh, Lacroix, Jouini, Chane-Ching, and Lacaze, "Polymer chain encapsulation followed by a quartz crystal microbalance during electropolymerization of bithiophene- $\beta$ -cyclodextrin hot-guest compounds in aqueous solution," pp. 1-14, Copyright 1999 with permission from Elsevier Science).



In fact, highly hydrophobic PBT chains have no affinity for the external hydrophilic HP $\beta$ CD surface. On the contrary, because of their affinity for the hydrophobic internal HP $\beta$ CD surface, the reduced PBT chains could be threaded into these molecules. The reduction process introduces a conformation change that would favor the entrance of HP $\beta$ CD molecules in the polymer. Obviously, in a thin and compact polymer layer, this reorganization is not sufficient to allow the insertion of HP $\beta$ CD molecules. In a thicker polymer layer the chains are less compact, allowing a change in conformation in order to become organized more or less perpendicularly to the surface, allowing the HP $\beta$ CD to diffuse along the polymer chains. Because of the loss of polymer rigidity during high HP $\beta$ CD inclusion, the EQCM technique (18) does not allow measurement of the insertion of more than one HP $\beta$ CD for ten BT units in the polymer, but the insertion level could be much higher. As stated above, from hydrophilic-hydrophobic considerations we propose that in the polymer layers the CD partially encapsulates the PBT chains.

### Electropolymerization of Thiophene Derivatives in Micellar Solutions

This approach is based on the use of the unique physical properties of surfactant molecules in aqueous solutions, which makes it possible to electropolymerize thiophene derivatives and to study the influence of micelles on the electropolymerization process and on the structures and properties of the resulting polymer films.



*Scheme 2. Surfactant monomer (M) – electrode interactions.*

The properties of surfactant molecules are (i) their ability to form different aggregate structures (micelles) above the critical micellar concentration (CMC), (ii) their ability to solubilize water-insoluble organic molecules (M) by hydrophobic-hydrophobic interactions, and (iii) their adsorption on electrodes changes the solution-metal interface, which alters redox reactions and produces template effects on the electrode surface (19) (Schem 2). SDS can be used to electropolymerize various thiophene derivatives such as EDOT, BT and MOT in aqueous solution.

### *Electropolymerization of Thiophene Derivatives in SDS Micelles*

The electrochemical behavior of  $10^{-3}$  M EDOT,  $10^{-3}$  M BT and  $10^{-3}$  M MOT in 0.1 M SDS and 0.1 M  $\text{LiClO}_4$  aqueous solutions cyclic voltammetry (CV) has been investigated by cyclic voltammetry (CV). The oxidation potentials of these monomers are shifted towards more negative potentials by about 130 to 200 mV, relative to the organic media (8, 20-21). This potential lowering is probably due to a better solvation of the resulting radical-cations with SDS.

The electropolymerization of these monomers in the above solution by CV or at constant current leads to the formation of thin, electroactive and homogeneous polymer films at Pt electrodes. For example, the successive CV of MOT in SDS micellar aqueous solutions is typical of conducting polymer growing on the electrode; each scan is performed between 0 and 1.3 V/SCE (Figure 3). The thickness increases regularly with the number of cycles. The resulting poly(MOT) films have well-defined redox peaks during the doping and undoping processes, indicating that they have a good electroactivity in aqueous solution (Figure 3). Similar results have been found for the electropolymerization of EDOT and BT in SDS micellar media.

The electropolymerization of these monomers at constant current under the same micellar conditions led to the formation of thin, electroactive polymer films. The electropolymerization of 0.05 M EDOT in 0.1 M SDS containing 0.1M  $\text{LiClO}_4$  in water at a Pt electrode began at very low current ( $j = 0.1 \text{ mA/cm}^2$ ), compared to that found in acetonitrile without SDS ( $j = 0.5 \text{ mA/cm}^2$ ). This phenomenon may be attributed to a specific effect of the SDS surfactant, which alters the oxidation potentials of EDOT. Thin, electroactive and conductive poly(EDOT) films can be synthesized in the above aqueous micellar solution at constant currents ranging from  $j = 0.1 \text{ mA/cm}^2$  to  $j = 5 \text{ mA/cm}^2$ . For  $j > 5 \text{ mA/cm}^2$ , the resulting poly(EDOT) films were non-electroactive and extremely degraded owing to the reaction between water molecules and the thieryl radical-cations formed (8).

### *Polythiophene Derivatives Structures*

All the polymer films resulting from SDS micelles were characterized by different spectroscopic techniques. UV-Vis analysis of poly(EDOT), PBT and Poly(MOT) films (0.5  $\mu\text{m}$  thickness) at ITO electrodes showed a strong absorption maximum band at  $\lambda_{\text{max}} = 590, 470$  and  $480 \text{ nm}$ , respectively,

**American Chemical Society  
Library**

1155 16th St. N.W.

In Conducting Polymers and Polymer Electrolytes; Rubinson, J., et al.; ACS Symposium Series 800; American Chemical Society: Washington, DC, 2002.

Washington, D.C. 20036

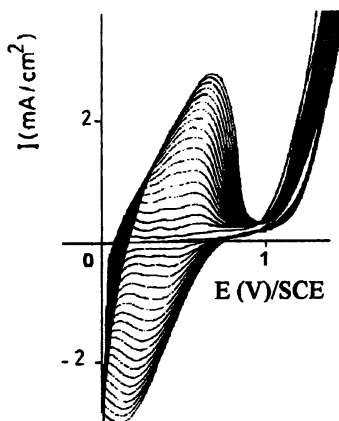


Figure 3. Electro-synthesis of Poly (MOT) at Pt electrode in aqueous micellar solution of 0.1 M SDS, 0.05 M MOT and 0.1 M LiClO<sub>4</sub> with butanol (4 vol. %).  $V = 100 \text{ mV s}^{-1}$

characteristic of a  $\pi - \pi^*$  electronic transition, which corresponds to highly conjugated polymer chains.

The analysis of these films by FTIR and Raman spectroscopies indicates that the polymer chains are formed mainly by  $\alpha$ - $\alpha'$  coupling of the corresponding monomers. This structure was supported by the presence of (i) two bands at 801 and 716  $\text{cm}^{-1}$  in poly(MOT) film corresponding to 2,5-disubstituted and 2-substituted 3-MOT, respectively, (ii) two bands at 789 and 701  $\text{cm}^{-1}$  in PBT films related to 2,5-disubstituted and 2-substituted thiophene, respectively, and (iii) two bands at 1220 and 891  $\text{cm}^{-1}$  in PEDOT films spectra characteristic of EDOT with  $\alpha$ - $\alpha'$  coupling (8, 20-21).

Resonance Raman spectra of PEDOT films ( $\lambda_{\text{ex}} = 514 \text{ nm}$ ) show that the polymer chains present a highly planar structure. The Raman peaks at 1127 and 1100  $\text{cm}^{-1}$ , related to distorted C-C inter-ring bonds, are weak and no bands appear at 682 and 655  $\text{cm}^{-1}$  related to defects in the polymer chains (8- 21).

The structure of PEDOT films was investigated by atomic force microscopy (AFM). AFM images of PEDOT films synthesized on graphite electrodes (HOPG) in SDS micelles show that the polymer film chains grew perpendicularly to the electrode surface, whereas PEDOT prepared in acetonitrile at the same electrochemical conditions grows parallel to the electrode surface (Figure 4). These observations provided from the electropolymerization mechanism of EDOT in SDS micelles; the polymer chains would be located parallel to surfactant chains, and thereby would grow perpendicularly to the electrode surface, leading to the hypothetical "columnar" structure (Figure 4). But this growth mode differs significantly from that observed in acetonitrile, in which polymer chains are probably located on the electrode surface, leading to a "plate" structure (Figure 4). Moreover, the incorporation of about 21% of dodecyl sulfate anions in PEDOT (estimated by XPS) supports the structure proposed for film synthesized in SDS micelles (8).

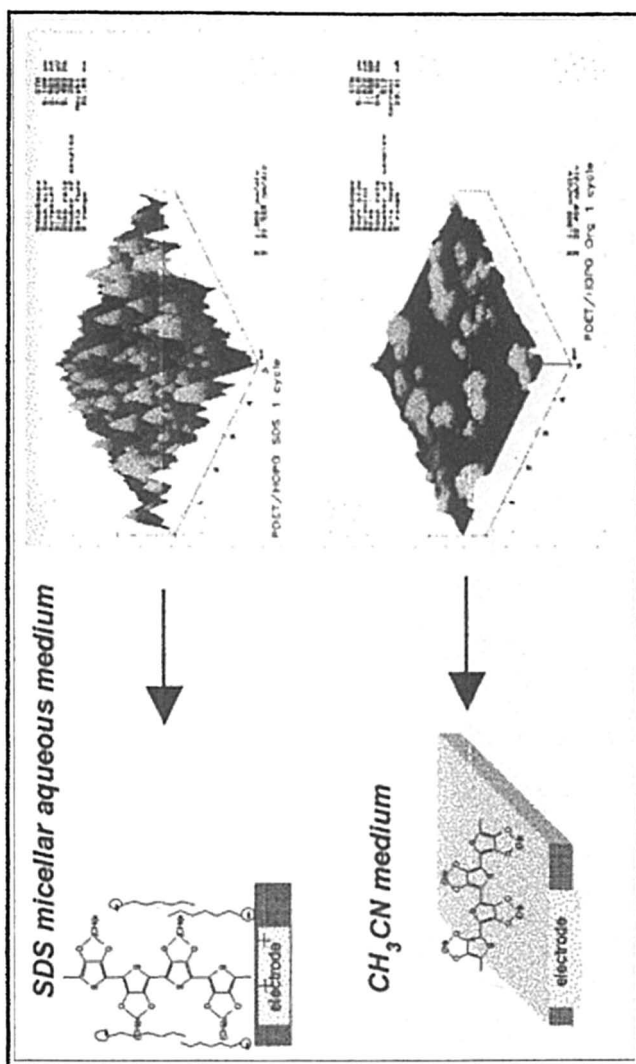
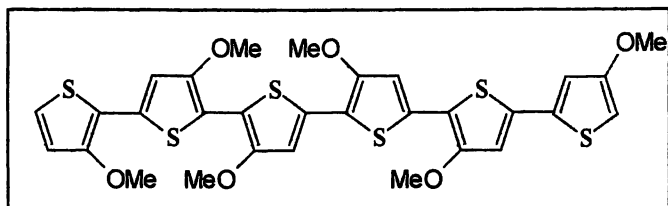


Figure 4. AFM images of PEDOT films electrosynthesized in SDS micelles (top) and in acetonitrile solution (bottom). Hypothetical proposed structures of these films (left)

The chain length of poly(MOT) films was determined by MALDI-TOF spectroscopy, because these polymers are soluble in usual organic solvents. They consist mainly of MOT hexamer (Scheme 3).



Scheme 3. Poly (MOT) structures prepared in SDS micelles.

## Conclusions

This work demonstrates new possibilities for the electropolymerization of thiophene derivatives and electrosynthesis of polythiophene derivative films in aqueous solution by using either CDs or SDS.

The interaction between CDs and thiophene derivatives such as BT and 3T increases their solubilities in water owing to the formation of inclusion complexes. CDs (hosts)-thiophene derivatives (guests) are stable inclusion complexes with high binding constants. The electropolymerization of BT-CD inclusion complex leads to: (i) the formation of PBT films with a high degree of polymerization and a high chain conjugation length and (ii) the formation of PBT molecular wire, which is partially encapsulated with CDs (polypseudorotaxane). However 3T-CD electropolymerization gives non-encapsulated polymer films, which consist of thiophene hexamer.

In SDS micelles, we show, that: (i) the solubility of thiophene derivatives in water increases, (ii) their oxidation potentials are lower than those found in organic media, (iii) the thienyl radical-cations formed are stabilized by electrostatic interactions with the dodecyl anions, (iv) the synthesis of thin, electroactive and conductive polymers films having well-defined structures (practically no defects) with a relatively high conjugation chain length has been realized. In addition, the resulting PEDOT films have a "columnar" structure.

## References

1. *Handbook of Conducting Polymers*; Skotheim, T.A., Ed., Marcel Dekker, New York, 1986; vol. 1 and 2.
2. *Handbook of Organic Conductive Molecules and Polymers*; Nalwa H.S., Ed., John Wiley & Sons, New York, 1997; vol. 2.

3. Roncali, J. *Chem. Rev.* **1997**, *97*, 173-205 and refs. Therein.
4. Bazzaoui, E.A.; Aeiyaeh, S.; Lacaze, P.C. *J. Electroanal. Chem.* **1994**, *364*, 63-69.
5. *Polymerization in organized media*; Paleos, C. M., Ed. Gordon and Breach Science Publishers: Philadelphia, PA, 1992.
6. Tamil Selvan, S.; Mani, A.; Pitchumani, S.; Phani, K.L.N. *J. Electroanal. Chem.* **1995**, *384*, 183-86.
7. Naol, K.; Oura, Y.; Maeda, M.; Nakamura, S. *J. Electrochem. Soc.* **1995**, *142*, 417-422.
8. Sakmeche, N.; Aeiyaeh, S.; Aaron, J.J.; Jouini, M.; Lacroix, J.C.; Lacaze, P.C. *Langmuir* **1999**, *15*, 2566-74.
9. Lagrost, C.; Lacroix, J.C.; Aeiyaeh, S.; Jouini, M.; Chane-Ching, K.I.; Lacaze, P.C., *Chem Commun.* **1998**, 489-90..
10. Lagrost, C.; Chane-Ching, K.I.; Lacroix, J.C.; Aeiyaeh, S.; Jouini, M.; Lacaze, P.C.; Tanguy, J., *J. Mater. Chem* **1999**, *9*, 2351-2358.
11. Lagrost, C.; Lacroix, J.C.; Aeiyaeh, S.; Chane-Ching, K.I.; Jouini, M.; Lacaze, P.C., *Adv. Mater. Chem.* **1999**, *11*, 664-667.
12. Szelti, J. *Cyclodextrins and Their Inclusion Complexes*; Akadematici Kiado: Budapest, Hungary, 1982.
13. Kaifer, A.E. *Acc. Chem. Res.* **1999**, *32*, 62-71.
14. Shen, X.; Belletête, M.; Durocher, G. *Chem. Phys. Lett.* **1998**, *298*, 201-10
15. Furukawa, Y.; Akimoto, M.A.; Harada, I. *Synth. Met.* **1987**, *18*, 151-156
16. Hoeve, W.ten; Wynberg, H.; Havinga, E.E.; Meijer, E.W. *J. Am. Chem. Soc.* **1991**, *113*, 5887-5889.
17. Xu, Z.G.; Horowitz, G. *J. Electroanal. Chem.* **1992**, *335*, 123-134.
18. Lagrost, C.; Tanguy, J.; Aeiyaeh, S.; Lacroix, J.C.; Jouini, M.; Chane-Ching, K.I.; Lacaze, P.C. *J. Electroanal. Chem.* **1999**, *476*, 1-14.
19. Rusling, J.F in *Electroanalytical Chemistry*; Bard, A.J Ed.; Marcel Dekker, New York, 1994; vol. 18, pp1-88
20. Bazzaoui, E.A.; Aeiyaeh, S.; Lacaze, P.C. . *Synth. Met.*, **1996**, *83*, 159-165
21. Fall, M.; Aaron, J.J; Sakmeche, N.; Aeiyaeh, S.; Dieng, M.M.; Jouini, M.; Lacroix, J.C.; Lacaze, P.C. *Synth. Met.* **1996**, *93*, 175-197.

## Chapter 4

# Electrochemical Behavior of Polyaniline and Polythiophene Derivatives in Various Electrolytes

Eric Naudin<sup>1</sup>, Hoang Anh Ho<sup>2</sup>, Livain Breau<sup>2</sup>,  
and Daniel Bélanger<sup>1</sup>

<sup>1</sup>Département de Chimie, Université du Québec à Montréal, Case Postale 8888, Succursale Centre-Ville, Montréal. Québec H3C 3P8, Canada

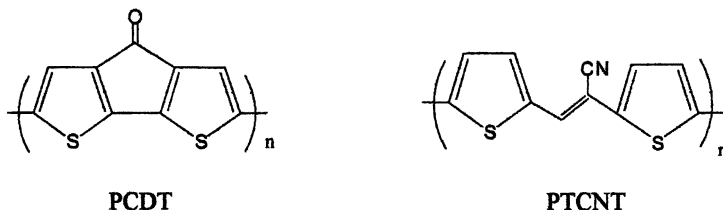
<sup>2</sup>Laboratoire de Synthèse Organique Appliquée, Département de Chimie, Université du Québec à Montréal, Case Postale 8888, Succursale Centre-Ville, Montréal. Québec H3C 3P8, Canada

The electrochemical behavior of three conducting polymers was investigated in the presence of various electrolytes, including an ionic liquid dissolved in acetonitrile, and the data indicated no significant difference in the initial cyclic voltammograms. The polymers investigated were polyaniline (PANI), poly(cyclopenta[2,1-b; 3,4-b']dithiophene -4-one) (PCDT) and poly-E- $\alpha$ -[(2-thienyl)methylene]-2-(3-methylthiophene) acetonitrile (PTCNT) electrochemically grown on a platinum electrode. The electrolytes were tetraethylammonium tetrafluoroborate (Et<sub>4</sub>NBF<sub>4</sub>), tetraethylammonium bis((trifluoromethyl)sulfonyl)imide (Et<sub>4</sub>NTFSI) and 1-ethyl-3-methylimidazolium bis((trifluoromethyl)sulfonyl) imide (EMITFSI) dissolved in acetonitrile.

## Introduction

Electronically conducting polymers have been extensively investigated due principally to their potential applications in energy storage systems such as rechargeable batteries and electrochemical supercapacitors, electrochromic devices, organic transistors and light-emitting diodes [1]. The performance of conducting polymers for these applications is dictated by a combination of a number of factors such as polymer morphology, substrate onto which the polymer is grown and the supporting electrolyte used for electrodeposition and during the galvanostatic cycling or cyclic voltammetry.

Our laboratory has been interested for the past few years, in application of conducting polymers as active electrode materials of electrochemical capacitors [2-5]. Most of our efforts so far have been devoted to the evaluation of several polymers but little attention has been paid to the electrolytes. In this study, we investigated the cyclic voltammetry behavior of three polymers; i) polyaniline (PANI); ii) poly(cyclopenta[2,1-b; 3,4-b']dithiophene-4-one) (PCDT) and iii) poly-E- $\alpha$ -[(2-thienyl)methylene]-2-(3-methylthiophene)acetonitrile (PTCNT) in the presence of various electrolytes. These electrolytes included tetraethylammonium tetrafluoroborate ( $\text{Et}_4\text{NBF}_4$ ), tetraethylammonium bis((trifluoromethyl)sulfonyl)imide ( $\text{Et}_4\text{NTFSI}$ ) and 1-ethyl-3-methylimidazolium bis((trifluoromethyl)sulfonyl)imide (EMITFSI) dissolved in acetonitrile. The structures of PCDT and PTCNT are given in Scheme 1.



Scheme 1. Structure of the low bandgap polymers investigated in this study.

## Experimental

A polyaniline film was deposited by electrochemical oxidation of aniline in aqueous acid solution on working electrode under an electric current of 5  $\text{mA}/\text{cm}^2$ . The electrolyte solution contained 1 M hydrofluoroboric acid and 0.5 M aniline. This film was immersed in 1 M hydrazine hydrochloride for 24 h and then dipped in an aqueous solution containing 30% w/v hydrazine for 48 h. The film was washed with acetonitrile and dried under vacuum at 80°C during 24 h [6]. PCDT films were grown from a solution containing 20 mM of CDT and 0.5 M of  $\text{Et}_4\text{NBF}_4/\text{ACN}$  and the electropolymerization was performed galvanostatically at a current density of 0.5  $\text{mA}/\text{cm}^2$  [2]. PTCNT films were



deposited galvanostatically at a current density of 0.1 mA/cm<sup>2</sup> and the electrolyte solution contained 20 mM of monomer TCNT and 0.5 M of Et<sub>4</sub>NBF<sub>4</sub>/ACN [4].

All measurements were performed in a glove box under a dry nitrogen atmosphere, in a closed three-electrode cell. The electrochemistry experiments were carried out with a PAR 263A potentiostat-galvanostat coupled to a PC with the Corrware Software for Windows (Scribner Associates, version 2.1b). The working electrode consisted in a platinum disk (diam. = 1 mm) sealed inside a glass tube or epoxy. Prior to any measurements, the platinum disk electrode was polished with a diamond polishing paste to the 1 μm level with aqueous alumina slurry (Techmet, Canada). The reference electrode was Ag/Ag<sup>+</sup> (10 mM AgNO<sub>3</sub>, 0.1 M tetrabutylammonium perchlorate in acetonitrile) and the counter electrode was a platinum grid (area = 1 cm<sup>2</sup>).

## Results and Discussion

The electrochemical behavior of polyaniline (PANI), poly(cyclopenta[2,1-b; 3,4-b']dithiophene-4-one) (PCDT) and poly-E-α-[(2-thienyl)methylene]-2-(3-methylthiophene) acetonitrile (PTCNT) was investigated in three different supporting electrolytes; tetraethylammonium tetrafluoroborate (Et<sub>4</sub>NBF<sub>4</sub>), tetraethylammonium bis((trifluoromethyl)sulfonyl)imide (Et<sub>4</sub>NTFSI) and 1-ethyl-3-methylimidazolium bis((trifluoromethyl)sulfonyl)imide (EMITFSI) dissolved in acetonitrile. The polymers were grown electrochemically (see EXPERIMENTAL) and initially characterized in 0.5 M Et<sub>4</sub>NBF<sub>4</sub>/acetonitrile to insure the uniformity of the films being investigated.

Figures 1-3 present the cyclic voltammograms (CV's) of PANI, PCDT and PTCNT, respectively, together with the doping levels for the n- and p-doping (x<sub>n</sub> and x<sub>p</sub>) processes in 0.5 M Et<sub>4</sub>NBF<sub>4</sub>/acetonitrile, 0.5 M Et<sub>4</sub>NTFSI/acetonitrile and 0.5 M EMITFSI/acetonitrile at a scan rate of 100 mV/s. The doping level for PANI was evaluated from [3]:

$$x = 2Q_{CV} / (Q_{dep} - Q_{CV}) \quad (1)$$

where Q<sub>CV</sub> is the voltammetric charge of the CV and Q<sub>dep</sub> is the charge consumed during the electrochemical polymerization. In the case of PCDT and PTCNT, which have two thiophene rings in their corresponding monomer, the doping level is calculated from [2,4]:

$$x = Q_{CV} / (Q_{dep} - Q_{CV}) \quad (2)$$

The CV's for PANI are characterized by at least one set of major waves for the three supporting electrolytes. The onset of oxidation is almost independent of the nature of the supporting electrolyte but some differences are observed for the oxidation waves. Indeed, one anodic peak appears at about -0.07 V in  $\text{Et}_4\text{NBF}_4$ , whereas two anodic peaks can be seen at -0.12 to 0.1 V in  $\text{Et}_4\text{NTFSI}$  and -0.1 to 0.05 V in EMITFSI. These peaks correspond to the oxidation of the fully reduced to the semiquinone form of PANI. On the other hand, previous studies have clearly demonstrated that the shape and the range of electroactivity of PANI in organic media can differ significantly [7-11]. Thus CV's like those shown in Figure 1 are observed when the positive potential limit is set at a low value of about 0.6-0.8 V whereas a second wave followed by a significant

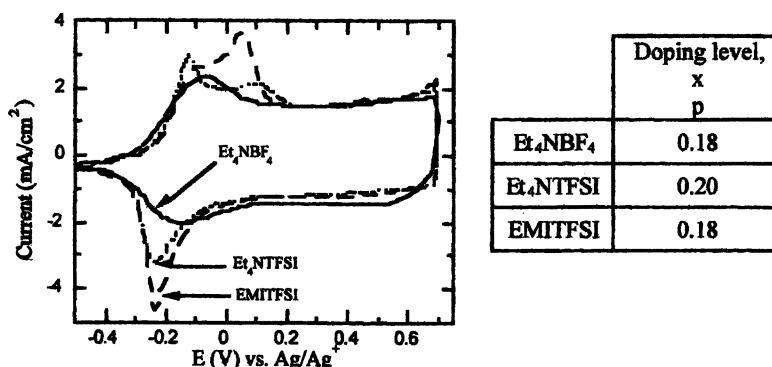


Figure 1. Cyclic voltammograms of PANI in the three supporting electrolytes with acetonitrile as solvent at a scan rate of 100 mV/s. The doping levels are also given.

decrease of current is seen when the potential limit is extended to about 1 V. The latter situation is usually avoided in order to limit the oxidative degradation of the polymer. The ratio of the anodic,  $Q_{\text{ox}(p)}$  and cathodic  $Q_{\text{red}(p)}$  voltammetric charges for the p-doping process for the polyaniline is close to 1 ( $> 0.9$ ) indicating a good reversibility for the redox process during potential cycling in the three supporting electrolytes. Moreover, doping levels of 0.18 to 0.20 are evaluated for assuming a polymerization efficiency of 100 %. These doping levels values are smaller than that usually found for PANI ( $\approx 0.4$ -0.5). This could be due to polymerization efficiency lower than 100% as evidenced by the formation of highly colored oligomers and to some loss of electroactivity of PANI as a result of the dehydration treatment of PANI following the electropolymerization in aqueous anodic media (see Experimental). Presumably, both phenomena contribute to the low doping level but the former is probably the most important since higher doping levels were obtained for

PANI grown on carbon paper [12]. In this case, a higher local concentration of cation radical can be generated within the porous carbon paper electrode, thus leading to a higher voltammetric charge and higher apparent doping level.

The cyclic voltammograms for a PCDT-coated platinum electrode in the same electrolytes are shown in Figure 2 and are characterized by two sets of redox waves. The redox waves between 0 and 1.1 V are associated with the p-doping process and the n-doping redox waves are centered at -1.4 V. The p- and n-doping redox waves are almost identical for the three supporting electrolytes. The shape of these CV's is similar to that reported by Lambert and Ferraris [13, 14] and Fusalba *et al.* [2]. The voltammetric charges for the anodic,  $Q_{\text{ox}(p)}$  and cathodic  $Q_{\text{red}(p)}$  branches of the p-doping wave and the cathodic  $Q_{\text{red}(n)}$  and for anodic  $Q_{\text{ox}(n)}$  branches of the n-doping process for PCDT

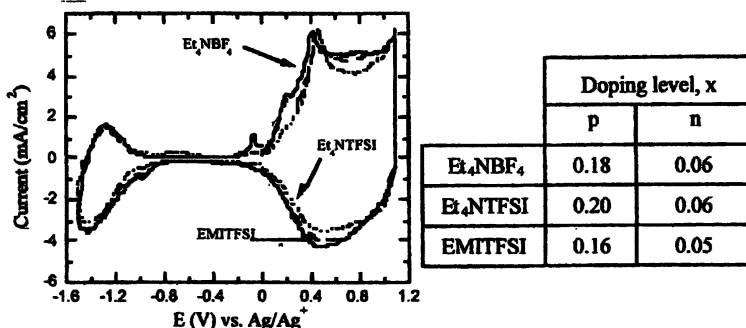


Figure 2. Cyclic voltammograms of PCDT in the three supporting electrolytes with acetonitrile as solvent at a scan rate of 100 mV/s. The p- and n-doping levels are also given.

were evaluated and we found that the ratio of doping-dedoping charge ( $Q_{\text{ox}(p)}/Q_{\text{red}(p)}$  and  $Q_{\text{red}(n)}/Q_{\text{ox}(n)}$ ) is always less than unity and average values of about 0.94 and 0.83 can be calculated for the p- and n-doping, respectively. The n-doping level (0.05 to 0.06) is clearly smaller than the p-doping level (0.16 to 0.20). This difference is attributed to a slower ionic transport in the n-doped polymer resulting from a stronger interaction of negative polarons of the polymer with the cations ( $\text{Et}_4\text{N}^+$  and  $\text{EMI}^+$ ) in comparison with that of anions ( $\text{BF}_4^-$  and  $(\text{CF}_3\text{SO}_2)_2\text{N}^-$ ) in the p-doped polymer. It is interesting to note that a higher n-doping level can be achieved for PCDT grown on carbon paper [2].

The cyclic voltammograms of PTCNT-coated platinum electrode, in the three supporting electrolytes, shown in Figure 3 are characterized by two sets of redox

waves centered at 0.75 and -1.5 V and in agreement with a previous report [4]. The first is associated with the p-doping process and the second corresponds to the n-doping process. The p-doping redox process is well defined in comparison to the irreversible n-doping process. In addition, the doping/dedoping charge ratios are much smaller ( $< 0.5$ ) than for PANI and PCDT. The doping levels for PTCNT are fairly low in comparison to those usually found for polythiophene [15, 16]. Similarly to PCDT, the n-doping level is significantly lower than the p-doping level. In addition, both doping levels are smaller than these reported for PTCNT grown on carbon paper electrode [4]. The reasons invoked for PCDT can be used for PTCNT as well to explain these differences. It is also worth noting that in a recent study, doping levels of 0.28 (instead of about 0.10) were found for chemically grown PTCNT electrodes, and these were unambiguously evaluated by weighing the mass of polymer used for the fabrication of the electrodes [17]. Finally, Figure 3 also demonstrates that PTCNT can be cycled over a potential window of about 2.8 V.

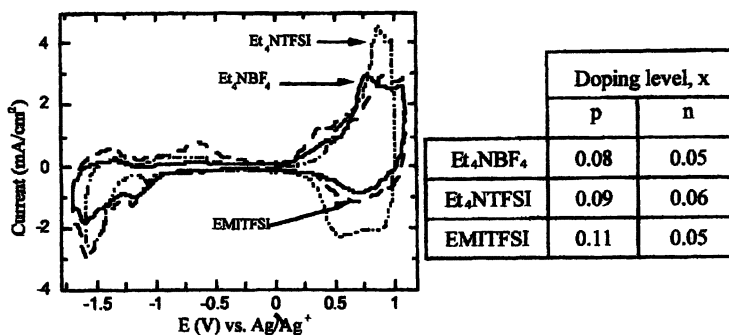


Figure 3. Cyclic voltammograms of PTCNT in the three supporting electrolytes with acetonitrile as solvent at a scan rate of 100 mV/s. The p- and n-doping levels are also given.

### Conclusion

The preliminary results presented here demonstrated that the electrochemical behavior of PANI, PCDT and PTCNT is not significantly influenced by the nature of the cationic and anionic species of the electrolyte. This might appear surprising at first sight since the size of these species differ considerably [18]. Typically, larger ions should hinder somehow the redox processes. On the other

hand, we have shown elsewhere that these polymers lost their charge capacity at a much faster rate in the presence of EMITFSI/acetonitrile than with the two other electrolytes [12]. Obviously, more work is needed in order to fully understand the behavior of conducting polymers in ionic liquid/acetonitrile media.

### Acknowledgments

This research was funded by the Natural Science and Engineering Research Council of Canada through a Strategic grant (to D. B. and L. B.). E. N. also wishes to acknowledge UQAM for a fellowship.

### References

1. *Handbook of Conducting Polymers*; Skotheim, T.; Elsembaumer, L.; Reynolds, J.R. 2<sup>nd</sup> Eds.; Marcel Dekker: New York, 1998.
2. Fusalba, F.; El Mehdi, N.; Breau, L.; Bélanger, D. *Chem. Mater.* **1999**, *11*, 2743.
3. Fusalba, F.; Bélanger, D., *J. Phys. Chem. B* **1999**, *103*, 9044.
4. Fusalba, F.; Ho, H.A.; Breau, L.; Bélanger, D. *Chem. Mater.* **2000**, *12*, 2581.
5. Fusalba, F.; Gouérec, P.; Villers, D.; Bélanger, D. *J. Electrochem. Soc.* **2000**, *148*, A1.
6. Villers, D.; Bélanger, D. work in progress.
7. Kanamura, K.; Kawai, Y.; Yonezawa, S.; Takehara, Z.-i. *J. Electrochem. Soc.* **1995**, *142*, 2894.
8. Yamada, K.; Teshima, K.; Kobayashi, N.; Hirohashi, R. *J. Electroanal. Chem.* **1995**, *394*, 71.
9. Yonezawa, S.; Kanamura, K.; Takehara, Z.-i. *J. Electrochem. Soc.* **1995**, *142*, 3309.
10. Garcia, B.; Fusalba, F.; Bélanger, D. *Can. J. Chem.* **1997**, *75*, 1536
11. Naudin, E.; Gouérec, P.; Bélanger, D. *J. Electroanal. Chem.* **1998**, *459*, 1.
12. Naudin, E.; Ho, H.A.; Breau, L.; Bélanger, D. *J. Electroanal. Chem.* submitted.
13. Lambert, T.L.; Ferraris, J.P. *J. Chem. Soc., Chem. Commun.* **1991**, 752.
14. Ferraris, J.P.; Lambert, T.L. *J. Chem. Soc., Chem. Commun.* **1991**, 1268.
15. Ferraris, J.P.; Eissa, M.M.; Brotherton, I.D.; Loveday, D. *Chem. Mater.* **1998**, *10*, 3528.
16. Sarker, H.; Gofer, Y.; Killiam, J.G.; Poehler, T.O.; Searson, P.C. *Synth. Met.* **1999**, *88*, 179.
17. Soudan, P.; Ho, H.A.; Breau, L.; Bélanger, D. *J. Electrochem. Soc.* in revision.
18. Mc Ewen, A.B.; Ngo, H.L.; Le Compte, K.; Goldman, J.L. *J. Electrochem. Soc.* **1999**, *146*, 1687.

## Chapter 5

# Electrochemical Quartz Crystal Microbalance Studies of the Growth of Perylene-Containing Films

V. Cammarata, N. Hao, J. Metz, and J. Liang

Department of Chemistry, Auburn University, Auburn, AL 36849-5312

Materials containing 3,4,9,10-perylene tetracarboxylic dianhydride and diimide have important photophysical properties such as high photoconductivity. These materials, in general, are insoluble and very difficult to process by conventional solution methods. We report the electrochemical synthesis and properties of poly(aromatic amine-imide) polymers containing the 3,4,9,10-perylene tetracarboxylic diimide group in the main chain. Using electrochemical quartz crystal microbalance (EQCM) measurements, we correlate the electrochemical growth of polymer films on surfaces with various solution parameters. Specifically we address the relative rates of precipitation versus dimerization in film formation and the efficiencies of these processes. We also show the effect of electrolytes and solvent on film processes.

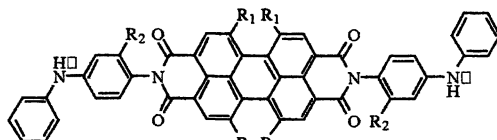
There are few reports of polymers synthesized with perylene tetracarboxylic diimide groups. Monomer materials containing this group have been used as photoconductors in xerographic materials (1), fluorescent solar collectors (2,3), and laser dyes (4-6). These applications are made possible by the photophysical properties of perylene tetracarboxylic diimide moiety, most importantly the high

quantum yield of the fluorescence, the fast electron transfer quenching and fast charge conduction in solutions and thin films made from these small molecules (7-9). Thin films have been synthesized primarily via vapor phase evaporation (10,11). Polymers containing the perylene tetracarboxylic diimide moiety have suffered from poor solubility. The intractability of these materials is a result of their strong intermolecular interactions. The formation of H-aggregates limits the maximum solubility of many of the monomeric materials to sub micromolar concentrations. In sublimed thin films of perylenetetracarboxylic dianhydride, the aromatic carbons are 3.21 Å apart (12). This aggregation promotes the delocalization of the molecular orbitals and significantly changes the electronic structure of the material (13). One strategy to increase solubility has been to form polymers with a rather diluted perylene component separated by a large aliphatic chain (14). Another strategy is to add bulky groups directly to the aromatic ring using steric bulk to prevent aggregation. Mullen and others successfully replaced the chlorines on 1,6,7,12-tetrachloroperylene tetracarboxylic dianhydride with aromatic ether groups effectively holding the two ring systems apart (15,16). Other substitutions to the perylene ring system afford more soluble materials.

Electrodeposition of polymers has been successfully used in many materials. However, the elucidation of the mechanism for many of these processes has been hampered by the lack of direct tools for measuring *in situ* the solid material produced at the electrode surface. A direct *in situ* tool for measuring the mass of the electrodeposit is the electrochemical quartz crystal microbalance (EQCM). This technique was originally described by Sauerbrey (17). Several good reviews exist on EQCM (18,19). For example, Inzelt has determined the complex ion transport properties during the doping and undoping of poly(pyrrole)(20). In another study, the difference between polymerizing poly(pyrrole) at a surface modified electrode as compared to a bare Au electrode was elucidated using EQCM (21). Our goal is to more thoroughly understand the growth mechanism of films that cannot be analyzed with conventional methods.

In previous work, we synthesized diimide and diamide monomers with diphenylamine endgroups (22-24). We showed, upon oxidation, these endgroups would dimerize to form diphenylbenzidine linkages. The materials formed were alternating copolymers of the diphenylbenzidine and either a diimide or diamide group. Diimides in particular can be reduced in two  $1e^-$  steps (25-28). Mazur and others found that when the two imides are attached to the same benzene ring the second  $e^-$  is transferred at a more negative potential, then if the imides are separated by a naphthalene ring (25). Depending on the intervening ring system, the first diimide reduction can be water stable and form extended  $\pi$ - $\pi$  n-mers of the radical anion (28). Diimide containing monomers, upon oxidation, can have both electron and hole transport properties resulting from the two different comonomer units (22-24). Here, we explored the electrosynthesis of materials where the monomers are insoluble in common

electrochemical solvents which necessitated the use of uncommon solvent systems. We have synthesized, characterized and electropolymerized monomers 1-4. The different monomers were soluble in different solvent systems so we



- 1-  $R_1 = R_2 = H$ , 2-  $R_1 = Cl$ ,  $R_2 = H$ , 3-  $R_1 = tBuPhO-$ ,  $R_2 = H$ ,  
4-  $R_1 = H$ ,  $R_2 = -CO_2Me$

employed EQCM to determine the initial deposition species in different electrolytes. By comparing the mass changes in films during various redox processes, we explored the relative contributions of counterions and solvent to these processes. We also show the relative kinetics of ion and solvent incorporation and expulsion in these materials.

## Experimental

### *Reagents, materials and apparatus*

$CH_2Cl_2$  and aniline were obtained from Fischer Scientific Co. and distilled from  $CaH_2$  (Aldrich Chemical Co.). 3,4,9,10-perylenetetracarboxylic dianhydride, 2-chloro-5-nitrobenzoic acid, sodium borohydride, copper (II) acetylacetonate, trifluoroacetic acid (TFA), tetrabutylammonium hexafluorophosphate (TBAPF<sub>6</sub>), dimethylacetamide (DMA), and N-phenyl-1,4-phenylenediamine were purchased from Aldrich Chemical Co. and used as received. Quinoline and triethylamine (TEA) (Aldrich Chemical Co.) were distilled in vacuo. IR spectra were obtained on a Bruker Equinox 55 Spectrometer. <sup>1</sup>H NMR spectra were obtained on a Bruker 250 multiprobe spectrometer. Elemental analyses were performed by Atlantic Microlabs. Mass spectrometry data were provided by the Auburn Mass Spectrometry Laboratory.

### *Synthesis of 1 (29)*

To 100 mL of quinoline were added 2.08 mmol (0.814 g) of perylenetetracarboxylic dianhydride, 4.67 mmol (0.859 g) of N-phenyl-1,4-phenylenediamine, and 0.635 mmol (0.139 g) of zinc acetate dihydrate. The solution was degassed with  $N_2$ , fitted with a reflux condenser and heated on an oil bath held at 230 °C for 22 hrs. The product was filtered and washed with 4 X



50 mL diethylether. It was then washed with 4 X 50 mL water and 4 X 50 mL diethylether. The product after drying *in vacuo* was dark red. Yield = 0.92 g (61%). Mass Spec. (EI)  $M^+$  = 725.  $^1\text{H-NMR}$  (TFA): 8.00 (m, 18H), 9.14 (s, 8H). IR (KBr,  $\text{cm}^{-1}$ ): 3374, 1701, 1663, 1594, 1577, 1516, 1496, 1432, 1403, 1359, 1320, 1255, 1177, 1123, 810, 746, 695. Elemental analysis: calculated (found) for  $\text{C}_{48}\text{H}_{28}\text{N}_4\text{O}_4$ : C, 79.55(77.58); H, 3.89(4.05); N, 7.73(7.47).

### Synthesis of 2

To 20 mL DMA were added 276 mg (1.5 mmol) N-phenyl-1,4-phenylenediamine and 265 mg (0.5 mmol) 1,6,7,12-tetrachloro-3,4,9,10-perylene dianhydride (30). The mixture was reacted at 130°C for 18 h under nitrogen with stirring. After cooling to room temperature, 60 mL diethyl ether was added to reaction mixture. The precipitate was filtered and was washed with diethyl ether (4 X 20 mL). After drying at 100°C *in vacuo* overnight, 248 mg black brown product was obtained. Yield = 59%. m.p. > 300°C. IR (KBr,  $\text{cm}^{-1}$ ): 3371, 1705, 1670 1591, 1525, 1384, 1325, 1300, 1242, 1173, 1116, 1025, 833, 789, 749, 687, 550, 524.  $^1\text{H-NMR}$  (TFA):  $\delta$  = 8.81 (s, 4H), 7.60 (m, 18H).

### Synthesis of 3

166 mg (0.9 mmol) N-phenyl-1,4-phenylenediamine, 296 mg (0.3 mmol) 1,6,7,12-tetrakis(4-t-butylphenoxy)-3,4,9,10-perylene dianhydride (15) and 29.6 mg zinc acetate were added to a 200 mL 3-neck flask. The mixture was reacted at 205 °C for 22 h under stirring and  $\text{N}_2$ . The workup was similar to that of 1. After drying at 70°C *in vacuo* overnight, 252 mg product was obtained. Yield = 63%. m.p. > 300°C. IR (KBr,  $\text{cm}^{-1}$ ): 3378, 2960, 1704, 1671, 1593, 1506, 1405, 1339, 1313, 1281, 1208, 1173, 1111, 1014, 878, 832, 749, 693, 557.  $^1\text{H-NMR}$  (TFA):  $\delta$  = 8.57 (s, 4H), 7.30 (m, 34H), 1.60(s, 36H). Elemental analysis: calculated (found) for  $\text{C}_{88}\text{H}_{72}\text{N}_4\text{O}_8$ : C, 79.52(77.84); H, 5.46(5.69); N, 4.22(4.49).

### Methyl 2-anilino-5-aminobenzoate

This material was synthesized using a similar procedure to Hanaya (31). 1 mmol (37.8 mg) sodium borohydride in 2 mL ethanol was added to a suspension of 0.2 mmol (52.4 mg) copper (II) acetylacetonate in 2 mL 2-propanol under  $\text{N}_2$  with stirring. To this solution were added 1.0 mmol (272 mg) methyl 2-anilino-5-nitrobenzoate (32) in 20 mL 2-propanol and then 2.0 mmol (75.7 mg)  $\text{NaBH}_4$  in 4 mL ethanol. The mixture was stirred under  $\text{N}_2$  for 4 h at 30°C. The reaction

was quenched with 25 mL water. 2-propanol and ethanol were removed with reduced pressure. The residue was extracted with chloroform (3 X 20 mL) and the collected chloroform solution was dried with anhydrous  $\text{Na}_2\text{SO}_4$ . After removing the solvent, 225 mg oil-like brown product was obtained and was used in the next step without further purification.

### *Synthesis of 4*

To 20 ml quinoline were added 221 mg (0.91 mmole) methyl 2-anilino-5-aminobenzoate, 119 mg (0.303 mmol) 3,4,9,10-perylenetetracarboxylic dianhydride and 27.7 mg zinc acetate. The mixture reacted at 220°C for 22 h under stirring and  $\text{N}_2$ . After cooling to room temperature, 60 mL diethyl ether was added to precipitate the product. The product was filtered and washed with diethyl ether (4 X 15 mL), water (4 X 15 mL) and diethyl ether (4 X 15 mL). After dried *in vacuo* at 100°C overnight, 231 mg product was obtained. Yield=91%. m.p> 300°C. IR (KBr,  $\text{cm}^{-1}$ ): 3364, 1700, 1664, 1593, 1514, 1355, 1319, 1253, 1076, 808, 748 589.  $^1\text{H-NMR}$  (TFA):  $\delta$  = 8.85 (s, 8H), 7.65 (m, 16H). Elemental analysis: calculated (found) for  $\text{C}_{52}\text{H}_{32}\text{N}_4\text{O}_8$ : C, 74.35(75.05); H, 3.84(3.88); N, 6.67(7.16).

### *Instrumentation*

Cyclic voltammetric experiments were performed on a modified AFRDE4 potentiostat (Pine Instrument Co.) with an EG&G PARC 175 programmer as an external analog signal, and a National Instruments Lab PC+ DAQ board was used to trigger the programmer and simultaneously collect and digitize the data. A series of LabVIEW programs were written for data acquisition, and storage. EQCM experiments were carried out with ELCHEMA EQCN-601 nanobalance instrument, EQCN-603 remote probe unit and EQCN-602 Faraday cage.

### *Electrodes and Cells*

A new 9.995 MHz polished quartz crystal electrode (QCE) (International Crystal Mfg. Co.) with 100 Å Cr and 1000 Å Au was mounted to a homemade 20 mL-volume cell with silicone glue and cured for at least 24 h. Before use, the new mounted cell was rinsed with fresh  $\text{CH}_2\text{Cl}_2$ . The keyhole shaped electrode had an area of 0.22  $\text{cm}^2$ . The solution was degassed with 99.999% Ar for 15 min in a Faraday cage which was purged with  $\text{CH}_2\text{Cl}_2$  saturated  $\text{N}_2$ . The reference electrode was Ag/AgCl saturated with KCl and all potentials are quoted vs. Ag/AgCl. The counter electrode was Pt gauze. Triethylammonium

trifluoroacetate, was synthesized by mixing TEA and TFA in a 1:1 mol:mol, then drying at 70 °C *in vacuo* for 24 h (Caution: this neutralization is very exothermic and can sputter hot material). All EQCM data are presented in  $\Delta_{\text{mass}}$  (change of mass from the beginning of the voltammetry) and are calculated from the frequency changes using the Sauerbrey equation (17).

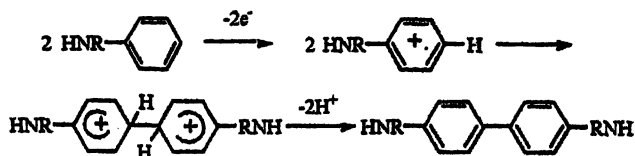
## Results and Discussion

### Synthesis of Monomers

Monomers 1-4 were synthesized via the condensation of 3,4,9,10-perylene-tetracarboxylic dianhydride or a similar derivative and an appropriate aminodiphenylamine using  $\text{Zn}(\text{OAc})_2$  as a Lewis acid catalyst. Each of the final monomer products was characterized using NMR, IR, Mass Spectrometry and elemental analysis. Yields were generally in the 60-90% range. The monomers varied from insoluble to moderately soluble (1 mM maximum solubility) in  $\text{CH}_2\text{Cl}_2$ , 1,2-dichloroethane and THF. In more typical electrochemical solvents such as  $\text{CH}_3\text{CN}$ , DMSO and DMF, all the compounds were insoluble.

### Electrooxidative polymerization of 1 - 4

Monomer 3 was moderately soluble in  $\text{CH}_2\text{Cl}_2$ , 1,2 dichloroethane and THF. Substitution on the perylene ring is expected to provide steric hindrance preventing strong  $\pi$ - $\pi$  interactions in the solid state. Also, 3 with the sterically more bulky *t*-butylphenoxy- groups is more soluble (1 mM vs. <0.05 mM) than 2 with chlorines attached to the ring. Figure 1A shows the cyclic voltammogram of a 0.4 mM 3 in a 0.1 M TBAPF<sub>6</sub> solution of  $\text{CH}_2\text{Cl}_2$ . The initial scan shows a peak at 1.15 V, very similar to analogous compounds based on naphthalene diimide (22). The voltammetry of 3 also shows a reversible peak at 1.45 V which has not been observed for other perylene diimides. We attribute this to the oxidation of the diarylether moiety of the main ring. Upon reversal, two reduction peaks at 0.7 and 0.95 V are observed and further potential cycling shows the growth of two oxidative peaks consistent with poly-3 having an electroactive diphenylbenzidine (DPB) linkage (Scheme 1). The original peak



Scheme 1. Radical dimerization mechanism of arylamines

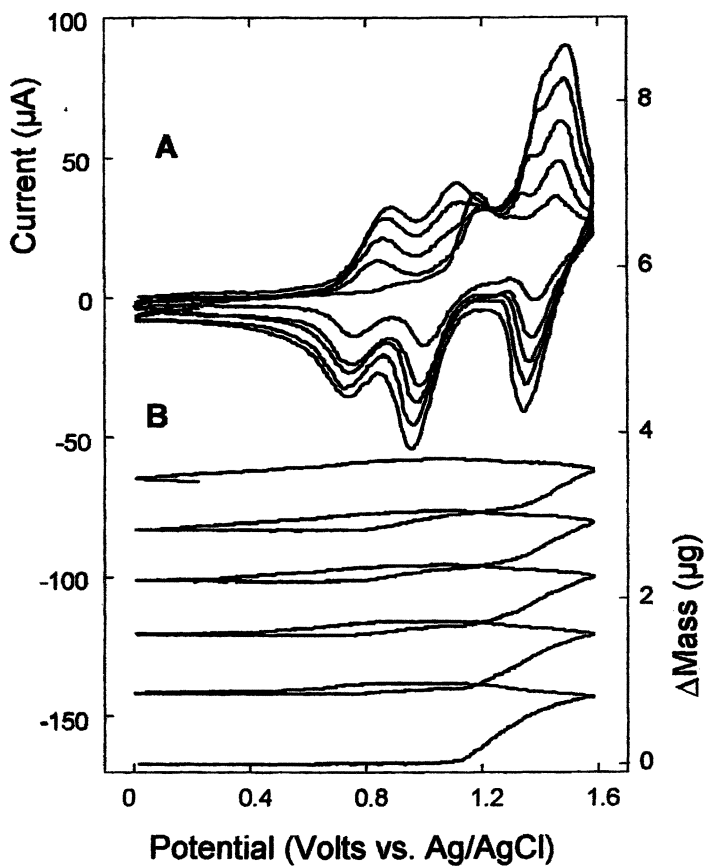


*Figure 1. (A) Solution cyclic voltammogram of 0.4 mM **3** in 0.1 M TBAPF<sub>6</sub> solution of CH<sub>2</sub>Cl<sub>2</sub>. Scan rate = 100 mV/s. Au electrode area = 0.24 cm<sup>2</sup>. (B) Simultaneous mass changes as recorded by the QCE.*

at 1.15 V decreased with increased number of scans. The DPB unit is formed by oxidative dimerization of the terminal diphenylamine groups (33).

Monomers 1, 2, and 4 are very insoluble in almost all organic solvents. Thus we had to explore non-traditional solvent systems to effect our electropolymerization. 1, 2, and 4 were found to be soluble in  $\text{CH}_2\text{Cl}_2$  and 1,2 dichloroethane with small amounts (<5% v:v) of TFA. Trifluoroacetic acid and TFA in  $\text{CH}_2\text{Cl}_2$  have been shown to stabilize radical cations formed during oxidation (34). Since the conductivity of this solution was low, we added 0.1 M TBAPF<sub>6</sub>, and subsequent excursions to oxidative potentials showed no clear oxidation peaks nor any products precipitating onto the electrodes. We reasoned that PF<sub>6</sub><sup>-</sup> maybe acid labile, so we synthesized triethylammonium trifluoroacetate as a supporting electrolyte and added TFA to solubilize the monomer. This solvent electrolyte system provided an excellent media for the electrooxidative polymerization of 1, 2, and 4.

The first voltammogram of a 0.35 mM solution of 1 (Figure 2A) in the above electrolyte solution shows a single irreversible oxidation peak at 1.05 V. Two reductive peaks at 0.75 V and 0.48 V are observed that correspond to the DPB<sup>2+/+</sup> and the DPB<sup>+0</sup> reduction, respectively. The second and subsequent scans show an oxidation peak at ~0.7 V corresponding to the DPB<sup>0/+</sup> linkage. The electropolymerization voltammograms of 4 are generally similar to the other monomers except the two DPB oxidations are merged into one. The initial oxidative scan differs since it shows a symmetric wave at 0.65 V that does not appear in subsequent scans. This process is a rearrangement of a chemisorbed species, or electrosorption or electrodesorption of a species from the Au/electrolyte interface.

We monitored the frequency changes of the QCE during the electropolymerization of each of the monomers. For analysis, we assigned the frequency of the QCE to zero in the monomer solution before any potential excursions. The frequencies were converted to mass changes for convenience (see Experimental). For the initial scans of 1-4 the mass at the electrode remains constant until the foot of the monomer oxidation wave (~1.0 V for  $\text{CH}_2\text{Cl}_2/\text{TBAPF}_6$  and ~0.9 V for  $\text{CH}_2\text{Cl}_2/\text{TEATFA}$ , see Figures 1B and 2B). At that point the mass at the electrode increases until the electrode potential becomes more negative of the oxidation potential. At that point, the mass does not change. The net mass change for the first cycle is typically the largest and net mass changes for subsequent scans are constant. As more material is deposited on the electrode subtle changes in the electrode mass between 0.0 V and 0.8 V become apparent. These mass changes correspond to the oxidation and reduction of the electroactive deposits and are discussed below. For the electrooxidation of 4, expansion of the initial oxidative sweep shows a slight decrease in mass at 0.65 V. This is consistent with the electrodesorption of some species, most likely chemisorbed 4.

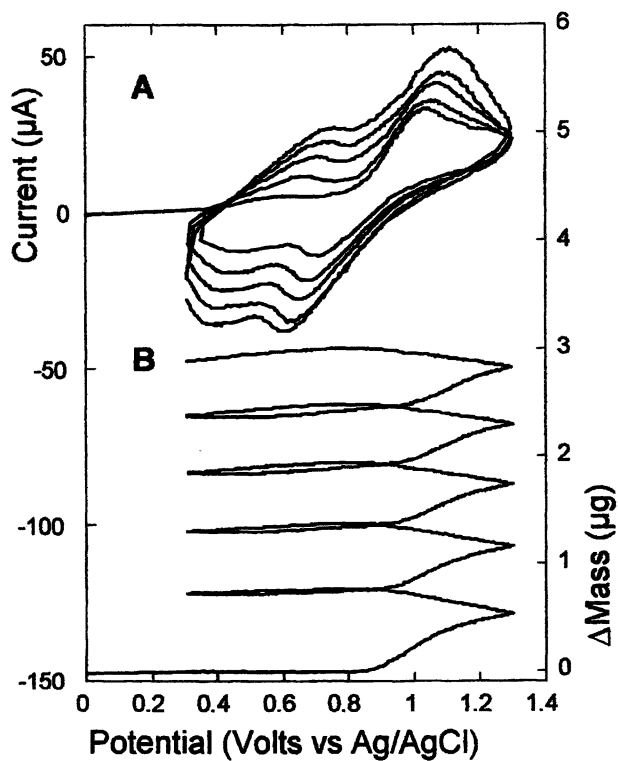


Figure 2. (A) Solution cyclic voltammogram of 0.35 mM **1** in 0.1 M TEATFA solution of  $\text{CH}_2\text{Cl}_2$ . Scan rate = 100 mV/s. Au electrode area =  $0.24 \text{ cm}^2$ . (B) Simultaneous mass changes as recorded by the QCE.

By integrating the cathodic current due to the reduction of the DPB linkage and taking  $2e^-$ /DPB unit, we can calculate the electroactive surface coverage added per scan. The frequency changes measure the amount of mass added to the electrode per scan. The ratio of these quantities is the average molecular weight of the depositing species. These results are summarized in Table I.

**Table I. EQCM Electrooxidative Deposition Data**

	<i>Supporting Electrolyte</i>	<i>MW<sup>a</sup> (obs)</i> (g/mol)	<i>Molecular Species</i>	<i>MW<sup>a</sup> (theory)</i> (g/mol)
1	TEAH <sup>+</sup> TFA <sup>-</sup>	1860	Dimer4H <sup>+</sup> 4CF <sub>3</sub> CO <sub>2</sub> <sup>-</sup>	1906
2	TEAH <sup>+</sup> TFA <sup>-</sup>	2446	Dimer6H <sup>+</sup> 6CF <sub>3</sub> CO <sub>2</sub> <sup>-</sup>	2412
3	TBA <sup>+</sup> PF <sub>6</sub> <sup>-</sup>	2654	Dimer	2634
4	TEAH <sup>+</sup> TFA <sup>-</sup>	2021	Dimer3H <sup>+</sup> 3CF <sub>3</sub> CO <sub>2</sub> <sup>-</sup>	2017

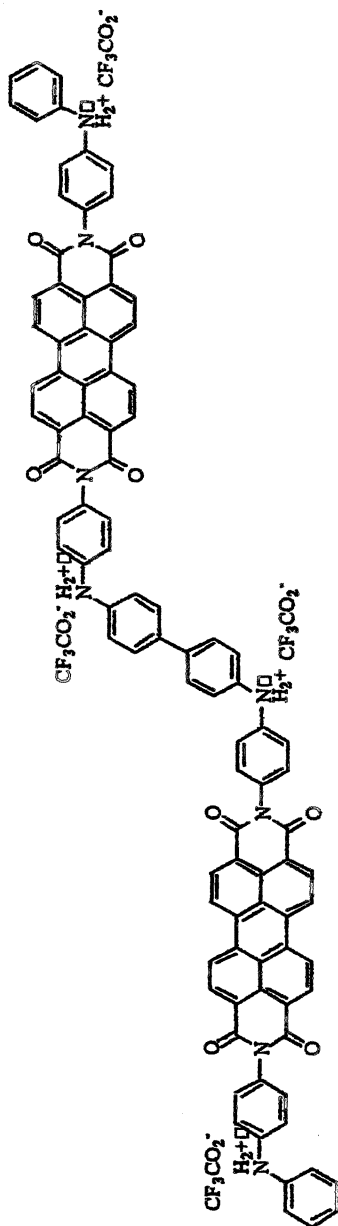
<sup>a</sup> We estimate the errors in mass and charge  $\pm 5\%$ .

For the precipitation of 1, the observed molecular weight of 1860 is very close to the C-C bond dimer with four trifluoroacetic acid groups protonating it (see Scheme 2). These data indicate that the dimer is the predominant species that initially precipitates onto the electrode. In the acidic solutions, the dimers are multiply protonated and deposit with multiple counter anions. Although the sites of protonation are unknown, most likely the aromatic nitrogens or carbonyl oxygens are good candidates. The molecular weight of the depositing species increases with increasing scans.

#### *Polymer films of 1 - 4*

After film deposition, the electrodes are rinsed with fresh CH<sub>2</sub>Cl<sub>2</sub> and evaluated using cyclic voltammetry. Figure 3A shows the cyclic voltammetry of poly-1 in a pure 0.1 M TBAPF<sub>6</sub>/CH<sub>2</sub>Cl<sub>2</sub> solution. The simultaneous mass changes were recorded in Figure 3B. For poly-1, there are two  $1e^-$  oxidations at 0.65 and 0.9 V. These redox waves are well-separated and consistent with previous work on diphenylamine endgroup polymers (22-24). These waves are symmetric and show a peak current proportional to scan rate as would be expected for a surface-confined species. For poly-3 those oxidation waves are also symmetric, indicative of surface-confined species (Figure 4A).

Poly-1, -2, and -4 all show two  $1e^-$  redox processes consistent with the DPB<sup>0/+</sup> and DPB<sup>+2+</sup> oxidations (22). For poly-3, two similar  $1e^-$  redox processes are observed near those potentials, but an additional  $2e^-$  process is observed at 1.4 V. This redox process clearly is associated with the t-BuPhO- groups on the perylene ring since cyclic voltammetry of (t-BuPhO-)<sub>4</sub>-perylene dianhydride shows a  $2e^-$  oxidation at that potential. At potentials <0.0 V, all four polymers show reversible electroactivity. For example in Figure 3A there is a multiple  $e^-$  reduction with a smaller wave at more positive potentials than a larger overlapping wave. Integrating the current associated with these processes reveals that for poly-1-4, there exists a total of  $3e^-$  transferred reversibly between



*Scheme 2. Tetraprotonated dimer of 1.*



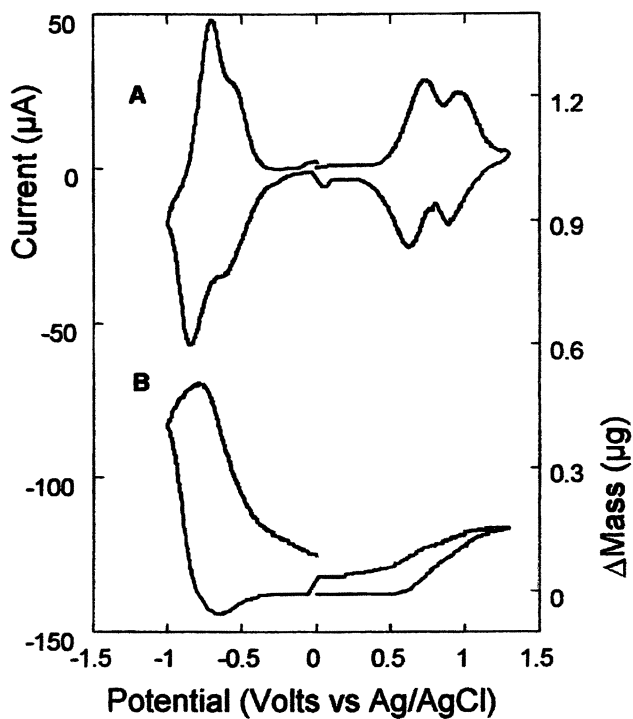


Figure 3. (A) Cyclic voltammogram of poly-1 film in 0.1 M TBAPF<sub>6</sub> solution of CH<sub>2</sub>Cl<sub>2</sub>. (B) Simultaneous mass changes as recorded by the QCE.

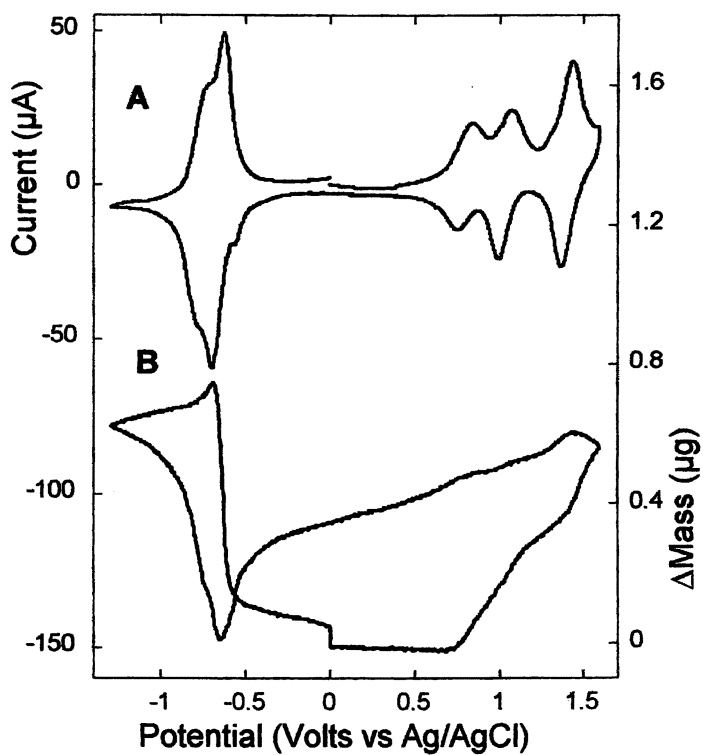


Figure 4. (A) Cyclic voltammogram of poly-3 film in 0.1 M TBAPF<sub>6</sub> solution of CH<sub>2</sub>Cl<sub>2</sub>. (B) Simultaneous mass changes as recorded by the QCE.

-0.5 and -1.0 V. Based on previous electrochemical results (22-29), one  $e^-$  reduces each imide ring and a third  $e^-$  reduces the perylene ring.

Figure 3B show the mass changes associated with the oxidation, rereduction, reduction and reoxidation of poly-1. A mass gain is observed with both the first and second  $e^-$  oxidation. Upon reversal that mass is lost. Scan rate dependence of mass gain and loss show kinetic limitations. Pausing at 0.0 V to allow the mass changes to decrease to zero and then scanning  $<0.0$  V, shows an initial decrease in mass associated with a reductive prewave (or possibly the first  $1 e^-$  reduction) followed by a rapid increase in mass. Upon reoxidation, that mass is lost in a kinetically sluggish process.

As shown in Table II, poly-1, -2 and -4 show  $\sim 150$  g/mol gain and then loss

**Table II. Potential-Mass Correlations  $>0.0$  V**

	<i>MW Gain (obs.) (g/mol)</i>	<i>Ion Change</i>	<i>MW Gain (theory) (g/mol)</i>
Poly-1	151 <sup>a</sup>	$-H^+, +PF_6^-$	144
Poly-2	160 <sup>a</sup>	$-H^+, +PF_6^-$	144
Poly-3	330 <sup>a</sup> , 370 <sup>b</sup>	$+2PF_6^-, +2PF_6^- + \text{solvent}$	290, 290+ <sup>b</sup>
Poly-4	140 <sup>a</sup>	$-H^+, +PF_6^-$	144

<sup>a</sup> All are two  $1e^-$  processes, we estimate the errors in mass and charge  $\pm 5\%$ .

<sup>b</sup> Poly-3 has an extra  $2e^-$  oxidation process.

upon oxidation and rereduction. Since this corresponds to a  $2 e^-$  oxidation the three possible processes that account for charge conservation are:

1. Two positive charges are lost from the polymer.
2. Two negative charges are incorporated into the polymer.
3. There is a loss of one negative and a gain of one positive charge.

The third possibility is most consistent with these data and is consistent with previous observations that this linkage is only electrochemically reversible in  $<pH 3$ , aqueous solutions (19). For poly-3, the data are more consistent with process 2 for the first set of two  $1e^-$  oxidations. For the next  $2e^-$  process, the mass gain is most consistent with incorporation two  $PF_6^-$  and some solvent. Upon rereduction the mass loss is kinetically slow. Not until the reduction at  $-0.7$  V does the mass return to zero. The more highly charged polymers such as [poly-3]<sup>4+</sup> might be expected to need solvent to stabilize the concentrated charges.

The redox processes  $<0.0$  V are, generally, more complicated to interpret that those  $>0.0$  V since the incorporation and expulsion of  $TBA^+$  groups is slower than that of  $PF_6^-$  (35). Poly-1 and -2 (Table III) both showed a loss of mass before a large increase of mass. This is most consistent with a loss of  $PF_6^-$  and then a gain in  $TBA^+$ . The incorporation of  $PF_6^-$  must initially occur upon addition of this film to the supporting electrolyte. For poly-3 and -4 mass increases  $> 3TBA^+$  are observed. In Figure 4B the reduction of the polymer and then reoxidation returns the polymer to the initial mass from the beginning of the scan. The mass changes are also very well correlated with the voltammetry. For poly-3 the ion/solvent kinetics  $>0.0$  V are slow, while  $<0.0$  V the kinetics are fast. Poly-4 (not shown) is kinetically reversible  $>0.0$  V; however scans  $<0.0$  V incorporate solvent that is very slow to be expelled upon return to 0.0 V.

**Table III. Potential-Mass Correlations <0.0 V**

	<i>MW Gain (obs.) (g/mol)<sup>a</sup></i>	<i>Ion change</i>	<i>MW Gain (theory) (g/mol)</i>
Poly-1	500	- PF <sub>6</sub> <sup>-</sup> , +2TBA <sup>+</sup>	484
Poly-2	99	- PF <sub>6</sub> <sup>-</sup> , +TBA <sup>+</sup>	97
Poly-3	869	+3TBA <sup>+</sup> + solvent	726 + solvent
Poly-4	920	+3TBA <sup>+</sup> + solvent	726 + solvent

<sup>a</sup> We estimate the errors in mass and charge  $\pm 5\%$ .

## Conclusions

We have shown that diphenylamine endgroup monomers can be electropolymerized in acidic, nonaqueous media. The initial process irreversibly deposits the dimer onto the electrode. Depending on the acidity of the solvent, either the neutral or protonated dimer predominates. The resulting films can be reversibly oxidized or reduced with mixed counterion incorporation and expulsion. For some films, it is necessary to invoke the incorporation of solvent to stabilize highly charged polymers. While cyclic voltammetry does not reveal sluggish solvent and ion movement, EQCM experiments can help identify mechanisms of film formation and slow kinetics of ion incorporation.

## Acknowledgments

The authors would like to acknowledge financial support from the Department of Energy, through the EPSCoR program.

## References

1. Law, K. -Y. *Chem. Rev.* **1993**, *93*, 449.
2. Seybold, G.; Wagenblast, G. *Dyes Pigm.* **1989**, *11*, 303.
3. Michot, C.; Daril, D.; Armand, M. *Sol. Energy Mater. Sol. Cells* **1995**, *39*, 289.
4. Sadrai, M.; Hadel, L.; Sauers, R. R.; Husain, S.; Krogh-Jespersen, K.; Westbrook, J. D.; Bird, G. R. *J. Phys. Chem.* **1992**, *96*, 7988.
5. Gvishi, R.; Reisfeld, R.; Burshtein, Z. *Chem. Phys. Lett.* **1993**, *213*, 338.
6. Danziger, J.; Dodelet, J. -P.; Armstrong, N. R. *Chem. Mater.* **1991**, *3*, 812.
7. Langhals, H. *Chem. Phys. Lett.* **1988**, *150*, 321.
8. Demming, S.; Langhals, H. *Chem. Ber.* **1988**, *121*, 225.
9. Rademacher, A.; Markle, S.; Langhals, H. *Chem. Ber.* **1982**, *115*, 2927.
10. Kam, A.; Aroca, R.; Duff, J.; Tripp, C. P. *Chem. Mater.* **1998**, *10*, 172.
11. Schlettwein, D.; Back, A.; Schilling, B.; Fritz, T.; Armstrong, N. R. *Chem. Mater.* **1998**, *10*, 601.

12. So, F. F.; Forrest, S. R. *Mol. Cryst. Liquid Cryst. Sci. Technol. B.* **1992**, *2*, 205.
13. Bulovic, V.; Burrows, P. E.; Forrest, S. R.; Cronin, J. A.; Thompson, M. E. *Chem. Phys.* **1996**, *210*, 1-12.
14. Wang, Z. Y.; Qi, Y.; Gao, J. P.; Sacripante, G. G.; Sundararajan, P. R.; Duff, J. D. *Macromolecules* **1998**, *31*, 2075
15. Dotcheva, D.; Klapper, M.; Muellen, K. *Macromol. Chem. Phys.* **1994**, *195*, 1905-11.
16. Quante, H.; Schlichting, P.; Rohr, U.; Geerts, Y.; Muellen, K. *Macromol. Chem. Phys.* **1996**, *197*, 4029-4044.
17. Sauerbrey, G. *Z. Phys.* **1959**, *155*, 206.
18. Buttry, D. A. In *Electroanalytical Chemistry*, Bard, A. J., Ed.; Vol. 17; Marcel Dekker: New York, 1991; p 1.
19. Bott, A. W. *Curr. Sep.* **1999**, *18*, 79.
20. Inzelt, G.; Kertesz, V.; Nyback, A.-S. *J. Solid State Electrochem.* **1999**, *3*, 251-257.
21. Wurm, D. B.; Kim, Y.-T. *Langmuir* **2000**, *16*, 4533-4538.
22. Wang, L.; Goodloe, G. W.; Stallman, B. J. Cammarata, V. *Chem. Mater.* **1996**, *8*, 1175.
23. Wang, L.; Cammarata, V. *Thin Solid Films*, **1996**, *284*, 297.
24. Wang, L.; Wang, Q. Q.; Cammarata, V. *J. Electrochem. Soc.* **1998**, *145*, 2648.
25. Mazur, S.; Lugg, P. S.; Yarnitzky, C. *J. Electrochem. Soc.* **1987**, *134*, 346.
26. Krause, L. J.; Lugg, P. S.; Speckharrrd, T. A. *J. Electrochem. Soc.* **1989**, *136*, 1379.
27. Viehbeck, A.; Goldberg, M. J.; Kovac, C. A. *J. Electrochem. Soc.* **1990**, *137*, 1460.
28. Zhong, C. -J.; Zinger, B.; Cammarata, V.; Kasai, P.; Miller, L. L. *Chem. Mater.*, **1991**, *3*, 787
29. Wang, L. Ph.D. thesis, Auburn University, Auburn, AL, **1997**.
30. Eilingsfeld, H.; Patsch, M. German Patent, 2519790, 1975.
31. Hanaya, K.; Muramatsu, T.; Kudo, H. *J. Chem. Soc., Perkin Trans. 1*, **1979**, *10*, 2409.
32. Dey, B. B.; Doraiswami, Y. G., *J. Indian Chem. Soc.* **1933**, *10*, 309.
33. Yang, H.; Bard, A. J. *J. Electroanal. Chem.* **1991**, *306*, 87.
34. Hammerich, O.; Moe, N. S.; Parker, V. D. *J. Chem. Soc., Chem. Commun.* **1972**, 156.
35. Wang, Q. M.S. thesis, Auburn University, Auburn, AL, **1998**.

## Chapter 6

# Preparation and Characterization of Polymeric Electrodeposits Modified with Dispersed Metallic Particles

M. A. del Valle\* and T. Pizarro

Facultad de Química, P. Universidad Católica de Chile, Av. V. Mackenna  
4860, Macul-Santiago, Chile  
\*email: mdvalle@puc.cl

Optimum conditions to electrodeposit poly(thiophene), poly(pyrrole) or poly(aniline) and to modify these electrodes by electrodeposition of Pt or Pt+Pb particles on these matrices have been established. The response of these electrodes was assayed for the oxidation of small molecules, showing that metal micro-particles in polymers are a promising route to obtain electrodic systems presenting very interesting electrocatalytic activity.

In addition, a study has been undertaken to optimize the electro-obtention of poly(o-phenylene diamine) because of the wide electrochemical window it shows in different electrolytes. Once the optimum conditions had been determined for the electrochemical deposit formation, the methodology to disperse Cu on the polymeric matrix was established. For this purpose, a procedure analogous to that employed to disperse Pb was followed. The response of this modified electrode was assayed as an amino-acid sensor.

## Introduction

The increasing amount of fundamental and applied research into conducting polymers is reflected in the number of papers and monographs devoted to this subject in the last twenty or thirty years, particularly those related to polyaniline (PANI), polythiophene (PTh) or polypyrrole (Ppy), and can be explained because of their extensive application in several areas (1-6). To prepare these materials, two main routes have been used: chemical and the electrochemical synthesis. Our work in the synthesis and characterization of new polymeric materials with specific properties has made it clear that electrochemical methods have important advantages when the aim is to obtain materials to be utilized in areas such as electrocatalysis, photovoltaic cells, diodes, analytical sensors, etc., since it is possible to simultaneously obtain electrochemical information and characterize the materials (7-16). In this area, our work has been focused specially on the preparation of polymer modified electrodes with metallic dispersed particles, with a view toward their application in electrocatalytic processes or as analytical sensors (13, 14). In this area, the first stage is to establish the optimal electrochemical working conditions to obtain an adequate polymer modified electrode. Thus, a previous study of the effect of the variables which governs the electropolymerization process is necessary (such as the electrolyte nature, its composition and the electrochemical perturbation) because the properties and particularly the electrodeposits' morphology are clearly influenced by these variables (15, 16). According to these results, it is possible to select the working conditions for the polymer electroformation (metal/polymer electrode) with adequate conductivity, electrochemical response and open morphology, allowing the metal particles to incorporate and easy substrate accessibility.

Considering the results reported for the electrocatalytic oxidation of some molecules by polymer dispersed metal systems and our previous systematic study on the electropolymerization of thiophene, in a first stage, we have attempted the preparation of polythiophene electrodes modified by electrodeposition of Pt and Pt+Pb for small molecule oxidation, such formation of formic acid (13). Later, and considering that polythiophene electrosynthesis requires very thorough working conditions control, a study of analogous systems using polyaniline or polypyrrole as polymeric matrices have been proposed in order to take advantage of the easy handling and good conductivity of these materials (14).

In addition, in view of the reports about poly(o-phenylenediamine), PoPDA, electro-obtention (17-23), indicating that this deposit is easily obtained from aqueous solutions and shows a wide electrochemical window, we infer that it will be adequate for redox reaction studies and we have considered its use in the case of metal dispersion for possible analytical sensors. Our first challenge has

been the preparation of an aminoacid sensor, particularly the interesting  $\gamma$ -aminobutyric acid, GABA, either for investigation of the activity of anesthetic and tranquilizer agents or as a characterizing element for wine producing grape varieties (24). So, we have undertaken a study to optimize the PoPDA electro-obtention and once the optimal conditions were determined for the electrodeposit formation, the methodology to disperse copper on the polymeric matrix was established. For this purpose, an procedure analogous to that employed to disperse Pb has been followed. We are currently working on the optimization of the response of this modified electrode in order to propose its use as aminoacid sensor.

## Experimental

The experimental conditions to prepare PANI, Ppy or PTh modified electrodes with Pt and Pt+Pb dispersed particles have been previously described (13, 14). Notice that in all these cases the Pt dispersion was based on the doping-undoping process of the modified electrode. After the support electrode was modified it was submerged in a Pt(IV) electrolytic solution and a very slow potential scan was run ( $1 \text{ mVs}^{-1}$ ) up to the positive limit to assure the anions incorporation in the polymeric matrix. A cathodic potential pulse was applied afterwards to assure the metal reduction (platinization cycle, PC). The amount of Pt included was varied by applying a repetitive PC and was estimated by integrating the charge of the  $j-t$  responses obtained during the potentiostatic step. These values were corrected by subtracting the respective polymer dedoping charge in a background electrolyte solution. For the studied polymeric deposits the PC number was optimized with respect to the formic acid response. To improve these electrodes response, lead was also included by submerging the platinum modified matrices into a Pb(II) solution. Thence these modified electrodes were transferred to another cell (after time  $t_i$ ) and a potentiostatic pulse was applied to reduce the metal ion present by diffusion in the polymeric matrix. The time  $t_i$  was optimized for each electrode with respect to its formic acid response.

In the case of PoPDA and copper modified electrodes the procedure was the following: platinum electrodes were modified with PoPDA working under previously reported conditions (17-23). A large area platinum coil was used as the auxiliary electrode and a Ag/AgCl electrode adjusted to 0.00 V vs SCE was used as the reference electrode (25). The polymerization on AISI 316 stainless steel electrodes with the same geometric area (0.3 cm diameter discs) was assayed under the same conditions. The PoPDA modified electrodes (M/PoPDA) were prepared either by applying successive potential scans (CV) between 0.0 and 1.0 V or by a potentiostatic pulse (PS) at 0.9 V for a time  $t$  in a 0.5 M sodium sulfate solution at pH 1.5 adjusted with sulfuric acid. Then,



copper insertion was attempted using an analogous procedure as that used for lead insertion in the other matrices. In this case the modified electrodes response was checked in a basic GABA solution. The electrodes film width was optimized by varying either the number of polymerization cycles,  $n$ , or the electrolysis time,  $t$ , and the copper amount being inserted into the matrix (by varying  $t_1$ ).

## Results and discussion

### Pt and Pt+Pb dispersion

The dispersion of Pt on PTh, PANI or PPy produces an electrocatalytic activity higher than that shown by pure Pt. Therefore, this observation confirms that platinum can be dispersed into all the three types of prepared polymers, exhibiting a lower catalytic site poisoning degree caused by the intermediate species fixation produced during formic acid oxidation. In addition to the current maxima obtained as result of this lower poisoning degree, a negative oxidation potential shift or a significant current increase as a function of potential is also observed in some instances. After a certain number of potentiodynamic scans a deactivation phenomenon is observed which is due either to platinum site poisoning, which cannot be avoided despite the presence of the metallic dispersion, or to a progressive decrease in the surface area of Pt caused by the electrochemical sintering that takes place during successive potentiodynamic cycles. Therefore, to obtain a more stable response with time, the addition of Pb represents a good alternative. Thus Pt/Polymer-Pt+Pb electrodes were prepared by immersing Pt/Polymer-Pt electrodes in Pb(II) aqueous solution for a period varying from 1 to 30 minutes ( $t_i$ ) and then immediately transferring it to the cell containing the electrolyte and applying a potential of -0.2 V for 5 s. The amount of Pb included was estimated in a similar way to that described above for Pt (13, 14).

In this way, a catalytic effect of Pb on the electro-oxidation of formic acid was clearly observed when its response was compared with the response obtained with the respective Pt/Polymer-Pt electrode under the same conditions. A noticeable increase in the current peaks associated with the direct oxidation of the substrate is observed in the three cases along with a clear decrease in the charge assigned to the oxidation of strongly adsorbed intermediates near 0.74 V. This observation confirms that the presence of lead precludes the fixation of poisoning intermediate species on platinum. It is necessary to emphasize that the presence of Pb(II) in the electrolyte is not required to obtain the  $j-t$  response for these modified electrodes.

In order to obtain optimum Pt/Polymer-Pt+Pb electrodes behaviour in the electro-oxidation of formic acid, its activity was investigated at a constant potential and was compared with the activity observed with a Pt/Polymer-Pt and a massive Pt electrode under the same conditions. For this purpose two E-t perturbation programs were applied to the three electrodes: the first one consists in a linear cyclic potential sweep from -0.2 ( $E_{an}$ , anodic potential) to 1.0 V ( $E_c$ , cathodic potential) at 0.1 Vs<sup>-1</sup>. After 18 cycles, a pulse sequence from  $E_{an}$  (during a time  $\tau$ ) to  $E_c$  (during a time  $\tau$ ) to  $E_{ox}$  is applied. The times  $\tau$  and  $\tau'$  values ranged from 5 to 120 s, and 20 s was the optimum time in both cases. Under these conditions the  $j-t$  responses show that the electrode's activity decreases with time, reaching a quasi-stationary value after about 15 minutes. However, the current magnitudes decreased in the order Pt/Polymer-Pt > Pt/Polymer-Pt+Pb > bulk Pt electrodes. After 15 min the circuit was opened for a time  $\tau''$  (optimum value 2 min) followed by application of a potential step  $E_{ox}$  and the electrode initial activity was partially recovered. A sequence of  $E_{an}$ ,  $E_c$  and  $E_{ox}$  pulses, followed by opening the circuit was performed and the  $j-t$  transient corresponding to the fourth cycle was recorded. This treatment resulted in complete restoration of the initial response of Pt/Polymer-Pt+Pb electrode.

These experiments showed that the electrode activity can be recovered by either opening the circuit or subjecting the electrode to an oxidation program of residual species and formic acid electro-adsorption, being the latter more effective. When this program is applied, stable electrode activity can be maintained for at least 36 h.

When the electrocatalytic activity decay percentages are plotted against time for the three electrodes, it is observed that the best behavior is obtained with the Pt/Polymer-Pt+Pb electrodes, which retain their activity near 20 % relative to the initial current value after 15 min, which is remarkably higher than that observed with the other electrodes.

The film thickness using a PTh matrix is much smaller than that for the other two studied matrices. In addition, only two platinization cycles are required to disperse the optimum amount of metal in this matrix. In the case of PANI and PPy a much higher number of potentiodynamic sweeps are required to obtain the most favourable film thickness and a higher number of platinization cycles are necessary to obtain an adequate amount of dispersed platinum. This effect can be ascribed to the different degree of porosity for these polymers and, particularly, to a hindrance of the ion exchange process responsible for the Pt(IV) inclusion in the matrix. The time of immersion of these electrodes in a Pb(II) solution has only a slight influence on their behavior, with being all efficient catalysts of the HCOOH oxidation. Electrodes formed by the PTh polymeric matrix, on the other hand, show higher current densities, and the electrocatalytic activity is more stable towards successive potentiodynamic cycles.

The electrocatalytic activity of the electrodes using PANI or PPy as the polymeric matrix decreases very rapidly with time because lead is transferred to the solution as the oxidation proceeds. The loss of lead in these systems can be explained considering the proposed model for the behavior of a platinum and lead polymeric matrix electrode: when the polymeric-Pt electrode system is in the reduced state the lead atoms are deposited on the surface of the platinum granules and on the polymeric matrix. The electro-adsorption of HCOOH takes place on the Pt active sites and the polymer eliminates anions through the undoping process. During oxidation the following processes take place: direct oxidation of HCOOH and partial polymer oxidation with subsequent anionic doping and Pb atoms total. So, in the oxidation process Pb(II) is not fixed when the polymer is either PANI or PPy. This effect is not observed when the polymeric matrix is PTh because a greater affinity holds between the cation and the sulfurs of the thiophene rings. Therefore, this system appears the most attractive or the most suitable, despite the fact that the preparation of PTh films is far more cumbersome and must be done in totally anhydrous solvent in order to obtain good reproducibility. The loss of Pb(II) from PANI or PPy indicates that in looking for suitable new materials to prepare these catalysts it is very important to consider, other than the morphology, the chemical affinity between the metal to be included in the polymer and the groups present as substituents in the original monomer.

### **Cu dispersion**

The *o*-PDA electropolymerization on AISI 316 stainless steel was first studied and the electrodeposit's response was compared with that of the polymer deposited on Pt using analogous conditions. The results indicated that after the film formation the modified electrode response is identical for both supporting materials. This is indicative that the supporting material affects only the initial electropolymerization stage and, once the film is generated, the polymers show an analogous response with a wide electrochemical window. Therefore, we have continued our study using this electrode.

The comparison of GABA response on SS/PoPDA, SS/PoPDA-Cu modified and bulk copper electrodes having the same geometrical area indicates (Figure 1) that GABA is electro-inactive on either SS or SS/PoPDA justifying copper insertion in the inert matrix. Moreover, a much higher current density is obtained in the case of SS/PoPDA-Cu than in the case of massive copper indicating that copper dispersion increases the effective electrode area favouring the detection system miniaturization.

The response was optimized by analyzing the following parameters' effects: type of electrochemical applied perturbation during the electropolymerization process (CV or PS), polymer film thickness (by either varying the number of voltammetric cycles,  $n$ , or the electrolysis time,  $t$ ). Each electrode was immersed

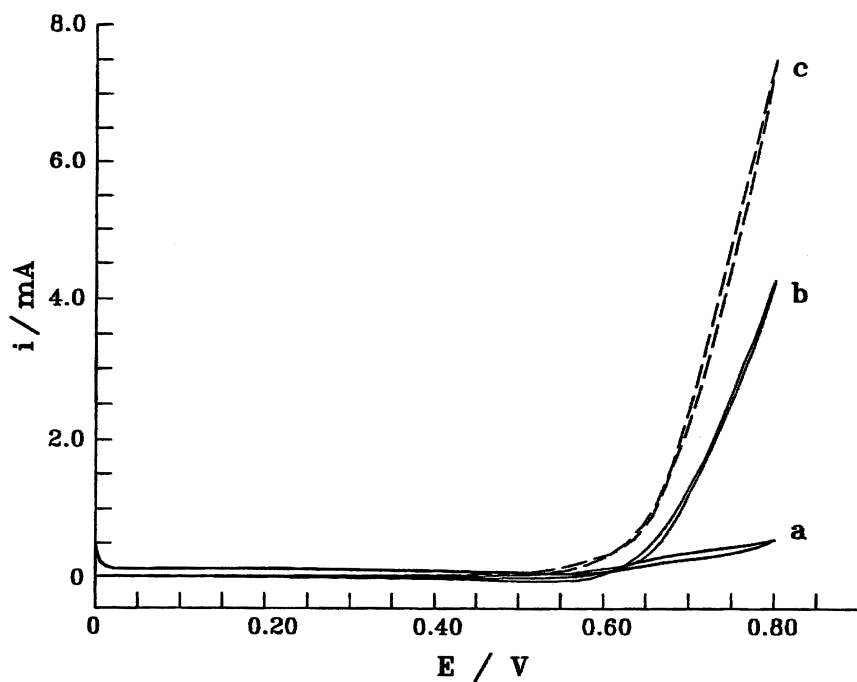


*Figure 1.* Potentiodynamic response of GABA (1 mg/L in 0.1M NaOH) on: (a)massive Cu; (b)SS/PopDA and (c)SS/PopDA-Cu electrodes.  $v = 100 \text{ mVs}^{-1}$ .

for different times ( $t_1$ ) in a Cu(II) solution and then a potential pulse at  $-0.3$  V was applied for a time  $t_2$  in order to introduce copper. Each electrode response was measured in a GABA solution and it was found that the highest current (maximum sensitivity) was obtained under the conditions summarized in Table 1.

**Table 1. Optimal conditions to prepare SS/PoPDA-Cu electrodes**

<i>Electrochem. perturbation</i>	<i>Film thickness<sup>a</sup></i>	$t_1$	$t_2$
CV (0-1.0 V; 50 mV/s)	$n$ : 50	5 min	3 min
PS (0.90 V)	$t$ : 15 min	5 min	3 min

<sup>a</sup>: expressed as function of either  $n$  or  $t$ .

It must be noticed that in both cases the optimum  $t_1$  and  $t_2$  values are the same, indicating that with either 50 PC cycles or applying a potential for 15 minutes the obtained polymeric deposits have similar characteristics. Considering that the PC preparation is faster and that this type of deposit presents a better response our study continued using the electrode modified under the conditions summarized in table 1 for this kind of electrochemical perturbation.

Figure 2 shows one of these electrodes' response (SS/PoDA(by PS)- Cu) in different concentrations GABA solutions. The measurements were made successively from (a) to (d) using the same modified electrode and the profiles shown are totally reproducible if the modified electrode has just been prepared. It can be observed that between 0.65 and 0.70 V the current increases initially, showing a linear dependence with GABA concentration. At concentration of 0.8 mg/L a deviation develops which can be attributed to a copper active site's "saturation" in the matrix. Nevertheless, if this electrode is replaced by a new, recently prepared identical one the response increases again linearly. This observation confirms that this behavior is a consequence of a degradation of the electrode after successive measurements.

Upon use of the same electrode to repeatedly measure a certain GABA solution the response remained constant for the first three determinations and it decreased after the third measurement. This result confirms that copper is lost from the polymeric matrix. Therefore, the measurements were repeated preparing a new electrode before each determination. Reproducible results were obtained which increased linearly with GABA concentration within the assayed range. However, the required rigourosity and the considerable waste of time and materials makes this system unattractive for its application.

These results are an indirect confirmation of the possibility of inserting copper in a polymeric matrix although it is not strongly retained when used as GABA sensor. As in the case of Pt and Pt + Pb the copper problem in the matrix might be solved modifying the polymer deposit incorporating a high

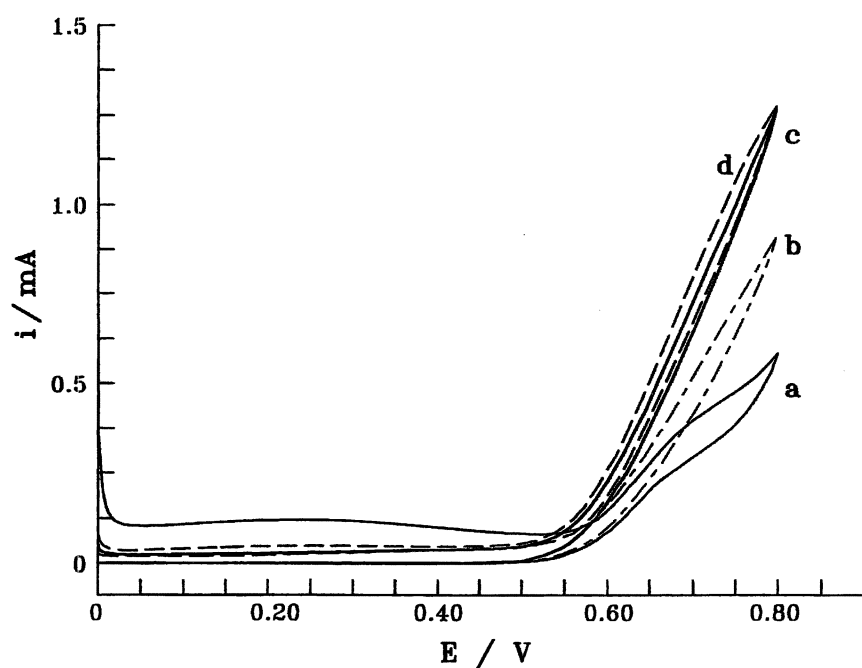


Figure 2. Potentiodynamic response of GABA on SS/PopDA-Cu electrode: (a)0.2; (b)0.4; (c)0.6 and (d)0.8 mg/L.  $v = 100 \text{ mVs}^{-1}$ .

coordinating capacity group. Two routes are tried to accomplish this modification:

1. Considering the possibility of electrochemical preparation of oPDA-hydroquinone co-polymer (26), which presents a wide electrochemical window, it is possible to attempt the obtention of an adequate morphology to insert copper and try its application as sensor for GABA and other aminoacids, taking advantage of the quinonic group coordinating capacity to assure the metal retention.
2. It is possible to modify the monomer with a copper coordinating group. So, we have undertaken a study to electropolymerize 2,3-diaminophenol, DAP which is analogue to oPDA with an hydroxylic group. On this time the optimal electropolymerization conditions has been established (27) and in the next future we will try to insert copper on this matrix.
- 3.

Even if the second option turns out to be interesting and good results should be obtained we plan to study also the first one because DAP, like Th, can be polymerized only under totally anhydrous conditions.

## Conclusions

We have demonstrated that electrochemical methods are not only a very useful tool for the synthesis and characterization of polymers, but also to study metals dispersion on polymeric matrices. This dispersion confers on them very interesting properties for areas of technological interest, although a great deal of previous study and fundamental research is required particularly in the new catalyst and sensors design based on dispersed metal particles.

The coordinating capacity of the metal ion toward groups present in the polymeric matrix must be considered to assure a stable response in time when the modified electrode is to be used in oxidation processes.

## Acknowledgements

The last part of this work was supported by Fondecyt grants N° 1990544 and 8970011. The invaluable contribution of profs. Dr. F. R. Díaz, Dr. M. E Bodini and R. Schrebler is also gratefully acknowledged.

## References

1. Skotheim, T. A.; *Handbook of Conducting Polymers*, Marcel Dekker: New York, NY, 1986.
2. Simonet, J.; Raoult-Berthelot, J. *Prog. Solid St. Chem.* **1991**, *21*, 1.

3. Radogan, A.; Lewenstam, A.; Ivaska, A. *Talanta* **1991**, *39*, 617.
4. Mastragostino, M.; Soddu, Y. *Electrochim. Acta* **1990**, *35*, 463.
5. Li, F.; Alberi, W. J. *Electroanal. Chem.* **1991**, *302*, 279.
6. Watanabe, Y.; Khong, J.; Rubner, M. J. *Chem. Soc., Chem. Commun.* **1989**, 123.
7. Díaz, F. R.; Sánchez, C. O.; del Valle, M. A.; Tagle, L. H.; Bernede, J. C.; Tregouet, Y. *Synth. Met.* **1998**, *92*, 99.
8. Díaz, F. R.; Sánchez, C. O.; del Valle, M. A.; Ugalde, L.; Gargallo, L. *Synth. Met.* **1999**, *105*, 161.
9. Díaz, F. R.; Sánchez, C. O.; del Valle, M. A.; Radic, D.; Bernede, J. C.; Tregouet, Y.; Molinie, P. *Synth. Met.* **2000**, *110*, 71.
10. Bernede, J. C.; D'Almeida, J.; Taoudi, H.; Martínez, F.; Neculqueo, G.; Díaz, F. R.; del Valle, M. A.; Lefrant, S.; Molinie, P. *Synth. Met.* **1999**, *101*, 646.
11. Díaz, F. R.; Sánchez, C. O.; del Valle, M. A.; Bernede, J. C.; Tregouet, Y. *Bol. Soc. Chil. Quim.* **2000**, *45*, 181.
12. Bernede, J. C.; Taoudi, H.; Kodjo, E.; del Valle, M. A.; Díaz, F. R.; Godoy, A. *Rec. Devel. Pol. Sci.* **1998**, *1*, 205.
13. Schrebler, R.; del Valle, M. A.; Gómez, H.; Veas, C.; Córdova, R. J. *Electroanal. Chem.* **1995**, *380*, 219.
14. del Valle, M. A.; Díaz, F. R.; Bodini, M. E.; Pizarro, T.; Córdova, R.; Gómez, H.; Schrebler, R. *J. Appl. Electrochem.* **1998**, *28*, 943.
15. Córdova, R.; del Valle, M. A.; Arratia, A.; Gómez, H.; Schrebler, R. J. *Electroanal. Chem.* **1994**, *377*, 75.
16. Schrebler, R.; Grez, P.; Cury, P.; Veas, C.; Merino, M.; Gómez, H.; Córdova, R.; del Valle, M. A. *J. Electroanal. Chem.* **1997**, *430*, 77.
17. Chiba, K.; Ohsaka, T.; Oyama, N. *J. Electroanal. Chem.* **1987**, *217*, 239.
18. Chiba, K.; Ohsaka, T.; Ohnuki, Y.; Oyama, N. *J. Electroanal. Chem.* **1987**, *219*, 117.
19. Ohsaka, T.; Watanabe, T.; Kitamura, F.; Oyama, N.; Tokuda, K. *J. Chem. Soc. Chem. Comm.* **1991**, 1072.
20. Levi, H. *Electrochim. Acta* **1992**, *37*, 635.
21. Oyama, N.; Ohsaka, T.; Chiba, K.; Takahashi, K. *Bull. Chem. Soc. Jpn.* **1988**, *61*, 1095.
22. Ogura, Y. *Electrochim. Acta* **1995**, *40*, 2707.
23. Komura, T.; Yamaguti, T.; Takahasi, K. *Electrochim. Acta* **1996**, *41*, 2865.
24. Lehtonen, P. *Am. J. Enol. Vitic.* **1996**, *47*, 127.
25. East, G.; del Valle, M. A. *J. Chem. Ed.* **2000**, *77*, 97.
26. Phani, K. L.; Pitchumani, S.; Muralidharan, S.; Ravichandran, S.; Iyer, S. V. *J. Electroanal. Chem.* **1993**, *353*, 315.
27. del Valle, M. A.; Silva, E. T.; Díaz, F. R.; Bodini, M. E.; Gargallo, L. *J. Pol. Sci. Part A: Pol. Chem.* **2000**, *38*, 1698.



## Chapter 7

# Conducting–Insulating Polymer Composites: Selectively Sensing Materials for Humidity and CO<sub>2</sub>

K. Ogura and H. Shiigi

Department of Applied Chemistry, Yamaguchi University,  
Ube 755–8611, Japan

Conducting/insulating polymer composites which respond selectively to humidity and CO<sub>2</sub> at room temperature have been prepared, and their sensing schemes disclosed. The logarithmic conductivity of a composite of emeraldine salt-type polyaniline (ES-PAn) with poly(vinyl alcohol)(PVA) is proportional to the humidity in a wide range ( $10^{-5}$  to  $10^{-1}$  Scm<sup>-1</sup>). The movement of protonic acid, that is, the shift of the salt-base equilibrium of the conducting polymer, occurring in the desiccating and moisturizing processes, causes the change in conductivity of the composite. On the other hand, the composite consisting of emeraldine base-type PAN (EB-PAn) and PVA makes no response to water because this type of polymer has no dopant anion to be released. In the presence of CO<sub>2</sub>, however, the carbonate ion formed by the hydrolysis of CO<sub>2</sub> can be incorporated into EB-PAn to generate ES-PAn, resulting in an increase in conductivity of the composite film. This is the basis for sensing CO<sub>2</sub> with the EB-PAn/PVA composite.

Extensive investigations on polyaniline (PAn) and its derivatives have been carried out (1) since they possess a moderate conductivity upon doping with protonic acid and an excellent stability under ambient conditions (2,3). PAn is simply prepared by the chemical and electrochemical oxidation of aniline or its derivatives in aqueous solution. In general, however, the chemical and electrochemical polymerization of aniline monomer lead merely to an insoluble powder and a thin brittle film, respectively. Hence, it is very difficult to process PAn for a practical use. In order to deal well with this problem, the improvement of processability of PAn has been studied by preparing polymer composites (4) and soluble PAn (5,6) and using plasma polymerization (7) and postsulfonation of PAn (8,9). Another approach to the preparation of processible PAn is to apply a precursor polymer, e.g., PAn can be produced by the thermal treatment of poly(anthranilic acid) (PANA) (10). This method is particularly useful for the preparation of processible PAn or its composites with other insulating polymers since it does not use external dopants that often cause an inconvenient situation associated with a practical use of the conducting polymer.

In the present study, PAn derived from PANA was characterized by thermogravimetric/mass (TG/MS) and Fourier transform infrared (FTIR) spectroscopies. The composites of PAn with insulating polymers have been found to be selectively sensing to humidity and CO<sub>2</sub> (11-14), and the application of PAn derived from PANA to humidity and CO<sub>2</sub> sensors is described here in detail.

## Experimental

The preparation of PANA was performed by the following procedure. An aqueous solution of 0.2 M (NH<sub>4</sub>)<sub>2</sub>S<sub>2</sub>O<sub>8</sub> was slowly poured with stirring into a 0.1 M H<sub>2</sub>SO<sub>4</sub> solution containing 50 mM anthranilic acid, and the polymerization was done at room temperature for 48 h. The precipitate was filtered, washed first with methanol and then with a 0.1 M H<sub>2</sub>SO<sub>4</sub> solution, and dried under vacuum. The powdery PANA obtained was dark brown. The conversion of PANA to PAn was achieved by the pyrolytic elimination of CO<sub>2</sub> at elevated temperature.

The chemical characterization of PANA and PAn was determined by a Jeol 220 TG/MS and a Shimadzu FTIR (Type 8100M). The TG/MS analyses were carried out under a helium atmosphere, and temperature was changed from 25 °C to 500 °C at the programmed heating rate of 5 °Cmin<sup>-1</sup>. The sample for this experiment was prepared by casting a dimethyl sulfoxide (DMSO) solution of the sample on a polyethylene substrate, evaporating the solvent in a vacuum, and

peeling the resulting film off from the substrate. FTIR spectra were obtained in the transmission mode as KBr tablets.

The PANA which was thus prepared was found to be in the form of emeraldine-salt polyaniline (ES-PAN). The solubility of PANA in DMSO was  $32 \text{ gL}^{-1}$ , and the electrical conductivity  $3.5 \times 10^{-2} \text{ Scm}^{-1}$ . The composite film consisting of PANA and poly(vinyl alcohol) (PVA) was very sensitive to humidity: the conductivity of this composite changed from conducting level to insulating upon the variation of relative humidity. The electrical conductivity was measured with a comb-shaped microelectrode that was made by depositing a thin platinum film in a comb shape on a glass substrate in a vacuum (11). A DMSO solution containing given quantities of PANA and PVA was cast on a microelectrode, and the solvent was removed under vacuum. The thickness of the applied composite was always 100 nm, which was estimated with a scanning electron microscope (SEM, Hitachi S-2300). The film-cast microelectrode was set in a measuring cell connected to a vacuum line permitting us to introduce a controlled pressure of water vapor at 25 °C. The conductivity was monitored by the two-probe direct current technique after the pressure was restored to 760 Torr by introducing nitrogen gas.

On the other hand, the composite consisting of emeraldine-base PAN (EB-PAN) and PVA did not respond to relative humidity but to  $\text{CO}_2$ . The EB-PAN was prepared by the pyrolytic elimination of  $\text{CO}_2$  from PANA. The pyrolysis was carried out at various elevated temperatures in a helium atmosphere. The electrical conductivity of the EB-PAN/PVA composite under varied conditions of humidity and  $\text{CO}_2$  concentration was measured with a comb-shaped microelectrode in the same manner as that described above.

## Results and Discussion

### Characterization of PANA and the preparation of EB-PAN

FTIR spectra of PANA and heat-treated PANAs were measured in the transmission mode as KBr tablets. The results are exhibited in Figure 1, where the heat-treatment was done at 150, 200, 250 and 280 °C for 2h. The absorption bands at 1690 and  $1450 \text{ cm}^{-1}$ , which are seen in the spectrum of PANA without heat-treatment (curve a), are attributable respectively to the C=O and C-O stretching vibration of the carboxyl group (15). The bands at 1570 and  $1380 \text{ cm}^{-1}$  are assignable respectively to the antisymmetric and symmetric stretching vibration of the ionized carboxyl group (15). Hence, both -COOH and -COO<sup>-</sup> groups are confirmed as being present in PANA without heat-treatment. On the other hand, the absorption intensities at 1690 and  $1450 \text{ cm}^{-1}$  are observed to decrease with elevating the treatment temperature,

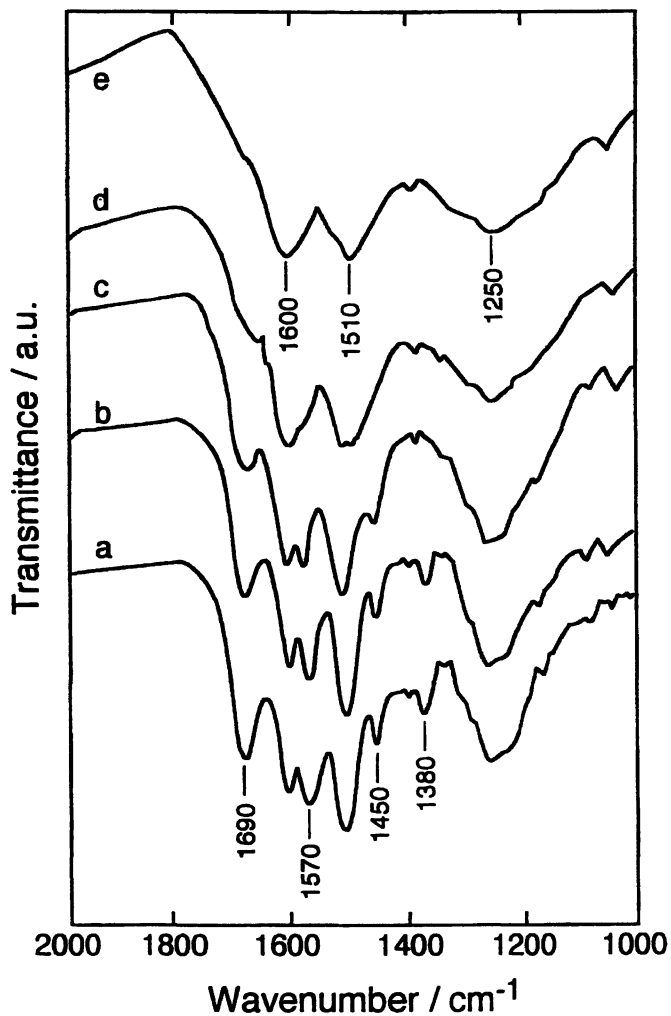


*Figure 1. FTIR spectra of the PANA powder treated at different temperatures: (a) without heat-treatment, (b) 150, (c) 200, (d) 250, (e) 280 °C.*

while the bands at 1570 and 1380  $\text{cm}^{-1}$  are almost invariable in magnitude up to 200  $^{\circ}\text{C}$ . It is therefore indicated that the carboxyl groups are readily detached from the PANA backbone with increasing the temperature while the ionized carboxyl group is thermally stable at least until 200  $^{\circ}\text{C}$ . The ionized form can be stabilized because this group acts as a self-dopant on PANA, i.e., the positive nitrogen atom interacts with the ionized carboxyl group (16). The spectrum of the PANA treated at the highest temperature (280  $^{\circ}\text{C}$ ) showed the disappearance of the bands belonging both to the carboxyl and ionized carboxyl groups, but distinct absorption bands are seen around 1600, 1510 and 1250  $\text{cm}^{-1}$  instead. These three bands are attributed to the stretching vibration of the benzenoid ring, quinoid ring and CN, respectively. The features of this spectrum is in good agreement with those of the spectrum for an emeraldine base of PAN prepared by the chemical oxidation of aniline monomer (17). Thus, EB-PAN is obtainable by the pyrolysis of PANA.

The TG curve of PANA and the corresponding MS spectra are shown in Figures 2 and 3, respectively. The TG curve demonstrates three major stages (I, II and III) of weight loss. A comparison between the two figures indicates that the weight loss observed at 85  $^{\circ}\text{C}$  (stage I) is due to  $\text{H}_2\text{O}$  ( $m/z=18$ ) desorbed from the polymer. The weight loss at stage II is caused by the decarboxylation ( $m/z=44$ ). Many MS peaks including the peak at  $m/z=93$  attributable to aniline occur at stage III, resulting from the pyrolysis of the PANA backbone.

In Figure 4, the MS chromatogram for  $\text{CO}_2$  ( $m/z=44$ ) and the electrical conductivity of PANA are shown as a function of the temperature at which PANA was heat-treated. The chromatographic intensity commences to increase from 100  $^{\circ}\text{C}$ , and reaches a maximum around 200  $^{\circ}\text{C}$  with a shoulder at about 170  $^{\circ}\text{C}$ . It is therefore indicated that the thermal decomposition of the carboxyl group to  $\text{CO}_2$  occurs via two steps, i.e., one decomposes around 170  $^{\circ}\text{C}$ , and the other at a temperature higher than 200  $^{\circ}\text{C}$ . This may support the existence of both  $-\text{COOH}$  and  $-\text{COO}^-$  groups intimated from the FTIR results. The decrease in MS intensity of heat-treated PANA beyond 200  $^{\circ}\text{C}$  is probably caused by the diminution in concentration of the remaining carboxyl groups. On the other hand, the electrical conductivity of PANA ( $1.7 \times 10^{-2} \text{ Scm}^{-1}$ ) heat-treated at 150  $^{\circ}\text{C}$  is comparable to that ( $3.5 \times 10^{-2} \text{ Scm}^{-1}$ ) without heat-treatment (25  $^{\circ}\text{C}$ ). The conductivity of PANA became much lower as the polymer was treated at a temperature above 150  $^{\circ}\text{C}$ , and it reached  $3.8 \times 10^{-4} \text{ Scm}^{-1}$  at 250  $^{\circ}\text{C}$ . Hence, it follows that the electrical conductivity of PANA is not related to the carboxyl group decomposed around 150  $^{\circ}\text{C}$  but to the ionized carboxyl group decomposed at more elevated temperature. The stabilization of the latter carboxyl group is brought about by the interaction with the positive nitrogen atom as noted above.

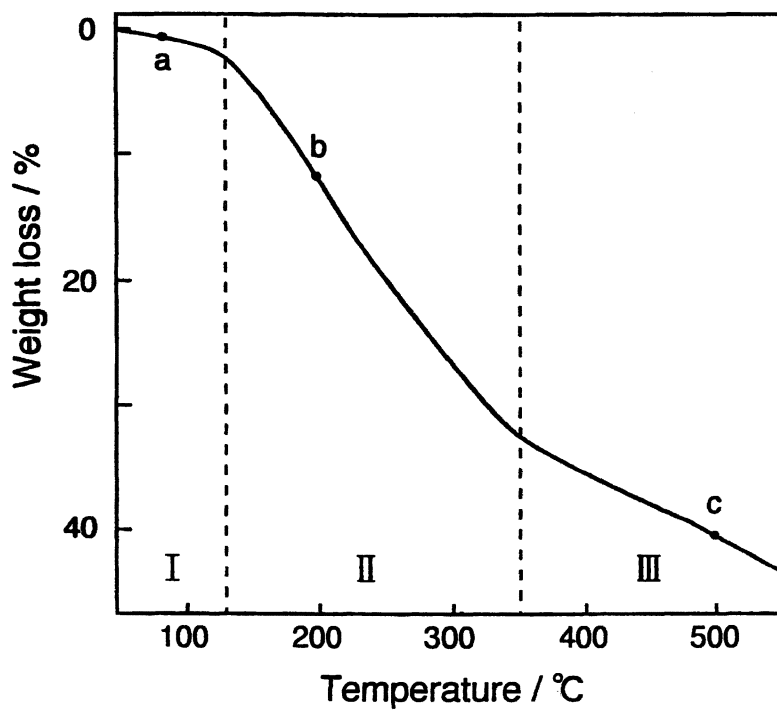


Figure 2. TG curve of PANA.

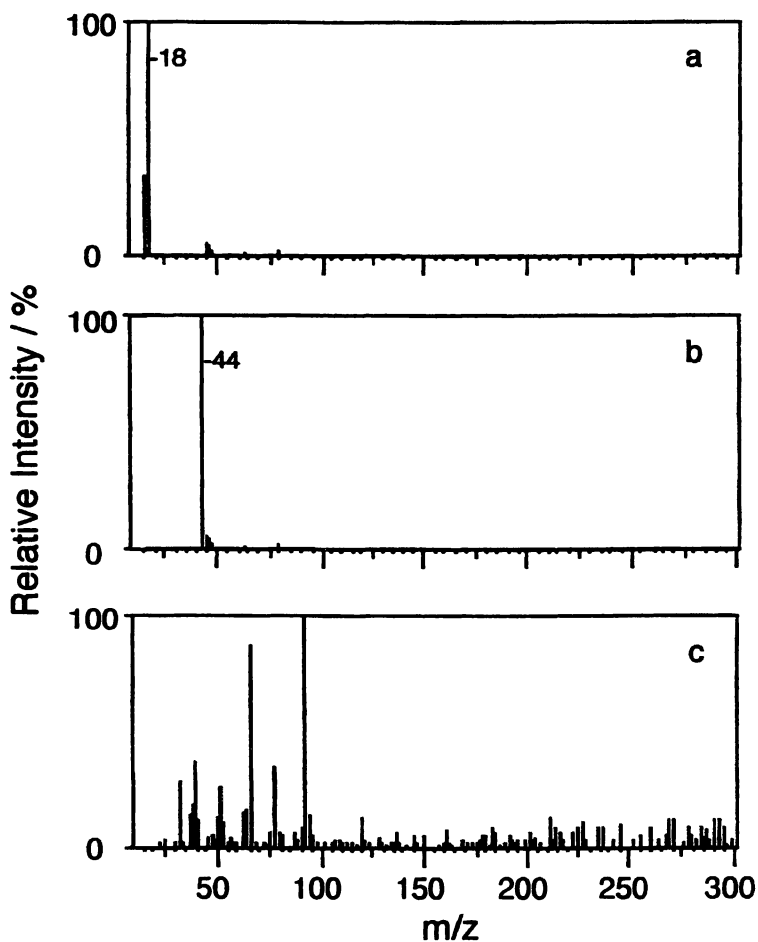


Figure 3. MS spectra of PANA taken at different temperatures : (a) 85, (b) 200, and (c) 500 °C.

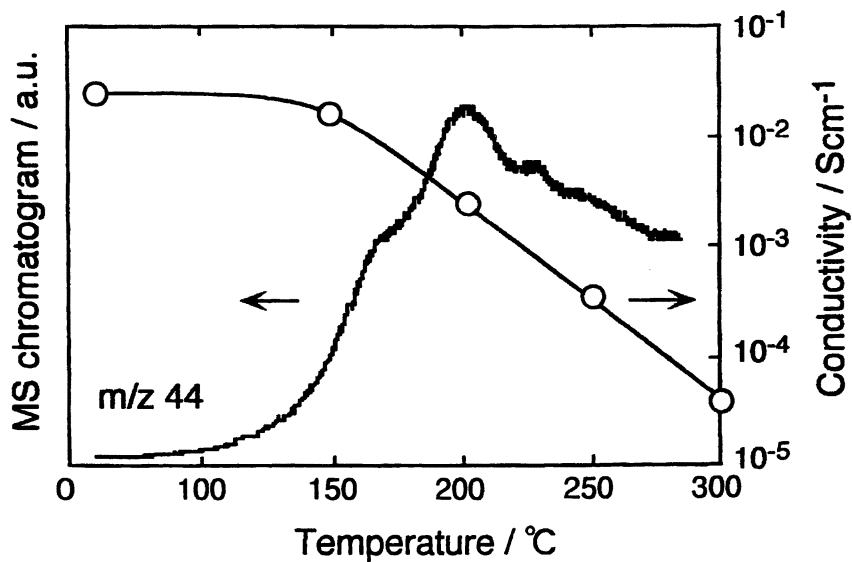


Figure 4. Relationship between the electrical conductivity of PANA and the treatment temperature.



From these results, the following scheme (Scheme I) can be given for the pyrolysis of PANA in which the decarboxylation occurs in two stages from -COOH and -COO<sup>-</sup> groups around 170 °C and 250 °C, respectively.

### **PANA/PVA composites as a humidity sensor**

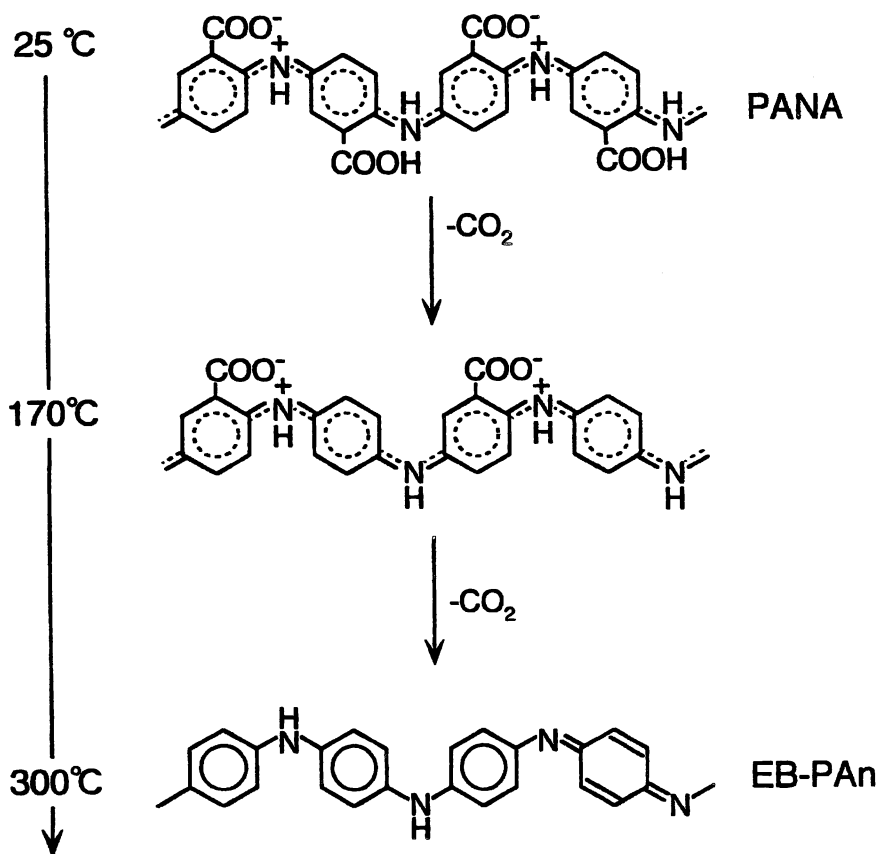
We have found that a composite film consisting of a conducting polymer and an insulating polymer is useful for a humidity sensor (11). The PANA as prepared and the PANA doped with surfuric acid (PANA-SA) were both used as the conducting polymer in the present study. The PANA-SA was prepared as follows. PANA was first heat-treated at 250 °C, and then the PANA was externally doped with surfuric acid. The electrical conductivity of PANA-SA was 6.2 Scm<sup>-1</sup>. This value is rather higher than that (5 Scm<sup>-1</sup>) (18) reported for the PAN prepared by the electrochemical and chemical polymerization of aniline monomer. In general, PAN is insoluble in DMSO, but PANA-SA is soluble to some extent (15 gL<sup>-1</sup>). The solubility of PANA-SA enables us to make a completely mixed composite of PANA-SA and PVA, which is very important for the preparation of a good humidity sensor with such a composite. The electrical conductivities of the PANA/PVA (a) and PANA-SA/PVA (b) composites measured under a constant humidity are shown in Figure 5. In both composites, the logarithmic conductivity is linearly related to the relative humidity, and there is no hysteresis in the measurements at the moistening and desiccating stages. The linearity is valid covering over 5 orders and 4 orders of magnitude for the PANA-SA/PVA (b) and PANA/PVA (a) composites, respectively.

The humidity-dependence of the PANA-SA/PVA composite can be explained on the basis of a salt-base transition of the conducting polymer (13). In the desiccating process, the protonic acid incorporated in the PANA-SA during its preparation is expelled and moves into the strongly bound water in PVA as shown in Scheme II. Hence, the conductivity of the composite decreases with a decrease of environmental humidity, and finally the composite becomes insulating. Conversely, in the moistening process, the external moisture is weakly rebound to the composite, and the protonic acid is likely to disperse over the composite, resulting in the recovery of the PANA-SA to the conducting level.

### **EB-PAN/PVA composite as a CO<sub>2</sub> sensor**

As mentioned above, there is a good linear relationship between the log of electrical conductivity and the relative humidity for the PANA/PVA composite, while the conductivity of the EB-PAN/PVA composite was about  $3 \times 10^{-5}$  Scm<sup>-1</sup> and was independent of the relative humidity. This signifies that PANA is completely converted to the base-type PAN and there is no dopant anion, (i.e.,

Scheme I.



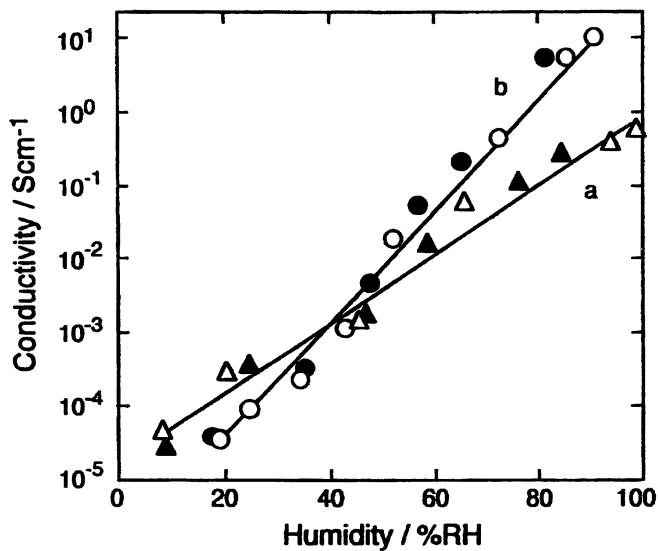
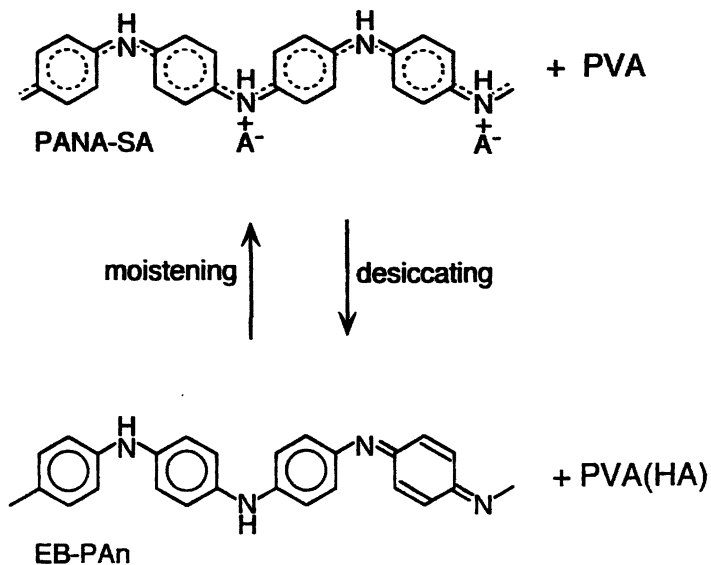


Figure 5. Dependence of electrical conductivity of a PANA/PVA (a) and a PANA-SA/PVA (b) composite on the relative humidity at the moistening (o,  $\Delta$ ) and desiccating ( $\bullet$ ,  $\blacktriangle$ ) stages.

Scheme II.



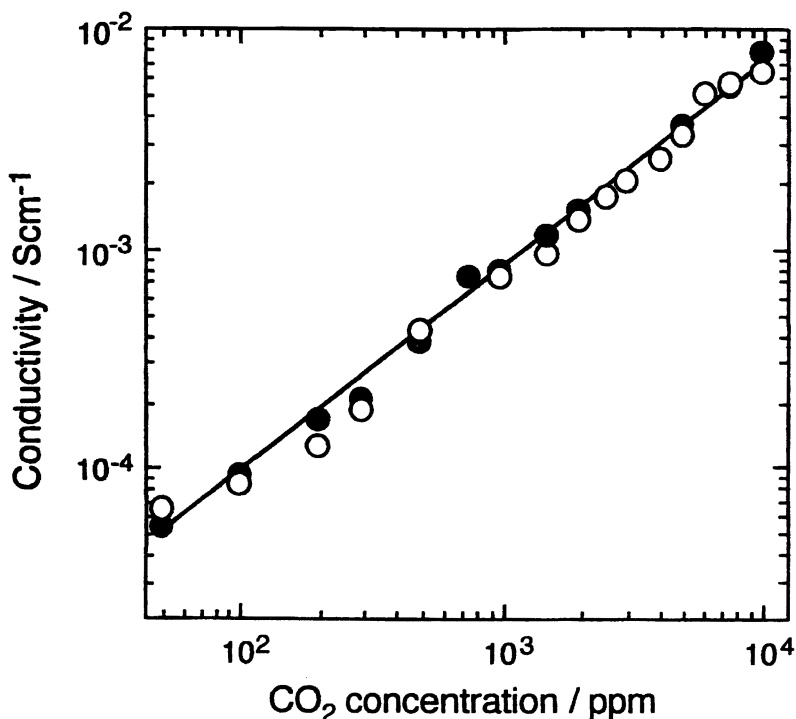


Figure 6. Dependence of electrical conductivity of a EB-PAN(14 wt%)/PVA (86 wt%) composite on the CO<sub>2</sub> concentration at the humidity of 30 %RH at 25 °C. The measurements were performed by increasing (○) and decreasing (●) the CO<sub>2</sub> concentration.

absence of self-dopant, -COO<sup>-</sup>) in the polymer. In the presence of CO<sub>2</sub> and humidity, however, the electrical conductivity of the EB-PAN/PVA composite was linearly related with the CO<sub>2</sub> concentration. In Figure 6, the logarithmic conductivity of EB-PAN (14 wt%) / PVA (86 wt%) is plotted versus the CO<sub>2</sub> concentration at the humidity of 30 %RH at 25 °C. The conductivity changes from  $5 \times 10^{-5} \text{ Scm}^{-1}$  to  $8 \times 10^{-3} \text{ Scm}^{-1}$  upon the variation of CO<sub>2</sub> concentration from 50 ppm to 1 %, and no hysteresis is involved in the measurements between the increasing and decreasing stages of CO<sub>2</sub> concentration.

In order to study the effect of humidity, the electrical conductivities of a EB-PAN/PVA composite upon the variation of CO<sub>2</sub> concentration were measured under various humidities, and the results are shown in Figure 7. At the humidity of 30 %RH, the logarithmic conductivity is proportional to the CO<sub>2</sub> concentration ranging from 50 ppm to 1%. At 90 %RH, however, the linear portion is rather limited, and the conductivity shows a constant value at

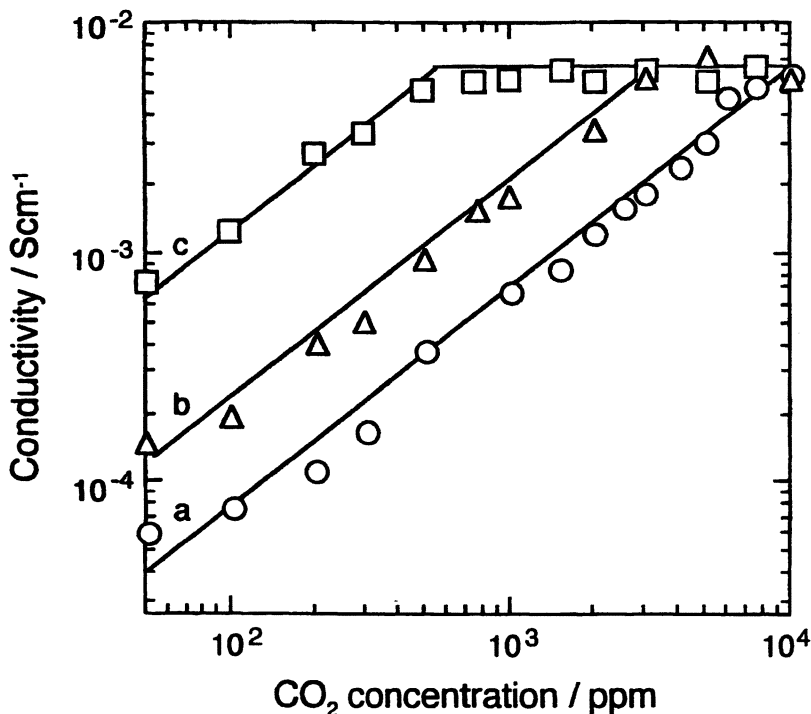
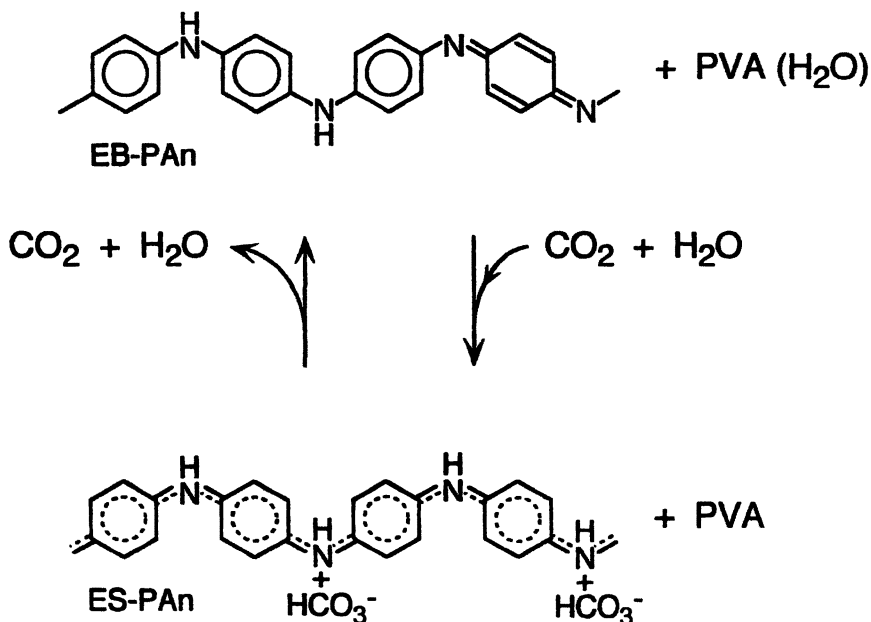


Figure 7. Dependence of electrical conductivity of a EB-PAN(14 wt%)/PVA (86 wt%) composite on the  $\text{CO}_2$  concentration at various humidities of (a) 30 %, (b) 50 %, and (c) 90%RH at 25 °C.

concentrations beyond 500 ppm. Interestingly, the slope of each straight line is independent of the humidity. These results mean that both  $\text{CO}_2$  concentration and humidity are involved directly in the variation of conductivity of the composite, and the  $\text{CO}_2$  sensing follows an identical scheme irrespective of the magnitude of humidity.

Based on these results, Scheme III by which the EB-PAN/PVA composite responds to  $\text{CO}_2$  molecules is proposed. In the absence of  $\text{CO}_2$ , the composite is insulating because EB-PAN is in the form of emeraldine base and no ionic species is present. In the addition of  $\text{CO}_2$  and humidity, however, carbonate ions are formed by the hydrolysis of  $\text{CO}_2$ , and the incorporation of these ions into EB-PAN leads to the generation of the emeraldine salt-type polyaniline (ES-PAN). The concentration of carbonate ions equilibrates with the concentration of the atmospheric  $\text{CO}_2$ , and the concentration of  $\text{CO}_2$  can be

Scheme III.



measured by monitoring the electrical conductivity of the composite. The EB-PAn/PVA composite does not respond to H<sub>2</sub>O, but once CO<sub>2</sub> coexists with H<sub>2</sub>O, the conductivity becomes dependent considerably on both concentrations of CO<sub>2</sub> and H<sub>2</sub>O. As shown in Figure 7, however, the slope of the log-log plot of electrical conductivity against the CO<sub>2</sub> concentration is a constant independent of humidity, and the contribution of the humidity to the total conductivity can be corrected without difficulty.

## References

1. MacDiarmid, A. G.; Epstein, A. J. *Faraday Discuss. Chem. Soc.* **1989**, *88*, 317-332.
2. Paul, E. W.; Ricco, A. T.; Wrighton, M. S. *J. Phys. Chem.* **1985**, *89*, 1441-1447.
3. Chiang, J. C.; MacDiarmid, A. G. *Synth. Met.* **1986**, *13*, 193-205.
4. Weiss, H.; Pfefferkorn, O.; Kotora, G.; Humphrey, B. D. *J. Electrochem. Soc.* **1989**, *136*, 3711-3714.
5. Inoue, M.; Navarro, R. E.; Inoue, M. B. *Synth. Met.* **1989**, *30*, 199-207.
6. Tzou, K.; Gregory, R. U. *Synth. Met.* **1993**, *53*, 365-377.
7. Hernandez, R.; Diaz, A. F.; Waltman, R.; Bargon, J. *J. Phys. Chem.* **1984**, *88*, 3333-3337.

8. Yue, J.; Epstein, A. J. *J. Am. Chem. Soc.* **1990**, *112*, 2800-2801.
9. Yue, J.; Wang, Z. H.; Cromack, K. R.; Epstein, A. J.; MacDiarmid, A. G. *J. Am. Chem. Soc.* **1991**, *113*, 2665-2671.
10. Toshima, N.; Yan, H.; Gotoh, Y.; Ishiwatari, M. *Chem. Lett.* **1994**, 2229-2232.
11. Ogura, K.; Shiigi, H.; Nakayama, M. *J. Electrochem. Soc.* **1996**, *143*, 2925-2930.
12. Ogura, K.; Saino, T.; Nakayama, M.; Shiigi, H. *J. Mater. Chem.* **1997**, *2*, 2363-2366.
13. Ogura, K.; Shiigi, H.; Nakayama, M.; Fujii, A. *J. Electrochem. Soc.* **1998**, *145*, 3351-3357.
14. Ogura, K.; Shiigi, H. *Electrochem. and Solid-State Lett.* **1999**, *2*, 478-480.
15. Bellamy, L. J. *The Infrared Spectra of Complex Molecules*, Chapman and Hall, London, 3rd ed., 1975; p.183.
16. Chan, H. S. O.; Ng, S. C.; Sim, W. S.; Tan, K. L.; Tan, B. T. G. *Macromolecules* **1992**, *25*, 6029-6034.
17. Tang, J.; Jing, X.; Wang, B.; Wang, F. *Synth. Met.* **1988**, *24*, 231-238.
18. Furukawa, Y.; Hara, T.; Hyodo, Y.; Harada, I. *Synth. Met.* **1986**, *16*, 189-198.

## Chapter 8

# Electrochemical Generation of Light in Conjugated Polymers

Danilo Dini<sup>1</sup>, Umamaheswari Janakiraman<sup>2</sup>, and Karl Doblhofer<sup>2</sup>

<sup>1</sup>Department of Chemistry, University of Rome "La Sapienza", p.le Aldo Moro 5, I-00185 Rome, Italy

<sup>2</sup>Fritz-Haber Institut der Max-Planck-Gesellschaft, Faradayweg 4-6, D-14195, Germany

Polyphenylene vinylene (PPV) and its derivatives represent the prototype systems for the realization of luminescent layers in electroluminescent LEDs. Recently they have been important in the development of light emitting electrochemical cells (LEC). The luminescent properties of the conducting polymer layer are determined not only the chemical species constituting the conducting polymer, but also the solid electrolyte of the electrochemical cell. In the present paper is reported a kinetics study of electrochemiluminescence (ECL) produced by 4-methoxy(2'ethylhexoxyl)-2,5-poly(phenylene vinylene), denoted herein as MEH-PPV, thin coatings when different electrochemical conditions are adopted. To our knowledge this represents one of the few critical studies on the features of ECL produced by polymer modified electrodes.

### Introduction

The emission of light induced by the application of an electric field in a conjugated molecule was reported for the first time in 1963 by C. Pope, *et al.*, who observed the electroluminescence (EL) produced by anthracene crystals sandwiched between Au and Na electrodes (1). The formation of light-emitting excited states in anthracene crystals was due to the recombination of the charge



carriers of opposite sign generated at the electrode/anthracene interfaces. The verification of EL thus indicated that crystals of conjugated molecules could be conducting due to the presence of mobile charge carriers. In 1977, after the discovery of conjugated polymers (CP) whose conductivity could be widely modulated in a controlled fashion (2), it was expected to be relatively easy matter to produce light from a CP through a mechanism of charge carrier recombination. As a matter of fact, it was only during 1990 that J.H. Burroughes *et al.* (3) reported on the possibility of producing EL from CPs, namely poly(p-phenylenevinylene) (PPV) derivatives, with the creation of the first organic light emitting diode (LED) based on a CP. A similar history can be traced for the progress of electrochemiluminescence (ECL), *i.e.*, the generation of light due to the occurrence of an electrochemical process from conjugated species. In fact, ECL with conjugated molecules was first reported in 1964 by Hercules (4) who showed the possibility of producing light during the electrolysis of rubrene and 9,10-diphenylanthracene in aprotic solvents. A gap of thirty years occurred before the appearance of the first report on ECL from a CP with the work of Richter, *et al.*, in 1994 (5). Once again the first CP that produced ECL was a PPV derivative, *i.e.*, 4-methoxy(2'-ethylhexoxyl)-2,5-poly(phenylenevinylene), hereafter indicated as MEH-PPV. The existence of such a gap is indicative of the difficulty in achieving polymeric materials with specific properties due to the problematic control of fundamental parameters such as molecular weight, chemical structure and molecular packing (6). PPV and its derivatives represent the prototype systems for the realization of luminescent layers in electroluminescent LEDs (7). Recently they have been in important in the development of light emitting electrochemical cells (LEC) (8,9). In these latter devices the luminescent properties of the CP layer are also determined by the chemical species constituting the solid electrolyte of the electrochemical cell. Such a feature is an interesting one because it can represent the starting point for the development of new electrochemical sensors whose response is the ECL produced as a consequence of CP interaction with the species dissolved in the electrolyte.

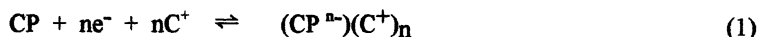
## Experimental

The synthesis of MEH-PPV has been accomplished according to the scheme presented in ref. (3). Due to the intrinsic insulating character of MEH-PPV in the pristine state (conductivity  $\sigma < 10^{-4}$  S cm<sup>-1</sup>), MEH-PPV must be deposited onto conductive electrodes to realize electrochemical redox processes. Thin films of MEH-PPV were deposited on Pt substrates by evaporation from a saturated MEH-PPV solution in xylene. The MEH-PPV film thickness was less than 10  $\mu$ m. The cell configuration was: MEH-PPV coated Pt substrate as the working electrode, Pt wires as the counter and quasi

reference electrodes. In all electrochemical experiments the electrolyte composition was 0.1 M tetraethylammonium tetrafluoroborate ( $\text{TEA}^+\text{BF}_4^-$ ) or tetraethylammonium hexafluorophosphate ( $\text{TEA}^+\text{PF}_6^-$ ) as supporting electrolytes (SE) in acetonitrile ( $\text{CH}_3\text{CN}$ ). The electrochemical experiments were carried out in an oxygen- and water-free atmosphere. The procedure for the purification of the solvent and electrolyte has been reported previously (11). Electrochemical measurements were accomplished with a homemade potentiostat. A Tektronix TDS 3014 digital oscilloscope was the data recorder. Potential pulses were applied to the cell by a Thandar TG 101 function generator via the potentiostat. The measurements of light intensity were accomplished by means of an RCA photomultiplier tube (type number 7326) polarized at -1200 V with a Keithley 246 high voltage supply.

## Results and discussion

The presence of an extended electronically conjugated network makes feasible the oxidation and/or reduction of a CP in an electrochemical cell by means of the application of a proper voltage. In fact, the existence of organic electrolytes possessing a sufficiently wide electrochemical stability combined with the polar character for the dissolution of SE allows the occurrence of electrochemically driven redox processes in CPs. These can be described as follows ( $e^-$ ,  $C^+$  and A represent, respectively, the elementary negative charge, a monovalent cation from SE, a monovalent anion from SE):



in the case of CP reduction and



in the case of CP oxidation.

When  $n = 1$ , a negative polaron  $p^-$  is formed in the CP (12). The negative polaron can be also identified as a mobile electron,  $e^-$ , if it is not necessary to consider the associated CP lattice distortion. When  $m = 1$  a positive polaron ( $p^+$ ) is formed and the polaron is a hole ( $h^+$ ). The further reduction (oxidation) of a negatively (positively) charged CP will lead to the formation of bipolarons  $bp^{2-}$  or  $bp^{2+}$  with  $n$  ( $m$ ) = 2 (13). From Equations (1) and (2) it is clear that an ionic complex between the reduced or oxidized CP and the charge compensating ion is formed. Therefore the reactions in Equations [1] and [2] involve the reversible exchange of ionic species between CP and the electrolyte as demonstrated by several techniques (14-16). The redox process in

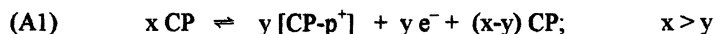
a CP is also called p doping or n doping, in analogy with the terminology adopted for inorganic semiconductors.

The general mechanism for the production of luminescence in Caps involves the following steps:

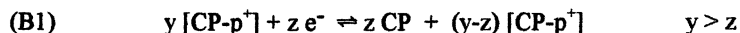
1. injection of electronic charge carriers with opposite signs into the polymer;
2. transport of the different electronic charge carriers within the polymer layer;
3. combination of the different electronic charge carriers;
4. formation of excited electronic states as a consequence of the step 3;
5. radiative decay from the excited electronic states.

In the present work the emission of ECL from MEH-PPV has been produced by stepping of the substrate potential between the values corresponding to the polymer oxidation and reduction (see Figure 1). This procedure allows the sequential injection of the different electronic charge carriers inside the polymeric layer only from the interface polymer/metal substrate. The opposite polymer/electrolyte interface will be thus involved solely in the insertion/expulsion of the ions compensating the polymeric charge. ECL from conjugated polymers is produced according to the following series of reactions:

1. Electrochemical formation of  $p^+$  in the conjugated polymer CP at a fixed value of anodic potential  $E^+$ , i.e.



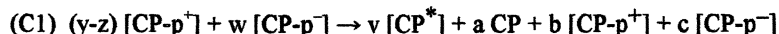
2. Electrochemical reduction of  $[\text{CP-p}^+]$  and the fraction of CP not oxidized in the first anodic step at a fixed value of cathodic potential  $E^-$ , i.e.



and

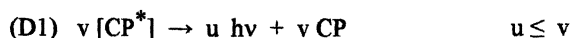


3. Chemical recombination of the species  $[\text{CP-p}^+]$  and  $[\text{CP-p}^-]$  produced respectively in the steps 1 and 2 with consequent formation of excited species  $[\text{CP}^*]$ , i.e.

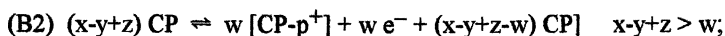
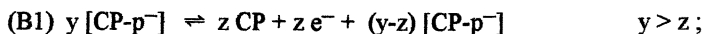
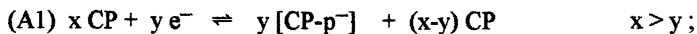


$$v \leq (y-z+w)/2 \quad \text{and} \quad (a+b+c) = (y-z+w-v)$$

4. Decay of  $[CP^*]$  with consequent emission of cathodic {anodic} ECL, i.e.



An analogous series of steps can be written for the n-doped polymer:



$$v \leq (y-z+w)/2 \quad \text{and} \quad (a+b+c) = (y-z+w-v)$$

For sake of simplicity the ionic exchanges associated with the processes of charge compensation have not been shown in the Equations (A1), (B1), (B2) and (C1). It will be shown that charge compensation is the primary factor in determining the kinetics of ECL emission and, in the first approximation, the possible effect of the nature of the charge compensating ion upon the emission efficiency of the electroactive polymer is neglected.

The cyclic voltammetry of MEH-PPV (Figure 1) shows the concomitant reversibility of both electrochemical processes of oxidation and reduction in MEH-PPV. Such features represent the first necessary condition for attainment of ECL as previously verified in the case of ECL produced by dissolved species (17). The electrochemical formation of the excited emitting states in PPV by means of the double potential step procedure is presented in Figure 2. The kinetics of anodic and cathodic ECL from MEH-PPV are reported in Figure 3 when  $SE=0.1$  M TEABF<sub>4</sub>. The kinetics differ in that cathodic ECL onset is delayed with respect to the potential switching at  $t=0$  s. Moreover the cathodic ECL has a sudden increase followed by a relatively fast decay in 0.5 s, whereas the anodic ECL increases gradually with time and reaches a constant value which holds for several seconds. The corresponding current transients (not shown here) are very similar for both anodic and cathodic ECL profiles, being characterized by a decay to zero in less than 0.2 s. The lack of correspondence between the time-profile of the injected charge in MEH-PPV and ECL profiles is indicative of light emission kinetics which is controlled by the rates of transport processes inside the CP (18). The rate of the latter is determined by the coupled movement of electronic and ionic carriers and an analysis of the experimental data of Figure 3 should account for the combination of electron

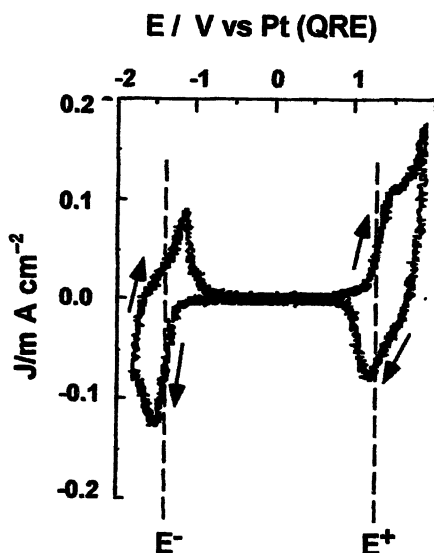


Figure 1. Cyclic voltammetry of an MEH-PPV coated Pt electrode; the electrolyte is 0.1 M TEABF<sub>4</sub> in CH<sub>3</sub>CN (scan rate: 100 mV s<sup>-1</sup>).

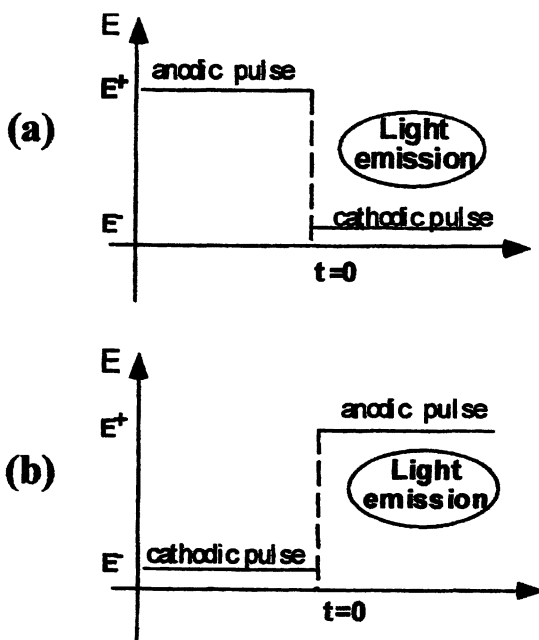


Figure 2. Potential step generating (a) cathodic and (b) anodic ECL.

hopping with the displacement of the charge compensating ion (19-21). The use of a different SE confirms the determining role of SE nature upon ECL kinetics of MEH-PPV, as verified when  $SE = 0.1 \text{ M TEAPF}_6$  (Figure 4). In the latter case anodic and cathodic ECL kinetics are qualitatively similar for the presence of a delay before ECL onset thus resembling the ECL kinetics of Figure 3(b). It seems that the existence of ECL onset delay can be associated with the movement of charge-compensating ionic species, being slower for ions of larger sizes, i.e.  $TEA^+$  [kinetics of Figures 3(b) and 4(b)] and  $PF_6^-$  [kinetics in Figure 4(a)]. In fact, only in the case of anodic ECL with  $TEABF_4$  (Figure 4a) in which, presumably, the smaller species  $BF_4^-$  should be intercalated inside MEH-PPV, the delay of ECL onset is not observed. This consideration leads to the conclusion that ionic diffusion inside the CP is a major factor in the control of  $p^+ - p^-$  recombination for the formation of excited polymeric species [Equation C1].

The kinetics of ECL depends also on the extent of oxidation or reduction which is achieved in the CP at the defined value of applied potential. The application of potential values leading to the formation of bipolarons in the CP inhibits the generation of excited species (Figure 5). This is because it is less probable to generate an excited state from bipolarons than for the bipolarons to recombine (22). Another ECL suppressing effect is the application of a potential step before the completion of ECL emission. In this latter case the occurrence of an electrochemical process involving excited species would lead to the elimination of the active emitting entities as observed with the quenching of ECL in Figure 6.

## Conclusions

In the present work we have shown that long-lived electrochemically generated chemiluminescence from conjugated polymers can be achieved using liquid electrolytes. Both anodic and cathodic ECL generated by a CP modified electrode, namely MEH-PPV, are reported when appropriate electrochemical conditions are adopted and an adequate degree of purity for the active polymer, solvent and supporting electrolyte is achieved. The emissive efficiency is generally higher during the anodic polarizations of MEH-PPV. The time-dependence of ECL is a function of the nature of the counter ion compensating the polymer charge. Such a finding leads to the conclusion that ionic movement is the main factor in controlling the rate of production of light emitting entities through the recombination of charge carriers with opposite signs.

## Acknowledgements

Prof. Andrew B. Holmes and Dr. Rainer E. Martin (Melville Laboratory, Department of Chemistry, University of Cambridge, England) are gratefully acknowledged for having provided the starting material for the electrochemiluminescence experiments.

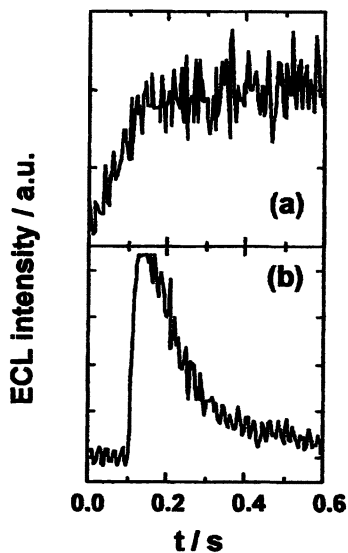


Figure 3. Electrochemiluminescence for MEH-PPV when potential is stepped between  $E^+ = 1.45 \text{ V}$  and  $E^- = -1.75 \text{ V}$  vs Pt (QRE). (a) anodic; (b) cathodic. Supporting electrolyte:  $0.1 \text{ M TEABF}_4$

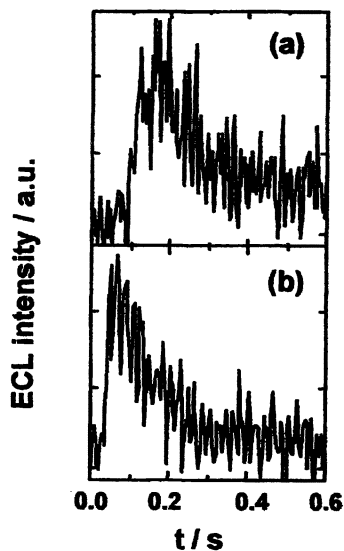


Figure 4. Electrochemiluminescence for MEH-PPV when potential is stepped between  $E^+ = 1.35 \text{ V}$  and  $E^- = -1.80 \text{ V}$  vs Pt (QRE). (a) anodic; (b) cathodic. Supporting electrolyte:  $0.1 \text{ M TEAPF}_6$

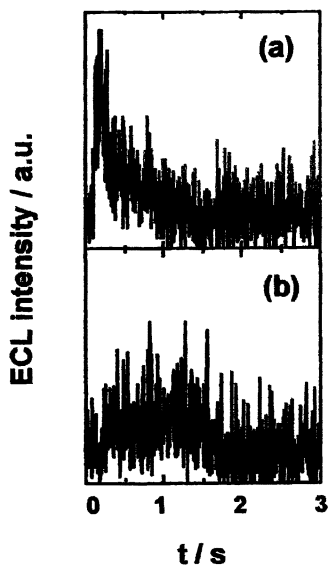


Figure 5. Anodic electrochemiluminescence for MEH-PPV when final potential is  $E^+$  = (a) 1.2 V and (b) 1.30 V vs Pt (QRE). (a) anodic; (b) cathodic. Supporting electrolyte: 0.1 M TEAPF<sub>6</sub>

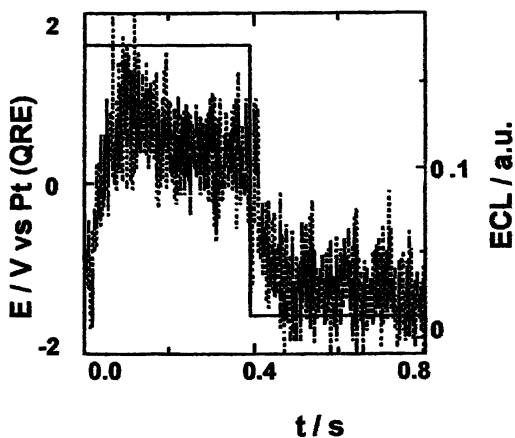


Figure 6. Effect of polarization change during anodic ECL (dotted line) when potential  $E$  (solid line) is stepped back to  $E^-$ . Supporting electrolyte: 0.1 M TEABF<sub>4</sub>



## References

1. Pope, M.; Kallmann, H.; Magnante, P. *J. Chem. Phys.* 1963, 38, 2042.
2. Shirakawa, H.; Louis, E.J.; MacDiarmid, A.G.; Chiang, C.K.; Heeger, A.J. *Chem. Commun.* 1977, 578.
3. Burroughes, J.H.; Bradley, D.D.C.; Brown, A.R.; Marks, R.N.; Mackay, K.; Friend, R.H.; Burns, P.L.; Holmes, A.B. *Nature* 1990, 347, 539.
4. Hercules, D.M. *Science* 1964, 145, 808.
5. Richter, M.M.; Fan, F.R.F.; Klavetter, F.; Heeger, A.J.; Bard, A.J. *Chem. Phys. Lett.* 1994, 226, 115.
6. Feast, W.J. In *Handbook of Conducting Polymers*; Skotheim, T.A., Ed.; Marcel Dekker: New York, 1986; vol.1, pp 1-44.
7. Kraft, A.; Grimsdale, A.C.; Holmes, A.B. *Angew. Chem.* 1998, 110, 417.
8. Pei, Q.; Yu, G.; Zhang, C.; Yang, Y.; Heeger, A.J. *Science* 1995, 269, 1086.
9. De Mello, J.C.; Tessler, N.; Graham, S.C.; Li, X.; Holmes, A.B.; Friend, R.H. *Synth. Met.* 1997, 85, 1277.
10. Nambu, H.; Hamaguchi, M.; Yoshino, K. *J. Appl. Phys.* 1997, 82, 1847.
11. Dini, D.; Doblhofer, K.; Ertl, G. *Phys. Chem. Chem. Phys.* 2000, 2, 1183.
12. Heeger, A.J.; Kivelson, S.; Schrieffer, J.R.; Su, W.P. *Rev. Mod. Phys.* 1988, 60, 781
13. Chance, R.R.; Bredas, J.L.; Silbey, R. *Phys. Rev. B* 1984, 29, 4491.
14. Dini, D.; Decker, F.; Zotti, G. *Electrochem. Solid St. Lett.* 1998, 1, 217.
15. Dini, D.; Decker, F.; Zotti, G.; Schiavon, G.; Zecchin, S.; Andreani, F.; Salatelli, E. *Chem. Mat.* 1999, 11, 3484.
16. Glenis, S.; Benz, M.; Le Goff, E.; Kanatzidis, M.G.; De Groot, D.C.; Schlinder, J.L.; Kannewurf, C.L. *Synth. Met.* 1995, 75, 213.
17. Rosenmund, J.; Doblhofer, K. *J. Electroanal. Chem.* 1995, 396, 77.
18. Pei, Q.; Yang, Y.; Yu, G.; Zhang, C.; Heeger, A.J. *J. Am. Chem. Soc.* 1996, 118, 3922.
19. Andrieux, C.P.; Saveant, J.M. *J. Phys. Chem.* 1988, 92, 6761.
20. Saveant, J.M. *J. Electroanal. Chem.* 1986, 201, 211.
21. Buck, R.P. *J. Electroanal. Chem.* 1986, 210, 1.
22. Pope, M.; Swenberg, C.E. *Electronic Processes in Organic Crystals and Polymers*; Monographs on the Physics and Chemistry of Materials 56; Oxford Science Publications: New York, 1999; 2nd edition.

## Chapter 9

# Photoelectrochemical Behavior of *p*-ATP/PANI Film and Nanoparticulate *p*-ATP/PANI/TiO<sub>2</sub> Film on Au Electrodes

Jin Luo<sup>1,2</sup>, Huaiguo Huang<sup>2</sup>, Zhonghua Lin<sup>2</sup>, and Maria Hepel<sup>1,\*</sup>

<sup>1</sup>Department of Chemistry, State University of New York at Potsdam, Potsdam, NY 13676

<sup>2</sup>State Key Laboratory for Physical Chemistry of the Solid Surface, Department of Chemistry, Xiamen University, Xiamen 361005, China

New multi-layer film electrodes for solar energy conversion applications, PANI (polyaniline) films on Au/*p*-ATP (*p*-aminothiophenol) substrates, and nano-particulate Au/*p*-ATP/PANI/TiO<sub>2</sub> films were prepared by electrochemical methods. The behavior and properties of Au/*p*-ATP, Au/*p*-ATP/PANI and Au/*p*-ATP/PANI/TiO<sub>2</sub> films were investigated by means of photocurrent spectroscopy and electrochemical quartz crystal nanobalance (EQCN) technique. Both cathodic and anodic photocurrents, generated in Au/*p*-ATP/PANI and Au/*p*-ATP/PANI/TiO<sub>2</sub> films upon illumination in different potential regions, were observed. The photocurrent spectra for Au/*p*-ATP/PANI film electrodes show a sub-bandgap excitation and follow the Fowler's rule. A model based on internal photoemission at semiconductor covered metal is proposed to describe the observed phenomena. The photocurrent spectra of nano-particulate Au/*p*-ATP/PANI/TiO<sub>2</sub> films show photoelectrochemical characteristics of both TiO<sub>2</sub> and PANI films. The wavelength region of the photocurrent generation in Au/*p*-ATP/PANI/TiO<sub>2</sub> films covers violet and red light regions.

## Introduction

Titanium dioxide is an important electrode material in semiconductor photoelectrochemistry. Much research has been focused on improving the conversion efficiency of solar energy using cells based on  $\text{TiO}_2$  in the anatase or rutile form (1-7).  $\text{TiO}_2$  nano-particulate film electrodes exhibit size-dependent optical and electronic properties, which differ from compact semiconductor electrodes. There are two processing routes for preparing nano-particulate semiconductor film electrodes. In the first approach, semiconductor particles are applied to a conducting substrate from a suspension and then sintered to form an electrical contact between the semiconductor particles and the substrate (8). In the second approach, semiconductor nano-particles are formed directly onto the substrate by an electrochemical or chemical deposition process (4, 5, 9). The nano-particulate semiconductor electrodes distinguish themselves by their porosity and high surface-to-volume ratio. The photosensitization of wide bandgap semiconductors by adsorbed dyes has been studied since the late 1960s. For  $\text{TiO}_2$ , the best charge transfer sensitizer investigated so far is  $\text{RuL}_2(\text{SCN})_2$  (L = 2, 2' - bipyridyl - 4, 4' - dicarboxylate). It accomplishes close to quantitative photon to electron conversion over the whole visible range (10). However, the conversion efficiencies in red light region are still lower than that in violet region.

Polyaniline (PANI) is one of the most extensively investigated polymers because of its high electrical conductivity in combination with good stability, ease of preparation, low cost of the monomer, and potential technological applications in batteries, electrochromic devices, and sensors (11-15). The fully reduced polyaniline (leucoemeraldine base) is an insulator whose large energy gap originates predominantly from extrinsic effects involving the overlap of molecular orbitals of neighboring phenyl rings and nitrogens (16). The presence of amine ( -NH- ) groups allows chemical flexibility so that other electronic states of the polymer can be obtained by removal of protons or hydrogen atoms, as well as electrons, from the polymer. These other forms of polyaniline are determined by the fraction of imine ( -N= ) nitrogens per four-ring repeat unit, which is labeled 1-y. The fully oxidized polyaniline (pernigraniline base, 1-y = 1) is also an insulator. The partially-oxidized polyaniline (emeraldine base, 1-y  $\cong$  0.5) has a good conductivity when protonated (14, 17). The models explaining conductivity of polyaniline involve mainly the "electron hopping assisted by proton exchange" model (18) and the granular metal island model (11, 19-21). Recent studies (16, 22, 23) have shown that emeraldine base has a broad absorption centered at 2 eV (the "exciton" band), an absorption band at  $\sim$  3.6 eV (the  $\pi$ - $\pi^*$  bandgap), and some absorption bands in the range from 0.9 to 3.0 eV (0.9 eV, 1.45 eV, 2.95 eV) which can be assigned to the formation of polarons within the gap. The bandgap for electrodeposited PANI, 2.85 eV, was determined by the Kubelka-Munk function (13). The PANI films prepared under

different conditions may have different band structures. Genies and coworkers (24, 25) discovered that PANI has a very fast photoresponse. Both cathodic and anodic photocurrent responses caused by the change in potentials have been observed for PANI films (26, 27). In comparison to Pt, PANI is a superior electrocatalyst for the reduction and oxidation of  $\text{Fe}(\text{CN})_6^{3-/4-}$  in acidic media (28). Recently, some photoelectrochemical studies on polyaniline growth, conductive properties, anion insertion and expulsion in polyaniline have been reported (12, 14). Maia and coworkers (14) proposed a model for charge carriers moving in response to the illumination of the PANI film with energy higher than bandgap energy. However, the wavelength distribution of photocurrents for PANI films has not been reported.

It is generally accepted that the electronic conductivity of PANI is limited by structural discontinuities and that the electrochemical performance is governed by morphological factors. A recent approach to studying electrochemical interactions at metal-organic interfaces involves the use of self-assembled monolayers (SAMs). An organized monolayer of thiols can be formed on a gold substrate by the self-assembly of thiol molecules through the strong coordination of mercapto groups to Au. PANI grown on Au/*p*-aminothiophenol (*p*-ATP) substrates is considerably denser than PANI grown on bare Au electrodes (29).

In this paper, we have developed new multi-layer film electrodes for solar cell application, composed of PANI and PANI/TiO<sub>2</sub> films deposited on Au/*p*-ATP substrates. Further investigations involved photoelectrochemistry and mechanism of photocurrent generation in these electrodes.

## Experimental

### Chemicals

Reagent-grade *p*-ATP (*p*-Aminothiophenol or 4-Aminothiophenol, 90%) was obtained from Aldrich Chemical Company and was used without further purification. Other reagents used in the experiments were of analytical reagent quality. Solutions were prepared using deionized water purified by a Milli-Pore Milli-Q purification system.

### Apparatus

The electrochemical experiments were carried out using a computer controlled electrochemical workstation (Model 660, CH Instruments). The Electrochemical Quartz Crystal Nanobalance (ELCHEMA EQCN-700) was used to measure the effective mass changes of the electrode. 10 MHz optically polished gold electrodes were used as substrates for films formation. For photocurrent monitoring, a homemade UV-Vis combined spectro-electrochemical measurement system was used. The light source was a 150 W Xe lamp with a high-throughput monochromator (ARC SpectraPro-275). The incident intensity was calibrated using a Rk-5710 power radiometer (LaserProbe

Inc.) with a RkP575 probe and a RkP576a probe. High resolution SEM (model S-520, Hitachi) was used to determine the size of TiO<sub>2</sub> nanoparticles.

### Film Preparation

*p*-ATP monolayers were prepared on Au polycrystalline electrodes after the appropriate surface treatment (30). Our previous studies (31) have shown that the adsorbed *p*-ATP molecules assume perpendicular orientation on a gold surface. A polyaniline film on such an ordered Au/*p*-ATP substrate was obtained by cycling the electrode potential 125 times between -0.2 and 0.7 V in solution of 1.0 mM aniline + 1 M HClO<sub>4</sub>. The oxidized, partially-oxidized, and reduced states of PANI films were obtained by applying the electrode potential of 1.00 V, 0.35 V, and -0.40 V for 10 minutes in 1 M HClO<sub>4</sub> aqueous solution, respectively. The electrode was rinsed with a large volume of deionized water and dried with N<sub>2</sub> gas. The resulting PANI film showed good adherence to the Au/*p*-ATP electrode.

The TiO<sub>2</sub> films on Au/*p*-ATP/PANI were obtained by electrodeposition. The cleaned Au/*p*-ATP/PANI electrode (in a partially-oxidized state) was biased at 0.1 V for 30 minutes in 0.05 M TiCl<sub>3</sub> solution which was adjusted to a pH of 2.2 with a deaerated solution of NaOH. The obtained Ti(IV) polymer film was carefully washed with deaerated 0.01 M HCl and ethanol and dried at room temperature in order to form a TiO<sub>2</sub> film.

All the potentials were measured and are quoted with respect to the saturated calomel electrode (SCE). The experiments were performed at room temperature (~20 °C).

## Results and Discussion

### Formation of Au/*p*-ATP Monolayer on Au

The effective mass-time transient recorded during the *p*-ATP self-assembly on a Au surface is presented in Figure 1. The total mass increase,  $\Delta m_{\text{PATP}}$ , which is due to the adsorption of *p*-ATP on Au was 25 ng, which corresponds to  $n_{\text{PATP}} = \Delta m_{\text{PATP}} / M_{\text{PATP}} = 0.200$  nmoles ( $M_{\text{PATP}} = 125.19$ ). The real surface area of the Au electrode in the EQCN cell,  $A_{\text{Au}}$ , is 0.25 cm<sup>2</sup>, while the number of adsorbed *p*-ATP molecules is  $\Gamma_{\text{PATP}} = 6.022 \times 10^{23} \times n_{\text{PATP}} / A_{\text{Au}} = 4.81 \times 10^{14}$  molecules/cm<sup>2</sup>. The cross-sectional area of a *p*-ATP molecule (30) is  $A_{\text{PATP}} \cong (0.43 \text{ nm})^2 = 1.85 \times 10^{-15}$  cm<sup>2</sup>. If *p*-ATP is adsorbed on Au as a monolayer, the number of *p*-ATP molecules is  $\Gamma_{\text{mono, PATP}} = 1 / A_{\text{PATP}} = 5.41 \times 10^{14}$  molecules/cm<sup>2</sup>.  $\Gamma_{\text{PATP}}$  is almost in agreement with  $\Gamma_{\text{mono, PATP}}$ . It is shown that a *p*-ATP monolayer can be obtained on the Au electrode after 100 seconds.

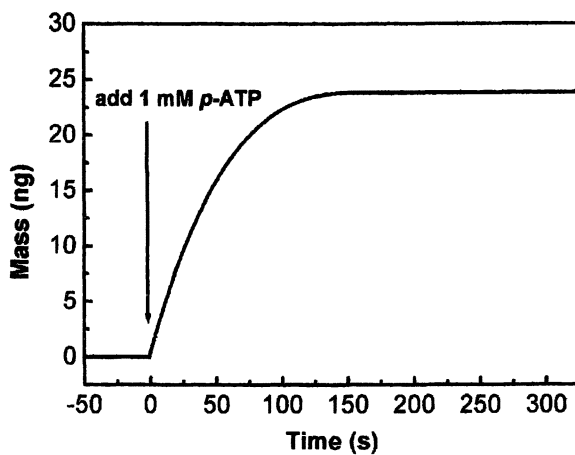


*Figure 1. Apparent mass change vs time transient for p-ATP adsorption on Au by self-assembly from 1 mM p-ATP ethanol solution.*

### Formation and Photoelectrochemical Behavior of PANI Film on Au/p-ATP Substrate

The gradual changes of *i-E* and *m-E* characteristics during the formation of polyaniline film on the Au/p-ATP substrate in a potential cycling experiment are shown in Figure 2. After the first cycle, the total mass increase at  $E = -0.2$  V,  $\Delta m_{LB1}$ , is 48 ng, which corresponds to the mass increase of a reduced PANI

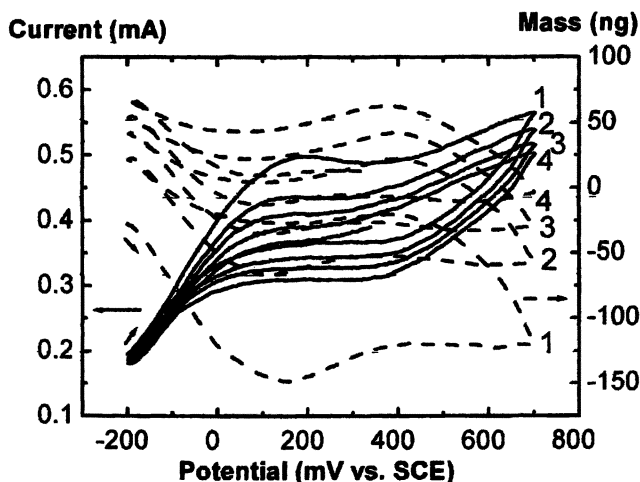


Figure 2. Variation of the current-potential (solid line) and apparent mass-potential (dashed line) characteristics during PANI film formation on an ordered Au/p-ATP substrate in 1 mM aniline + 1 M HClO<sub>4</sub> aqueous solution (1: first cycle; 2: second cycle; 3: third cycle; 4: fourth cycle). Sweep rate: 100 mV/s.

(leucoemeraldine,  $[-(C_{24}H_{20}N_4)_x-]$ ) (22). It can be estimated that the number of deposited leucoemeraldine molecules ( $M_{LB} = 364.45$ ) is  $x_{LB1} = 6.022 \times 10^{23} \times \Delta m_{LB1} / (M_{LB} \times A_{Au}) = 3.17 \times 10^{14}$  molecules/cm<sup>2</sup>. Similarly, the number of deposited leucoemeraldine molecules is  $1.12 \times 10^{14}$  molecules/cm<sup>2</sup>,  $0.99 \times 10^{14}$  molecules/cm<sup>2</sup>, and  $0.99 \times 10^{14}$  molecules/cm<sup>2</sup>, in the second, third and fourth cycle, respectively. It is seen that the rates of polyaniline formation remain approximately constant after the second cycle. There is a difference between the mass of PANI in the reduced and oxidized state, which is caused by the water / anions insertion. After cycling the electrode potential 125 cycles, the number of molecules of the leucoemeraldine base formed is ca.  $1.3 \times 10^{16}$  molecules/cm<sup>2</sup>. The thickness of polyaniline films obtained after 125 cycles was approximately 0.05  $\mu$ m, as estimated from the EQCN and cyclic voltammetric data (cf. Ref. 32). Cyclic voltammetric measurements utilizing the electron transfer probe of Fe(CN)<sub>6</sub><sup>3-/4-</sup> show that the conductivity of PANI films is dependent on the state of oxidation and the insertion of ClO<sub>4</sub><sup>-</sup> ions. It has been found that the

partially oxidized PANI polymer film on ordered Au/*p*-ATP substrate has a good electron transfer characteristic.

For all of the three forms (oxidized \ partially-oxidized \ reduced states) of PANI films, both cathodic and anodic photocurrents were observed in different potential regions in a 0.05M Fe(CN)<sub>6</sub><sup>3-</sup>/ Fe(CN)<sub>6</sub><sup>4-</sup> solution as shown in Figure 3.

The partially-oxidized PANI film shows a high photoelectrochemical activity. Figure 4 presents the photocurrent spectra of the partially-oxidized and reduced PANI films on Au/*p*-ATP in the same 0.05M Fe(CN)<sub>6</sub><sup>3-</sup>/ Fe(CN)<sub>6</sub><sup>4-</sup> solution. The incident-photon-to-current efficiencies (IPCE) are defined by the equation:

$$\text{IPCE} = jhc/\lambda Pe \quad (1)$$

where *j* is the photocurrent density, *h* is the Planck constant, *c* is the velocity of light, *λ* is the wavelength, *P* is the light power, and *e* is the elemental charge. The photocurrent spectrum of the oxidized PANI film was not obtained because of the weak photocurrent signal. As shown in Figure 4, the anodic and cathodic photocurrents extend from 450 nm to 760 nm (1.6 eV-2.8 eV). There are tails observed at long wavelength regions of the photocurrent peaks. They indicate that both partially-oxidized and reduced PANI films show the characteristics of sub-bandgap photocurrent spectra.

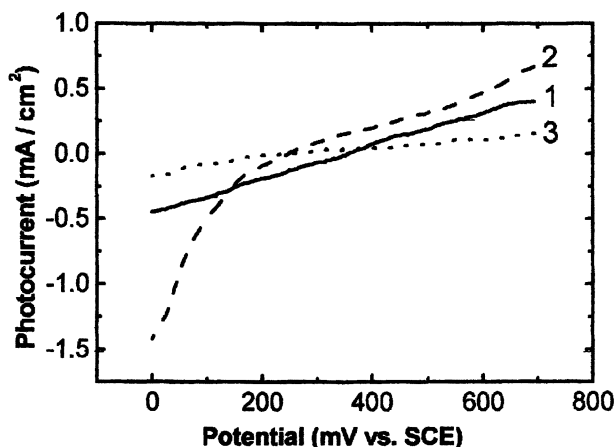
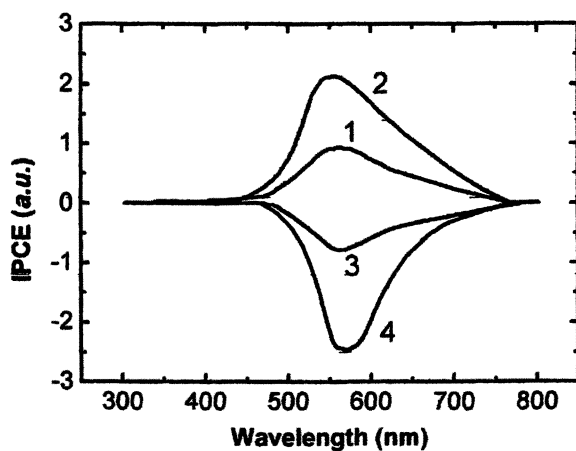


Figure 3. The potential dependence of the photocurrent for (1) reduced state, (2) partially-oxidized state and (3) oxidized state of PANI film on ordered Au/*p*-ATP substrate in 0.05 M K<sub>3</sub>Fe(CN)<sub>6</sub>/ K<sub>4</sub>Fe(CN)<sub>6</sub> aqueous solution under illumination of a Xe lamp without filtering. Sweep rate: 5 mV/s.





*Figure 4. Photocurrent spectra of a PANI film on an ordered Au/p-ATP substrate in 0.05M  $K_3Fe(CN)_6 / K_4Fe(CN)_6$  aqueous solution.*

*(1) reduced PANI film at 0.7 V; (2) partially-oxidized PANI film at 0.7 V;  
(3) reduced PANI film at 0 V; (4) partially-oxidized PANI film at 0 V.*

To explain the conductivity of polyaniline, the granular metal island model has been used (19-21). In this model, fully protonated metallic regions are isolated by unprotonated (insulating or semiconducting) regions in polyaniline. A photoelectrochemical model of internal photoemission at semiconductor covered metal may be invoked to interpret the photocurrent behavior of PANI films on Au/*p*-ATP (33-35). Based on a granular metal island model for polyaniline, the Fowler plots ( $IPCE^{1/2} \sim h\nu$ ) are obtained from the photocurrent spectra of partially-oxidized Au/*p*-ATP/PANI film and are displayed in Figure 5. The functional form appears to be linear and the photocurrent onset wavelengths can be obtained by extrapolation. Linear Fowler plots are indicative

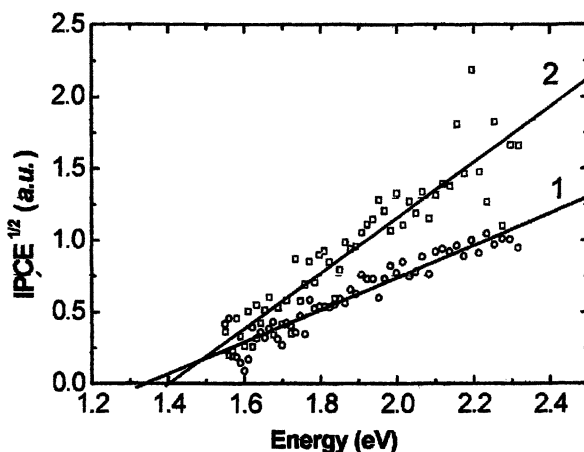


Figure 5. Fowler plots of the photocurrent data for (1) anodic photocurrent and (2) cathodic photocurrent of the PANI film on ordered Au/*p*-ATP substrate in 0.05M  $K_3Fe(CN)_6 / K_4Fe(CN)_6$  aqueous solution. Extrapolated photocurrent onsets indicate the energy barrier difference between the Fermi level of metallic region and the conduction band (cathodic photocurrent) or the valence band (anodic photocurrent) of semiconducting region in PANI film.

(Reproduced with permission from reference 10. Copyright 2000.)

of the internal photoemission of holes or electrons from the metallic region of PANI into the appropriate electronic band of the semiconducting region. The onset energy indicates a minimum energy required for the promotion of an electron (hole) from the Fermi level of metallic region to the conduction band (valence band) of semiconducting region. From Figure 5, the onset energies of photoelectron emission and photohole emission are 1.40 eV and 1.34 eV,

respectively. The sum of the onset minima for anodic and cathodic photocurrents should approximate the bandgap energy of the semiconducting region of polyaniline, presuming the Fermi level of metallic region does not shift with respect to the band edges of semiconducting region as a function of the applied bias. This is approximately correct for the PANI films given the determination of an indirect bandgap at about 2.74 eV. This bandgap is close to the absorption band (3.0 eV) of polyaniline (22). Thus, for the PANI on Au/*p*-ATP, the Fermi level position of the metallic region would be about 1.34 eV above the valence band of semiconducting region (Figure 6). The photocurrent was not detected when incident light energy was larger than the bandgap (2.74 eV). This might be due to the existence of powerful recombination sites, such as the polaron energy band, in the bandgap.

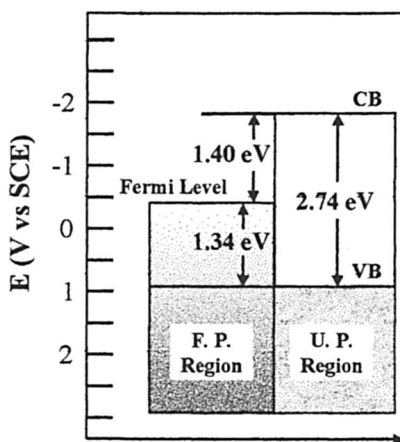


Figure 6. Energy band diagram for the metal island model of granular polyaniline film. CB: conduction band; VB: valence band; F. P. Region: fully protonated (metallic) region; U. P. Region: Unprotonated (semiconducting) region.

### Photoelectrochemical Behavior of PANI/TiO<sub>2</sub> Film on Au/*p*-ATP Substrate

The SEM images of the nano-particulate TiO<sub>2</sub> film prepared on the Au/*p*-ATP/PANI film and on the bare Au electrode were shown in our previous paper (36). They show that the nano-particulate TiO<sub>2</sub> film formed on Au/*p*-ATP/PANI is denser than the nano-particulate TiO<sub>2</sub> film formed on a bare Au. The size of the TiO<sub>2</sub> particles is approximately 200 nm.

The photocurrent response of a PANI/TiO<sub>2</sub> film on Au/*p*-ATP substrate (Figure 7) shows that composite Au/*p*-ATP/PANI/TiO<sub>2</sub> films also generate both the anodic and cathodic photocurrents in different potential regions. Comparing with the photocurrent of the Au/*p*-ATP/PANI film, the anodic photocurrent of the Au/*p*-ATP/PANI/TiO<sub>2</sub> film is higher and the cathodic photocurrent is lower. It confirms that the nano-particulate TiO<sub>2</sub> film is an n-type semiconductor.

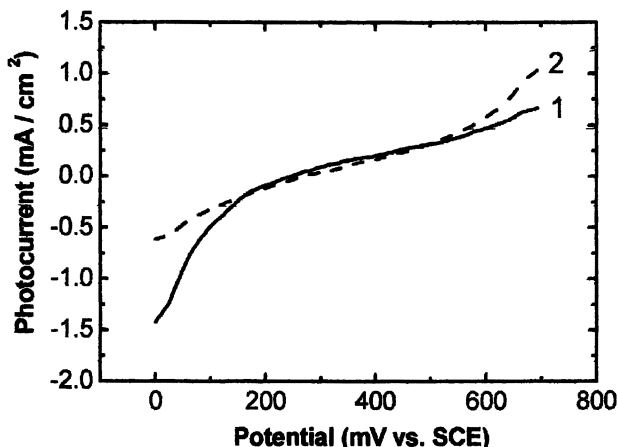


Figure 7. Photocurrent vs potential dependence for (1) the PANI film and (2) the PANI/TiO<sub>2</sub> film on ordered Au/*p*-ATP substrate in 0.05M K<sub>3</sub>Fe(CN)<sub>6</sub> / K<sub>4</sub>Fe(CN)<sub>6</sub> aqueous solution under illumination of a Xe lamp without filtering.

The photocurrent spectra of a composite Au/*p*-ATP/PANI/TiO<sub>2</sub> film in 0.05M Fe(CN)<sub>6</sub><sup>3-</sup> / Fe(CN)<sub>6</sub><sup>4-</sup> solution are shown in Figure 8. In contrast to the Au/*p*-ATP/PANI films, there are two anodic photocurrent peaks appearing in the anodic photocurrent spectrum (Figure 8a). It is obvious that the peak at 300~400 nm (3.1~4.1 eV) is related to the direct inter-band transition originated in TiO<sub>2</sub> particles and the peaks at 450~760 nm (1.6~2.8 eV) are related to the subband-gap transition originated in the PANI species. The photocurrent spectrum for the composite Au/*p*-ATP/PANI/TiO<sub>2</sub> film is an overlap of that for a pure TiO<sub>2</sub> film and a PANI film.

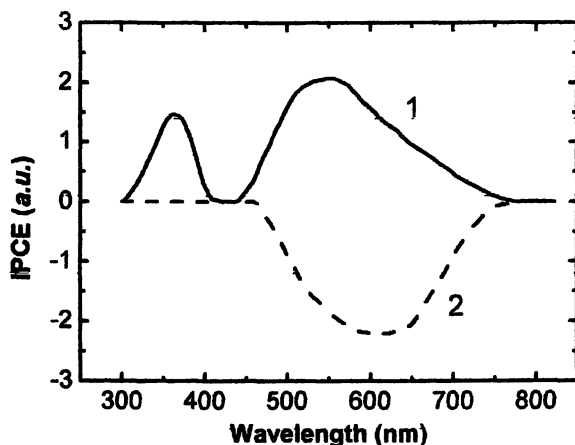


Figure 8. Photocurrent spectra of the PANI/TiO<sub>2</sub> film on ordered Au/p-ATP substrate at (1) 0.7 V and (2) 0 V in 0.05M K<sub>3</sub>Fe(CN)<sub>6</sub> / K<sub>4</sub>Fe(CN)<sub>6</sub> aqueous solution.

The photoelectrochemical behavior of the composite Au/p-ATP/PANI/TiO<sub>2</sub> film can be ascribed to the porosity of the nano-particulate TiO<sub>2</sub> film. For a lightly doped semiconductor particle, an internal electrostatic field is not necessary for separation of the photogenerated electron-hole pairs and to transport carriers in the particle toward the particle-solution interface by diffusion. In this case, the process of charge separation is controlled by the interfacial dynamics at semiconductor particles-solution interface, the applied electric field and the carrier concentration gradients. We assume that the solution can penetrate through the nano-particulate TiO<sub>2</sub> film (see also Peter and coworkers (9)). Both the TiO<sub>2</sub> particles and PANI species are thus in contact with the solution and can generate electron-hole pairs under illumination with the UV/Vis light. At the potential of 0.7 V, the photogenerated electrons in both TiO<sub>2</sub> particles and PANI species traverse through the interconnected aniline chains to the gold substrate, where they are withdrawn as anodic photocurrents in wavelength regions of 300–400 nm and 450–760 nm. At the potential of 0 V, only PANI species can generate electron-hole pairs under illumination of the UV/Vis light. Under influence of the applied electric field, the photogenerated electrons in PANI species transport to the PANI-solution interface or traverse through the interconnected TiO<sub>2</sub> particles to the TiO<sub>2</sub> particles-solution interface to reduce oxidized species in the solution, and photogenerated holes in PANI

species traverse through the interconnected aniline chains to the gold substrate, where they are withdrawn as cathodic photocurrents in wavelength regions of 450–760 nm. In comparison to the pure TiO<sub>2</sub> film and the PANI film prepared under the same conditions, the Au/*p*-ATP/PANI/TiO<sub>2</sub> film widens the wavelength region for solar energy conversion and has a better adherence to the Au substrate. It is, therefore, expected that this kind of film should have a higher photoelectrochemical conversion efficiency.

## Conclusion

The photoelectrochemical behavior of Au/*p*-ATP/PANI and Au/*p*-ATP/PANI/TiO<sub>2</sub> films was investigated. PANI films were formed on well-ordered Au/*p*-ATP substrates. The monolayer coverage of *p*-ATP on Au,  $\Gamma_{\text{PATP}} = 4.81 \times 10^{14}$  molecules/cm<sup>2</sup>, was determined using EQCN technique. This experimental value is close to the theoretical  $\Gamma_{\text{mono, PATP}} = 5.41 \times 10^{14}$  molecules/cm<sup>2</sup>, based on the *p*-ATP molecule dimensions and perpendicular orientation.

The Au/*p*-ATP/PANI films generate both cathodic and anodic photocurrents in different potential regions. A photoelectrochemical model based on internal photoemission in semiconductor covered metal is proposed to explain the photocurrent behavior of PANI films on Au/*p*-ATP substrate. Based on this model, an indirect bandgap of 2.74 eV in the PANI films was determined and the Fermi level position of the metallic region was estimated to be *ca.* 1.34 eV above the valence band of the semiconducting region.

For the Au/*p*-ATP/PANI/TiO<sub>2</sub> films, both cathodic and anodic photocurrents were also observed in different potential regions. The wavelength range of generating photocurrent for Au/*p*-ATP/PANI/TiO<sub>2</sub> films covers violet light and red light regions. This kind of Au/*p*-ATP/PANI/TiO<sub>2</sub> film widens the wavelength region for solar energy conversion and is expected to improve the efficient absorption of solar light.

## Acknowledgements

This work was partially supported by ACS-PRF grant no. 33190-B5, and by the National Natural Science Foundation of China (29703006 and 29833060).

## References

1. Hagfeldt, A.; Gratzel, M. *Chemical Reviews*, **1995**, *95*, 49.
2. O'Regan, B.; Gratzel, M. *Nature*, **1991**, *353*, 737.
3. Shiyonovskaya, I.; Hepel, M. *J. Electrochem. Soc.*, **1998**, *145*, 3981; **1999**, *146*, 243.

4. Kavan, L.; O'Regan, B.; Kay, A.; Gratzel, M. *J. Electroanal. Chem.*, **1993**, *346*, 291.
5. Natarajan, C.; Nogami, G. *J. Electrochem. Soc.*, **1996**, *143*, 1547.
6. Kamat, P. V. *Chemtech.*, **1995**, 6-22.
7. Vlachopoulos, N.; Liska, P.; Augustynski, J.; Gratzel, M. *J. Am. Chem. Soc.*, **1988**, *110*, 1216.
8. O'Regan, B.; Moser, B.; Anderson, M.; Gratzel, M. *J. Phys. Chem.*, **1990**, *94*, 8720.
9. Hodes, G.; Howell, I. D. J.; Peter, L. M. *J. Electrochem. Soc.*, **1992**, *139*, 3136.
10. Nazeruddin, M. K.; Kay, A.; Rodicio, I.; Humphry-Baker, R.; Muller, E.; Liska, P.; Vlachopoulos, N.; Gratzel, M. *J. Am. Chem. Soc.*, **1993**, *115*, 6382.
11. MacDiarmid, A. G.; Epstein, A. J. *Faraday Discuss. Chem. Soc.*, **1989**, *88*, 317.
12. Kilmartin, P. A.; Wright, G. A. *Electrochim. Acta*, **1996**, *41*, 1677; **1998**, *43*, 3091.
13. Das Neves, S.; Da Fonseca, C. N. P.; De Paoli, M.-A. *Synth. Met.*, **1997**, *89*, 167.
14. Maia, D. J.; Das Neves, S.; Alves, O. L.; De Paoli, M.-A. *Electrochim. Acta*, **1999**, *44*, 1945.
15. Gabrielli, C.; Keddani, M.; Nadi, N.; Perrot, H. *J. Electroanal. Chem.*, **2000**, *485*, 101.
16. Stafstrom, S.; Bredas, J. L.; Epstein, A. J.; Woo, H. S.; Tanner, D. B.; Huang, W. S.; MacDiarmid, A. G. *Phys. Rev. Lett.*, **1987**, *59*, 1464.
17. Pouget, J. P.; Laridjani, M.; Jozefowicz, M. E.; Epstein, A. J.; Scherr, E. M.; MacDiarmid, A. G. *Synth. Met.*, **1992**, *51*, 95.
18. Nechtschein, M.; Santier, C.; Travers, J. P.; Chroboczek, J.; Alix, A.; Ripert, M. *Synth. Met.*, **1987**, *18*, 311.
19. Lundberg, B.; Salaneck, W. R.; Lundstroem, I. *Synth. Met.*, **1987**, *21*, 143.
20. Epstein, A. J.; Ginder, J. M.; Zuo, F. *Synth. Met.*, **1987**, *18*, 303.
21. Zuo, F.; Angelopoulos, M.; MacDiarmid, A. G.; Epstein, A. J. *Phys. Rev. B*, **1987**, *36*, 3475.
22. McCall, R. P.; Ginder, J. M.; Leng, J. M.; Ye, H. J.; Manohar, S. K.; Masters, J. G.; Asturias, G. E.; MacDiarmid, A. G.; Epstein, A. J. *Phys. Rev. B*, **1990**, *41*, 5202.
23. Roe, M. G.; Ginder, J. M.; Wigen, P. E.; Epstein, A. J.; Angelopoulos, M.; MacDiarmid, A. G. *Phys. Rev. Lett.*, **1988**, *60*, 2789.
24. Genies, E. M.; Lapkowski, M. *Synth. Met.*, **1988**, *24*, 69.
25. Genies, E. M.; Hany, P.; Lapkowski, M. *Synth. Met.*, **1988**, *25*, 29.
26. Shen, P. K.; Tian, Z. Q. *Electrochim. Acta*, **1989**, *34*, 1611.
27. Yaohua, D.; Shaolin, M. *Electrochim. Acta*, **1991**, *36*, 2015.
28. Desilvestro, J.; Haas, O. *Electrochim. Acta*, **1989**, *36*, 361.
29. Sabatani, E.; Gafni, Y.; Rubinstein, I. *J. Phys. Chem.*, **1995**, *99*, 12305.
30. Kim, Y. T.; Mcarley, R. L.; Bard, A. J. *J. Phys. Chem.*, **1992**, *96*, 7416.

31. Luo, J.; Zhang, H. P.; Huang, H. G.; Wu, L. L.; Lin, Z. H. *Molecular Crystals and Liquid Crystals*, **1999**, 337, 157.
32. Greef, R.; Kalaji, M.; Peter, L. M. *Faraday Discuss. Chem. Soc.*, **1989**, 88, 277.
33. Sukamto, J. P. H.; McMillan, C. S.; Smyrl, W. *Electrochim. Acta*, **1993**, 38, 15.
34. Watanabe, T.; Gerischer, H. J. *Electroanal. Chem.*, **1981**, 122, 73.
35. Helman, J. S.; Sanchez-Sinencio, F. *Phys. Rev. B*, **1973**, 7, 3702.
36. Luo, J.; Huang, H. G.; Zhang, H. P.; Wu, L. L.; Lin, Z. H.; Hepel, M. *J. New Mat. Electrochem. Systems*, **2000**, 3, 249.



## Chapter 10

# Conjugated Organic Polymers for Anticorrosion Coating

S. Aeiya<sup>1</sup>, K. I. Chane-Ching<sup>1</sup>, J. C. Lacroix<sup>1</sup>, J. Petitjean<sup>2</sup>, and P. C. Lacaze<sup>1,\*</sup>

<sup>1</sup>Institut de Topologie et de Dynamique des Systèmes de l'Université Paris 7-Denis Diderot, Associé au CNRS (UPRES-A 7086), 1 rue Guy de la Brosse, 75005 Paris, France

<sup>2</sup>USINOR-Recherche et Développement-LEDDEP, 17 Avenue des Tilleuls, BP 70011, 57191 Florange Cedex, France

Conjugated organic polymers such as polypyrrole (PPy), polyaniline (PANI) and their derivatives can be used for protection of oxidizable metals against corrosion. Direct electrosynthesis of these polymers by oxidation of the corresponding monomer on oxidizable metals is particularly convenient for industrial applications, but difficulties arising from the large potential gap between the oxidation potential of the monomer and the dissolution potential of the metal have to be solved. We demonstrate that well-chosen experimental conditions, including a preliminary surface treatment, allow the deposition of adherent polymer films without any dissolution of the metal. Moreover, in the case of pyrrole, we describe a novel one-step general procedure that leads to the deposition of PPy films at ultra-high rates (1  $\mu\text{m}/\text{sec}$ ) on a large variety of oxidizable metals (Fe, Zn, Cu, Al...).

## Introduction

Protection of metals by organic coatings has reached a level of perfection that guarantees more than 10 years protection against corrosion. This coating quality is due to the presence of chromated pigments incorporated in the coating and also to a mixed chromating phosphating treatment of the metallic surface. Unfortunately, application of environmental protection rules will prohibit chromating in the near future, and this means that replacement techniques must soon be found.

Recently, the use of oxidized PANI has been recognized as an interesting means of protecting oxidizable metals. Deberry (1) was the first to show that a PANI film coated on stainless steel by electrochemical oxidation of aniline acted as a protective primer. This protection has been explained by a redox effect of the doped PANI, which maintains the metallic oxide film in its passive state. These results were confirmed by MacDiarmid et al. (2) and later, Wessling et al. (3) showed that chromating could be replaced by the direct deposition of a PANI dispersion on the metal.

At the same time, much work has been done on PPy. Indeed, among the various heterocyclics, only pyrrole can be electropolymerized from aqueous electrolytes over a pH range between 3 and 9 (4). Moreover, pyrrole has a rather good solubility (*ca.* 1 M) in water, a relatively low oxidation potential, and does not lead to carcinogenic degradation products as does PANI, which gives benzidine derivatives. Several groups have investigated the possibility of depositing PPy films on oxidizable metals with the aim of corrosion protection, using the electropolymerization technique well described for noble metals (5).

This technique, which can be easily automated, constitutes a very attractive metal-coating technique for industrial applications. Adherent conducting polymer films can be easily obtained on Pt or Au by electrochemical oxidation of common monomers such as pyrrole, aniline, thiophene and their derivatives. The layer thickness of these polymers can be varied from 10 to 30  $\mu\text{m}$  by controlling the current and the medium.

Unfortunately, the thermodynamic conditions for the electropolymerization of monomers such as pyrrole or aniline are very unfavorable with common oxidizable metals such as iron and zinc. Indeed, electropolymerization of these monomers needs a positive potential (0.7 V/ SCE for pyrrole at pH 5 and 0.8 V/ SCE for aniline in 1M  $\text{H}_2\text{SO}_4$ ) that is much higher than the metal dissolution potential (- 0.7 V/ SCE for iron, - 0.96 V/ SCE for zinc at pH < 8). Consequently, it is obvious that attempts to deposit PPy or PANI by electrochemical oxidation of pyrrole or aniline on iron or zinc will be unsuccessful if we consider only the thermodynamic data related to the pure metals and the monomers.

Work reported by several groups confirmed these difficulties, in particular the occurrence of metal dissolution and the lack of adhesion of the PPy film onto the metal. Nevertheless, some experiments were successful. Beck et al., using oxalic acid as an electrolyte and after prepassivation of iron with  $\text{KMnO}_4$ , obtained adherent PPy films with negligible metal dissolution (6-8).

These results show that a preliminary modification of the electrode surface changes dramatically its electrochemical behavior, and makes it possible to perform electropolymerization in spite of initial unfavourable thermodynamic prediction.

In conclusion, the success of the electrochemical technique relies upon the search for suitable pretreatment of the surface or on the choice of a specific electrolyte, which in this latter case will provide a slight passivation of the electrode without preventing electropolymerization. Two strategies can be envisaged: either a two-step process including a preliminary treatment of the metallic surface followed by electropolymerization, or a one-step process that is more suitable for industrial application. In the latter case, a specific electrolyte is required: it must inhibit the metal dissolution by a slight passivation of the surface without disturbing the electropolymerization process. In this work, we show that strongly adhesive PPy coatings can be deposited on iron, or other oxidizable metals like zinc, in aqueous media, by a two-step or one-step process.

## Experimental

All compounds, potassium oxalate, sodium oxalate, sodium sulfide, sodium salicylate and salicylic acid, were purchased from Acros, Fluka or Prolabo and used without further purification. Pyrrole (Acros) was distilled twice under argon. Water was purified by passing through a Millipore purification system.

All voltammetric and galvanostatic experiments were performed using a one-compartment three-electrode cell as described previously (9).

The working electrodes were iron, mild steel, aluminum, copper, tin or zinc (polished in water with 1200-grit paper), or 2 to 3  $\mu\text{m}$  zinc-electroplated steel. The counter-electrode was a stainless steel plate and the reference electrode a Tacussel KCl saturated calomel (SCE). The rotating disk electrode was an EDI Radiometer monitored with a CTV 101 Radiometer speed control unit.

Photoelectron (XPS) spectra were determined with a VG Escalab MK1 apparatus (10).

## Two-Step PPy Deposition on Mild Steel

The first attempts to electrosynthesize PPy on oxidizable metals, reported by Stockheim et al. (11), were carried out in organic media. The main difficulties encountered were due to marked anodic dissolution of the metals. Many works have been devoted to the optimization of the electrolytic medium; organic or aqueous, in order to passivate the metal surface toward corrosion without stopping electropolymerization. In particular, during our investigations on PPy

deposition on iron or steel in aqueous media, we demonstrated the crucial role of metal pretreatment by dilute nitric acid (9).

### **Effect of the Surface Treatment on the Electrochemical Response of Iron**

Iron passivity and transpassivity were investigated in aqueous solutions of either sodium sulfate ( $\text{Na}_2\text{SO}_4$ ) or potassium nitrate ( $\text{KNO}_3$ ) after different pretreatments. In all cases, the first treatment consisted of an alkaline rinsing in order to remove grease from the surface. Then, we compared the effect of treatment in various aqueous media:

- 4 min in 10%  $\text{HNO}_3$
- 10 min in 30%  $\text{HCl}$
- 10 min in 10%  $\text{H}_2\text{SO}_4$
- 10 min in 10%  $\text{H}_3\text{PO}_4$

The electrochemical behavior of iron in aqueous solution in the absence and in the presence of pyrrole was studied. In addition, the effect of iron pretreatment on the formation of very adherent PPy films was investigated.

#### *Sodium Sulfate Solution*

The behavior of mild steel substrates was first examined in a 0.1 M solution of  $\text{Na}_2\text{SO}_4$  in water. It appears that substrate pretreatment with nitric acid is the only one that allows effective protection. Indeed, the use of  $\text{HCl}$ ,  $\text{H}_2\text{SO}_4$  or  $\text{H}_3\text{PO}_4$  as pretreatment reagent leads to substrates that are strongly corroded as soon as a potential of - 0.6 V is reached. On the other hand, when  $\text{HNO}_3$  is used, a considerable passivation region is observed up to a polarization potential of + 1.25 V, where water oxidation occurs. Such a pretreated mild steel electrode acts like a platinum one, when polarized in the same medium. However, an important difference appears during the back sweep in the potential region below + 0.15 V, since an oxidation wave appears when mild steel is used whereas none is observed on platinum. The substrate surface was examined by XPS spectroscopy, which shows that nitrogenous species are first formed during nitric acid action and strongly absorbed on the metal surface. During the back sweep, the nitrogenous species are partially desorbed at + 0.15 V and replaced by sulfate anions.

When 0.1 M pyrrole is added to the sodium sulfate solution, no electropolymerization occurs with the samples pretreated in  $\text{HCl}$ ,  $\text{H}_2\text{SO}_4$  or  $\text{H}_3\text{PO}_4$ . As in the absence of pyrrole, the metal is strongly corroded at potentials higher than - 0.6 V and the electrolyte solution becomes yellow, indicating extensive iron dissolution. On the other hand, when the electrode is pretreated

with dilute  $\text{HNO}_3$ , we observe a considerable passivation up to + 0.7 V where deposition of PPy occurs, as far in a platinum electrode. During the back sweep, a large anodic peak is observed as in the absence of pyrrole. Such deposition can be obtained in the galvanostatic mode at a relatively low current density of 2  $\text{mA}/\text{cm}^2$  and with a good coulombic yield (about 70%). Thus, the polarization of a mild steel electrode under these conditions and for 30 min leads to a film thickness of 6.6  $\mu\text{m}$ , i.e. a growth rate of about 2.2  $\mu\text{m}/\text{min}$ . The resulting polymer films are strongly adherent (100% adherence) according to the standard stollotape test. Using higher current densities than 4  $\text{mA}/\text{cm}^2$  leads to partial metal dissolution, and poor quality films were obtained.

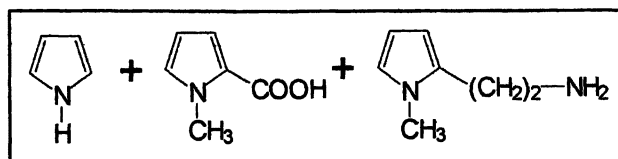
#### *Potassium Nitrate Solution*

The significant effect of nitrate anions is evidenced when a mild steel electrode is polarized in a 0.1 M  $\text{KNO}_3$  solution. Indeed, whatever the surface pretreatment (dilute  $\text{HNO}_3$ ,  $\text{HCl}$ ,  $\text{H}_2\text{SO}_4$  or  $\text{H}_3\text{PO}_4$ ), the cyclic voltammogram indicates a very efficient passivation of the mild steel electrode up to + 1.2 V where an oxidation wave arises. The same behavior is observed when a platinum electrode is used, indicating once again an effective passivation of the mild steel surface in nitrate medium.

When pyrrole is added to the electrolytic solution, PPy film growth occurs in all cases at + 0.7 V. However, when the steel is pretreated in  $\text{HCl}$ ,  $\text{H}_2\text{SO}_4$  or  $\text{H}_3\text{PO}_4$ , the resulting films of PPy are very poorly adherent (0% adhesion), whereas the sample pretreated with dilute nitric acid affords very adherent films (100% adhesion). Moreover, an optimized coulombic yield of about 95% is obtained in the galvanostatic mode. With a current density of 4  $\text{mA}/\text{cm}^2$ , a very adherent film of PPy is synthesized with a growth rate of 0.55  $\mu\text{m}/\text{min}$ .

#### *Anticorrosion Properties of PPy Films*

To test the anticorrosion behavior of polymer films prepared in nitrate medium using mild steel pretreated with dilute nitric acid, we synthesized simple PPy films (referred to as  $(\text{PPy})_i$ ) and modified PPy films (referred to as  $(\text{PPy})_m$ ).  $(\text{PPy})_m$  is obtained by copolymerization of a 5 : 0.5 : 0.5 mixture of pyrrole, N-methylpyrrole-2-carboxylic acid and N-methyl-2[ethylamino]pyrrole (total concentration: 0.1M). The structures of these monomers are shown in scheme 1



*Scheme 1. Structures of pyrrole and its copolymerized derivatives*

Both (PPy)<sub>s</sub> and (PPy)<sub>m</sub> films were prepared in the galvanostatic mode ( $j = 4 \text{ mA/cm}^2$ ) and had thickness between 3 and 10  $\mu\text{m}$ . The (PPy)<sub>m</sub> films heated at 180°C for 30 min in order to achieve polycondensation of the modified polymer chains. Both samples were over-coated with cathaphoretic paints (total thickness about 28  $\mu\text{m}$ ) and then compared in salt spray tests with phosphated steels covered with the same thickness of cataphoretic paint. These tests were performed for 500 h, after which adherence was checked. It is found that the adherence properties are similar for all samples. The main difference is that corrosion propagation around the streaks is twice as small for (PPy)<sub>m</sub> than as for (PPy)<sub>s</sub>, which shows behavior identical with that of the phosphated steel system (12).

## Two-Step PPy Deposition on Zinc

From an application point of view, we have chosen to pursue our investigations in using zinc as substrate, because this metal is widely used in industry. As mentioned in the Introduction, its use is particularly difficult since it is more electropositive than iron and no insulating oxide layer like for aluminum protects it. Among various attempts to inhibit corrosion in aqueous medium, we found that preliminary chemical treatment of its surface by sulfide compounds allowed the deposition of PPy without metal dissolution. Two methods were investigated, consisting of an immersion process (13,14) and an electrochemical pretreatment (15), respectively. Details are given below.

### *Surface Pretreatment by Immersion*

The direct polarization of a Zn electrode (only mechanically polished with abrasive paper) in a 0.1 M  $\text{K}_2\text{C}_2\text{O}_4$  aqueous solution shows a very strong oxidation peak at - 0.7 V ( $j = 10 \text{ mA/cm}^2$ ). The electrochemical behavior is totally different when the electrode is submitted to a preliminary immersion in a 0.2 M  $\text{Na}_2\text{S}$  solution: the anodic peak below 0 V vanishes and we observe only the oxidation of oxalate anions at + 0.9 V. The resulting anodically polarized electrode is strongly passivated by a mixed layer containing zinc sulfide and zinc oxide, as confirmed by XPS analysis. During the back sweep from + 2 V to - 1 V, a very low current intensity (about 0.5  $\text{mA/cm}^2$ ) is observed.

When 0.5 M pyrrole is added to the oxalate solution, its polymerization is difficult on non-pretreated Zn: the metal surface is too strongly passivated and we obtain at best dendritic and inhomogeneous films. Good film qualities are obtained only when the Zn has been pretreated with  $\text{Na}_2\text{S}$ . These films are synthesized in galvanostatic mode under specific experimental conditions. Whatever the electrolysis current chosen from 4 to 30  $\text{mA/cm}^2$ , the electrical

yield is about 95% and the corresponding deposition rate ranges from 0.6 to 3.5  $\mu\text{m}/\text{min}$ , respectively. This procedure, however, requires quite long times of substrate immersion before electropolymerization, at least 12 hours being necessary to achieve an adequate surface modification. For this reason, we have improved the operating mode by replacing the chemical treatment by an electrochemical one.

### *Electrochemical Zinc Surface Pretreatment*

In order to shorten the time of pretreatment, we have investigated a novel procedure consisting of an electrochemical conversion of zinc substrates in aqueous  $\text{Na}_2\text{S}$  solution. Thus, instead of simple dipping, the anodic electrolysis of Zn in a 0.2 M  $\text{Na}_2\text{S}$  solution leads to the same important modification. Full characterization of pretreated Zn by potentiodynamic polarization, impedance measurements and XPS analysis, indicates that the protective layer consists of a mixture of ZnS and zinc oxides such as  $\text{ZnO}_x\text{H}_y$ , where  $1 \leq x \leq 2$  and  $0 \leq y \leq 1$ . As shown in Figure 1, the optimized conditions correspond to a polarization of the zinc surface at 0.35  $\text{mA}/\text{cm}^2$  for 3 min in a 0.2 M  $\text{Na}_2\text{S}$  solution, followed by PPy electrosynthesis in an aqueous solution containing 0.1 M  $\text{Na}_2\text{C}_2\text{O}_4$  and 0.9 M pyrrole at  $j = 4 \text{ mA}/\text{cm}^2$ .

With a long pretreatment time (more than 10 min), the protective layer is too thick. The resulting surface resistance is too high and inhibits the synthesis of polymer films. On the contrary, when too short a pretreatment time is used (less than 2 min), we observe a long induction time corresponding to Zn dissolution prior to PPy deposition. The best conditions are obtained with the intermediate time of 3 min.

We obtain PPy films as adherent on Zn electrodes as previously (Zn chemically pretreated by immersion) and with equivalent electrical yield. However, the total time of deposition remains too long for an industrial application that requires:

- No pretreatment of the metal surface
- Direct electropolymerization with vigorous stirring
- Very high deposition rates: *ca.* 2 to 3  $\mu\text{m}$  in 3 sec
- Strong adherence of PPy to the metal
- Possibility of coating the PPy layer with other paint layers

That is why we have developed a new and very promising process involving the use of sodium salicylate as the electrolyte salt for PPy deposition on Zn.

### **One-Step PPy Deposition on Zinc**

A few years ago we found that zinc or zinc-electroplated steel can be covered by adherent PPy coatings by using an aqueous solution of sodium salicylate (NaSac) and pyrrole at pH 5, with very high current densities and without metal dissolution (16).

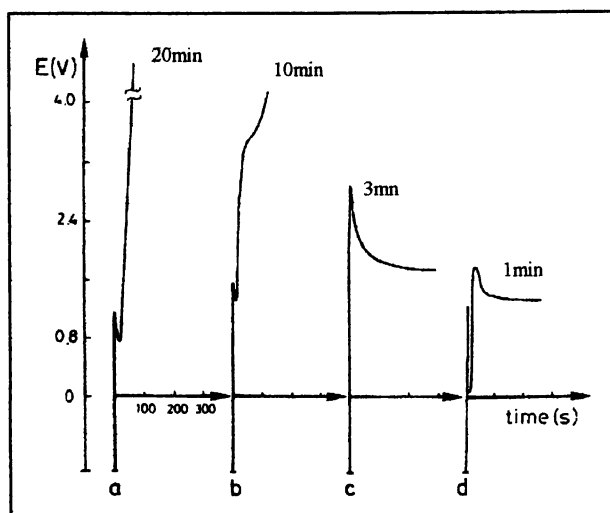


*Figure 1. Galvanostatic curves for pyrrole oxidation (0.9 M) in 0.1 M  $\text{Na}_2\text{C}_2\text{O}_4$  solution at  $j = 4 \text{ mA/cm}^2$  with different times of pretreatment. Curves a, b, c and d correspond to Zn pretreated in 0.2 M  $\text{Na}_2\text{S}$  at  $j = 0.35 \text{ mA/cm}^2$  for 20, 10, 3 and 1 min, respectively.*



### Voltammetric Study

The voltammetric response of a Zn electrode in an aqueous solution of 1 M NaSac + 0.5 M pyrrole at pH 5 (optimized electrolytic solution) is presented in Figure 2. It should be noted that the rotation speed of the working electrode has no great effect upon the voltammogram. Four regions denoted A, B, C and D appear on the anodic curve. Region A corresponds to a slight dissolution of the metal immediately followed by the precipitation of ZnSac which makes up the passivating layer (peaks P<sub>1</sub> and P<sub>2</sub>). In region B, a low oxidative current is observed. This current is due to a residual dissolution of Zn. In region C, the anodic current diminishes markedly. The P<sub>3</sub> peak is attributed to a synergic effect of pyrrole, NaSac and the Zn surface, since it is not observed on a Pt electrode, or in the absence of monomer. The mechanism corresponding to the sudden stop of Zn dissolution has been well elucidated with the help of XPS analysis. It has been demonstrated that at about + 0.5 V, the pyrrole and the salicylate ions absorbed in the passivating layer are oxidized, leading to a modified electrode covered mainly by PPy. This polymer layer constitutes a film sufficiently dense to inhibit further Zn dissolution. Then, PPy formation takes place (onset at + 0.6 V) and gives a very strong wave, as when a Pt electrode is used. During the back sweep, no current is noticed in the anodic region, but only a cathodic current at around - 0.9 V (peak P<sub>4</sub>) due to polymer reduction. This preliminary study shows that the optimized conditions (aqueous solution of 1 M NaSac + 0.5 M pyrrole at pH 5) allow us to form regular and very adherent films of PPy. This result encouraged us to investigate the galvanostatic mode, which corresponds better to the industrial criteria mentioned above.

### Galvanostatic Study

For this purpose, we have checked, on the laboratory scale, the possibility of simulating the hydrodynamic conditions of a production line, using a disk electrode rotating at 4000 rpm in the galvanostatic mode. Under these conditions, when a current density of 5 mA/cm<sup>2</sup> is used, homogeneous PPy films are formed at about 0.65 V, with a growth rate of 1 μm/min, i.e. a polymerization level of about 100%. However, this polymerization rate is too low for industrial use that requires 2 to 3 μm of polymer film in 3s. In this case, the theoretical current density is 20 A/dm<sup>2</sup> (200 mA/cm<sup>2</sup>). In order to use such a high current density, we have examined the possibility of reducing the bath resistivity. It was found that for a pyrrole concentration of 0.5 M, the conductivity of the bath is increased from 37 to 50 S cm<sup>-1</sup> when the NaSac

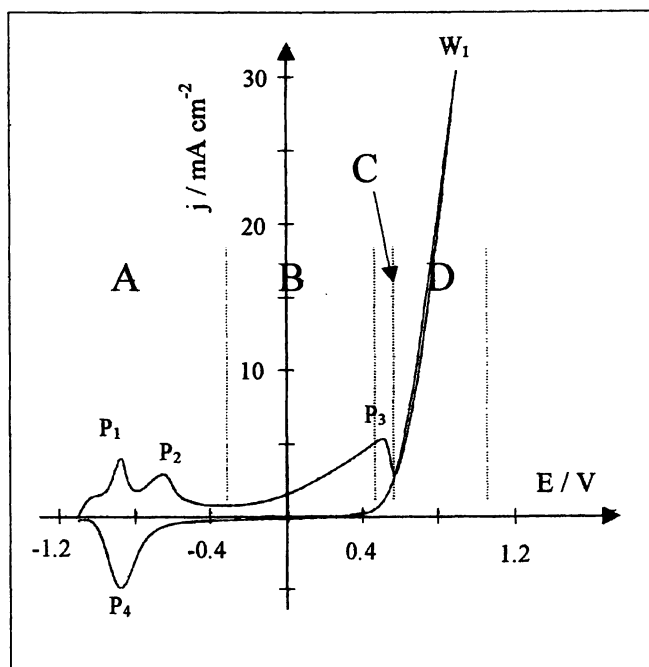
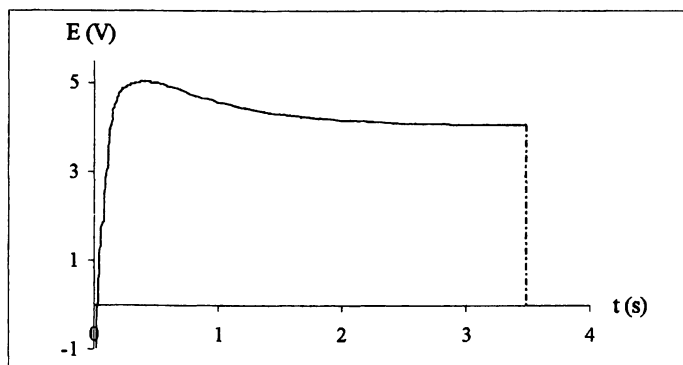


Figure 2. Cyclic voltammogram of a Zn electrode in an aqueous solution of 1 M NaSac and 0.5 M pyrrole at pH 5 (scan rate: 10 mV/s)

concentration increased from 1 to 2 M. Using the high NaSac concentration, PPy films can be synthesized in the galvanostatic mode at  $j = 20 \text{ A/dm}^2$  with a very short induction time and at a potential stabilized at about 4 V (see Figure 3). Under these conditions, it is demonstrated that very adherent deposits are obtained with a good electrical yield (about 100%) and with the required polymer film growth of  $2 \mu\text{m}$  in 3s.



*Figure 3. Galvanostatic response of a Zn electrode during electropolymerization of PPy at  $j = 20 \text{ A/dm}^2$  in an aqueous solution of 2 M NaSac + 0.5 M pyrrole at pH 5. Rotation speed of the electrode: 4000 rpm*

Figure 4 shows a micrographic cut of a PPy film deposited under the optimized conditions on  $2 \mu\text{m}$  zincated steel. It can be seen that the PPy film is homogeneous and without any defect.

Another very important fact is the high versatility of this process which makes it very attractive. Indeed, several zincated electrodes with various surface states (more or less oxidized or rough) as well as different substrates (iron, mild steel, aluminum, copper and tin) were tested. In every case, PPy is synthesized without any difficulty with the same electrochemical behavior.

## Conclusion

We have shown that pyrrole can be electropolymerized on various oxidizable metals such as iron, mild steel, aluminum, copper, tin and zinc, and that this can be achieved in one or two steps. During our investigations, the strategy adopted was to circumvent the unfavorable thermodynamic data by the optimization of kinetic conditions. To this end, we have developed various processes, in which the metal is initially passivated with respect to corrosion

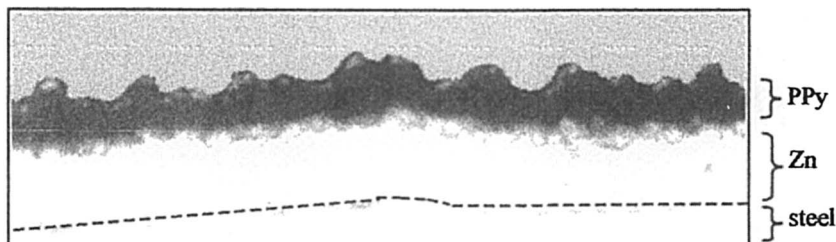


Figure 4. Micrographic cut of PPy/Zn/Steel synthesized in galvanostatic mode at  $j = 20 \text{ mA/dm}^2$  during 3 s in aqueous solution consisting of 2 M NaSac and 0.5 M pyrrole at pH 5. Rotation speed of the electrode: 4000 rpm.

while remaining suitable for electropolymerization. The first one consists of a two-step process, in which the metal is preliminarily treated with dilute nitric acid (mild steel) and sodium sulfate solution, chemically or electrochemically (zinc). In order to satisfy industrial requirements, a one-step process has been developed, using an aqueous salicylate electrolyte. In this way, polymerization of pyrrole in aqueous solution containing 2 M SacNa + 0.5 M pyrrole at pH 5 leads to very adherent films with a coulombic yield of 100% and at a deposition rate of  $2 \mu\text{m}$  in 3s. To our knowledge, the possibility of introducing the electrochemical deposition of PPy into an industrial process is described for the first time.

## References

1. Deberry, D.W. *J. Electrochem. Soc.* **1985**, *132*, 1022-1026.
2. Ginder, J.M.; Richter, A.F.; MacDiarmid, A.G.; Epstein, A.J. *Solid State Commun.*, **1987**, *63*, 97-101.
3. Wessling, B. *Mater. Corros.* **1996**, *47*, 439-445.
4. Beck, F.; Michaelis, R. *Werkstoffe und corrosion* **1991**, *42*, 341-345.
5. Shirmeisen, M.; Beck, F. *J. Appl. Electrochem.* **1989**, *19*, 401-409.
6. Beck, F.; Michaelis, R. *J. Coat. Technol.* **1992**, *64*, 59-67.
7. Beck, F.; Huelsner, P.; Michaelis, R. *Bull. Electrochem.* **1992**, *8*, 35-44.
8. Beck, F.; Michaelis, R.; Schloten, F.; Zinger, B. *Electrochimica Acta* **1994**, *39*, 229-234.
9. Ferreira, C.A.; Aeiych, S.; Aaron, J.J.; Lacaze, P.C. *Eletrochim. Acta* **1996**, *41*, 1801-1809.
10. Ferreira, C.A.; Aeiych, S.; Delamar, M.; Lacaze, P.C. *J. Electroanal. Chem.* **1990**, *284*, 351-359.

11. Prejza, J.; Lundstrom, J.; Stockheim, T. A. *J. Electrochem. Soc.* **1982**, *129*, 2685-2692.
12. Ferreira, C.A.; Aeiyaeh, S.; Coulaud, A.; Lacaze, P.C. *J. Appl. Electrochem.* **1999**, *29*, 259-263.
13. Lacaze, P.C.; Ferreira, C.A.; Aeiyaeh, S. French Patent 9214092, 1992.
14. Ferreira, C.A.; Aeiyaeh, S.; Aaron, J.J.; Lacaze, P.C. In *Organic Coatings*; Lacaze, P.C., Ed; ALP Press, Woodbury: New York, US, 1996; Vol. 354, PP 159-165.
15. Zaïd, B.; Aeiyaeh, S.; Lacaze, P.C.; Takenouti, H. *Electrochim. Acta* **1998**, *43*, 2331-2339.
16. Aeiyaeh, S.; Lacaze, P.C.; Hedayatullah, M.; Petitjean, J. French Patent 9315395, 1993.

## Chapter 11

# Selective Electrocatalytic Reduction of CO<sub>2</sub> on Electroprepared [Ru(L)(CO)<sub>2</sub>]<sub>n</sub> Polymeric Film: L = 2,2'-Bipyridine Derivatives

A. Deronzier

Laboratoire d'Electrochimie Organique et de Photochimie Rédox, UMR  
CNRS 5630, Université Joseph Fourier Grenoble 1, BP 53, 38041 Grenoble  
Cedex 9, France

We describe here an original electrochemical proceeding for elaboration of a new kind of organometallic polymer having the generic formula : [Ru(L)(CO)<sub>2</sub>]<sub>n</sub> (L = 2,2'-bipyridine derivatives). The polymer displays outstanding electrocatalytic activity toward reduction of carbon dioxide. These molecular cathodes are prepared as thin films on conductive materials by electroreduction of a mononuclear ruthenium complex precursor like [Ru(L)(CO)<sub>2</sub>Cl<sub>2</sub>]. The overall process involves the addition of two electron per complex associated with the loss of two Cl<sup>-</sup> ligands. It has been demonstrated that polymerization occurs by an electrochemical propagation process. Characterization of the [Ru(L)(CO)<sub>2</sub>]<sub>n</sub> polymer has been made using various physico-chemical techniques. These modified electrodes have been applied with success to electrocatalytic reduction of CO<sub>2</sub> into CO or HCOO<sup>-</sup> in pure aqueous electrolyte, the selectivity of the reaction depending on the nature of the L ligand.

## Introduction

Interest in the electrocatalytic reduction of  $\text{CO}_2$  with a view to the construction of artificial photosynthetic systems has been increasing very rapidly in the last 10 years (1, 2). A large variety of transition metal complexes has been studied as electrocatalysts (3), however only a few appear to be effective in pure aqueous electrolyte. The accompanying reduction of protons limits the efficiency of the electrocatalysis. One solution to this problem is to use complexes in a polymer-confined system deposited on metallic cathode surfaces. Some attempts have been reported recently in the literature (4), but successes obtained with this type of device have been very scarce.

In view to reach this goal we have developed over the last few years (5) an electrocatalytic system based on a new kind of organometallic polymeric films, such as  $[\text{Ru}(\text{L})(\text{CO})_2]_n$  ( $\text{L} = 2,2'$ -bipyridine derivatives), containing metal-metal bonds (Fig. 1(a)). These molecular cathodes appear to be highly selective for reduction of  $\text{CO}_2$  into  $\text{CO}$  or  $\text{HCOO}^-$  at a rather low overvoltage in pure aqueous electrolyte (6-8).

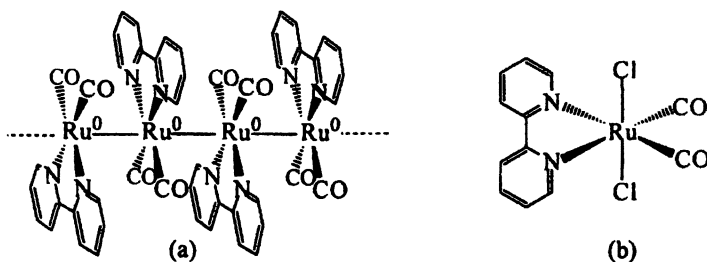


Figure 1 : Formula of the polymer  $[\text{Ru}(\text{L})(\text{CO})_2]_n$  (a) and precursor  $[\text{Ru}(\text{L})(\text{CO})_2\text{Cl}_2]$  (b) ;  $\text{L} = 2,2'$ -bipyridine

## Results

### Film formation

Films of  $[\text{Ru}(\text{L})(\text{CO})_2]_n$  can be easily obtained by the two-electron reduction of a mononuclear ruthenium(II) complex precursor like  $[\text{Ru}(\text{L})(\text{CO})_2\text{Cl}_2]$ . Two Cl ligands per molecule of precursor are released during the electropolymerization. Equation (1) summarizes the overall process.

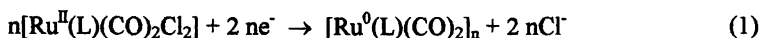


Fig. 2 shows for instance, the cyclic voltammogram of a solution of  $[\text{Ru}(\text{bpy})(\text{CO})_2\text{Cl}_2]$   $\text{bpy} = \text{regular } 2,2'\text{-bipyridine}$  in  $\text{CH}_3\text{CN} + 0.1 \text{ M TBAP}$  at a Pt electrode. It exhibits a two-electron irreversible cathodic peak associated on the reverse scan with an irreversible anodic peak. The shape of this cathodic-anodic peak system is typical of an electroprecipitation redissolution phenomena. Iterative CV between  $-0.80 \text{ V}$  and  $-2.00 \text{ V}$  (Fig. 3) or electrolysis at  $-1.65 \text{ V}$  induces the electropolymerization and then produces the growth of an electroactive organometallic polymer of  $[\text{Ru}(\text{bpy})(\text{CO})_2]_n$  on the working electrode

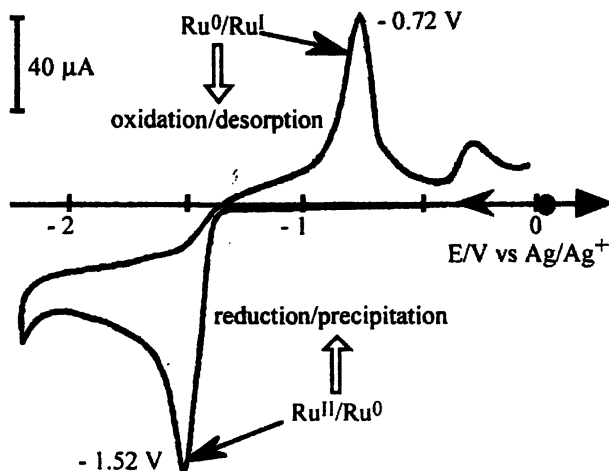
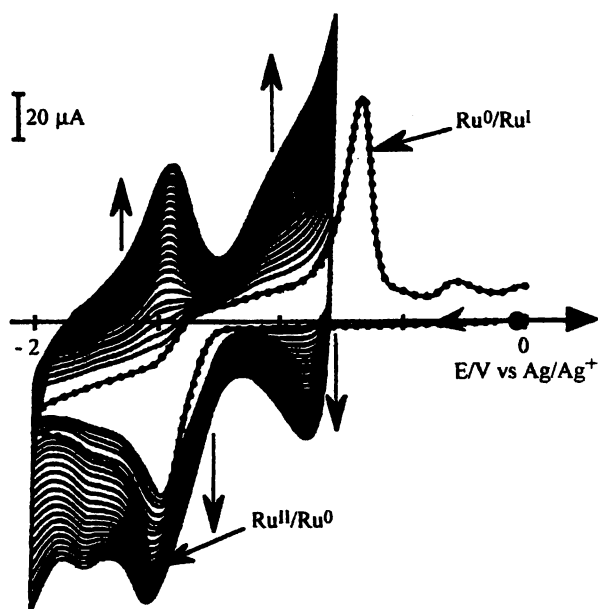


Figure 2: Cyclic voltammogram in  $\text{CH}_3\text{CN} + 0.1 \text{ M TBAP}$  of  $[\text{Ru}(\text{bpy})(\text{CO})_2\text{Cl}_2]$  ( $1 \text{ mM}$ ) at a Pt electrode (diam.  $5 \text{ mm}$ ). Scan rate  $100 \text{ mV s}^{-1}$ .

Fig. 4 illustrates the redox properties of the polymer after its transfer into a pure electrolyte solution  $\text{CH}_3\text{CN} + 0.1 \text{ M TBAP}$ . Films are prepared here on a vitreous carbon (VC) electrode. The electroactivity is stable when scan limit potentials are conveniently chosen. It is characterized essentially by two redox system at  $E_{1/2} = -1.51 \text{ V}$  and at  $-0.92 \text{ V}$  corresponding respectively to electronic transfers localized on the ligand ( $\text{bpy}^{0/-}$ ) and the metal ( $\text{Ru}^{0/1}$ ) within the polymer. However this organometallic polymer is irreversibly oxidized at potentials higher than  $-0.70 \text{ V}$ . For instance successive scans beyond the desorption potential show the fast progressive disappearance of the initial strong oxidation peak at  $-0.72 \text{ V}$  causing the desorption of the polymer film in electrolyte solution. A first exhaustive one-electron oxidation carried out at  $0.2 \text{ V}$  surface.



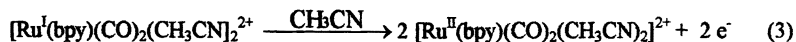


*Figure 3 : Iterative cyclic voltammograms between - 0.80 V and - 2.00 V. Scan rate  $100 \text{ mV s}^{-1}$ .*

V leads mainly to a dimeric soluble ruthenium(I) complex according to equation (2).



A two-electron oxidation which induces the cleavage of all Ru-Ru (bonds) is obtained by a further oxidation at 1 V leading to the mononuclear ruthenium(II) complex  $[\text{Ru}^{\text{II}}(\text{bpy})(\text{CH}_3\text{CN})(\text{CO})_2]^{2+}$  (equation 3).



Similar films can be easily obtained by reduction of precursors containing substituted bipyridine and even some phenanthroline instead of the regular 2-2, bipyridine (9). Polymerization occurs when electron-donating or withdrawing groups are present on the chelating bpy ligand on the 4,4'-positions, except with nitro groups. In fact, the electron properties of this substituted bpy undergo a strong stabilization of the reduced forms of the complex due to an efficient electron delocalization mostly centered on the bidentate ligand preventing the formation of the polymer. It has been also shown that the substitution on the 6,6'-positions of the bpy ligand by a moderately bulky group does not prevent the polymerization process. On the other hand precursors containing other leaving groups than  $\text{Cl}^-$  ligands give similar  $[\text{Ru}(\text{bpy})(\text{CO})_2]_n$  films as demonstrated for the case of  $\text{CH}_3\text{CN}$ ,  $\text{CH}_3\text{CO}_2^-$ ,  $\text{CF}_3\text{SO}_3^-$  or  $\text{SCN}^-$  ligands.

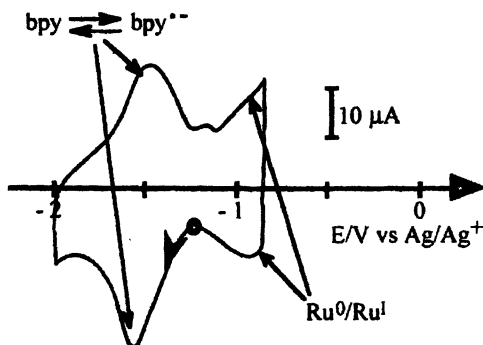


Figure 4: Cyclic voltammogram between -0.85 and -2.00 V of a VC/ $[\text{Ru}^0(\text{bpy})(\text{CO})_2]_n$  modified electrode (diam. 3 mm) in  $\text{CH}_3\text{CN} + 0.1 \text{ M TBAP}$ . Scan rate  $100 \text{ mV s}^{-1}$ .

*Physico-chemical characterization of films*

In order to confirm the identity of the oxidized and reduced form of films we used EPR spectroelectrochemistry at 100°K. Experiments were conducted with a  $[\text{Ru}(\text{L})(\text{CO})_2]_n$  polymer containing 4,7-diphenyl-2,9-phenanthroline as ligand L. This film is EPR silent initially, but when the modified electrode is held at constant potential of -1.80 V corresponding to the reduction peak of the ligand in the film,  $\text{L}^\cdot$  radical anions are generated. The narrow and symmetrical EPR signal with  $g = 2.0034$  observed is typical of paramagnetic organic species having an unpaired electron localized on the  $\Pi$  orbitals of the ligand.

The absence of hyperfine splitting is due to intramolecular electron hopping between close ligand. In a similar fashion the EPR spectrum obtained at -0.95 V ( $\text{Ru}^{0/1}$  couple) is typical of a film containing a  $\text{Ru}^{\text{I}}$  metal centre. The  $g$  value is then higher ( $g = 2.0132$ ) confirming that in this electrogenerated species the electron is predominantly metal centered.

A full characterization of this kind of film is difficult to obtain since the films are unstable at potentials higher than -0.60 V, so they cannot be handled in air. However, the formulation of their structure as  $[\text{Ru}(\text{L})(\text{CO})_2]_n$  is strongly supported by the following observations:

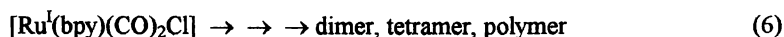
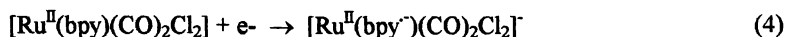
1. The great insolubility of films, even in solvents like DMF and DMSO, is in favor of a polymeric structure.
2. Elemental analyses are consistent with the formulation  $[\text{Ru}^0(\text{L}_2)(\text{CO})_2]_n$ .
3. FAB-MS studies (using *m*-nitrobenzyl alcohol (*m*-NBA)/ $\text{CH}_3\text{CN}$  as a matrix) show peaks at  $m/z$  values of 1137, 966, and 794 corresponding to the fragments  $[\text{Ru}_3(\text{L})_3(\text{CO})_6(\text{m-NBA})(\text{CH}_3\text{CN}) + \text{H}]$ ,  $[\text{Ru}_2(\text{L})_3(\text{CO})_5(\text{m-NBA})(\text{CH}_3\text{CN}) + \text{H}]$ , and  $[\text{Ru}_2(\text{L})_2(\text{CO})\text{H}_3(\text{m-NBA})]$ , respectively ; L = 2,2'-bipyridine.
4. The absorption of the film electrodeposited on an optically transparent electrode exhibits three intense bands in the visible region ( $\lambda_{\text{max}} = 475, 600,$  and  $760$  nm). The shape of this absorption spectrum strongly suggests the presence of metal-metal bonds in the film.
5. The presence of metal-metal bonds ( $\text{Ru}^0\text{-Ru}^0$ ) is confirmed by the presence of a band around  $170\text{ cm}^{-1}$  in the FT-IR spectrum. No  $\nu_{\text{Ru-Cl}}$  stretching vibration is detected. Those films exhibit several vibrations between  $1920$  and  $2010\text{ cm}^{-1}$  and the usual bands due to the vibrations of the bipyridine ligand in the  $1620\text{-}1540\text{ cm}^{-1}$  region.

The fact that quantitative desorption and oxidation of  $[\text{Ru}(\text{L})(\text{CO})_2]_n$  (with L = bpy) in  $\text{CH}_3\text{CN}$  leads successively to the soluble dimer  $[\text{Ru}^{\text{I}}(\text{L})(\text{CO})_2(\text{CH}_3\text{CN})]_2^{2+}$  and monomer  $[\text{Ru}^{\text{II}}(\text{L})(\text{CO})_2(\text{CH}_3\text{CN})]^{2+}$  supports strongly the propounded structure. This indicates unambiguously that the basic

structure of the precursor is retained in the polymeric film. In other words, only simple chemical reactions like dimerization or polymerization (no loss of CO or bpy ligand for instance) occur during the electroreduction. The two initial Cl<sup>-</sup> ligands are replaced by two CH<sub>3</sub>CN ligands since the film is dissolved in pure CH<sub>3</sub>CN which does not contain any Cl<sup>-</sup> anions. The morphology of the film [Ru(L)(CO)<sub>2</sub>]<sub>n</sub> has been examined by scanning electron microscopy. The surface of the film exhibits a quasi-homogeneous distribution of the polymeric nuclei (~3000-6000 Å). Some excrescences are clearly visible and are due to growths like “cotton flower” of the polymer on the nuclei. The presence of ruthenium atoms is confirmed by a strong signal observed at 2.5 keV by EDXRA experiments.

### Polymerization mechanism

We have shown (10) that polymerization occurs upon reduction of [Ru(bpy)(CO)<sub>2</sub>Cl<sub>2</sub>] by an electrochemical propagation process (equations 4-6).



This is a consequence of the easier or similar reducibility of the dimer [Ru(bpy)(CO)<sub>2</sub>Cl]<sub>2</sub> and parent oligomers. An electrochemical study conducted on the independently chemically prepared dimer has demonstrated that the latter is reduced at a less cathodic potential (E<sub>p</sub> = -1.46 V) than the precursor [Ru(bpy)(CO)<sub>2</sub>Cl<sub>2</sub>], E<sub>p</sub> = -1.52 V.

In terms of mechanism it means that the polymerization proceeds via the initial formation of the instable anion radical of the bpy ligand (equation 4) leading to an Ru<sup>I</sup> species by the break of the Ru-Cl bond. This other instable species (17 electron complex) dimerizes into the dimer which is reduced at a close potential.

A crucial point for the formation of the polymeric structure is the presence of two leaving groups. For instance, the mononuclear complex [Ru(bpy)(CO)<sub>2</sub>(C(O)OCH<sub>3</sub>)Cl] bearing a C(O)OMe group, known to be a poor leaving group, instead of a Cl<sup>-</sup> ligand undergoes a one-electron (E<sub>p</sub> = - 1.68 V) electrochemical dimerization. This corresponding dimer has been isolated and

characterized but does not polymerize and exhibits a quasi reversible one-electron reduction at a more cathodic potential ( $E_{1/2} = -1.98$  V).

At this stage of the study it should be recalled that the mononuclear precursor  $[\text{Ru}^{\text{II}}(\text{bpy})(\text{CO})_2\text{Cl}_2]$  exists in two stereoisomeric forms having *trans*-Cl/*cis*-CO (a) and *cis*-Cl/*cis*-CO (b) configurations (Fig. 5). These two stereoisomers can be easily distinguished by  $^1\text{H}$  NMR experiments. The aromatic parts of the  $^1\text{H}$  NMR spectra are shown in Fig. 5 for comparison purposes. Insets on this figure show the structures and attribution of the aromatic patterns. For the *cis*-Cl isomer the spectrum (Fig. 5B) shows eight well resolved signals (each integrate for one proton) as expected for eight unique non symmetric aromatic protons. The spectrum is consistent with an asymmetry in the equatorial plan of the bipyridine ligand. It should be noted that the same splitting pattern is observed for the  $^{13}\text{C}$ -NMR spectra of the isomers. In contrast only four sets of protons are observed for the *trans*-Cl isomer (Fig. 5A).

At negative potentials this *cis*-Cl isomer exhibits the same kind of cyclic voltammogram that of the *trans*-Cl one with an electroprecipitation-redissolution phenomenon. A slight shift (- 40 mV) of the cathodic peak potential is observed compared with the value obtained for the *trans*-Cl complex. This statement confirms that the electronic density inherent to the reduction process is probably located on the bidentate bipyridyl ligand since it is only very slightly influenced by the structure of the complex. Iterative CV between - 0.85 V and - 2.00 V or electrolysis at - 1.60 V induces the electropolymerization and then produces the growth of an electroactive organometallic polymer of  $[\text{Ru}(\text{bpy})(\text{CO})_2]_n$  on the working electrode surface. It should be noted that this polymer is less adherent than the one obtained from the *trans* chloro complex. Electrochemical properties and physico-chemical characteristics of this films are essentially the same as those of the polymer obtained by electroreduction of the *trans*-Cl isomer. So regardless of the complex stereochemistry, the two-electron reduction leads to the formation of an organometallic polymer (11).

### Electrocatalytic activity vs $\text{CO}_2$ reduction of $[\text{Ru}(\text{L})(\text{CO})_2]_n$ films

Fig. 6 shows the cyclic voltammogram under Ar and  $\text{CO}_2$  of the  $[\text{Ru}(\text{bpy})(\text{CO})_2]_n$  film in an aqueous medium. The electroactivity of the modified electrode remains almost identical to that observed in  $\text{CH}_3\text{CN}$  under Ar. Bubbling  $\text{CO}_2$  induces a strong increase of the cathodic current indicating a strong electrocatalytic phenomenon. Electrolysis at - 1.20 V on a carbon felt electrode coated with  $[\text{Ru}^0(\text{bpy})(\text{CO})_2]_n$  (prepared by passing 1.5 C) produces CO with current efficiency > 97 % after 60 C has been consumed. By this time, the electrolysis current had dropped to 40 % of its initial value and a pseudo-plateau was reached.

Taking into account the proposed structure of the polymeric film we suggest the following mechanism for the electrocatalytic cycle. The initial step involves a

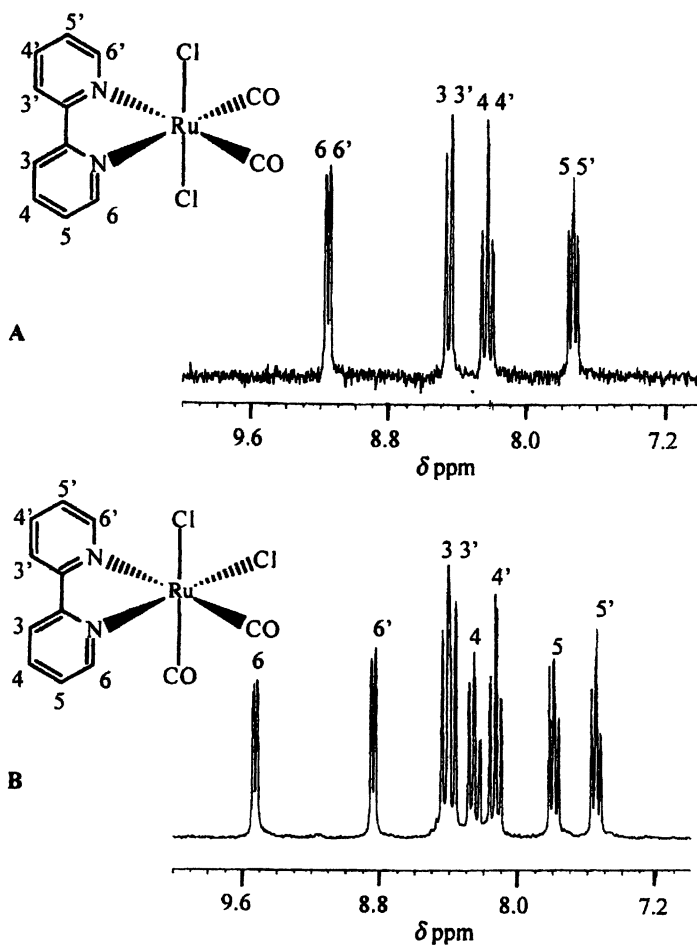


Figure 5 : Aromatic regions of  $^1\text{H-NMR}$  spectra of (A) *trans-Cl* isomer (B) *cis-Cl* isomer.

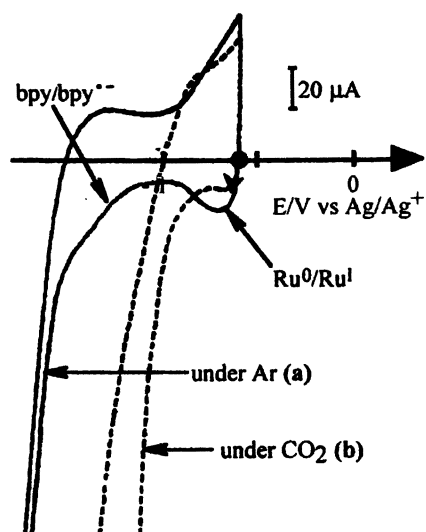


Figure 6 : Cyclic voltammogram in  $\text{H}_2\text{O} + \text{LiClO}_4 10^{-1} \text{ M}$  of a film of  $[\text{Ru}(\text{bpy})(\text{CO})_2]_n$  ; under (a) Ar and (b)  $\text{CO}_2$ . Scan rate  $100 \text{ mV s}^{-1}$ .

one-electron reduction of the electroactive  $[\text{Ru}(\text{bpy})(\text{CO})_2]$  unit in the polymeric film to give  $[\text{Ru}(\text{bpy}^{\cdot-})(\text{CO})_2]$ . This species is not fully stable and may liberate CO, generating a pentacoordinated species  $[\text{Ru}(\text{bpy}^{\cdot-})(\text{CO})]$ . In the presence of  $\text{CO}_2$ , the latter coordinates this species to produce  $[\text{Ru}(\text{bpy})(\text{CO})_2]^+$  via  $[\text{Ru}(\text{bpy})(\text{CO})(\text{C}(\text{O})\text{OH})]$  in the presence of water, which acts as a proton source. At that potential  $[\text{Ru}(\text{bpy})(\text{CO})_2]^+$  is reduced back to  $[\text{Ru}(\text{bpy})(\text{CO})_2]$ , which is ready for participation in another electrocatalytic cycle. Electrogeneration of pentacoordinated metallic carbonyl complexes like  $[\text{Ru}^0(\text{bpy})_2(\text{CO})]$  and  $[\text{Re}^1(\text{bpy})(\text{CO})_2\text{Cl}]$  has been postulated previously as a key species in some homogeneous electrocatalytic processes (12, 13).

An important feature of this kind of polymer is that the product distribution of the electrocatalytic reduction can be changed dramatically with films using a bpy ligand disubstituted on the 4,4' position with electron withdrawing groups like esters, since  $\text{HCOO}^-$  is now the main product of the reduction of  $\text{CO}_2$  over a large pH range ( $\text{pH} > 5$ ). An optimum current efficiency of 90% for  $\text{HCOO}^-$  was obtained at pH 12. However, it should be noted that  $\eta_{\text{HCOO}^-}$  decreases slowly as the charge passed increases, for instance when 30 C has been consumed then production of  $\text{HCOO}^-$  reaches a plateau ( $\eta = 80\%$ ). Since in this case  $\text{HCOO}^-$  is the reduction product, the mechanism involved is probably different although the  $[\text{Ru}(\text{L}^{\cdot-})(\text{CO})]$  species should be considered as the key transient intermediate. One plausible hypothesis is that  $\text{CO}_2$  coordinates the metal in a formate form ( $\text{M}-\text{O}-\text{C}(\text{O})\text{H}$ ) instead of an hydroxycarbonyl form ( $\text{M}-\text{C}(\text{O})\text{OH}$ ). The origin of this formate bond could result from an initial formation of an metal-hydride followed by insertion of  $\text{CO}_2$ . A similar mechanism has been proposed with other metal complexes able to reduce  $\text{CO}_2$  into  $\text{HCOO}^-$  ions more or less selectively [14]. Here the presence of electron withdrawing ester groups induces a strong decrease of the electronic density on the metal site favoring formation of an oxygen-metal bond at the expense of a carbon-metal bond. It should be mentioned that some effects of the bpy substitution on the selectivity of the electrocatalyzed reduction of  $\text{CO}_2$  by  $[\text{Ru}(\text{bpy})_2(\text{CO})_2]^{2+}$  complexes have been observed previously [13]. Electron donating groups such as Me on the bpy ligand increases the amount of CO (99%).

The main difficulty relative to the utilization of  $[\text{Ru}(\text{L})(\text{CO})_2]_n$  cathodes arises from their instability at potentials higher than - 0.70 V. The presence of molecular oxygen also induces oxidation of the polymeric material into dimeric and monomeric complexes and disintegration of the molecular cathodes. As a consequence  $[\text{Ru}(\text{L})(\text{CO})_2]_n$  films cannot be handled easily in air. In order to circumvent this difficulty molecular electrodes e.g. *ppyrr*- $[\text{Ru}(\text{L})(\text{CO})_2\text{Cl}_2]$  with preformed films of monomeric  $[\text{Ru}(\text{L})(\text{CO})_2\text{Cl}_2]$  complexes can be used. They are prepared as functionalized polypyrrolic films (15) by anodic oxidation of the corresponding monomeric complex containing a bipyridine ligand having pyrrole groups as substituents. The formation of metal-metal bonds within the film via a mechanism similar to that of  $[\text{Ru}(\text{bpy})(\text{CO})_2]_n$  formation from *trans*-Cl-



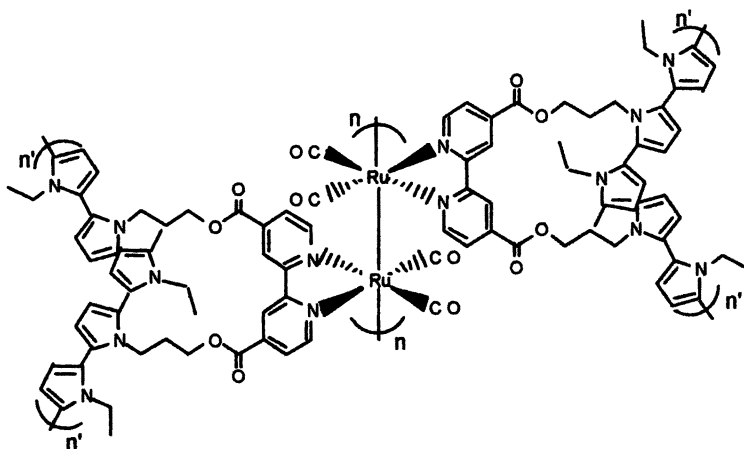


Figure 7 : Schematic structure of the  $ppy\text{-}[\text{Ru}(\text{L}_2)(\text{CO})_2]_n$  composite material

$[\text{Ru}(\text{bpy})(\text{CO})_2\text{Cl}_2]$  can be easily achieved electrochemically by continuous cycling the potential of the Pt or the VC  $| ppy\text{-}[\text{Ru}_1(\text{L}_1)(\text{CO})_2\text{Cl}_2]$  modified electrode in the cathodic range ( $-0.9 \rightarrow -2.0$  V for instance) or by potentiostating the electrode at  $-1.28$  V and  $-1.60$  V depending on the ligand L used. Fig. 7 shows the proposed structure of the resulting  $ppy\text{-}[\text{Ru}(\text{L}_2)(\text{CO})_2]_n$  composite material with a ligand also substituted by an ester group  $\text{L}_2$ . Like  $[\text{Ru}(\text{bpy})(\text{CO})_2]_n$ ,  $ppy\text{-}[\text{Ru}(\text{L}_1)(\text{CO})_2]_n$  films give CO as the main product of the reduction of  $\text{CO}_2$ .

The same study has been carried out with C  $| ppy\text{-}[\text{Ru}(\text{L}_2)(\text{CO})_2]_n$  films. As expected, the orientation of the  $\text{CO}_2$  reduction toward  $\text{HCOO}^-$  brought about by the ester groups is maintained in the preformed polypyrrole film. It should be noted that the catalytic current decreased slowly as the charge passed increased (about 30 % after 100 C ;  $\text{H}_2\text{O} + 0.1$  M  $\text{Na}_2\text{SO}_4$  in the presence of phosphate buffers). The utilization of a more conductive medium :  $0.5$  M  $\text{Na}_2\text{SO}_4$  without phosphate ions or  $0.5$  M  $\text{Na}_2\text{SO}_4 + 0.1$  M  $\text{NaHCO}_3$  allows perfectly stable catalytic currents to be obtained. No noticeable decrease in current intensity was observed after 800 C has been consumed. Moreover this kind of modified electrodes can be reused five times without any change in the intensity of the catalytic steady current. Under these conditions a formate current efficiency of 99% can be reached at a very low overvoltage ( $-0.75$  V) (16).

## Acknowledgments

I express my sincere appreciation to my coworkers involved in this research program, especially Dr. Sylvie Chardon (CNRS senior scientist), my students (Dr. Marie-Noëlle Collomb-Dunand-Sauthier, Dr. Daniela Zsoldos, Dr. Chrystelle Cecillon-Caix and Philippe Da Costa) and my colleague Dr. Raymond Ziessel from the Ecole Européenne Chimie des polymères, Matériaux, Strasbourg - France and Pr. Pakkanen from the University of Joensuu - Finlande.

## References

1. Ziessel, R. in *Photosensitization and Photocatalysis Using Inorganic and Organometallic Compounds* ; Kalyanasundaram, K. ; Grätzel, M., Eds ; Kluwer : Dordrecht, 1993 ; p. 217-240.
2. *Electrochemical and Electrocatalytic Reaction of Carbon Dioxide* ; Sullivan, B.P. ; Krist, K. ; Guards, H.E., Eds ; Elsevier : Amsterdam, 1993.
3. Collin, J.-P. ; Sauvage, J.-P. *Coord. Chem. Rev.* **1989**, 93 245.
4. Abe, T. ; Yoshida, T. ; Tokita, S. ; Taguchi, F. ; Imai, H. ; Kaneko, M. *J. Electroanal. Chem.* **1996**, 412, 125 and references therein.
5. Collomb-Dunand-Sauthier, M.-N. ; Deronzier, A. ; Ziessel, R. *J. Electroanal. Chem.* **1993**, 350, 43.
6. Collomb-Dunand-Sauthier, M.-N. ; Deronzier, A. ; Ziessel, R. *J. Chem. Soc., Chem. Commun.* **1994**, 189.
7. Collomb-Dunand-Sauthier, M.-N. ; Deronzier, A. ; Ziessel, R. *Inorg. Chem.* **1994**, 33, 2961.
8. Chardon-Noblat, S. ; Deronzier, A. ; Ziessel, R. ; Zsoldos, D. *J. Electroanal. Chem.* **1998**, 444, 253.
9. Caix-Cecillon, C. ; Chardon-Noblat, S. ; Deronzier, A. ; Haukka, M. ; Pakkanen, T.A. ; Ziessel, R. ; Zsoldos, D. *J. Electroanal. Chem.* **1999**, 466, 187.
10. Chardon-Noblat, S. ; Deronzier, A. ; Zsoldos, D. ; Ziessel, R. ; Haukka, M. ; Pakkanen, T.A. ; Venäläinen, T. *J. Chem. Soc. Dalton Trans.* **1996**, 2581.
11. Chardon-Noblat, S. ; Da Costa, P. ; Deronzier, A. ; Haukka, M. ; Pakkanen, T.A. ; Ziessel, R. *J. Electroanal. Chem.* in press.
12. Lehn, J.-M. ; Ziessel, R. *J. Organomet. Chem.* **1990**, 382, 157.
13. Ishida, H. ; Fujiki, K. ; Ohba, T. ; Ohkuba, K. ; Tanaka, K. ; Terada, T. ; Tanaka, T. *J. Chem. Soc., Dalton Trans.* **1990**, 2155.
14. Pugh, J.R. ; Bruce, M.R.H. ; Sullivan, B.P. Meyer, T.J. *Inorg. Chem.* **1991**, 30, 86.
15. Collomb-Dunand-Sauthier, M.-N. ; Deronzier, A. ; Ziessel, R. *J. Phys. Chem.* **1993**, 97, 5973.
16. Chardon-Noblat, S. ; Collomb-Dunand-Sauthier, M.-N. ; Deronzier, A. ; Orillon, M. ; Ziessel, R. ; Zsoldos, D., patent n° WPB 1997, 39500.

## Chapter 12

# Modification of Electroactive Biomaterials for Neural Engineering Applications

Christine Schmidt<sup>1,2</sup>, Tyrell Rivers<sup>2</sup>, Terry Hudson<sup>2</sup>,  
and Joel Collier<sup>1</sup>

<sup>1</sup>Biomedical Engineering Program, The University of Texas at Austin,  
Austin, TX 78712-1084

<sup>2</sup>Department of Chemical Engineering, The University of Texas at Austin,  
Austin, TX 78712-1062

New tissue engineering technologies will rely increasingly more on interactive biomaterials that can both physically support tissue growth and stimulate specific cell functions. In our research, we have focused on a biomaterial with electrical properties (i.e., the electrically conducting polymer, polypyrrole) that has been shown to improve the regeneration of several tissues including nerve. We have modified polypyrrole for tissue engineering applications by either incorporating biological molecules that can specifically trigger desired cellular responses (e.g., the formation of new blood vessels), or by adding unique linkage sites within the polypyrrole backbone to control its degradation and mechanical integrity. To this end, we are synthesizing two distinct materials: (1) composites of polypyrrole and the polysaccharide hyaluronan which stimulates angiogenesis as it degrades; and (2) conducting pyrrole oligomers of three units in length connected using degradable ester linkages. These materials are promising candidates for tissue engineering applications, such as nerve repair, that may benefit from electrical stimulation and/or enhanced vascularization.

## Introduction

The emergence of new tissue engineering technologies will ultimately require that biomaterials be designed both to physically support tissue growth as well as to elicit desired receptor-specific responses from particular cell types. One way of achieving such interactive biomaterials is with the incorporation of biological molecules into synthetic matrices. Further specificity may be gained by choosing a material with inherent properties that enhance desired cellular responses – for example, an electroactive material that can stimulate electrically responsive cell types such as bone or nerve. In this paper, we summarize our research to further modify an electrically conducting polymer, polypyrrole, for neural tissue engineering applications by (1) the incorporation of biological molecules (i.e., hyaluronan) that can specifically trigger desired cellular responses (e.g., the formation of new blood vessels), and (2) the addition of unique linkage sites within the polypyrrole backbone to control its degradation, mechanical integrity, processibility, and electrical properties.

### The Clinical Need for New Biomaterials in Neural Tissue Engineering

Current clinical treatments for peripheral nerve injury are surgical end-to-end anastomoses and autologous nerve grafts. Surgical end-to-end repair involves the direct reconnection of individual nerve fibers, and is useful only if the damaged nerve ends are adjacent (1). To repair a large nerve defect, autologous nerve grafts are used to bridge the gap and to guide the regenerating axons (2). However, there are several drawbacks to this approach, including loss of function at the donor site and the need for multiple surgeries.

In an effort to surpass these limitations, research is focused on creating the ideal scaffold that can be used to bridge damaged nerve ends (Figure 1).

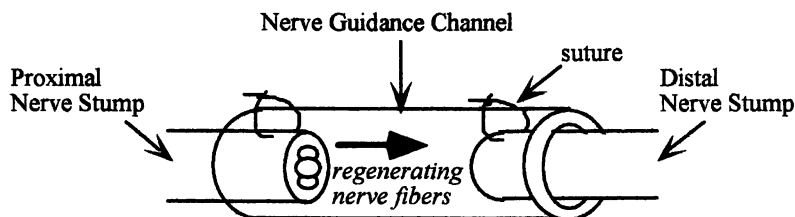


Figure 1. Schematic of surgical placement of a nerve guidance channel.

These nerve guidance channels help direct axons sprouting off the regenerating (proximal) nerve end, provide a conduit for diffusion of neurotrophic factors secreted by the damaged nerve ends, and minimize infiltrating fibrous tissue. Over the years, researchers and surgeons have used various existing natural and synthetic materials to physically bridge nerve defects; however, none of these materials has matched the effectiveness of nerve grafts. As a result, researchers are now focusing on the combination of existing materials with adhesive and growth-promoting molecules and the creation of new materials that can actively stimulate the repair process.

### **Polypyrrole (PP) as a Biomaterial**

In its oxidized form (Figure 2a), polypyrrole (PP) is a polycation with delocalized positive charges along its highly conjugated backbone. The conjugated backbone permits electron transfer between different chains, giving rise to electronic conduction. Negatively charged counter ions or dopant ions ( $X^-$  in Figure 2a) associate with polycationic PP to yield overall charge neutrality.

Several biomedical applications have been developed based on the electrochemical properties of PP including its use as a matrix for controlled delivery of the neurotransmitter dopamine (3) and as a biosensor for glucose detection (4). PP can also be easily fabricated electrochemically into thin films for use with in vitro microscopy studies or into thick films for use with in vivo implantation studies. Studies with PP have shown that it is not toxic to cells, and that this material can be formed into conduits (i.e., nerve guidance channels) to support the regeneration of damaged peripheral nerves in rats (5). Research has also shown that in vitro electrical stimulation of PC12 cells (i.e., a neuron-like cell line) using PP as the substratum results in nearly a two-fold enhancement of neurite (axon) outgrowth compared to unstimulated controls (5).

Another useful property of PP is that its synthesis requires the incorporation of negatively charged dopant ions. By selecting an appropriate dopant, the properties of PP can be tailored. In the past, PP has been doped with a wide variety of materials, including small anions (6), polymeric anions (7), and biologically active anions such as ATP (8) and heparin (9). As part of the studies summarized here, we incorporated hyaluronan as a biologically-active dopant ion as a means to trigger angiogenesis and enhance nerve regeneration.

### **Hyaluronan and the Role of Angiogenesis in Nerve Regeneration**

We sought to couple the ability of PP to electrically stimulate tissue regeneration with the specific biological activity of hyaluronan or hyaluronic acid (HA) (10). HA, a major component of the extracellular matrix (ECM), is a

high molecular weight glycosaminoglycan composed of a disaccharide repeat of N-acetylglucosamine and D-glucuronic acid (Figure 2b). Each glucuronic acid unit contains one carboxyl group, giving rise to HA's polyanionic character at physiologic pH. HA was chosen because it can be used as a negative dopant ion during PP synthesis, as well as for its known beneficial role in wound healing, as described below. HA's high density of negative charges also yields a highly hydrophilic nature. In water, HA expands in volume 1000 times. HA is thought to play roles as space filler, lubricant, and osmotic buffer in the ECM.

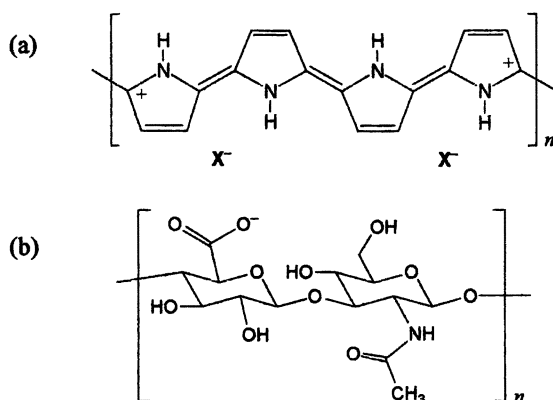


Figure 2. Chemical structure of oxidized polypyrrole (a) and hyaluronan (b).

HA is also involved in cell signaling events including migration, attachment, and neuronal sprouting (11). These matrix-induced processes are mediated through a group of proteins collectively called hyaladherins or hyaluronan binding proteins (HA-binding proteins). Hyaladherins include two types of binding proteins: those that network HA with other ECM molecules, and those, such as the receptor for HA-mediated motility (RHAMM), that are found on the cell surface and act as receptors for HA (12). Therefore, HA may affect cell behavior indirectly by altering the physical and hydrodynamic properties of the ECM or directly via cell surface receptors (13).

In addition, and of key interest for tissue regeneration, fragments of HA appear to promote angiogenesis. While long chain HA has been shown to inhibit angiogenesis, degradation products of 4-25 disaccharide units have been shown to stimulate in vivo capillary growth (14) and 3-16 disaccharide units have been shown to induce in vitro endothelial proliferation, migration and tube formation (15-17). The cellular mechanisms by which HA oligosaccharides promote

angiogenesis are not completely understood, although studies suggest that binding of the CD44 cell surface receptor to HA is involved (15,18).

The vasculature plays a critical role in wound healing by supporting the metabolism of regenerating cells. Various researchers have found vasculature to limit nerve regeneration in nerve guidance channels – increases in capillary number and permeability appear in a wave, proceeding neurite outgrowth (19, 20). Thus, targeting angiogenesis, in combination with the use of electroactive nerve guidance channels, should further enhance the nerve repair process.

### **The Need for a Biodegradable and Processible Form of PP**

PP in its present form (Figure 2a) is not easily processed into various forms and is non-degradable. Although several applications that exploit the electronic conductivity (glucose sensors) and reversible electrochemistry (dopamine release) of PP have been explored, these applications for PP could be expanded if it possessed reasonable processibility. For example, in tissue engineering, the control over three-dimensional architecture in a predictable fashion is crucial to elicit desired cellular responses. Hence, the synthesis of PP with some degree of processibility and pliability would be an enormous contribution. Furthermore, although PP appears to exhibit good short-term and long-term tissue compatibility, a biodegradable form of the material would be ultimately desired. The long-term presence of any foreign material, especially with implants in the nervous system, always poses a potential risk. As a result of the possible dangers associated with permanent materials, the use of biodegradable materials in clinical applications has become more attractive (21).

## **Materials and Methods**

### **Synthesis and Characterization of Polypyrrole-HA Composites**

#### *PP/HA Material Synthesis*

PP/HA films were compared to PP films doped with poly(styrenesulfonate) (PSS) because PP/PSS films have been well characterized (5). PP/HA *bilayer* films were synthesized because films composed entirely of PP/HA (i.e., no underlying PP/PSS) were mechanically and electrically inferior (10). Bilayer films consist of a PP/PSS layer that provides bulk polymeric properties (good mechanical and electrical properties) and a PP/HA layer that provides biological activity. PP/HA bilayer films were electrochemically synthesized by polymerizing a film of PP/PSS onto an ITO-coated glass slide (from a solution

of 0.1 M pyrrole, 0.1 M PSS) and polymerizing a PP/HA layer on top of the PP/PSS film (from a solution of 0.1 M pyrrole, 2 mg/ml HA). Film thickness was varied between 0.15 and 2  $\mu\text{m}$ , depending on the application (e.g., animal implantation studies require thick, strong films). For consistency in HA content, the PP/HA layer thickness was kept at 0.05  $\mu\text{m}$ , and the underlying PP/PSS layer thickness was varied to give the desired total thickness.

### *PP/HA Material Characterization*

PP conductivity was measured using a four-point probe technique (10). Nickel print conductive bus material was applied to the corners of PP films (2  $\mu\text{m}$ ). A constant current was applied between two adjacent corners, and the voltage across the other two corners was measured. Conductivities were calculated from these measurements using the equations of Van der Pauw (22).

To detect HA on the surfaces of PP films, a colorimetric enzyme-based assay was used. PP/PSS and PP/HA bilayer films (0.15  $\mu\text{m}$ ) were blocked using 3% BSA and then incubated in biotinylated HA binding protein (bHABP) solution. Avidin-biotin-peroxidase complex (Vectastain kit PK-4000, Vector Laboratories) and o-phenylenediamine dihydrochloride (OPD) substrate were used to create a colored product. Absorbances were measured at 490 nm.

In vivo vascularization in response to PP films were evaluated. PP/PSS and PP/HA bilayer films (2  $\mu\text{m}$ ) were synthesized and laminated to poly(lactic acid-co-glycolic acid) (PLGA) films to prevent folding during implantation. Small subcutaneous pouches were created near the shoulder blades of male rats under general anesthesia, and squares (1 x 1 cm) of PLGA-laminated PP/PSS and PP/HA bilayer films were implanted. Films were harvested after 2 and 6 weeks, and the explanted tissues were fixed in formalin and stained using a standard hematoxylin and eosin protocol. For each sample, 5 images within a 550  $\mu\text{m}$  vicinity of the implant were captured using brightfield microscopy. NIH Image software was used to measure the total area occupied by blood vessels (expressed as %blood vessels, relative to total area of tissue in image).

Additional detailed characterization studies of PP/HA using cyclic voltammetry, scanning electron microscopy, x-ray photoelectron spectroscopy, and reflectance-absorbance infrared spectroscopy are described elsewhere (10).

### **Synthesis of a Biodegradable Form of Polypyrrole**

We are in the process of synthesizing a polymer containing electrically conducting oligomers of pyrrole coupled to one another via degradable ester linkages. The resulting polymer is expected to not only be electronically



conductive upon chemical or electrochemical oxidation but also exhibit excellent mechanical properties and processibility.

The goal is to synthesize electrically conducting units of three pyrroles connected via aliphatic chains and degradable ester linkages (Figure 3). The motivation for this particular structure is based on several considerations. (1) In an electrochemically synthesized PP film, the conjugation length is typically 3-5 pyrrole units. Beyond this length, the conjugation is disrupted as the result of a defect, possibly in the form of a C-C inter or intra-chain bond from radical coupling. This suggests that a minimum PP chain of approximately 3-5 pyrrole units would be sufficient to impart conductivity. (2) Conductivity in PP, unlike with other organic conductors such as polyacetylene or poly(p-phenylene), results primarily from the hopping of electrons between chains (inter chain) and not along the chain (intra chain). Thus, for the microphase separated structure of the proposed polymer, good  $\pi$ - $\pi$  overlap could be expected and the electrical conductivity should be preserved within an order of magnitude. (3) The aliphatic chain separating the terpyrrole oligomers will impart an overall flexibility to the final polymer structure. In addition, the alkyl chain length can be varied to alter the mechanical and degradation properties of the final polymer. (4) The ester linkages will be degraded in vivo by hydrolysis and enzymes, giving rise to biodegradable characteristics.

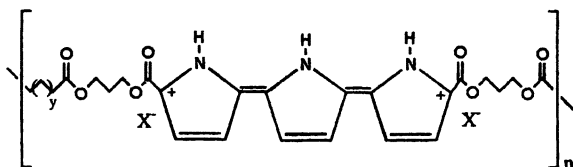


Figure 3. Schematic of conductive terpyrrole units connected via degradable ester linkages and flexible aliphatic chains.

The synthesis of biodegradable PP is being carried out in five major steps:

1. Terpyrroles with methyl ester groups at their  $\alpha$  positions will be synthesized, using modified procedures of Wallace et al. (23) and Merrill and LeGoff (24).
2. The methyl esters of the terpyrrole will be hydrolyzed to form diacids.
3. The diacids will be converted to esters with hydroxyl groups at the end.
4. The hydroxy-terminated oligomers will be reacted with an alkyl diacid chloride to yield the biodegradable PP.
5. The polymer will be transformed to its conductive form (Figure 3) via either chemical and/or electrochemical oxidation.

## Results

### Synthesis and Characterization of Polypyrrole-HA Composites

PP/HA bilayer films have electrical conductivities ( $\sigma = 8.02 \pm 0.21$  S/cm,  $n = 3$ ) statistically indistinguishable from those of PP/PSS films ( $\sigma = 9.25 \pm 1.68$  S/cm,  $n = 3$ ). The conductivities of PP/PSS and the PP/HA bilayer films are typical of conductivities of doped PP materials reported in the literature (25). These data demonstrate that the electrical characteristics of the PP backbone were not compromised by the inclusion of HA as a dopant ion.

We used a biotinylated HA binding protein (bHABP) to probe for HA on the PP films. The PP/HA bilayer films stain heavily with bHABP, and the PP/PSS films are statistically indistinguishable from the blank values. The absorbance for PP/HA bilayer films ( $0.955 \pm 0.222$ ,  $n = 6$ ) is statistically higher than that for PP/PSS ( $0.081 \pm 0.007$ ,  $n = 6$ ) ( $p < 0.005$ ). This suggests that HA is present and biologically active on the surfaces of the PP/HA bilayer films.

Because degradation products of HA are known to stimulate angiogenesis, we evaluated the vascularization response to PP films. Compared to PP/PSS films, PP/HA bilayer films exhibit enhanced vascularization (Figure 4).

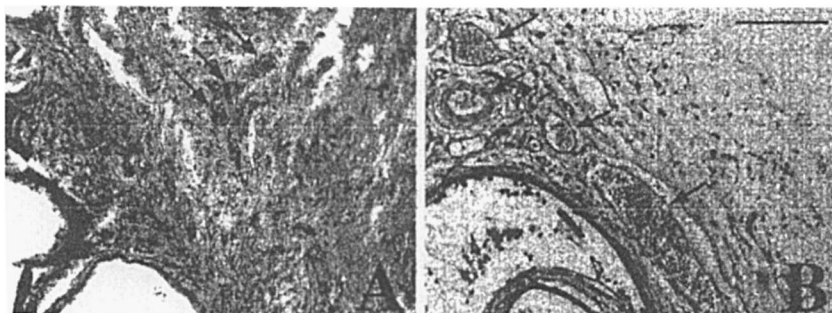


*Figure 4. In vivo vascularization surrounding PP/PSS (a) and PP/HA (b) films. Scale bar, 100  $\mu$ m.*

*(Reproduced with permission from reference 36. Copyright 2000 J. Bio-med. Mater. Res.)*

As shown in Figure 4b, numerous blood vessels (indicated by arrows) are found to surround the PP/HA bilayer implant (black material in figure) after 2 weeks of implantation, compared to fewer vessels surrounding PP/PSS films (Figure 4a). Furthermore, the blood vessels surrounding the PP/HA bilayer implants are consistently larger. Vascularization of tissue surrounding the

PP/PSS films ( $2.4 \pm 1.2\%$ ,  $n = 9$ ) ( $p < 0.005$ ). This represents nearly a two-fold enhancement of blood vessel growth near the PP/HA implants compared to vascularization near PP/PSS implants after 2 weeks of implantation.

### Synthesis of a Biodegradable Form of Polypyrrole

The synthesis of the biodegradable form of polypyrrole was initiated using the five steps outlined under Material and Methods. As part of this scheme, the synthesis of terpyrrole diacids (step 2) and their subsequent conversion to esters bearing hydroxyl groups (step 3) is crucial to the formation of the final polymer. However, it was found that the diacid was sparingly soluble in common organic solvents. Since polythiophenes demonstrate the same conductive properties as polypyrrole and are noted for having increased solubilities, the center nitrogen of the terpyrrole was replaced by a sulfur atom to form a thiophene unit. The diacid of this terpyrrole derivative is soluble in common organic solvents and is being used for the remainder of the synthesis. Thus, Figure 5 summarizes our altered chemical strategy to produce a biodegradable form of polypyrrole. Figure 5a represents the terpyrrole derivative that has already been synthesized, as described below, and Figure 5b gives the predicted final structure of the polymer using the terpyrrole derivative as a precursor.

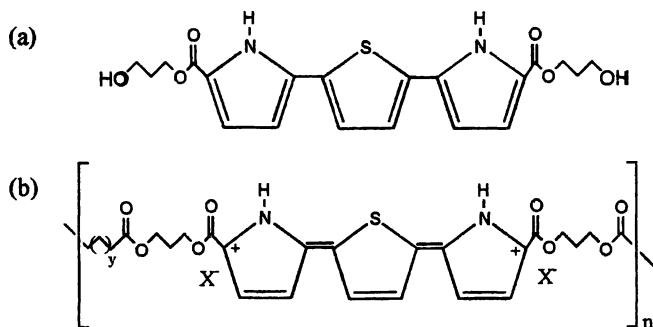


Figure 5. (a) Structure of new terpyrrole derivative with thiophene unit.  
(b) Final predicted structure of biodegradable polypyrrole-derivative.

Currently, the hydroxy-terminated terpyrrole derivative (as shown in Figure 5a) has been successfully synthesized and characterized using NMR ( $^1\text{H}$  and  $^{13}\text{C}$ ) and mass spectroscopy. Figure 6 shows the proton NMR of the terpyrrole derivative that is depicted in Figure 5a. The peak located farthest downfield

represents the pyrrole proton (12.22), followed by the aromatic ring protons (H-thiophene, 7.55; H-pyrrole-thiophene 6.80; H-pyrrole-ester, 6.39). The remaining peaks correspond to the hydroxyl proton (4.56) and the propyl protons ( $C_{\alpha}$ , 3.52;  $C_{\beta}$ , 1.82; and  $C_{\gamma}$ , 4.27). These peaks are consistent with the structure given in Figure 5a. We are currently in the process of creating the full biodegradable polymer (as shown in Figure 5b) from this precursor, following the methods outlined in the Materials and Methods section.

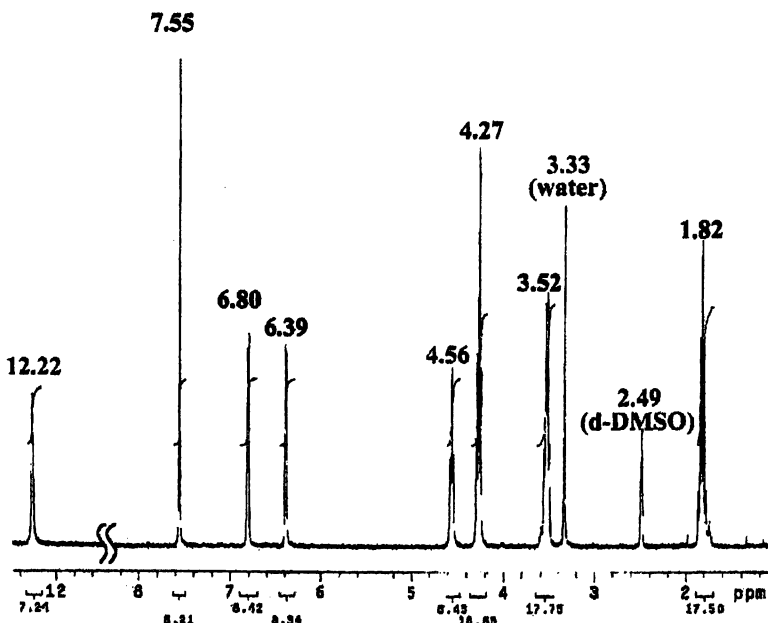


Figure 6. Proton ( $^1\text{H}$ ) NMR for terpyrrole derivative in Figure 5a. NMR obtained using a Varian Ultra Plus (300 MHz).

## Conclusions

In this paper, we summarized our research to further modify PP for neural tissue engineering applications by (1) the incorporation of biological molecules (i.e., hyaluronan) that can specifically trigger angiogenesis, and (2) the addition of unique linkage sites within the PP backbone to control its degradation, mechanical integrity, processibility, and electrical properties. In the first set of experiments, we were able to produce PP/HA composite materials with good electrical conductivity and electrochemical properties. In addition, PP/HA biomaterials were found to increase the formation of new blood vessels by two-fold compared to controls when implanted into rats. Another aspect of our research that is discussed in this paper is our goal to synthesize a biodegradable

and more processible form of PP, which will ultimately have the positive attributes of being inherently electrically conductive and also have the clinical appeal of being biodegradable. To accomplish this goal, we are in the process of synthesizing a polymer containing electrically conducting oligomers of pyrrole coupled to one another via hydrolyzable ester linkages. In summary, both materials – PP/HA composites and biodegradable PP – are promising candidates for tissue engineering applications, such as nerve repair, that may benefit from electrical stimulation and/or enhanced vascularization.

The authors thank Collaborative Laboratories for the gift of HA, Paraskevi Heldin for bHABP, and Glenn Prestwich, Koen Vercruyse, and Grant Willson for technical consultation. This work was supported by grants from NSF (BES-9733156, BES-9702882) and a gift from the Gillson Longenbaugh Foundation.

## References

1. Millesi, H.; Meissl, G.; Berger, A. The interfascicular nerve-grafting of the median and ulnar nerves. *J. Bone and Joint Surgery*, **1972**, *54A*, 727.
2. Millesi, H. Indications and techniques of nerve grafting. In *Operative Nerve Repair and Reconstruction*; Gelberman, R. H., Ed.; J.B. Lippincott: Philadelphia, PA, 1991; pp. 525-544.
3. Miller, L. L.; Zhou, Q.-X. Poly(N-methylpyrrolylium)poly(styrene-sulfonate). A conductive, electrically switchable cation exchanger that cationically binds and anodically releases dopamine. *Macromolecules* **1987**, *20*, 1594-1597.
4. Couves, L. D. Polypyrrole as a potentiometric glucose sensor. *Synth. Metals* **1989**, *28*, C761-C768.
5. Schmidt, C. E.; Shastri, V. R.; Vacanti, J. P.; Langer, R. Stimulation of neurite outgrowth using an electrically conducting polymer. *Proc. Natl. Acad. Sci.* **1997**, *94*, 8948-8953.
6. Vork, F.T.A.; Schuermans, B.C.A.M.; Barendrecht E. Influence of inserted anions on the properties of polypyrrole. *Electrochim Acta* **1990**, *35*, 567-75.
7. Prezyna, L. A.; Qiu, Y.-J.; Reynolds, J. R.; Wnek, G. E. Interaction of cationic polypeptides with electroactive polypyrrole/poly(styrenesulfonate) and poly(N-methylpyrrole)/ poly(styrenesulfonate) films. *Macromolecules* **1991**, *24*, 5283-5287.
8. Boyle, A.; Genies, E.; Fouletier, M. Electrochemical behaviour of polypyrrole films doped with ATP anions. *J. Electroanal. Chem.* **1990**, *279*, 179-186.
9. Garner, B.; Georgevich, B.; Hodgson, A. J.; Liu, L.; Wallace, G. G. Polypyrrole-heparin composites as stimulus-responsive substrates for endothelial cell growth. *J. Biomed. Mater. Res.* **1999**, *44*, 121-129.

10. Collier, J. H.; Camp, J. P.; Hudson, T. W.; Schmidt, C. E. Synthesis and Characterization of Polypyrrole/Hyaluronic Acid Composite Biomaterials for Tissue Engineering. *J. Biomed. Mater. Res.* **2000**, *50*, 574-584.
11. Laurent, T. C.; Fraser, J. R. Hyaluronan. *Faseb J.* **1992**, *6*, 2397-2404.
12. Nagy, J. I.; Hacking, J.; Frankenstein, U. N.; Turley, E. A. Requirement of the hyaluronan receptor RHAMM in neurite extension and motility as demonstrated in primary neurons and neuronal cell lines. *J. Neurosci.* **1995**, *15*, 241-252.
13. Knudson, C. B.; Knudson, W. Hyaluronan-binding proteins in development, tissue homeostasis, and disease. *Faseb J.* **1993**, *7*, 1233-1241.
14. West, D. C.; Hampson, I. N.; Arnold, F.; Kumar, S. Angiogenesis induced by degradation products of hyaluronic acid. *Science* **1985**, *228*, 1324-1326.
15. Trochon, V.; Mabilat, C.; Bertrand, P.; Legrand, Y.; Smadja-Joffe, F.; Soria, C.; Delpech, B.; Lu, H. Evidence of involvement of CD44 in endothelial cell proliferation, migration and angiogenesis in vitro. *Int. J. Cancer* **1996**, *66*, 664-668.
16. Deed, R.; Rooney, P.; Kumar, P.; Norton, J. D.; Smith, J.; Freemont, A. J.; Kumar, S. Early-response gene signalling is induced by angiogenic oligosaccharides of hyaluronan in endothelial cells. Inhibition by non-angiogenic, high-molecular-weight hyaluronan. *Int. J. Cancer* **1997**, *71*, 251-256.
17. Rahmanian, M.; Pertoft, H.; Kanda, S.; Christofferson, R.; Claesson-Welsh, L.; Heldin, P. Hyaluronan oligosaccharides induce tube formation of a brain endothelial cell line in vitro. *Exp. Cell Res.* **1997**, *237*, 223-230.
18. Lokeshwar, V. B.; Iida, N.; Bourguignon, L. Y. The cell adhesion molecule, GP116, is a new CD44 variant (ex14/v10) involved in hyaluronic acid binding and endothelial cell proliferation. *J. Biol. Chem.* **1996**, *271*, 23853-23864.
19. Hobson, M. I.; Brown, R.; Green, C. J.; Terenghi, G. Inter-relationships between angiogenesis and nerve regeneration: a histochemical study. *Br. J. Plast. Surg.* **1997**, *50*, 125-131.
20. Podhajsky, R. J.; Myers, R. R. The vascular response to nerve transection: neovascularization in the silicone nerve regeneration chamber. *Brain Res.* **1994**, *662*, 88-94.
21. Langer, R.; Vacanti, J. P. Tissue engineering. *Science* **1993**, *260*, 920-926.
22. Van der Pauw, L. J. A method of measuring specific resistivity and hall effect of discs of arbitrary shape. *Phillips Res. Rep.* **1958**, *13*, 1-9.
23. Wallace, D.; Leung, S.; Senge, M.; Smith, K. *J. Org. Chem.* **1993**, *58*, 7245.
24. Merrill, B.; LeGoff, E. *J. Org. Chem.* **1990**, *55*, 2904.
25. Diaz, A. F.; Bargon, J. Electrochemical Synthesis of Conducting Polymers. In *Handbook of Conducting Polymers*; Skotheim, T.A., Ed; Marcel Dekker: New York, 1978.

## Chapter 13

# Conducting Polymer-Supported Fuel Cell Catalysts

Zhigang Qi<sup>1,2</sup>, Jingning Shan<sup>1</sup>, and Peter G. Pickup<sup>1,\*</sup>

<sup>1</sup>Department of Chemistry, Memorial University of Newfoundland, St. John's, Newfoundland A1B 3X7, Canada

<sup>2</sup>Current address: H Power Corporation, 60 Montgomery Street, Belleville, NJ 0

The use of conducting polymer supported metal catalysts for the main fuel cell reactions (oxygen reduction, hydrogen oxidation, and methanol oxidation) is reviewed and new results are presented for oxygen reduction at polyaniline supported Pt and methanol oxidation at poly(3,4-ethylenedioxythiophene) supported Pt-Ru. It is shown that polymer supported electrodes can provide performances that approach those of commercial carbon supported catalysts, but that stability problems currently make applications in fuel cells impractical.

The potential use of polymer supports in electrocatalysis has been one of the major factors driving the development of polymer modified electrodes over the past 20 years (1, 2). The early focus was on the use of molecular catalysts such as porphyrins and other macrocyclic complexes. However, such systems provide limited activity and durability and are therefore not suitable for application in fuel cells. There has therefore been an increasing focus on the use of bulk metals, alloys, and oxides on polymer supports.

Polymer supports are attractive for use in fuel cells because their properties can (in theory) be tailored to provide the most efficient use of precious metal

catalysts. Key parameters are the electronic and proton conductivity of the support, its porosity and ability to facilitate and maintain dispersion of the catalytic particles, and its hydrophilicity. The latter is important in that the catalyst layer in the fuel cell must remain sufficiently hydrated to provide good proton conductivity and electrochemical kinetics, while rejecting water to prevent flooding of its pores.

The need for high electronic conductivity has meant that work has focused on the use of the so called conducting polymers, exemplified by polypyrrole, polyaniline and polythiophene (Structures 1 to 3). These materials must be in their p-doped (partially oxidized) states (right hand side of eq. 1, for example) to exhibit sufficient electronic conductivity. Unfortunately, the p-doped polymers are cationic and will therefore tend to exclude the protons needed for the fuel cell reactions. To circumvent this problem, composites of conducting polymers with cation exchange polymers have been used. Thus p-doped polypyrrole / poly(styrene-4-sulphonate) (PSS), for example, exhibits both proton and electron conductivity (8).

Platinum has been the most widely used catalyst, since it (and its alloys) is the only sufficiently efficient catalyst material for oxygen reduction in low temperature (< 120 °C) fuel cells. For fuel cell anodes, Pt-Ru alloys provide better tolerance to CO in the fuel stream (hydrogen from reformed methane or methanol) and have been found to be most effective for methanol oxidation.

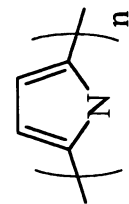
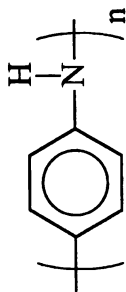
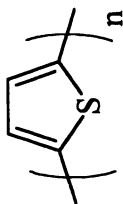
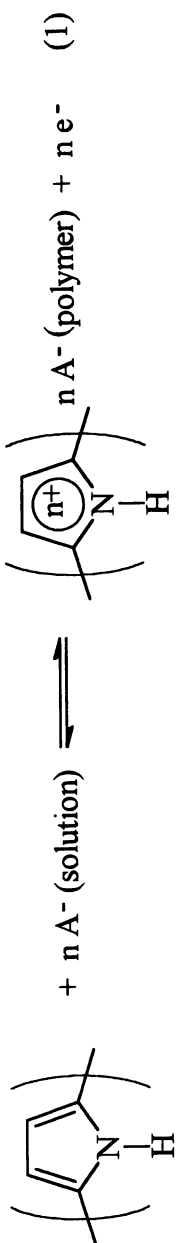
## Catalysts for Oxygen Reduction

### Polypyrrole Supported Catalysts

The first demonstration of oxygen reduction at a polypyrrole supported Pt catalyst appears to have been by Holdcroft and Funt (3). They electrochemically deposited a polypyrrole film on a glassy carbon electrode and then electrochemically deposited Pt from  $\text{H}_2\text{PtCl}_6$  onto and within this polymer matrix. The use of various Pt deposition protocols allowed the spacial distribution in the polypyrrole film to be varied. It was found that electrodes in which Pt was dispersed homogeneously through the film, in order to increase its surface area, suffered severe mass transport limitation due to the low oxygen permeability of the polypyrrole matrix. This therefore offsets the the advantage of dispersing the Pt over simply depositing it on a flat surface.

Rajeshwar and coworkers (4-6) took the important step of using colloidal Pt particles, which are necessary to provide efficient use of the expensive Pt catalyst. They electrochemically deposited polypyrrole onto glassy carbon electrodes from a colloidal Pt suspension containing pyrrole. These authors draw the interesting conclusions that the polypyrrole support itself shows some activity for oxygen



**1: polypyrrole****2: polyaniline****3: polythiophene**

reduction, and that the rate of oxygen reduction in their system is not limited by permeation of oxygen into the film, despite the uniform Pt distribution.

Although electrochemically prepared polypyrrole films are useful for fundamental studies, they are not practical for use in fuel cells. Apart from the difficulty of their large scale production, their permeability is insufficient for generation of the large current densities ( $> 500 \text{ mA cm}^{-2}$ ) required of commercial cells. To circumvent these problems, we have used chemically prepared polypyrrole/poly(styrene-4-sulphate) powders, which we have rendered catalytic by the chemical deposition of Pt particles by various methods (7-9). These polypyrrole supported Pt catalysts can easily be mass-produced, and can be formed into catalyst layers for fuel cell gas diffusion electrodes using the technology currently used commercially for carbon supported catalysts.

Although some of these catalysts provided encouraging performances for oxygen reduction in gas diffusion electrodes, yielding current densities as high as  $100 \text{ mA cm}^{-2}$  (8), we were unable to produce materials with both sufficiently small Pt particles and sufficient electronic conductivity. Deposition of Pt nanoparticles (ca. 4 nm) by formaldehyde reduction of  $\text{Pt}(\text{NH}_3)_4\text{Cl}_2$  (or  $\text{H}_2\text{PtCl}_6$ ), or  $\text{PtO}_2$  nanoparticles (ca. 2 nm) by  $\text{H}_2\text{O}_2$  oxidation of  $\text{Na}_6\text{Pt}(\text{SO}_3)_4$ , both resulted in a loss of electronic conductivity of the polypyrrole support to ca.  $10^{-5} \text{ S cm}^{-1}$  (7). Pt deposition by reduction of  $\text{K}_2\text{PtCl}_4$  with  $\text{H}_2$  produced a catalyst with a much higher electronic conductivity (ca.  $0.3 \text{ S cm}^{-1}$ ), but large (ca. 200 nm) Pt particle size. Use of citrate to reduce  $\text{H}_2\text{PtCl}_6$  to colloidal Pt (4) does not degrade the conductivity of the polypyrrole as much as formaldehyde, but we have not been able to prepare effective catalysts by this method.

Another problem encountered in this work was that both the uncatalysed polypyrrole/PSS support and catalysed samples lost conductivity during storage. The conductivity of an uncatalysed polypyrrole/PSS sample decreased from  $3 \text{ S cm}^{-1}$  to  $0.1 \text{ S cm}^{-1}$  over a period of 9 months under vacuum, while the conductivity of a Pt catalysed sample dropped from  $0.3 \text{ S cm}^{-1}$  to  $10^{-4} \text{ S cm}^{-1}$ . These observations indicate that polypyrrole supported catalysts are unlikely to be suitable for oxygen reduction in fuel cells.

## Polyaniline

Polyaniline has only recently been employed to support Pt particles for oxygen reduction (10, 11). In one approach, polyaniline films were cast onto glassy carbon electrodes from a solution of camphorsulfonic acid doped polyaniline, and then Pt was electrochemically deposited from a  $\text{H}_2\text{PtCl}_6$  solution. The polyaniline film was found to provide a higher surface area for Pt deposition but exhibited limited permeability to oxygen. Use of a composite of polyaniline and Nafion (a proton conducting polymer commonly used in the fabrication of fuel cell electrodes) resulted in better oxygen permeability (11).

We have investigated the use of chemically prepared polyaniline and polyaniline/poly(styrene-4-sulphonate) powders rendered catalytic with Pt by various chemical deposition methods. Heating polyaniline in the presence of formaldehyde decreases its conductivity to unacceptably low values, and so effective catalysts could not be prepared by formaldehyde reduction of Pt compounds. Nanometer size (ca. 10 nm) Pt particles could be deposited by citrate reduction of  $\text{H}_2\text{PtCl}_6$  without unaccepted loss of conductivity (to  $10^{-2} \text{ S cm}^{-1}$ ), but the catalytic activity of this catalyst was not investigated since more promising results were obtained by  $\text{H}_2$  reduction of  $\text{K}_2\text{PtCl}_4$ , as described here.

Fig. 1 shows cyclic voltammograms (under nitrogen) of gas diffusion electrodes catalysed with polyaniline and polyaniline/PSS supported Pt. Oxygen reduction polarization curves for the same electrodes are shown in Fig. 2. The polyaniline based catalysts exhibit voltammetric peaks in the 0 to +1 V region characteristic of the electrochemistry of the polyaniline support, and increasing cathodic currents at potentials below ca. -0.25 V due to hydrogen evolution. Interestingly, the composite with PSS gives much lower polyaniline peaks, but higher hydrogen evolution currents than the polyaniline without PSS. Although no waves due to hydrogen adsorption/desorption on Pt within the catalyst layer can be observed in the cyclic voltammograms in Fig. 1, the presence of electroactive Pt is confirmed by the substantial hydrogen evolution currents and the activity of the electrodes for oxygen reduction. Interestingly, some other polyaniline supported catalysts did show significant hydrogen adsorption/desorption waves (e.g. Fig. 3) but these proved to be less effective catalysts for oxygen reduction. We speculate that the appearance of hydrogen adsorption/desorption waves depends on the conductivity of the polyaniline at potentials below 0 V, which can vary quite significantly between samples because in this potential region the polymer is only lightly doped. Oxygen reduction, which is studied at potentials where all samples are presumably sufficiently conducting, will be influenced more by the porosity and ionic conductivity of the catalyst layer.

The polarization curves in Fig. 2 show that polyaniline is a more effective catalyst support than its composite with PSS, and that its effectiveness can be enhanced considerably by addition of a proton conductor (Nafion) to the catalyst layer. The beneficial effect of Nafion here is not surprising because polyaniline is not likely to be a good proton conductor.

The best oxygen reduction performance observed to date for a polyaniline supported catalyst is comparable to the best obtained with polypyrrole (Fig. 4) (8). As for polypyrrole, polyaniline supported catalysts lose conductivity during storage and are therefore unlikely to be suitable for use in fuel cells.

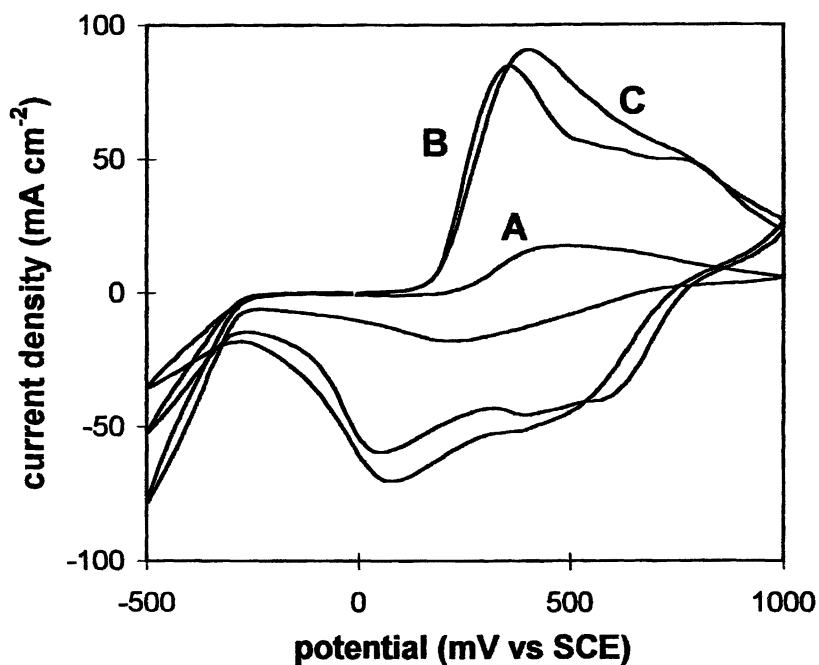
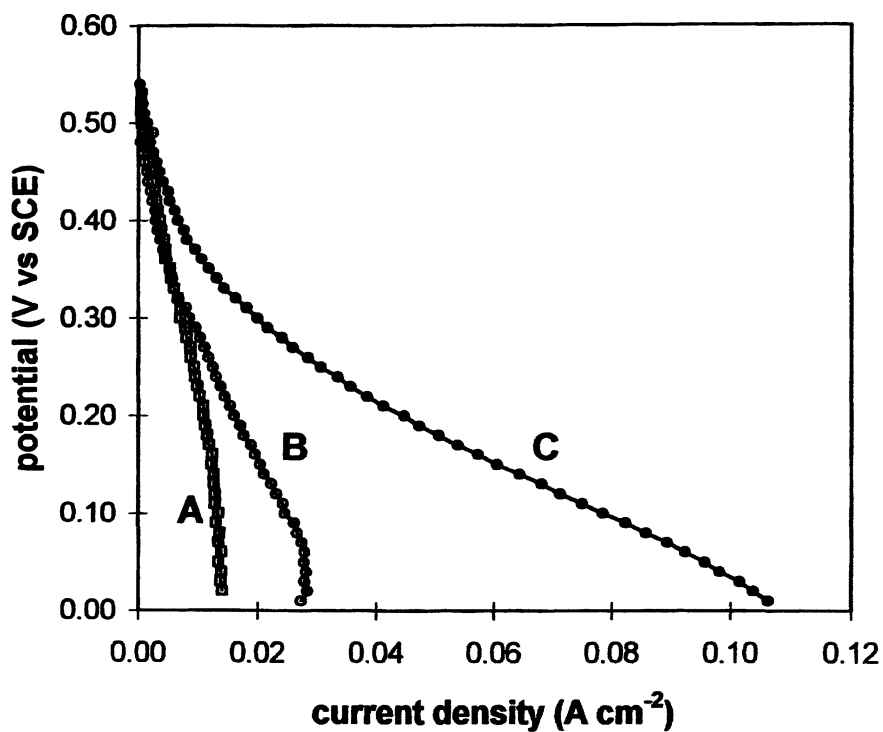
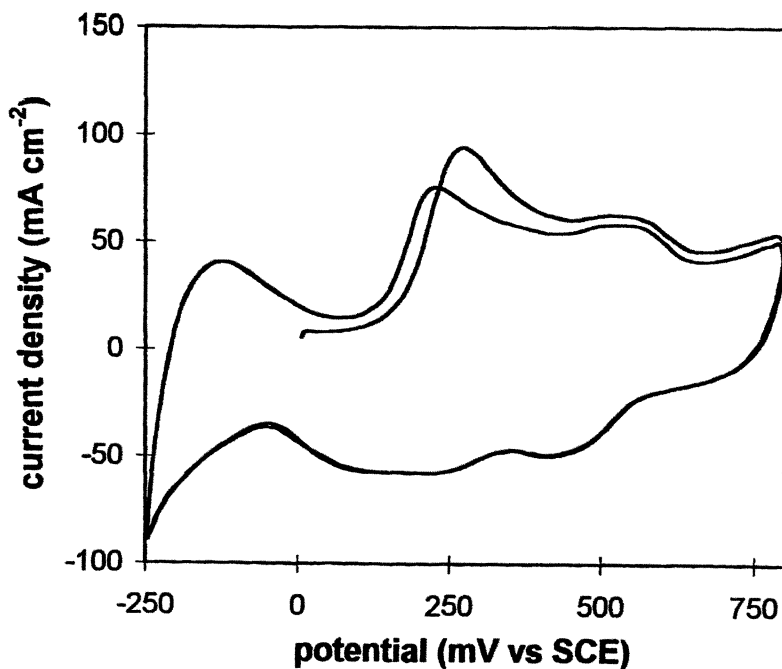


Figure 1. Cyclic voltammograms ( $100 \text{ mV s}^{-1}$ , under  $\text{N}_2$ ) of CFP | catalyst layer | Nafion 117 electrodes in  $1 \text{ M H}_2\text{SO}_4(\text{aq})$ . A. Pt on polyaniline/PSS; B. Pt on polyaniline; C. Pt on polyaniline with Nafion ( $0.1 \text{ mg cm}^{-2}$ ) added to the catalyst layer. Pt loadings were all nominally ca.  $0.2 \text{ mg cm}^{-2}$ .



*Figure 2. Normal Pulse (12 s step time; 2 s pulse width) oxygen reduction polarization curves for the electrodes described for Fig. 1.*



*Figure 3. Cyclic voltammograms ( $100 \text{ mV s}^{-1}$ , under  $\text{N}_2$ ) of a CFP | catalyst layer | Nafion 117 electrode in  $1 \text{ M H}_2\text{SO}_4(\text{aq})$ . The catalyst layer was Pt on polyaniline with Nafion added.*

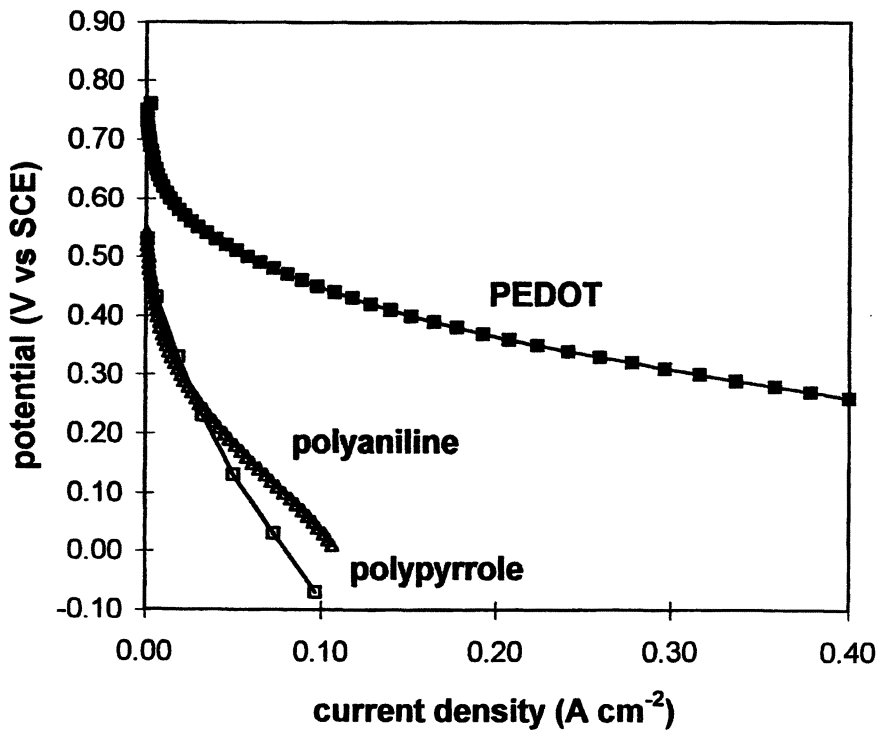


*Figure 4. Oxygen reduction polarization curves for our best electrodes containing PEDOT/PSS, polypyrrole/PSS, and polyaniline supported catalysts. Pt loadings were 0.9, 0.8, and 0.2 mg cm<sup>-2</sup>, respectively.*

## Polythiophenes

The outstanding stability reported for poly(3,4-ethylenedioxythiophene) (PEDOT) prompted us to switch our attention to it as an oxygen reduction catalyst support. Much earlier, Yassar et al. (12) had described the use of Pd modified poly(3-methylthiophene) for oxygen reduction with promising results.

Our approach followed that used for preparing polypyrrole and polyaniline supported catalysts. Thus we prepared PEDOT/PSS composite powders by oxidative chemical polymerization of 3,4-ethylenedioxythiophene in the presence of NaPSS (13), and deposited Pt particles onto these via formaldehyde reduction of  $\text{H}_2\text{PtCl}_6$  (14, 15). These catalysts have provided much better oxygen reduction performances than any other polymer supported catalysts (see Fig. 4 for a comparison with our polypyrrole and polyaniline supported catalysts) but are still inferior to commercial carbon supported catalysts (15). Our failure to beat the performance of carbon, thus far, appears to result from a combination of factors, including electronic isolation and poisoning of Pt particles, and our slightly higher Pt particles sizes (16).

The main advantage of PEDOT over other conducting polymers is that it is sufficiently stable that we have been able to deposit colloidal Pt on it without incurring a large loss of conductivity. It is probable that polypyrrole and polyaniline catalysts with similar performances can be prepared under sufficiently mild Pt deposition conditions. However, the problem of long term stability remains even with PEDOT (15). The electronic conductivities of PEDOT/PSS supported Pt catalysts drop from 0.1-1  $\text{S cm}^{-1}$  to typically ca.  $10^{-2} \text{S cm}^{-1}$  over a period of months in air. However, more disturbingly, they lose much of their catalytic activity for oxygen reduction within days of storage in air. It is not clear at this stage whether this is due to local loss of conductivity, causing electronic isolation of the Pt particles, or some sort of slow poisoning effect.

## Catalysts for Hydrogen Oxidation

Hydrogen oxidation has been studied at electrodes coated with Pt supported on electrochemically deposited films of polypyrrole (5, 17), polyaniline (17, 18), and poly(pyrrole-co-dithiophene) (19). It appears that the kinetics and mechanism of  $\text{H}_2$  oxidation are similar to those on bulk Pt (18), as long as the Pt is deposited on the surface of the polymer to avoid mass transport limitation in the polymer matrix (17) and the polymer is sufficiently conductive at the  $\text{H}^+/\text{H}_2$  formal potential (17). The latter point is particularly important since the electronic conductivities of all these p-doped conducting polymers decrease with decreasing potential, and can



vary considerably between samples at low potentials. This presumably explains why Vork et al. (17) found that the onset of hydrogen oxidation was shifted to higher potentials at Pt/polyaniline coated electrodes, while Lamy and coworkers (18) did not. Inspection of Chen et al.'s (5) voltammograms for hydrogen oxidation at polypyrrole supported Pt reveals a positive shift that was not observed by Vork et al (for polypyrrole) (17). Chen et al. (5) claim a five-fold rate enhancement for their polypyrrole supported colloidal Pt electrodes over bulk Pt, due to formation of an efficient three-dimensional reaction zone and a catalyst-polymer interaction. However, these conclusions are based on inverse Levich plots which yield significant uncertainties and may be influenced by other factors, such as turbulence due to electrode roughness and inaccurate subtraction of background currents.

Our results for hydrogen oxidation at gas diffusion electrodes containing Pt supported on chemically prepared PEDOT/PSS have been disappointing, with large overpotentials required to drive practical current densities (e.g. ~400 mV at 0.5 A cm<sup>-2</sup>) (15). This was attributed to the limited electronic conductivity of the polymer support at the H<sup>+</sup>/H<sub>2</sub> formal potential.

In light of the excellent performances of carbon supported catalysts for hydrogen oxidation in fuel cells, and the problem of obtaining and maintaining sufficient conductivity for polymer supports at the low potentials required, the prospects for polymer supported catalysts appear to be weak.

## Catalysts for Methanol Oxidation

The relatively high operating potentials of methanol anodes, and slowness and mechanistic complexity of the methanol oxidation reaction provide considerable incentive to develop polymer supported catalysts, and this has resulted in much research activity. Polypyrrole has been most widely used as a support, presumably because its conductivity extends to lower potentials than for most other conducting polymers. Polyaniline has also attracted significant attention, and some polythiophenes are attractive for their enhanced stability.

### Polypyrrole Supported Catalysts

All reported studies of methanol oxidation at polypyrrole supported catalysts have involved the use of electrochemically prepared films of the polymer on a solid electrode. Strike et al. (20), who electrochemically deposited Pt onto such electrodes from a H<sub>2</sub>PtCl<sub>6</sub> solution, reported current densities for methanol oxidation that were enhanced by factors of 10-100 over those at bulk Pt and platinumized gold electrodes. Furthermore, a less rapid decay of the current with time

indicated that the polypyrrole supported particles were less susceptible to poisoning by intermediates.

Since the advantages of the polypyrrole support appear to stem from dispersion of the Pt particles (20-22), other ways of producing the Pt particles have been explored. One promising approach is to incorporate  $\text{PtCl}_4^{2-}$  into the polypyrrole film during its formation, and subsequently reduce this to form a uniform distribution of Pt particles within the film (23).

Poly(N-methylpyrrole) has been used in several studies because of its higher stability than unsubstituted polypyrrole (24, 25). A poly(N-methylpyrrole)/Nafion composite was found to be an effective support, and is attractive for use in fuel cells because of its proton conductivity (24). Incorporation of polynuclear ruthenium oxide/cyanoruthenates into poly(N-methylpyrrole) containing Pt particles produced a synergistic increase in methanol oxidation activity (25).

## **Polyaniline**

Studies of methanol oxidation with polyaniline supported catalysts have focused on the use of bimetallic catalysts. As for the bulk metals and carbon supported metals, Pt-Ru and Pt-Sn are both more effective than Pt for methanol oxidation when supported on polyaniline (26, 27). Pt-Ru also provides more complete oxidation of methanol to  $\text{CO}_2$  (27).

The more porous, fibrous structure of polyaniline (26) makes it a more attractive support than polypyrrole, and the high dispersion of the catalyst that can be achieved has produced current densities for methanol oxidation as high as  $65 \text{ mA cm}^{-2}$  (26). The polyaniline support also appears to prevent the absorption of CO on Pt, resulting in less poisoning (28).

## **Poly(3,4-ethylenedioxythiophene) / poly(styrene-4-sulphonate)**

The excellent oxygen reduction performances that we obtained for Pt supported on chemically prepared PEDOT/PSS powders, and the known superior activity of Pt-Ru alloys over Pt for methanol oxidation, prompted us to prepare a series of PEDOT/PSS supported Pt-Ru catalysts (15). Preliminary results (15) showed them to be quite effective catalysts for methanol oxidation, although not as effective as Pt-Ru supported on carbon. Some new results for methanol oxidation at a PEDOT/PSS supported catalyst are reported here.

To provide more controlled experimental conditions, and to allow more accurate comparisons with literature data for films of polymer supported catalysts on electrodes, we have immobilized our catalyst powders on glassy carbon rotating disc electrodes using a procedure reported by Gojkovic et al. (29). Thus, an

appropriate amount of catalyst is suspended in a 5 % Nafion solution and a small amount of this suspension is applied to the carbon electrode and allowed to dry. The resulting thin films do not significantly restrict mass transport to the catalytic sites and are sufficiently robust for extended rotating disc studies. For carbon supported Pt catalysts virtually 100 % of the Pt surface area is electrochemically active, while PEDOT/PSS catalysts show only 30-50% activity (16). The lower activity of the polymer supported catalysts appears to be due to electronic isolation of some Pt particles and/or poisoning.

Fig. 5 shows normal pulse voltammograms for methanol oxidation at a rotating electrode coated with PEDOT/PSS supported Pt-Ru. The pulse width of 10 s corresponds to a similar timescale to the linear scan rate of  $5 \text{ mV s}^{-1}$  used by Hable and Wrighton (26) in their study of polyaniline supported Pt-Ru. At ambient temperature, our electrode with a Pt-Ru loading of  $0.1 \text{ mg cm}^{-2}$  gave a current density of ca.  $3 \text{ mA cm}^{-2}$  at 0.5 V vs SCE. Extrapolation of Hable and Wrighton's data to the same loading produces a similar current density (ca.  $2.5 \text{ mA cm}^{-2}$ ). We also see the strong temperature dependence reported by Hable and Wrighton, with currents rising by a factor of about ten when the temperature is increased to  $60 \text{ }^\circ\text{C}$ .

These comparisons show that our PEDOT/PSS supported catalysts are as active for methanol oxidation as the best polymer supported catalysts reported in the literature. However, a question that must be answered is whether polymer supported catalysts can provide superior performance to commercially available carbon supported catalysts. To answer this, the PEDOT/PSS supported catalyst used for the experiments in Fig. 5, was compared with a commercial (E-TEK) carbon supported Pt-Ru alloy catalyst. Fig. 6 shows normal pulse voltammograms at  $60 \text{ }^\circ\text{C}$ , while Fig. 7 shows the results of constant potential experiments (at  $22 \text{ }^\circ\text{C}$ ) over a much longer time period. In both experiments, and over all timescales studied, the carbon supported catalyst delivers currents that are as much as 10 times higher than for the polymer supported catalyst. The only conditions under which the polymer supported catalyst is superior are at short times and high potentials, which are not relevant to fuel cell operation.

The inferiority of the PEDOT/PSS supported catalyst to the carbon supported catalyst can largely be accounted for by the slightly higher Pt-Ru particle size, which decreases the available surface area, and lower catalyst utilization (16). Thus optimization of the support material (to prevent poisoning and conductivity loss) and metal deposition procedure should allow one to achieve comparable, if not superior, performances to commercial carbon supported catalysts.

## Concluding Remarks

Although a wide range of conducting polymers have been shown to be effective supports for electrocatalysts, there have been few attempts to assess and

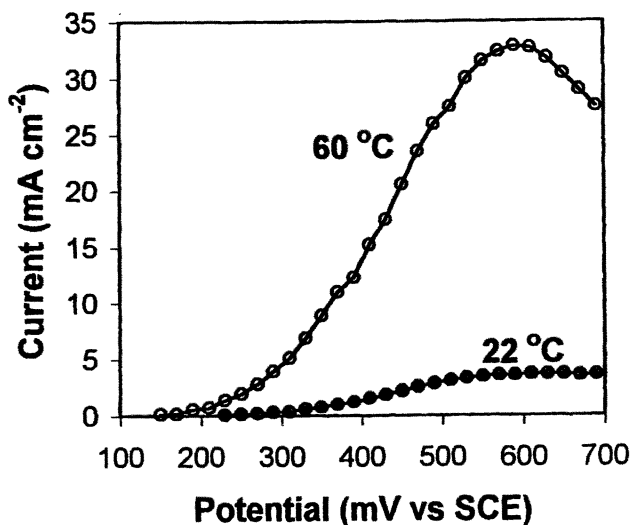


Figure 5. Normal Pulse voltammograms (20 s step time; 10 s pulse width) for methanol (1 M in 1 M  $H_2SO_4(aq)$ ) oxidation at glassy carbon rotating (1500 rpm) disc electrodes coated with 35% Pt-Ru (0.10  $mg\ cm^{-2}$ ; 1.3:1 Pt:Ru) on PEDOT/PSS in a Nafion matrix.

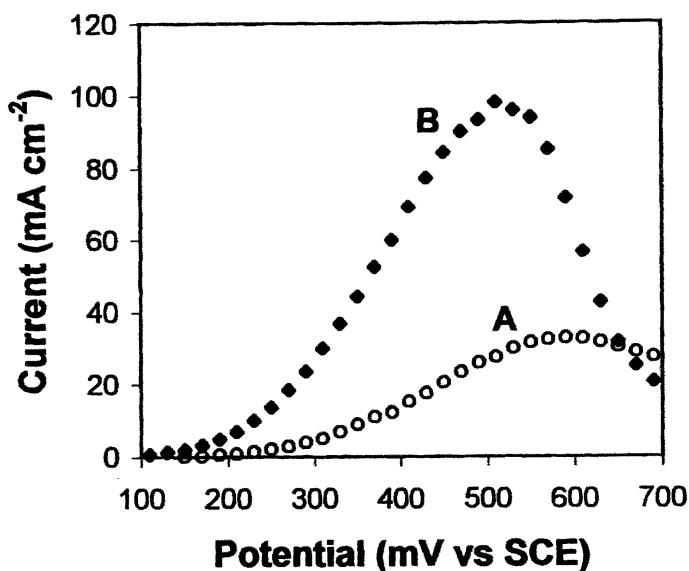
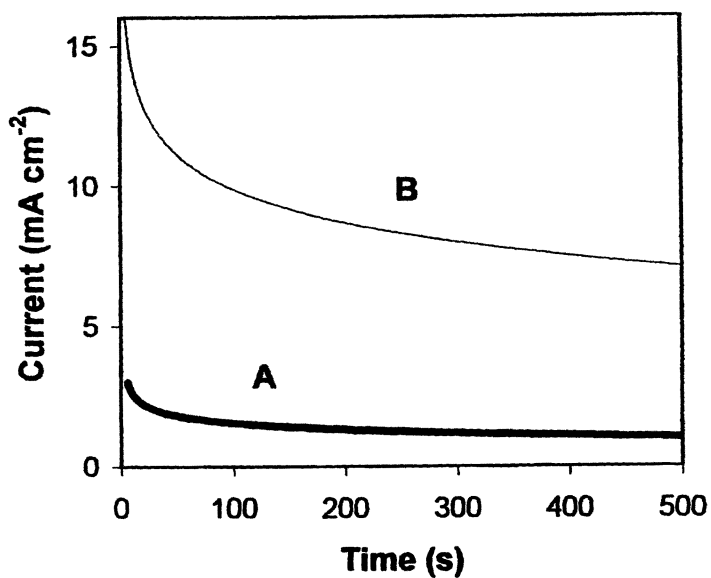


Figure 6. Normal Pulse voltammograms for methanol oxidation at 60 °C as in Fig. 6. A. 35% Pt-Ru (0.10  $mg\ cm^{-2}$ ; 1.3:1 Pt:Ru) on PEDOT/PSS; B. 20% Pt-Ru (0.10  $mg\ cm^{-2}$ ; 1:1 Pt:Ru) on Vulcan XC-72 carbon (E-TEK).



*Figure 7. Chronoamperometry for methanol oxidation (22 °C; +0.5 V) at rotating disc electrodes under the conditions described for Fig. 5, for the electrodes described for Fig. 6.*

optimize the performance of these materials in fuel cell electrodes. Most studies have focused on thin films of the polymer on solid electrodes, and so have failed to demonstrate sufficient current densities for use in fuel cells. More seriously, this type of study has failed to reveal the limited durability of polymer supported catalysts.

Our studies of chemically prepared catalyst powders in gas diffusion electrodes have demonstrated that conducting polymer supported catalysts can provide similar current densities to commercial carbon supported catalysts. They indicate that with further optimization, the ion conducting properties of certain polymer supported catalysts may allow them to exceed the performance of carbon supported catalysts. However, it is clear that substantial improvements in the stability of the polymer support materials will have to be made before applications in fuel cells can be realized.

## Experimental

Polyaniline was prepared by oxidation of aniline (2.5 mmol) with  $(\text{NH}_4)_2\text{S}_2\text{O}_8$  (2.9 mmol) in ca. 25 mL of 0.5 M  $\text{H}_2\text{SO}_4(\text{aq})$ . The reaction mixture was centrifuged after ca. 1 h, and the precipitate was washed with 0.5 M  $\text{H}_2\text{SO}_4(\text{aq})$ . Half of the sample was dried and the electronic conductivity of a pressed pellet was measured to be ca.  $4 \text{ S cm}^{-1}$ . The other half (ca. 100 mg) was stirred with 25 mL of 5 mM  $\text{K}_2\text{PtCl}_4$  (24 mg Pt) for 24 h, and then  $\text{H}_2$  was bubbled through the suspension for 1 h. The catalysed polymer was collected, washed with 0.5 M  $\text{H}_2\text{SO}_4(\text{aq})$ , and dried under vacuum at ambient temperature. It had an electronic conductivity of ca.  $0.1 \text{ S cm}^{-1}$ .

Polyaniline/PSS was prepared by oxidation of aniline (0.80 mmol) with  $(\text{NH}_4)_2\text{S}_2\text{O}_8$  (0.96 mmol) in ca. 25 mL of 0.1 M  $\text{H}_2\text{SO}_4(\text{aq})$  containing NaPSS (0.40 mmol  $-\text{SO}_3^-$ ; Aldrich). The reaction mixture was centrifuged after ca. 1.5 h, and the precipitate was catalysed with Pt (24 mg) as described above for polyaniline.

The synthesis and characterization of the PEDOT/PSS supported catalyst followed a previously reported procedure (13, 15), with formaldehyde as the reductant for metal deposition. A 4:1  $\text{RuCl}_3:\text{H}_2\text{PtCl}_6$  mole ratio was required to provide a Ru:Pt mole ratio close to the target of 1:1.

Oxygen reduction studies and cyclic voltammetry were carried out at ambient temperature ( $22 \pm 2^\circ\text{C}$ ) in  $1 \text{ cm}^2$  gas diffusion electrodes as previously described (8). The catalyst, mixed with ca. 50 mass % PTFE as a binder (and Nafion solution in one case), was spread on carbon fibre paper (CFP; Toray TGPH090), which was then hot-bonded to a Nafion 117 membrane. In the cell, a controlled flow of gas ( $\text{O}_2$ , or  $\text{N}_2$  for cyclic voltammetry) was passed over the CFP and the membrane was in contact with a 1 M  $\text{H}_2\text{SO}_4(\text{aq})$  solution containing counter and reference (SCE) electrodes.

Methanol oxidation was studied at 0.071 cm<sup>2</sup> glassy carbon rotating disc electrodes coated with a thin film of catalyst in a Nafion matrix (16).

### Acknowledgement

This work was supported by the Natural Sciences and Engineering Research Council of Canada (Strategic Grant) and Memorial University.

### References

1. Lyons, M. E. G. *Analyst* **1994**, *119*, 805.
2. Malinauskas, A. *Synthet. Metal.* **1999**, *107*, 75.
3. Holdcroft, S.; Funt, B. L. *J. Electroanal. Chem.* **1988**, *240*, 89.
4. Bose, C. S. C.; Rajeshwar, K. *J. Electroanal. Chem.* **1992**, *333*, 235.
5. Chen, C. C.; Bose, C. S. C.; Rajeshwar, K. *J. Electroanal. Chem.* **1993**, *350*, 161.
6. Rajeshwar, K.; Bose, C. S. C. *US Patent* **1994**, *5,334,292*.
7. Qi, Z.; Pickup, P. G. *Chem. Commun.* **1998**, 15.
8. Qi, Z.; Lefebvre, M. C.; Pickup, P. G. *J. Electroanal. Chem.* **1998**, *459*, 9.
9. Qi, Z.; Pickup, P. G. In *Quantum Confinement: Nanoscale Materials, Devices, and Systems*; The Electrochemical Society Proceedings Series, 1997; Vol. 97-11, pp. 28-34.
10. Lai, E. K. W.; Beattie, P. D.; Holdcroft, S. *Synthet. Metal.* **1997**, *84*, 87.
11. Lai, E. K. W.; Beattie, P. D.; Orfino, F. P.; Simon, E.; Holdcroft, S. *Electrochim. Acta* **1999**, *44*, 2559.
12. Yassar, A.; Roncali, J.; Garnier, F. *J. Electroanal. Chem.* **1988**, *255*, 53.
13. Lefebvre, M. C.; Qi, Z.; Rana, D.; Pickup, P. G. *Chem. Mater.* **1999**, *11*, 262.
14. Qi, Z.; Pickup, P. G. *Chem. Commun.* **1998**, 2299.
15. Lefebvre, M. C.; Qi, Z.; Pickup, P. G. *J. Electrochem. Soc.* **1999**, *146*, 2054.
16. Shan, J.; Pickup, P. G. *Electrochim. Acta* **2000**, *46*, 119.
17. Vork, F. T. A.; Janssen, L. J. J.; Barendrecht, E. *Electrochim. Acta* **1986**, *31*, 1569.
18. Croissant, M. J.; Napporn, T.; Leger, J. M.; Lamy, C. *Electrochim. Acta* **1998**, *43*, 2447.
19. Laborde, H.; Leger, J.-M. *J. Appl. Electrochem.* **1990**, *20*, 524.

20. Strike, D. J.; De Rooij, N. F.; Koudelka-Hep, M.; Ulmann, M.; Augustynski, J. *J. Appl. Electrochem.* **1992**, *22*, 922.
21. Yang, H.; Lu, T. H.; Xue, K. H.; Sun, S. G.; Lu, G. Q.; Chen, S. P. *J. Electrochem. Soc.* **1997**, *144*, 2302.
22. Xue, K. H.; Cai, C. X.; Yang, H.; Zhou, Y. M.; Sun, S. G.; Chen, S. P.; Xu, G. *J. Power Sources* **1998**, *75*, 207.
23. Hepel, M. *J. Electrochem. Soc.* **1998**, *145*, 124.
24. Morita, M.; Matsuno, M.; Matsuda, Y. *Denki Kagaku* **1996**, *64*, 749.
25. Kulesza, P. J.; Matczak, M.; Wolkiewicz, A.; Grzybowska, B.; Galkowski, M.; Malik, M. A.; Wieckowski, A. *Electrochim. Acta* **1999**, *44*, 2131.
26. Hable, C. T.; Wrighton, M. S. *Langmuir* **1993**, *9*, 3284.
27. Laborde, H.; Leger, J. M.; Lamy, C. *J. Appl. Electrochem.* **1994**, *24*, 1019.
28. Laborde, H.; Leger, J. M.; Lamy, C. *J. Appl. Electrochem.* **1994**, *24*, 219.
29. Gojkovic, S. L.; Zecevic, S. K.; Savinell, R. F. *J. Electrochem. Soc.* **1998**, *145*, 3713.



## Chapter 14

# Estimating Concentrations of Condensed Counterions around a Polyelectrolyte by Chemical Trapping

Barbara A. McKernan, Gerald S. Manning,  
and Laurence S. Romsted\*

Department of Chemistry, Wright-Rieman Laboratories, Rutgers,  
The State University of New Jersey, New Brunswick, NJ 08903

We have developed a novel experimental method for estimating the concentration of “condensed” counterions in the immediate vicinity of the anionic polyelectrolyte sodium polyacrylate, NaPAA, based on product yields from dediazonation of 2,4,6-trimethylbenzenediazonium ion, 1-ArN<sub>2</sub><sup>+</sup>. 1-ArN<sub>2</sub><sup>+</sup> reacts with the pendent carboxylate groups of NaPAA to give an aryl ester tag, and with water in the condensed volume and water in the bulk to give a phenol. HPLC measurements of the fraction of reactive groups tagged are combined with the independently measured selectivity of the dediazonation reaction toward carboxylate groups and water and the exchange constant between Na<sup>+</sup> and 1-ArN<sub>2</sub><sup>+</sup>, measured by <sup>23</sup>Na NMR, to estimate Na<sup>+</sup> and 1-ArN<sub>2</sub><sup>+</sup> concentrations in the condensed region.

Counterions condense on a polyelectrolyte when the charge density,  $\xi$ , created by the head groups along the polyelectrolyte exceeds a critical value (1). As  $\xi$  increases, more counterions condense so that the net charge density of the polyelectrolyte remains at the critical value. Constant net charge density has been demonstrated by using pH (2,3), refractive index (4), ultrasound absorption (5), and  $^{13}\text{C}$  NMR relaxation rates (6).

Counterion condensation theory (CCT) predicts the concentration of bound counterions (1-5). However, traditional experimental methods only measure the fraction of counterions bound and not their concentration within the condensed volume. The chemical trapping method provides this information (7-11). Here, we use chemical trapping to estimate the concentration of counterions in the condensed volume of an anionic polyelectrolyte, sodium polyacrylate, NaPAA and compare our result with that obtained from CCT.

### Condensed Counterion Theory

CCT has been described in detail (1,12,13). The concentration of univalent counterions in the condensed volume,  $c_1^{\text{loc}}$  (1), can be calculated from:

$$c_1^{\text{loc}} = \frac{1000\theta_1}{V_p} = \frac{24.3}{\xi b^3} \quad (1)$$

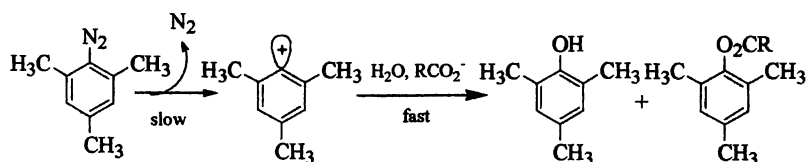
where  $\theta_1$  is the number of condensed counterions per charged group on the polyelectrolyte,  $V_p$  is the volume in which those counterions are found in units of  $\text{cm}^3/\text{mol}$ . The second equality permits estimation of  $c_1^{\text{loc}}$  from the charge density,  $\xi$ , and the average spacing between charged groups along the polyelectrolyte chain,  $b$ . The final units are moles of counterion per liter of condensed volume surrounding the polyelectrolyte. Values of  $\xi$  and  $b$  for a variety of polyelectrolytes are available in the literature (1, 14).

### Chemical Trapping

The chemical trapping method was originally developed to estimate the interfacial nucleophile compositions of surfactant aggregates and the assumptions of the method and the information it provides have been discussed in detail (7-11).

In chemical trapping experiments in aqueous solutions of NaPAA, counterions are assumed to be either bound ions or free, i.e., a two-site model, and 2,4,6-trimethylbenzenediazonium ions,  $1\text{-ArN}_2^+$ , added as its tetrafluoroborate salt, exchange with  $\text{Na}^+$  in the condensed volume. Bound  $1\text{-ArN}_2^+$  reacts with the carboxylate groups of NaPAA to form ester "tags",

1-ArO<sub>2</sub>CR, and with water in the condensed volume to form 2,4,6-trimethylphenol, 1-ArOH, Scheme 1. 1-ArN<sub>2</sub><sup>+</sup> in the bulk reacts with water to form the phenolic product. Three pieces of information are needed to determine the concentration of condensed counterions: (a) the exchange constant for Na<sup>+</sup> and 1-ArN<sub>2</sub><sup>+</sup> between the condensed region and the bulk aqueous solution; (b) the selectivity of 1-ArN<sub>2</sub><sup>+</sup> towards RCO<sub>2</sub><sup>-</sup>/RCO<sub>2</sub>H versus water; and (c) the percent tagging of the polyelectrolyte by 1-ArN<sub>2</sub><sup>+</sup>. The exchange constant,  $K_{1-ArN_2}^{Na^+}$ , was determined from <sup>23</sup>Na NMR relaxation rates; the selectivity,  $S_w^{OAc}$ , from reaction of 1-ArN<sub>2</sub><sup>+</sup> in aqueous acetic acid/acetate solutions as a model system for the condensed volume; and the percent tagging from product yields measured by reverse phase HPLC.



Scheme 1. Dediazonation mechanism.  $R = (CH_2CH)$  monomer unit for NaPAA,  $CH_3$  for acetate ion.

## Results

### Ion Exchange Constant

In aqueous solutions of NaPAA containing added 1-ArN<sub>2</sub><sup>+</sup>, the distribution of the two cations between the condensed volume and the bulk water is described by an exchange constant:

$$K_{1-ArN_2}^{Na^+} = \frac{[Na_b^+][1-ArN_{2,w}^+]}{[Na_w^+][1-ArN_{2,b}^+]} \quad (2)$$

where  $Na_w^+$ ,  $Na_b^+$ ,  $1-ArN_{2,w}^+$  and  $1-ArN_{2,b}^+$  are, respectfully: the concentration of Na<sup>+</sup> in the bulk water, the concentration of Na<sup>+</sup> in the condensed volume, the concentration of 1-ArN<sub>2</sub><sup>+</sup> in the bulk water, and the concentration of 1-ArN<sub>2</sub><sup>+</sup> in the condensed volume. Square brackets here and throughout the text indicate units of moles per liter of *solution volume* to explicitly differentiate bulk

concentrations from moles per liter of *condensed volume* indicated by subscript 'cv' (see below).

The equilibrium constant for this exchange was obtained by using  $^{23}\text{Na}$  NMR (15,16) to measure the change in the relaxation time of  $\text{Na}^+$  as a function of added  $[1\text{-ArN}_2^+]$ . We assume that the total number of counterions in the condensed volume remains constant, i.e. one-to-one exchange of counterions. The assumption of one-to-one exchange is supported by the repeated observation that the fraction of counterions bound to a polyelectrolyte is unaffected by dilution or added electrolyte (1,6,12,13,17,18).

$\text{Na}_w^+$  and  $\text{Na}_b^+$  exchange rapidly on the NMR time scale and give a single weighted average spin lattice relaxation time,  $T_1$ , in  $^{23}\text{Na}$  NMR (15). In pulsed experiments (See Experimental), the rate of relaxation,  $R_{\text{obs}}$ , ( $R_{\text{obs}} = 1/T_1$ ) of the total sodium ion,  $\text{Na}_T^+$ , in the system is the weighted sum of the relaxation rates of  $\text{Na}_b^+$  and  $\text{Na}_w^+$ :

$$R_{\text{obs}} = f_b R_b + f_w R_w \quad (3)$$

where  $f_b$ ,  $f_w$ ,  $R_b$ , and  $R_w$ , are, respectfully, the fraction of sodium ions condensed on the polyelectrolyte, the fraction of sodium ions "free" in the bulk water, the relaxation of the  $\text{Na}^+$  in the condensed region, and the relaxation of the  $\text{Na}^+$  in the bulk water (19,20).

$R_w$  was obtained by measuring the relaxation time of  $\text{Na}^+$  in a solution of NaCl at 19.9 °C in the absence of NaPAA, equation 3 at  $f_b = 0$ ;  $R_w = 26.6 \text{ s}^{-1}$ , in good agreement with literature values (21,22).  $R_b$  was determined by measuring the relaxation time of  $\text{Na}^+$  in NaPAA solutions. The degree of ionization of fully deprotonated NaPAA is 35% (23), i.e. 35% of the  $\text{Na}^+$  are free in the bulk solution. Thus  $f_w = 0.35$  and  $f_b = 0.65$ , because  $f_b = 1 - f_w$  in a two site model (20). Measurements of  $R_{\text{obs}}$  on NaPAA solutions at 19.9 °C gave  $R_b = 179 \text{ s}^{-1}$ .  $R_b \gg R_w$  is to be expected because a bound  $\text{Na}^+$  has a longer relaxation rate due to its more constricted environment (15,16).

Values of  $K_{1\text{-ArN}_2^+}^{\text{Na}^+}$ , were estimated from a series of  $R_{\text{obs}}$  measurements with increasing amounts of  $1\text{-ArN}_2^+$  in NaPAA solutions. Equation 4, obtained by combining equation 3 with  $f_w + f_b = 1$ , was used to estimate the fraction of  $\text{Na}^+$  displaced,  $f_w$ :

$$f_w = \frac{R_{\text{obs}} - R_b}{R_w - R_b} \quad (4)$$

and then  $f_b$ . The values for  $f_w$  and  $f_b$  were used to estimate  $[\text{Na}_w^+]$  and  $[\text{Na}_b^+]$  from:

$$[\text{Na}^+_w] = f_w [\text{Na}^+_T] \quad (5)$$

$$[\text{Na}^+_b] = f_b [\text{Na}^+_T] \quad (6)$$

$[1\text{-ArN}_2^+_b]$  is calculated from  $[\text{Na}^+_b]$  and  $\beta[\text{NaPAA}]$ , the total fraction of bound counterions.

$$[1\text{-ArN}_2^+_b] = \beta[\text{NaPAA}] - [\text{Na}^+_b] \quad (7)$$

$[1\text{-ArN}_2^+_w]$  is given by:

$$[1\text{-ArN}_2^+_w] = [1\text{-ArN}_2^+_T] - [1\text{-ArN}_2^+_b] \quad (8)$$

where  $[1\text{-ArN}_2^+_T]$  is the stoichiometric concentration of  $1\text{-ArN}_2^+$ .

Concentrations obtained from equations 5 - 8 are used to estimate  $K_{1\text{-ArN}_2^+}^{\text{Na}^+}$ , equation 2. The results, Table I, show that as  $[1\text{-ArN}_2^+_T]$  increases, the value of  $K_{1\text{-ArN}_2^+}^{\text{Na}^+}$  decreases from about 4 to 1. This decrease is attributed to an ionic strength effect.  $^{23}\text{Na}$  relaxation experiments carried out at constant total counterion concentration, i.e. by varying the concentration ratio of  $1\text{-ArN}_2\text{BF}_4$  and  $\text{NaCl}$ , but keeping their total constant show that at constant total counterion concentration,  $K_{1\text{-ArN}_2^+}^{\text{Na}^+} \cong 1$ , Table II.

### Selectivity of $1\text{-ArN}_2^+$ towards $\text{RCO}_2^-/\text{RCO}_2\text{H}$ versus $\text{H}_2\text{O}$

Solutions of sodium acetate/acetic acid were used as a model system for the condensed volume.  $1\text{-ArN}_2^+$  reacts with water and acetate ion, Scheme 1, and also acetic acid to give stable products. The selectivity of the  $1\text{-ArN}_2^+$  toward acetate versus water is then defined as (7):

$$S_w^{\text{OAc}} = \frac{[\text{H}_2\text{O}](\%1\text{-ArOAc})}{[\text{OAc}](\%1\text{-ArOH})} \quad (9)$$

where  $\%1\text{-ArOAc}$  and  $\%1\text{-ArOH}$  are the normalized yields of ester and phenolic products from reaction with acetate ion and acetic acid and  $\text{H}_2\text{O}$ , respectively.  $[\text{H}_2\text{O}]$  is calculated from the measured weight of water in each solution and  $[\text{OAc}]$  is the total concentration of  $\text{HOAc}$  and  $\text{OAc}^-$  in solution.

Values for  $S_w^{\text{OAc}}$  were obtained in solutions over a concentration range of 1 - 5 M total acetate at pH values of 3, 5 and 7, spanning the  $\text{pK}_a$  of acetic acid

**Table I.**  $^{23}\text{Na}$  relaxation times used to determine the exchange constant for  $\text{Na}^+$  and  $1\text{-ArN}_2^+$  on NaPAA at  $5.0\text{ }^\circ\text{C}$ .

$[1\text{-ArN}_2^+ \tau]$ (M)	$[\text{Na}^+ \tau]$ (M) <sup>a</sup>	$R_{\text{obs}}$ ( $\text{s}^{-1}$ )	$[\text{Na}^+ b]$ (M)	$[\text{Na}^+ w]$ (M)	$[1\text{-ArN}_2^+ b]$ (M)	$[1\text{-ArN}_2^+ w]$ (M)	$K_{1\text{-ArN}_2^+}^{\text{Na}^+}$
0	0.0237	133	0.0155	0.0071	0	0	--
0.0094	0.0213	116	0.0117	0.0096	0.0022	0.0072	4.0
0.0179	0.0237	109	0.0119	0.0118	0.0035	0.0144	4.1
0.0278	0.0237	93.5	0.0097	0.0140	0.0057	0.0221	2.7
0.0387	0.0237	75.8	0.0071	0.0166	0.0083	0.0304	1.6
0.0534	0.0237	60.2	0.0048	0.0189	0.0106	0.0428	1.0
0.0688	0.0237	55.2	0.0041	0.0196	0.0113	0.0575	1.1

a. The total sodium ion concentration,  $[\text{Na}^+ \tau] = [\text{NaPAA}]$ .

**Table II.  $^{23}\text{Na}$  relaxation times used to determine the exchange constant for  $\text{Na}^+$  and  $1\text{-ArN}_2^+$  on NaPAA at constant ionic strength at  $5.0\text{ }^\circ\text{C}$ .**

$[1\text{-ArN}_2^+ \tau]$ (M)	$[\text{NaCl}]$ (M)	$R_{\text{obs}}$ ( $\text{s}^{-1}$ )	$[\text{Na}^+ \tau]$ (M) <sup>a</sup>	$[\text{Na}^+ b]$ (M)	$[\text{Na}^+ w]$ (M)	$[1\text{-ArN}_2^+ b]$ (M)	$[1\text{-ArN}_2^+ w]$ (M)	$K_{1\text{-ArN}_2^+}$
0.0090	0.0609	54.0	0.0846	0.0140	0.0706	0.0014	0.0076	1.1
0.0177	0.0520	55.2	0.0757	0.0131	0.0626	0.0023	0.0154	1.4
0.0282	0.0370	52.9	0.0607	0.0096	0.0511	0.0058	0.0224	0.7
0.0397	0.0330	52.9	0.0567	0.0090	0.0477	0.0064	0.0333	1.0
0.0519	0.0200	59.0	0.0437	0.0086	0.0351	0.0068	0.0451	1.5
0.0688	0	55.2	0.0237	0.0041	0.0196	0.0113	0.0575	1.1

a.  $[\text{Na}^+ \tau] = [\text{NaCl}] + [\text{NaPAA}]; [\text{NaPAA}] = 0.237\text{ M}$ .

(4.76). As the total acetate concentration increases, the yield ratio of 1-ArOAc to 1-ArOH, at each pH, also increases, but the selectivity remains about constant, Table III. At pH 3, 5, and 7, the average selectivities are 1.8, 2.4, and 1.6, respectively. Despite the change in acetate from primarily acetic acid, to about 50:50 acetic acid and acetate ion, to primarily acetate ion, the selectivities are almost constant and the average value is about 2.0.

**Table III. Selectivity of 1-ArN<sub>2</sub><sup>+</sup> towards total acetate (HOAc and OAc) versus water at pH = 3, 5, and 7 from normalized yields at 40 °C.**

<i>pH</i>	<i>[OAc](M)</i>	<i>%(1-ArOAc)<sup>a</sup></i>	<i>%(1-ArOH)<sup>a</sup></i>	<i>[H<sub>2</sub>O] (M)<sup>b</sup></i>	<i>S<sub>w</sub><sup>OAc</sup></i>
3	1.0	3.0	97.0	52.5	1.6
	2.0	7.2	92.8	49.7	1.9
	4.0	15.5	84.5	43.8	2.0
5	1.0	4.0	96.0	52.8	2.2
	2.0	8.5	91.5	50.0	2.3
	3.0	14.4	85.7	46.9	2.6
	4.0	18.6	81.4	44.7	2.6
	5.0	22.8	77.3	42.2	2.5
7	1.0	3.3	96.8	52.9	1.7
	2.0	6.2	93.7	50.0	1.7
	3.0	7.7	92.3	46.7	1.3
	4.0	11.7	88.3	45.4	1.5

a. Normalized yields.

b. Calculated from measured weights of H<sub>2</sub>O in each solution.

### Percent Tagging

Dediazotiation reactions were carried out over a range of NaPAA concentration ranges, 1.57–8.22 g/L (0.0167–0.0874 M). The “tagged” polyelectrolyte was isolated by size exclusion chromatography, subjected to alkaline hydrolysis to remove the ester tags, followed by neutralization to give 1-ArOH. The yield 1-ArOH, which is equivalent to the amount of tagging, was determined by reverse phase HPLC using fluorescence instead of UV detection because of the low 1-ArOH yield. The percent tagging of NaPAA is given by equation 10:

$$\text{percent tagging} = \frac{[1 - \text{ArOH}]}{[1 - \text{ArN}_2^+]} * 100\% \quad (10)$$



where  $[1\text{-ArOH}]$  is concentration of phenol formed from hydrolysis of tagged NaPAA and  $[1\text{-ArN}_2^+_{\text{T}}]$  is the stoichiometric concentration of arenediazonium ion, Table IV. The percent tagging is essentially constant over the NaPAA concentration range used, and has an average value of about 0.28%.

**Table IV. Percent tagging of NaPAA by  $1\text{-ArN}_2^+$  at 40 °C.**

$[\text{NaPAA}] \text{ (M)}^a$	$[1\text{-ArN}_2^+] \text{ (M)}$	Percent Tagging
0.0167	$5.07 \times 10^{-4}$	0.24
0.0185	$5.51 \times 10^{-4}$	0.27
0.0248	$7.51 \times 10^{-4}$	0.26
0.0287	$8.69 \times 10^{-4}$	0.34
0.0323	$9.75 \times 10^{-4}$	0.15
0.0457	$1.44 \times 10^{-3}$	0.27
0.0646	$2.03 \times 10^{-3}$	0.23
0.0874	$2.62 \times 10^{-3}$	0.38
Average:		$0.28 \pm 0.06$

a. Molarity of the monomer unit ( $\text{CH}_2\text{CHCO}_2\text{Na}$ ) of NaPAA.

## Discussion

The polyelectrolyte NaPAA was selected because it is 90% ionized at  $\text{pH} \leq 7$  and adopts the extended rod conformation (24) and no other reactions compete with dediazonium (7, 25).

To estimate local concentration of counterions in the immediate vicinity of NaPAA, we first calculated the local concentration of pendent carboxylate groups by using equation 11,

$$\text{PCO}_2^{\text{cv}} = \frac{\text{H}_2\text{O}_{\text{cv}} (\%1 - \text{ArO}_2\text{CP})}{S_{\text{w}}^{\text{OAc}} (\%1 - \text{ArOH}_b)} \quad (11)$$

and the results are summarized in Table V.

Equation 11 is based on the assumption that the selectivity of the chemical trapping reaction within the immediate vicinity of NaPAA, is the same as the average value of the selectivity in aqueous acetate solutions, i.e.,  $S_{\text{w}}^{\text{OAc}} = 2.0$ . This is based on an assumption made in the chemical trapping method that the selectivity of the reaction is the same in bulk solution as it is the the interfacial region of micelles.(7-10, 26) Equation 11 is formally equivalent to equation 9

except that the molarity of water,  $H_2O_{cv}$ , the percent yield of phenol, %1-ArOH<sub>b</sub>, and the percent yield of trapped pendent carboxylate groups on NaPAA, %1-ArO<sub>2</sub>CP, are for reaction within the condensed volume around NaPAA. The concentrations of carboxylate groups and Na<sup>+</sup> and 1-ArN<sub>2</sub><sup>+</sup> counterions in the condensed volume are relatively small, and we assume that  $H_2O_b = 55$  M.

**Table V. Estimated concentrations of counterions in the condensed region of NaPAA by chemical trapping at 40 °C..**

$[NaPAA]$ (M) <sup>a</sup>	$[1-ArN_2^+_b]$ (M) ( $\times 10^6$ )	$[1-ArO_2CP]$ (M) ( $\times 10^6$ )	%1-ArO <sub>2</sub> CP	$PCO_2^-_{cv}$	$C_{cv}$
0.0167	1.61	1.22	0.76	0.21	0.14
0.0185	1.75	1.49	0.85	0.24	0.15
0.0248	2.38	1.95	0.82	0.23	0.15
0.0287	2.76	2.95	1.10	0.30	0.19
0.0323	3.09	1.46	0.47	0.13	0.09
0.0457	4.57	3.89	0.85	0.24	0.15
0.0646	6.44	4.67	0.73	0.20	0.13
0.0874	8.31	9.96	1.20	0.33	0.22
Average:					0.15 ± 0.04

a.  $[1-ArN_2^+_T] = [NaPAA]/33$

Values for %1-ArO<sub>2</sub>CP and %1-ArOH<sub>b</sub> for each chemical trapping experiment are obtained as follows.

The yield of tagged carboxylate groups, %1-ArO<sub>2</sub>CP, is obtained from equation 12 and the phenol yield from reaction with local water is obtained by difference from equation 13:

$$\%1-ArO_2CP = \frac{[1-ArO_2CP]}{[1-ArN_2^+_b]} * 100\% \quad (12)$$

$$(\%1-ArOH_b) = 100 - (\%1-ArO_2CP) \quad (13)$$

Values of  $[1-ArN_2^+_b]$  for each tagging experiment are obtained from equation 2, setting  $[1-ArN_2^+_w] = [1-ArN_2^+_T] - [1-ArN_2^+_b]$  and  $K_{1-ArN_2^+}^{Na^+} = 4.0$  (see Results).

We assume that net surface charge density (5) and similarly the fraction of bound counterions to NaPAA, are independent of counterion type. Thus the total concentration of  $\text{Na}^+$  and  $1\text{-ArN}_2^+$  counterions is 65% of that of the pendent carboxylate groups,  $\theta_V = 0.65$ . Over a 5-fold polymer dilution, the average interfacial counterion concentration in the condensed volume,  $C_{cv}$  around NaPAA is about 0.14 M estimated by chemical trapping.

We then compare our experimental estimate to the theoretical estimate made by CCT using equation 1. For NaPAA, the distance in angstroms,  $b$ , between the charged sites is  $b = 2.5/\alpha$  and the linear charge density is  $\xi = 2.85\alpha$ , where  $\alpha$  is the degree of neutralization (1). Our chemical trapping experiments were carried out at  $\text{pH} = 7$ , where  $\alpha = 0.9$  for NaPAA (24). For these conditions,  $c_1^{\text{loc}} = 0.44$  M around NaPAA. The local concentration of the counterion condensate is predicted by CCT to be constant at 0.44 M as long as the bulk concentration is less than 0.44 M. The average value 0.15 M, obtained by chemical trapping, is within a factor of 3 of the CCT estimate of 0.44 M.

Several factors may contribute to the 3 fold difference between the CCT and chemical trapping estimate of counterion concentration in the condensed volume. CCT treats ions as point charges, but the exchange constant between  $1\text{-ArN}_2^+$  and  $\text{Na}^+$  in NaPAA solutions is 4, indicating stronger specific interactions between  $\text{Na}^+$  and carboxylate groups than  $1\text{-ArN}_2^+$  and carboxylate groups along the polyion chain. How to best treat this problem is still unresolved. In these initial experiments, the NMR exchange constants were estimated at 5 °C to minimize decomposition of  $1\text{-ArN}_2^+$ , but the chemical trapping experiments were carried out at 40 °C. We are currently determining the temperature dependence of exchange constants. Finally, the assumption of constant  $\alpha$  for different counterions might not be exact and the exchange constant might be better treated as a variable.

## Conclusions

Chemical trapping with an arenediazonium ion provides the first experimental estimate of counterion concentration in the condensed volume around an anionic polyelectrolyte, NaPAA. The method can be applied to other polyelectrolyte systems. Inherent advantages of the method are the low selectivity of the probe towards a variety of nucleophiles and its insensitivity to medium effects such that product yields are almost directly proportional to nucleophile concentration. We are currently using chemical trapping to estimate the concentration of condensed counterions around sodium polystyrene

sulfonate, NaPSS, where specific counterion effects should not be as significant. Sulfonic acids are stronger acids than carboxylic acids and are not expected to bind counterions as specifically. Our unpublished estimate of the exchange constant for  $\text{Na}^+$  and  $1\text{-ArN}_2^+$  in NaPSS solutions is approximately 1, consistent with the weaker binding of  $\text{Na}^+$  to PSS than PAA.

## Experimental

### Materials

Polyacrylic acid, sodium salt (35% solution, MW ~ 60,000) was purchased from Polysciences. A 5% solution was prepared and passed over a size exclusion chromatography (SEC) PD-10 Sephadex, G-25M column in 2.5 ml portions to remove acrylic acid and other low molecular weight impurities. The NaPAA was dried by lyophilization to constant weight to ensure removal of all water. 2,4,6-Trimethylphenol, 1-ArOH (99%), Aldrich, was purified by repeated dissolution in acetonitrile followed by precipitation with pentane. A single peak was obtained in its HPLC chromatograms. HPLC grade methanol, sodium acetate, acetic acid, and HEPES buffer were purchased from Sigma Aldrich and used as received. Isopropanol, acetonitrile, sodium hydroxide solutions, sulfuric acid and hydrochloric acid were purchased from Fisher Scientific and used as received. The preparation of 2,4,6-trimethylbenzenediazonium tetra-fluoroborate,  $1\text{-ArN}_2\text{BF}_4$ , and 2,4,6-trimethylphenyl acetate, 1-ArOAc, have been described (7, 9). All aqueous solutions were prepared by using distilled water that was passed over activated carbon and deionizing resin and redistilled.

### Methods

UV/visible spectra and kinetic data were collected on a Perkin-Elmer 559A spectrophotometer or a Perkin Elmer Lambda 40 spectrophotometer. Product yields were determined on a Perkin-Elmer LC-235 HPLC equipped with a 235C diode-array detector measuring absorbance at  $\lambda = 220$  nm and a LC 240 fluorescence detector, (ex.  $\lambda = 210$  nm, em.  $\lambda = 330$  nm). The HPLC was fitted with a Rainin Microsorb-MV C-18 reverse phase column (4.6 mm ID x 25 cm; 5-nm particle size); a 200  $\mu\text{l}$  sample loop. The mobile phase for product separation was 80% MeOH/20%  $\text{H}_2\text{O}$  with a flow rate of 0.8 ml/min for all runs. Reported peak areas are averages of triplicate injections. Solution pH was measured with an Orion combination pH microelectrode, model 8103.  $^{23}\text{Na}$  spin-lattice relaxation times,  $T_1$ , were measured on a Varian VXR-200 and

determined by an inversion recovery Fourier transform method (27, 28), using an  $180^\circ$ - $t$ - $90^\circ$  pulse sequence over a range from 0.001 to 0.05 seconds.

### **$^{23}\text{Na}$ NMR Experiments**

Stock solutions of NaCl and NaPAA were prepared in 50:50  $\text{H}_2\text{O}:\text{D}_2\text{O}$ . Weighed samples of solid  $1\text{-ArN}_2\text{BF}_4$  were added to 5.00 mL portions of PAA stock solution to give final  $1\text{-ArN}_2^+$  concentrations of 0.008 M to 0.07 M. Experiments were run at  $5^\circ\text{C}$  to minimize  $1\text{-ArN}_2^+$  decomposition.

### **Determination of Selectivity**

Sodium acetate, NaOAc, acetic acid, HOAc, solutions were prepared at pH = 3, 5, and 7 by adjusting the NaOAc/HOAc molar ratio, over a concentration range of 1-5 M. Reaction was initiated by injecting aliquots of freshly prepared, ice cold, stock solutions of  $1\text{-ArN}_2\text{BF}_4$ , 0.01 M in methanol, to give final concentrations of  $1\text{-}5 \times 10^{-4}$  M. Solutions were layered with cyclohexane to minimize loss of volatile products (7). Reaction flasks were placed in  $40^\circ\text{C}$  water bath for a minimum of eight hours. Product solutions were made homogeneous by adding sufficient isopropanol, *i*-PrOH, to dissolve both the cyclohexane and aqueous phase and then analyzed by HPLC using UV detection in triplicate 20  $\mu\text{l}$  injections.

Product yields of  $1\text{-ArOH}$  and  $1\text{-ArOAc}$  from reaction with water and acetate ion, respectfully, were identified in HPLC chromatograms by spiking experiments using independently prepared  $1\text{-ArOAc}$  (9) and commercially available  $1\text{-ArOH}$ . Calibration curves were prepared from peak areas by using stock solutions of each product in MeOH over a concentration range of  $1 \times 10^{-4}$  –  $5 \times 10^{-3}$  M. Plots of peak area as a function of  $1\text{-ArX}$  ( $\text{X} = \text{OH}$  or  $\text{OAc}$ ) concentration are linear and give an equation of the form  $\text{Area} = m[1\text{-ArX}]$ . Concentrations were calculated by multiplying peak areas by  $1/m$ . The values of  $m$  are  $4.06 \times 10^9 \mu\text{V}\cdot\text{sec}/\text{M}$  (cc. = 1.000) and  $2.83 \times 10^9 \mu\text{V}\cdot\text{sec}/\text{M}$  (cc. = 1.000) for  $1\text{-ArOH}$  and  $1\text{-ArOAc}$ , respectfully.

### **Tagging Experiments**

Aqueous sodium polyacrylate solutions were prepared in  $1 \times 10^{-3}$  M HEPES buffer at pH 7. Solid  $1\text{-ArN}_2\text{BF}_4$  was added to each solution such that the ratio of polyelectrolyte to  $1\text{-ArN}_2^+$  was approximately 33:1. Solutions were placed in a  $40^\circ\text{C}$  constant temperature water bath for a minimum of ten half lives.

Product solutions were passed over a size exclusion chromatography column to remove 1-ArOH formed from reaction of 1-ArN<sub>2</sub><sup>+</sup> with water. These solutions containing tagged polyelectrolyte were hydrolyzed in 1 M NaOH at ambient temperature for 30 hours to ensure complete hydrolysis of the ester linkages. The half-life for the hydrolysis of the model compound 1-ArOAc is only about 5 minutes under these conditions based on its measured second order rate constant of  $2.8 \times 10^{-3} \text{ M}^{-1} \text{ sec}^{-1}$ . After the hydrolyses were complete, the pH of each solution was adjusted to 7.0 by titrating with 6 M HCl and monitoring with a pH meter. The yields of 1-ArOH were analyzed by HPLC by fluorescence detection in triplicate 100  $\mu\text{L}$  injections.

## Kinetics

De Diazonation reactions rates were carried out in NaOAc and NaPAA at various pH's. NaOAc solutions are self buffered, and NaPAA solutions were buffered with  $1 \times 10^{-3} \text{ M}$  HEPES. Reactions were monitored at  $40 \text{ }^\circ\text{C} \pm 0.1 \text{ }^\circ\text{C}$ , and were followed for at least 10 half lives at  $\lambda = 285 \text{ nm}$ . Reactions were initiated by injecting aliquots ( $\sim 50 \text{ }\mu\text{L}$ ) of 1-ArN<sub>2</sub>BF<sub>4</sub>, of a freshly prepared ice cold 0.01 – 0.02 M stock solutions in CH<sub>3</sub>CN, into 5.0 – 10.0 mL of reaction solution to give final [1-ArN<sub>2</sub>BF<sub>4</sub>] of  $\sim 1 \times 10^{-4} \text{ M}$ . Plots of  $\ln(A_\infty - A)$  versus time were linear for 3 – 4 half lives with  $cc \geq 0.998$ . The de Diazonation rate is essentially constant from pH 4 to 9 ( $k_{\text{obs}} = 3.4 \times 10^{-4} \text{ s}^{-1}$ , 8 data points). The reaction in NaPAA solutions pH 7.0 is slightly faster,  $k_{\text{obs}} = 5.0 \times 10^{-4} \text{ s}^{-1}$ .

The rate of alkaline hydrolysis of 1-ArOAc to form 1-ArOH was monitored at  $25 \text{ }^\circ\text{C} \pm 0.1 \text{ }^\circ\text{C}$ , and was followed for 10 half lives at  $\lambda = 275 \text{ nm}$ .  $1 \times 10^{-4} \text{ M}$  1-ArOAc was dissolved in 0.1 M NaOH. The plots of  $\ln(A_\infty - A)$  versus time were linear for 3 – 4 half lives with  $cc \geq 0.998$ . The second order rate constant for hydrolysis is  $2.8 \times 10^{-3} \text{ M}^{-1} \text{ sec}^{-1}$ . Reported rates of alkaline hydrolysis for phenyl acetate and *p*-tolyl acetate are 0.576 and  $0.310 \text{ M}^{-1} \text{ sec}^{-1}$ , respectively (29). The rate of alkaline hydrolysis of 1-ArOAc should be slower than that of phenyl acetate and *p*-tolyl acetate because of the two ortho-methyl groups of 1-ArOAc, are electron-donating and sterically hinder attack of the OH.

## Acknowledgements

We appreciate assistance from Lanzhen Zhuang in the preparation of 1-ArOAc and helpful discussions with Pat O'Connor, Suzie Sheng, and Ruth Saxl. BAM thanks the U.S. Department of Education for the GAANN fellowship that provided partial support for her Ph.D. research. LSR appreciates

financial support of NSF Organic Dynamics Division (CHE-9985774) and NSF International Programs (INT97-22458).

## References

1. Manning, G. S. *Quart. Rev. Biophys.* **1978**, *11*, 179-246.
2. Gregor, H. P.; Frederick, M. J. *Poly. Sci.* **1957**, *23*, 451-465.
3. Rinaudo, M.; Milas, M. In *Polyelectrolytes and Their Applications*; Rembaum, A.; Selegny, E., Eds. Holland, 1975; pp 31-49.
4. Ikegami, A. *J. Poly. Sci. Part A* **1964**, *2*, 907-921.
5. Zana, R.; Tondre, C.; Rinaudo, M.; Milas, M. *J. Chim. Phys. Physicochim. Biol.* **1971**, *68*, 1258-1266.
6. Ni, J. X. *New J. Chem.* **1999**, *23*, 1071-1073.
7. Chaudhuri, A.; Loughlin, J. A.; Romsted, L. S.; Yao, J. J. *Am. Chem. Soc.* **1993**, *115*, 8351-8361.
8. Chaudhuri, A.; Romsted, L. S.; Yao, J. J. *Am. Chem. Soc.* **1993**, *115*, 8362-8367.
9. Romsted, L. S.; Zhang, J.; Zhuang, L. J. *Am. Chem. Soc.* **1998**, *120*, 10046-10054.
10. Romsted, L. S.; Yao, J. *Langmuir* **1999**, *15*, 326-336.
11. Cuccovia, I. M.; Romsted, L. S.; Chaimovich, H. J. *Colloid Interface Sci.* **1999**, *220*, 96-102.
12. Ray, J.; Manning, G. S. *Langmuir* **1994**, *10*, 2450-2461.
13. Manning, G. S. *Ber. Bunsenges. Phys. Chem.* **1996**, *100*, 909-922.
14. Record, M. T.; Woodbury, C. P.; Lohman, T. M. *Biopolymers* **1976**, *15*, 893-915.
15. Paulsen, M. D.; Anderson, C. F.; M. Thomas Record, J. *Biopolymers* **1988**, *27*, 1249-1265.
16. Shannon, P.; Lochhead, R. Y. *Polymer Preprints* **1995**, *36*, 61-62.
17. Essafi, W.; Lafuma, F.; Williams, C. E. *Eur. Phys. J. B* **1999**, *9*, 261-266.
18. Konop, A. J.; Colby, R. H. *Macromolecules* **1999**, *32*, 2803-2805.
19. Gustavsson, H.; Lindman, B. *J. Am. Chem. Soc.* **1975**, *97*, 3923-3930.
20. Forsen, S.; Lindman, B. *Chem. Br.* **1978**, *14*, 29-34.
21. Klink, J. J. v. d.; Zuiderweg, L. H.; Leyte, J. C. *J. Chem. Phys.* **1974**, *60*, 2391-2399.
22. Levij, M.; Bleijser, J. D.; Leyte, J. C. *Chem. Phys. Lett.* **1981**, *83*, 183-191.
23. Fixman, M.; Skolnick, J. *Macromolecules* **1978**, *11*, 863-867.
24. Nagasawa, M.; Murase, T.; Kondo, K. *J. Phys. Chem.* **1965**, *69*, 4005-4012.
25. Banerjee, R.; Das, P. K.; Chaudhuri, A. *Biochim. Biophys. Acta* **1998**, *1373*, 299-308.

26. Romsted, L. S.; Yao, J. *Langmuir* **1996**, *12*, 2425-2432.
27. Robb, I. D.; Smith, R. *J. Chem. Soc. Faraday Trans. I* **1974**, *70*, 287-292.
28. Yoshida, T.; Taga, K.; Okayashi, H.; Matsushita, K.; Kamaya, H.; Ueda, I. *J. Colloid Interface Sci.* **1986**, *109*, 336-340.
29. Tommila, E.; Hinshelwood, C. N. *J. Chem. Soc.* **1938**, 1801-1810.



## Chapter 15

# Challenges and Opportunities: Where Do We Go from Here?

Harry B. Mark, Jr.<sup>1</sup>, and Judith F. Rubinson<sup>2</sup>

<sup>1</sup>Department of Chemistry, University of Cincinnati,  
Cincinnati, OH 45221-0172

<sup>1</sup>Department of Chemistry, Georgetown University,  
Washington, DC 20057-1227

Editors of a volume such as this are instructed that they should include a chapter addressing the questions “Where do we go from here?” or “What are the directions that are seen for future research and development in the area?” Truth be told, we felt that it would be more than a little risky to make any specific predictions at this time. After all, when Alan MacDiarmid, the 2000 Nobel Laureate in Chemistry, published the definitive papers on the conductivity properties of the inorganic polymer, poly(sulfur nitride), a few electrochemists took notice because they could see that this polymer, as an electrode material, would have a very different solution/electrode interface structure and, perhaps, different electron transfer kinetics. No grand new applications were envisioned. However, when his first seminal publications on the organic conducting polymer, polyacetylene, appeared, great breakthroughs and/or new materials were instantaneously predicted. These included superlight all-organic batteries, highly efficient solar energy conversion systems, and organic room temperature superconductors. Although these lines of research have not yet proved as successful as anticipated, the “detours” along the way have led to a multitude of specialized electrochemical applications that never could have been developed without the unique properties of these organic conducting polymer materials.

We think it *is* safe to say that there will be practical batteries developed that rely on a combination of electronic- and ionic-conducting organic polymers, the so-called “Jelly Roll.” Although long-term stability is still a problem with these systems, they have been shown to have very rapid charge/discharge characteristics, and it is just a matter of time before more stable polymers are synthesized. Furthermore, synthetic research will produce materials for “super capacitors” for

massive energy storage and for stable fuel cells. Synthesis of derivatives of the the original conducting polymers have produced , and are likely to continue to produce, great strides in the area of photovoltaic devices.

The ability to tailor the behavior of these polymers by way of attachment of specific structural groups will, no doubt, lead to expansion of their capabilities in areas ranging from electrocatalysis to sensors with a high degree of specificity. Corrosion science should benefit from the work of those presently looking at the mechanisms by which conducting polymers lead to inhibition of corrosion. Another area in which we expect to see widespread application is in the area of biomedical research and engineering. The promising results in terms of biocompatibility will very likely lead to their use both for *in vitro* and *in vivo* purposes.

A colleague recently remarked that “Conducting polymers are not the answer to everything!” However, drawing on the expertise brought to the table by interdisciplinary teams such as those presently exploring their possibilities, the types and numbers of applications will doubtless continue to expand in the years to come.

# Author Index

- Aaron, J. J., 38  
Aeiyaeh, S., 38, 128  
Bélanger, Daniel, 52  
Breau, Livain, 52  
Cammarata, V., 59  
Chane-Ching, K. I., 38, 128  
Collier, Joel, 154  
del Valle, M. A., 75  
Deronzier, A., 141  
Dini, Danilo, 103  
Doblhofer, Karl, 103  
Galal, Ahmed, 18  
Hao, N., 59  
Hepel, Maria, 113  
Ho, Hoang Anh, 52  
Huang, Huaiguo, 113  
Hudson Terry, 154  
Janakiraman, Umamaheswari, 103  
Jouini, M., 38  
Lacaze, P. C., 38, 128  
Lacroix, J. C., 38, 128  
Liang, J., 59  
Lin, Zhonghua, 113  
Luo, Jin, 113  
Manning, Gerald S., 184  
Mark, Harry B., Jr., 203  
McKernan, Barbara A., 184  
Metz, J., 59  
Naudin, Eric, 52  
Ogura, K., 88  
Petitjean, J., 128  
Pickup, Peter G., 166  
Pizarro, T., 75  
Qi, Zhigang, 166  
Rivers, Tyrell, 154  
Romsted, Laurence S., 184  
Rubinson, Judith F., 2, 203  
Schmidt, Christine, 154  
Shan, Jingning, 166  
Shiigi, H., 88  
Tanguy, J., 38

# Subject Index

## A

Adhesion, conducting polymers, 4  
*p*-Aminothiophenol (*p*-ATP)  
  film preparation method, 116  
  formation of Au/*p*-ATP monolayer  
    on Au, 116  
  *See also* Multi-layer film electrodes  
Angiogenesis, role in nerve  
  regeneration, 156–158  
Aniline  
  thermodynamic conditions for  
    electropolymerization, 129–130  
  *See also* Polyaniline  
Anthracene crystals,  
  electroluminescence, 103–104  
Antibodies, immobilization for  
  sensing or catalysis, 7, 11  
Anticorrosion coatings  
  conducting polymers, 5–6  
  effect of surface treatment on  
    electrochemical response of iron,  
      131–133  
  electrochemical zinc surface  
    pretreatment, 134  
  experimental, 130  
  galvanostatic curves for pyrrole  
    oxidation, 135*f*  
  galvanostatic response of Zn  
    electrode during  
      electropolymerization of  
      polypyrrole (PPy), 138*f*  
  galvanostatic study, 136, 138  
  micrographic cut of PPy/Zn/steel in  
    galvanostatic mode, 139*f*  
  one-step PPy deposition on zinc, 134,  
    136, 138  
  properties of PPy films, 132–133  
  protection of metals, 129

  structures of pyrrole and  
    copolymerized derivatives, 132  
  surface pretreatment by immersion,  
    133–134  
  thermodynamic conditions for  
    electropolymerization of pyrrole or  
    aniline, 129–130  
  two-step PPy deposition on mild  
    steel, 130–133  
  two-step PPy deposition on zinc,  
    133–134  
  use of oxidized polyaniline (PANI),  
    129  
  voltammetric study, 136, 137*f*  
  work on PPy, 129  
Anti human serum albumin,  
  immobilization for sensors, 9*t*  
Arsenic analysis, conducting  
  polymers, 12  
Au/*p*-aminothiophenol (*p*-ATP)  
  substrates. *See* Multi-layer film  
  electrodes

## B

Batteries, electronic and ionic-  
  conducting organic polymers, 203  
Biodegradable polymers. *See*  
  Biomaterials, electroactive  
Biomaterials, electroactive  
  chemical structure of oxidized  
    polypyrrole (PP) and hyaluronan,  
      157*f*  
  clinical need for new biomaterials for  
    neural tissue engineering, 155–  
      156  
  <sup>1</sup>H NMR for terpyrrole derivative,  
    163*f*

- hyaluronan and role of angiogenesis  
in nerve regeneration, 156–  
158
- hyaluronic acid (HA) in cell  
signaling events, 157
- in vivo vascularization surrounding  
PP/PSS [poly(styrenesulfonate)]  
and PP/HA films, 161*f*
- need for biodegradable and  
processable form of PP, 158
- PP as biomaterial, 156, 157*f*
- predicted structure of biodegradable  
PP derivative, 162*f*
- schematic of conductive terpyrrole  
units connected via degradable  
ester linkages and flexible  
aliphatic chains, 160*f*
- schematic of surgical placement of  
nerve guidance channel, 155*f*
- structure of new terpyrrole derivative  
with thiophene unit, 162*f*
- synthesis and characterization  
methods of PP–HA composites,  
158–159
- synthesis and characterization of PP–  
HA composites, 161–162
- synthesis method of biodegradable  
form of PP, 159–160
- synthesis of biodegradable form of  
PP, 162–163
- Biomedical applications, conducting  
polymers, 11–12
- Biomedical research and engineering,  
204
- Biotinylated hepatitis C probe,  
immobilization for sensor  
applications, 8*t*
- Bipyridine (bpy) ligands. *See*  
Organometallic polymer  
[Ru(L)(CO)<sub>2</sub>]<sub>n</sub>
- Bithiophene (BT)  
inclusion complexes formation with  
cyclodextrins, 41–43  
*See also* Thiophene derivatives
- Bode-[Z] diagrams  
effect of exposing poly(3-  
methylthiophene) film to iodine,  
31*f*  
poly(3-methylthiophene) films, 21,  
23*f*, 24
- ## C
- Capacitance, poly(3-methylthiophene)  
films, 24
- Capacitors, conducting polymers, 5
- Carbon dioxide (CO<sub>2</sub>)  
electrocatalytic reduction, 142  
emeraldine base-type  
polyaniline/poly(vinyl alcohol)  
(EB-PAn/PVA) composite, 96,  
99–101  
response of CO<sub>2</sub> to EB-PAn/PVA,  
100–101  
*See also* Organometallic polymer  
[Ru(L)(CO)<sub>2</sub>]<sub>n</sub>
- Catalysis, conducting polymers, 7, 11
- Catalysts. *See* Polymer supported fuel  
cell catalysts
- Cell culture, conducting polymers,  
11–12
- Cell signaling events, hyaluronic acid,  
157
- Characterization  
conducting polymers, 3–4  
electrochemical impedance  
spectroscopy (EIS), 19  
electrochemical quartz crystal  
microbalance (EQCM), 60
- Chromate reduction, conducting  
polymers, 12
- Coatings. *See* Anticorrosion coatings
- Composites. *See* Biomaterials,  
electroactive; Polymer composites
- Conducting polymers  
adhesion, 4  
anticorrosion, 5–6  
applications, 4–12  
characterization, 3–4

- electrocatalysis, 4–5
- electronics, 5
- entrapment and release of bioactive substances, 11
- environmental monitoring and remediation, 12
- fuel cell design, 6
- future of, electrodes, 203–204
- immobilization of enzymes, polynucleotide, and antibodies, 7, 11
- morphology, 3–4
- neuroscience and cell culture applications, 11–12
- photovoltaics, 5
- sensing or catalysis, 7, 11
- sensors and detection, 6–7
- solid-state reference electrodes, 12
- synthesis, 3
- tailoring behavior, 204
- See also* Poly(3-methylthiophene)
- Conductivity
  - polymer, 4
  - See also* Polymer composites
- Conjugated polymers
  - anodic electrochemiluminescence (ECL) for 4-methoxy(2'-ethylhexoxyl)-2,5-poly(*p*-phenylenevinylene) (MEH–PPV), 111*f*
  - cyclic voltammetry of MEH–PPV coated Pt electrode, 108*f*
  - derivatives of PPV, 104
  - effect of polarization change during anodic ECL, 111*f*
  - electrochemiluminescence (ECL) by reactions, 106–107
  - electrochemiluminescence for MEH–PPV, 110*f*
  - electroluminescence, 103–104
  - emission of ECL from MEH–PPV, 106, 108*f*
  - experimental, 104–105
  - general mechanism for production of luminescence, 106
  - kinetics of ECL, 109, 111*f*
  - light emission kinetics, 107, 109
  - MEH–PPV synthesis, 104–105
  - oxidation and/or reduction, 105–106
  - potential step generated cathodic and anodic ECL, 108*f*
  - See also* Anticorrosion coatings
- Copper. *See* Polymeric electrodeposits with metallic particles
- Counterions, condensed
  - chemical trapping, 185–186
  - comparing experimental to theoretical estimates, 194
  - dediazonation mechanism, 186
  - dediazonation reaction rates, 197
  - determination of selectivity, 196
  - equilibrium constant for obtaining <sup>23</sup>Na NMR, 187
  - estimated concentrations in region of sodium polyacrylate (NaPAA) by chemical trapping at 40°C, 193*t*
  - estimating local concentrations, 192–193
  - experimental materials, 195
  - experimental methods, 195–196
  - factors contributing to difference between theory and chemical trapping estimate, 194
  - ion exchange constant, 186–188
  - kinetics, 197
  - <sup>23</sup>Na NMR experiments, 196
  - NaPAA selection, 192
  - <sup>23</sup>Na relaxation times for determining exchange constant for Na<sup>+</sup> and 1-ArN<sub>2</sub><sup>+</sup> on NaPAA, 189*t*, 190*t*
  - percent tagging, 191–192
  - rate of alkaline hydrolysis, 197
  - rate of relaxation, 187
  - selectivity of 1-ArN<sub>2</sub><sup>+</sup> toward acetate versus water, 188, 191
  - tagging experiments, 196–197
  - theory (CCT), 185
  - yield of tagged carboxylate groups, 193–194
- Cyclodextrins (CDs)

- electropolymerization of host-guest complexes with thiophene derivatives, 40–46  
 guests in host-guest complexes, 40  
 host-guest inclusion complexes formation, 41–43  
 host-guest polymerization, 43  
*See also* Thiophene derivatives
- D**
- Detection, conducting polymers, 6–7  
 Diaminopyridine, immobilization for sensors, 8*t*  
 Dispersed metallic particles. *See* Polymeric electrodeposits with metallic particles  
 Dopamine, entrapment and release, 11  
 Dopant, addition to organic polymer, 18–19
- E**
- Electroactive biomaterials. *See* Biomaterials, electroactive  
 Electrocatalysis, conducting polymers, 4–5  
 Electrocatalytic reduction of CO<sub>2</sub>, 142  
 Electrochemical impedance spectroscopy (EIS)  
 electrochemically active polymers, 19  
 parameters for poly(3-methylthiophene) films, 28*t*  
*See also* Poly(3-methylthiophene)  
 Electrochemical quartz crystal microbalance (EQCM)  
 characterization method, 60  
 EQCM electrooxidative deposition data, 68*t*  
*See also* Perylene containing films  
 Electrochemiluminescence (ECL)  
 anodic ECL for 4-methoxy(2'-ethylhexoxy)-2,5-PPV (MEH-PPV), 111*f*  
 effect of polarization change during anodic ECL, 111*f*  
 emission of ECL from MEH-PPV, 106, 108*f*  
 kinetics, 109, 111*f*  
 potential step generating cathodic and anodic ECL, 108*f*  
 reactions for ECL from conjugated polymers, 106–107  
*See also* Conjugated polymers  
 Electrochemistry. *See* Poly(3-methylthiophene)  
 Electrodes  
 future of conducting polymer, 203–204  
 in vivo applications, 12  
 solid-state reference, 12  
*See also* Multi-layer film electrodes; Polymeric electrodeposits with metallic particles  
 Electroluminescence  
 anthracene crystals, 103–104  
*See also* Conjugated polymers  
 Electrolytes, cyclic voltammograms of polyaniline and polythiophene derivatives, 55–57  
 Electronics, conducting polymers, 5  
 Electrooxidative polymerization. *See* Perylene containing films  
 Electropolymerization  
 factors hindering thiophene derivatives, 39  
 host-guest complexes of thiophene derivatives-cyclodextrins, 40–46  
 thermodynamic conditions for pyrrole and aniline, 129–130  
 thiophene derivatives in aqueous solution, 39  
 thiophene derivatives in micellar solutions, 46–50  
*See also* Thiophene derivatives

Emulsion polymerization. *See*  
 Micelles  
 Energy band diagram, metal island  
 model, 122*f*  
 Environmental monitoring and  
 remediation, conducting polymers,  
 12  
 Enzymes, immobilization for sensing  
 or catalysis, 7, 11  
 1-Ethyl-3-methylimidazolium  
 bis((trifluoromethyl)sulfonyl)imide  
 (EMITFSI), cyclic voltammograms  
 of polyaniline and polythiophene  
 derivatives, 55–57  
 3,4-Ethylenedioxythiophene (EDOT).  
*See* Thiophene derivatives

## F

Fuel cell design, conducting polymers,  
 6  
 Fuel cells. *See* Polymer supported fuel  
 cell catalysts

## G

Galvanostatic study  
 zinc, 136, 138  
*See also* Anticorrosion coatings  
 Glucose oxidase, immobilization for  
 sensor, 9*t*, 10*t*  
 Gold electrodes. *See* Multi-layer film  
 electrodes  
 Granular metal island model,  
 explaining conductivity of  
 polyaniline, 121–122

## H

Horseradish peroxidase (HPR),  
 immobilization for sensor, 9*t*  
 Host-guest complexes

cyclodextrins, 40  
 electropolymerization, 40–46  
 formation of inclusion complexes,  
 41–43  
 polymerization, 43  
*See also* Thiophene derivatives  
 Humidity  
 dependence of electrical conductivity  
 of poly(anthranilic  
 acid)/poly(vinyl alcohol)  
 (PANA/PVA) and PANA–  
 SA(doped with sulfuric acid)/PVA  
 composite on humidity, 98*f*  
 PANA/PVA composite as sensor, 96,  
 98  
*See also* Carbon dioxide (CO<sub>2</sub>)  
 Hyaluronan  
 cell signaling events, 157  
 chemical structure, 157*f*  
 role of angiogenesis in nerve  
 regeneration, 156–158  
 synthesis and characterization of  
 polypyrrole–hyaluronic acid (HA)  
 composites, 158–159, 161–162  
*See also* Biomaterials, electroactive  
 Hydrogen oxidation, catalysts, 175–176

## I

Immobilization  
 enzymes, polynucleotide, or  
 antibodies, 7, 11  
 sensor applications, 8*t*, 9*t*, 10*t*  
 Incident-photon-to-current efficiencies  
 (IPCE), definition, 119  
 Iodine  
 doping poly(3-methylthiophene), 24,  
 28  
 effect of exposure of poly(3-  
 methylthiophene) as Bode-[Z]  
 plot, 31*f*  
 effect of exposure of poly(3-  
 methylthiophene) by testing  
 electrode, 28, 29*f*, 30*f*



- See also* Poly(3-methylthiophene)  
 Ion-selective conducting polymer. *See*  
 Poly(3-methylthiophene)
- Iron  
 effect of surface treatment on  
 electrochemical response, 131–133  
*See also* Anticorrosion coatings
- J**
- Jelly Roll, conducting organic  
 polymers, 203
- L**
- Lead. *See* Polymeric electrodeposits  
 with metallic particles
- Light-emitting diodes, conducting  
 polymers, 5
- Luminescence  
 general mechanism for production,  
 106  
*See also* Conjugated polymers
- M**
- MacDiarmid, Alan, poly(sulfur  
 nitride), 203
- Metal catalysts. *See* Polymer  
 supported fuel cell catalysts
- Metal island model  
 energy band diagram, 122*f*  
 explaining conductivity of  
 polyaniline, 121–122
- Metallic particles. *See* Polymeric  
 electrodeposits with metallic  
 particles
- Metals. *See* Anticorrosion coatings
- Methanol oxidation  
 catalysts, 176–178  
 chronoamperometry, 180*f*  
 experimental, 182
- normal pulse voltammograms,  
 179*f*
- poly(3,4-ethylenedioxythiophene)/  
 poly(styrene-4-sulphonate), 177–  
 178
- polyaniline, 177
- polypyrrole supported catalysts, 176–  
 177  
*See also* Polymer supported fuel cell  
 catalysts
- 3-Methoxythiophene (MOT). *See*  
 Thiophene derivatives
- Micelles  
 atomic force microscopy (AFM)  
 images of poly(3,4-  
 ethylenedioxythiophene) (PEDOT)  
 films electrosynthesized in sodium  
 dodecylsulfate (SDS), 49*f*  
 electropolymerization of thiophene  
 derivatives, 46–50  
 electropolymerization of thiophene  
 derivatives in SDS, 47  
 electrosynthesis of poly(3-  
 methoxythiophene) [poly(MOT)]  
 at Pt electrode, 48*f*  
 poly(MOT) structures prepared in  
 SDS, 50  
 surfactant monomer-electrode  
 interactions, 46  
*See also* Thiophene derivatives
- Mild steel  
 two-step polypyrrole deposition,  
 130–133  
*See also* Anticorrosion coatings
- Model, granular metal island, for  
 polyaniline, 121–122
- Morphology, conducting polymers, 3–  
 4
- Mott Schottky plots, poly(3-  
 methylthiophene) films in LiClO<sub>4</sub>,  
 34*f*, 35*f*
- Multi-layer film electrodes  
 apparatus, 115–116  
 apparent mass change vs. time  
 transient for *p*-aminothiophenol

(*p*-ATP) adsorption on Au by self-assembly, 117*f*  
 chemicals, 115  
 energy band diagram for metal island model of granular polyaniline (PANI) film, 122*f*  
 experimental, 115–116  
 film preparation method, 116  
 formation and photoelectrochemical behavior of PANI film on Au/*p*-ATP, 118–122  
 formation of Au/*p*-ATP monolayer on Au, 116  
 Fowler plots of photocurrent data for anodic and cathodic photocurrent of PANI film on ordered Au/*p*-ATP, 121*f*  
 granular metal island model, 121–122  
 incident-photon-to-current efficiencies (IPCE), 119  
 photocurrent spectra of PANI film on ordered Au/*p*-ATP, 120*f*  
 photocurrent spectra of PANI/TiO<sub>2</sub> film on ordered Au/*p*-ATP, 124*f*  
 photocurrent vs. potential dependence for PANI and PANI/TiO<sub>2</sub> films on Au/*p*-ATP, 123*f*  
 photoelectrochemical behavior of PANI/TiO<sub>2</sub> film on Au/*p*-ATP, 122–125  
 potential dependence of photocurrent for reduced, partially-oxidized, and oxidized states of PANI film on ordered Au/*p*-ATP, 119*f*  
 use of self-assembly monolayers, 115  
 variation of current-potential and apparent mass-potential characteristics during PANI film formation on Au/*p*-ATP, 118*f*

## N

Nanojunction switch, polyaniline, 5  
 Nano-particulate Au/*p*-aminothiophenol/polyaniline/TiO<sub>2</sub> films  
 photocurrent spectra of polyaniline (PANI)/TiO<sub>2</sub> film on ordered Au/*p*-ATP, 124*f*  
 photocurrent vs. potential dependence for PANI and PANI/TiO<sub>2</sub> films on ordered Au/*p*-ATP, 123*f*  
 photoelectrochemical behavior, 122–125  
*See also* Multi-layer film electrodes  
 Nerve guidance channel, schematic of surgical placement, 155*f*  
 Nerve regeneration, hyaluronan and role of antiogenesis, 156–158  
 Neural tissue engineering, need for new biomaterials, 155–156  
 Neuroscience, conducting polymers, 11–12  
 Nyquist diagram, poly(3-methylthiophene) films, 21, 22*f*, 24

## O

Oligonucleotide, immobilization for sensor applications, 8*t*, 9*t*  
 Organic polymers  
 addition of dopant, 18–19  
 batteries relying on electronic and ionic-conducting, 203  
*See also* Anticorrosion coatings; Poly(3-methylthiophene)  
 Organometallic polymer [Ru(L)(CO)<sub>2</sub>]<sub>n</sub>  
 aromatic regions of <sup>1</sup>H-NMR spectra of *trans*-Cl and *cis*-Cl isomers, 149*f*

- cyclic voltammogram of vitreous carbon (VC)/[Ru<sup>0</sup>(bpy)(CO)<sub>2</sub>]<sub>n</sub> modified electrode, 143, 145*f*
- cyclic voltammograms in CH<sub>3</sub>CN + TBAP of, at Pt electrode, 143*f*
- cyclic voltammogram under Ar and CO<sub>2</sub> in aqueous medium, 150*f*
- difficulty in utilization of, cathodes, 151–152
- electrocatalytic activity vs. CO<sub>2</sub> reduction of, films, 148, 151–152
- film formation, 142–147
- formula of polymer and precursor, 142*f*
- iterative cyclic voltammograms, 144*f*
- observations supporting formulation, 146
- physico-chemical characterization of films, 146–147
- polymerization mechanism, 147–148
- product distribution of electrocatalytic reduction, 151
- schematic structure of polypyrrole–[Ru(L<sub>2</sub>)(CO)<sub>2</sub>]<sub>n</sub> composite material, 152*f*
- Oxygen reduction experimental, 181
- polyaniline, 169–170
- polypyrrole supported catalysts, 167, 169
- polythiophene, 175
- See also* Polymer supported fuel cell catalysts
- P**
- Perylene containing films aggregation, 60 applications, 59 cyclic voltammograms of poly-1 film and simultaneous mass changes, 70*f*
- cyclic voltammograms of poly-3 film and simultaneous mass changes, 71*f*
- diimide and diamide monomers with diphenylamine endgroups, 60–61
- electrochemical quartz crystal microbalance (EQCM), 60
- electrodes and cells, 63–64
- electrooxidative polymerization of monomers, 64–66, 68
- EQCM electrooxidative deposition data, 68*t*
- experimental, 61–64
- frequency changes of quartz crystal electrode (QCE) during electropolymerization of monomers, 66
- instrumentation, 63
- photophysical properties, 59–60
- polymer films, 68, 72
- potential mass correlations >0.0V, 72*t*, 73*t*
- radical dimerization mechanism of arylamines, 64
- reagents, materials, and apparatus, 61
- solution cyclic voltammograms of monomer 1 in triethylamine and trifluoroacetic acid (TEATFA) solution of CH<sub>2</sub>Cl<sub>2</sub>, 67*f*
- solution cyclic voltammograms of monomer 3 in tetrabutylammonium hexafluorophosphate (TBAPF6) solution of CH<sub>2</sub>Cl<sub>2</sub>, 65*f*
- synthesis, 60
- synthesis of methyl 2-anilino-5-aminobenzoate, 62–63
- synthesis of monomers, 61–63, 64
- tetraprotonated dimer of monomer 1, 69
- Photovoltaics, conducting polymers, 5
- Platinum alloy, immobilization for sensor applications, 10*t*

- Platinum electrodes. *See* Polymeric electrodeposits with metallic particles
- Polyacetylene  
 addition of dopant, 18–19  
 predictions, 203
- Polyacrylate, sodium (NaPAA). *See* Counterions, condensed
- Polyaniline  
 applications and properties, 114–115  
 chemical characterization, 89–90  
 chemical structure, 168  
 cyclic voltammograms in electrolytes, 55–56  
 cyclic voltammograms of gas diffusion electrodes catalyzed with, and polyaniline/poly(styrenesulfonate) supported Pt, 171*f*  
 electronics, 5  
 experimental, 53–54  
 formation and photoelectrochemical behavior of, film on Au/*p*-aminothiophenol substrate, 118–122  
 granular metal island model, 121–122  
 hydrogen adsorption/desorption waves, 173*f*  
 hydrogen oxidation, 175–176  
 methanol oxidation, 177  
 oxygen reduction, 169–170  
 oxygen reduction performance for best electrodes, 174*f*  
 oxygen reduction polarization curves, 172*f*  
 preparation, 77–78, 89, 181  
 protecting oxidizable metals, 129  
*See also* Anticorrosion coatings; Multi-layer film electrodes; Polymer composites; Polymer supported fuel cell catalysts; Polymeric electrodeposits with metallic particles
- Poly(anthranilic acid) (PANA)  
 characterization, 90, 92  
 FTIR spectra, 91*f*  
 mass spectra at different temperatures, 94*f*  
 PANA/poly(vinyl alcohol) (PVA) composite as humidity sensor, 96, 98  
 preparation, 89  
 relationship between electrical conductivity and temperature, 92, 95*f*  
 sulfuric acid (SA) doping, 96  
 thermogravimetric curve, 93*f*  
*See also* Polymer composites
- Poly(bithiophene) (PBT)  
 host-guest polymerization, 43  
 structures, 44–46  
*See also* Thiophene derivatives
- Poly(cyclopenta[2,1-b;3,4-b']dithiophene-4-one) (PCDT)  
 cyclic voltammograms in electrolytes, 56  
 structure, 53  
*See also* Thiophene derivatives
- Polyelectrolyte. *See* Counterions, condensed
- Poly(3,4-ethylene dioxythiophene) (PEDOT), synthesis, 3
- Poly(3,4-ethylene dioxythiophene)/poly(styrene-4-sulphonate), methanol oxidation, 177–178
- Polyheteroaromatic films  
 interest, 39  
*See also* Thiophene derivatives
- Polymer composites  
 characterization of poly(anthranilic acid) (PANA) and preparation of emeraldine base-type polyaniline (EB-PAn), 90, 92, 96  
 chemical characterization of PANA and polyaniline (PAn), 89–90  
 dependence of electrical conductivity of EB-PAn/poly(vinyl alcohol)

- (PVA) composite on CO<sub>2</sub> concentration, 99*f*
- dependence of electrical conductivity of EB-PAN/PVA composite on CO<sub>2</sub> concentration at various humidities, 100*f*
- dependence of electrical conductivity of PANA/PVA and PANA-SA(doped with sulfuric acid)/PVA composites on humidity at moistening and desiccating stages, 98*f*
- EB-PAN/PVA composites as CO<sub>2</sub> sensor, 96, 99–101
- experimental, 89–90
- FTIR spectra of PANA and heat-treated PANAs, 91*f*
- mass spectra (MS) spectra of PANA at different temperatures, 94*f*
- PANA/PVA composites as humidity sensor, 96, 98
- polyaniline preparation, 89
- preparation of PANA, 89
- pyrolysis of PANA, 97
- relationship between electrical conductivity of PANA and treatment temperature, 92, 95*f*
- response of EB-PAN/PVA composite to CO<sub>2</sub>, 100–101
- thermogravimetric (TG) curve of PANA, 93*f*
- Polymer electrodes, arsenic analysis, 12
- Polymer supported fuel cell catalysts
- catalysts for hydrogen oxidation, 175–176
- catalysts for methanol oxidation, 176–178
- catalysts for oxygen reduction, 167–175
- chronoamperometry for methanol oxidation, 180*f*
- cyclic voltammograms of gas diffusion electrodes catalyzed with polyaniline and
- polyaniline/poly(styrene-4-sulphonate) (PSS) supported Pt, 171*f*
- experimental, 181–182
- hydrogen adsorption/desorption waves, 173*f*
- normal pulse oxygen reduction polarization curves for electrodes catalyzed with polyaniline and polyaniline/PSS supported Pt, 172*f*
- normal pulse voltammograms for methanol oxidation, 179*f*
- oxygen reduction polarization curves for best electrodes, 174*f*
- platinum use, 167
- polyaniline for methanol oxidation, 177
- polyaniline for oxygen reduction, 169–170
- poly(3,4-ethylenedioxythiophene)/PSS (PEDOT/PSS) for methanol oxidation, 177–178
- polypyrrole supported catalysts, 167, 169, 176–177
- polythiophenes for oxygen reduction, 175
- potential use, 166–167
- structures of polypyrrole, polyaniline, and polythiophene, 168
- Polymeric electrodeposits with metallic particles
- catalytic effect of Pb on electro-oxidation of formic acid, 78
- Cu dispersion, 80–84
- electrocatalytic activity of electrodes using polyaniline (PANI) or polypyrrole (PPy), 80
- electrocatalytic oxidation of molecules, 76
- electro-obtention of poly(*o*-phenylenediamine) (PoPDA), 76–77
- experimental, 77–78

- film thickness using polythiophene (PTh) matrix, 79
- $\gamma$ -aminobutyric acid (GABA)  
response on SS/PoPDA,  
SS/PoPDA-Cu modified, and Cu  
electrodes, 81*f*
- obtaining optimum Pt/polymer-Pt +  
Pb electrodes behavior, 79
- optimal conditions to prepare  
SS/PoPDA-Cu electrodes, 82*t*
- platinum electrodes modified with  
PoPDA, 77–78
- preparation, 76
- Pt and Pt + Pb dispersion, 78–80
- response of electrodes in different  
GABA concentrations, 83*f*
- Polymerization. *See* Thiophene  
derivatives
- Poly(3-methylthiophene)  
behavior of electrodes, 19
- Bode-[Z] diagrams of films in  
tetrabutyl ammonium  
hexafluorophosphate/acetonitrile  
(TBAHFP/AcN), 21, 23*f*, 24
- comparing AC impedance  
characteristics, 24, 28
- effect of exposing film to iodine as  
Bode-[Z] plot, 28, 31*f*, 32
- effect of exposure of film to iodine  
by testing electrode in TBAHFP  
and LiClO<sub>4</sub>, 28, 29*f*, 30*f*
- effect of iodine doping, 24, 28, 32
- EIS curves for films in LiClO<sub>4</sub>, 26*f*,  
27*f*
- EIS (electrochemical impedance  
spectroscopy), 19
- equivalent circuit for doped and  
undoped, 24, 25*f*
- experimental, 20–21
- Mott Schottky plots for films in  
LiClO<sub>4</sub>, 34*f*, 35*f*
- Nyquist diagram of film at different  
potentials, 21, 22*f*
- phase angle/frequency plots of film  
in TBAHFP/AcN, 33*f*
- polymer film parameters for oxidized  
and reduced states, 28*t*
- relation between change in electrical  
properties and sensor behavior of  
polymer, 32
- sample preparation, 20–21
- synthesis, 3
- Polynucleotide, immobilization for  
sensing or catalysis, 7, 11
- Poly(*o*-phenylenediamine) (PoPDA)  
electro-obtention, 76–77  
*See also* Polymeric electrodeposits  
with metallic particles
- Poly(phenylene vinylene) (PPV)  
cyclic voltammetry of 4-methoxy(2'-  
ethylhexoxy)-2,5-PPV (MEH-  
PPV), 106, 108*f*
- electrochemical formation of excited  
emitting states, 107
- electrochemiluminescence for MEH-  
PPV, 110*f*
- electroluminescence, 104
- emission of ECL from MEH-PPV,  
106, 108*f*
- MEH-PPV synthesis, 104–105  
*See also* Conjugated polymers
- Polypyrrole  
anticorrosion properties of films,  
132–133
- biomaterial, 156
- chemical structure, 168
- chemical structure of oxidized, 157*f*
- chromate reduction, 12
- entrapment and release of bioactive  
substances, 11
- films on oxidizable metals, 129
- galvanostatic study on zinc, 136, 138
- hydrogen oxidation, 175–176
- immobilization for sensor  
applications, 8*t*, 9*t*, 10*t*
- in vivo applications, 12
- micrographic cut of film on zinc,  
139*f*
- need for biodegradable and  
processable form, 158

- one-step deposition on zinc, 134, 136, 138  
 preparation, 77–78  
 supported catalysts for methanol oxidation, 176–177  
 synthesis and characterization of polypyrrole–hyaluronic acid (HA) composites, 158–159, 161–162  
 synthesis of biodegradable form, 159–160, 162–163  
 two-step deposition on mild steel, 130–133  
 two-step deposition on zinc, 133–134  
 voltammetric study on zinc, 136, 137f  
*See also* Anticorrosion coatings; Biomaterials, electroactive; Polymer supported fuel cell catalysts; Polymeric electrodeposits with metallic particles
- Poly(pyrrole-*co*-dithiophene), hydrogen oxidation, 175–176
- Polysaccharide hyaluronan. *See* Biomaterials, electroactive
- Poly(styrenesulfonate) (PSS). *See* Biomaterials, electroactive
- Poly(sulfur nitride), 203
- Poly(terthiophene) (P3T)  
 host-guest polymerization, 43  
 structures, 44–46  
*See also* Thiophene derivatives
- Poly-E- $\alpha$ -[(2-thienyl)methylene]-2-(3-methylthiophene)acetonitrile (PTCNT)  
 cyclic voltammograms in electrolytes, 56–57  
 structure, 53
- Polythiophene  
 chemical structure, 168  
 oxygen reduction, 175  
 preparation, 77–78  
*See also* Polymeric electrodeposits with metallic particles; Polymer supported fuel cell catalysts
- Polythiophene derivatives  
 cyclic voltammograms of poly(cyclopenta[2,1-b; 3,4-b']dithiophene-4-one (PCDT), 56  
 cyclic voltammograms of poly-E- $\alpha$ -[(2-thienyl)methylene]-2-(3-methylthiophene)acetonitrile (PTCNT), 56–57  
 experimental, 53–54  
 structures of PCDT and PTCNT, 53
- Poly(vinyl alcohol) (PVA). *See* Polymer composites
- Potassium nitrate, iron passivity and transpassivity, 132
- Pyrrrole  
 structure, 132  
 thermodynamic conditions for electropolymerization, 129–130
- ## R
- Remediation, conducting polymers, 12
- Ruthenium. *See* Organometallic polymer [Ru(L)(CO)<sub>2</sub>]<sub>n</sub>
- ## S
- Sensing, conducting polymers, 7, 11
- Sensor applications, immobilization, 8t, 9t, 10t
- Sensors  
 conducting polymers, 6–7  
*See also* Polymer composites
- Sodium dodecylsulfate (SDS)  
 electropolymerization of thiophene derivatives, 46–50  
*See also* Micelles; Thiophene derivatives
- Sodium polyacrylate (NaPAA). *See* Counterions, condensed
- Sodium sulfate, behavior of mild steel, 131–132

Solid-state reference electrodes,  
conducting polymers, 12  
Steel, mild. *See* Anticorrosion  
coatings  
Sulfuric acid, doping poly(anthranilic  
acid), 96  
Surface pretreatment  
electrochemical zinc, 134, 135*f*  
zinc by immersion, 133–134  
Surface treatment, electrochemical  
response of iron, 131–133  
Surgical end-to-end repair, nerve  
fibers, 155  
Synthesis, conducting polymers, 3

## T

Terthiophene (3T)  
inclusion complexes formation with  
cyclodextrins, 41–43  
*See also* Thiophene derivatives  
Tetraethylammonium  
bis((trifluoromethyl)sulfonyl)imide  
(Et<sub>4</sub>N<sup>+</sup>TFSI<sup>-</sup>), cyclic voltammograms  
of polyaniline and polythiophene  
derivatives, 55–57  
Tetraethylammonium  
tetrafluoroborate (Et<sub>4</sub>N<sup>+</sup>BF<sub>4</sub><sup>-</sup>), cyclic  
voltammograms of polyaniline and  
polythiophene derivatives, 55–57  
Theory, condensed counterion, 185  
Thiophene derivatives  
atomic force microscopy (AFM)  
images of poly(3,4-  
ethylenedioxythiophene) (PEDOT)  
films electrosynthesized in SDS  
micelles and in acetonitrile  
solution, 49*f*  
bithiophene (BT) or terthiophene  
(3T), 41  
cyclodextrins (CDs) as guest, 40  
electropolymerization in micellar  
solutions, 46–50  
electropolymerization in sodium  
dodecylsulfate (SDS) micelles,  
47  
electropolymerization of host-guest  
derivatives in aqueous solutions,  
40–46  
electrosynthesis of poly(3-  
methoxythiophene) [poly(MOT)]  
at Pt electrode in aqueous micellar  
solution, 48*f*  
experimental, 39–40  
fluorescence spectra of BT with  
increasing cyclodextrin derivative,  
42*f*  
frequency and admittance changes  
observed under double potential  
steps, 45*f*  
host-guest inclusion complexes  
formation, 41–43  
host-guest polymerization, 43  
polybithiophene (PBT), 43  
poly(MOT) structures in SDS  
micelles, 50  
polyterthiophene (P3T), 43  
polythiophene derivatives structures,  
47–48, 50  
structures of PBT and P3T, 44–46  
surfactant monomer (M)–electrode  
interactions, 46  
Tissue engineering  
clinical need for new biomaterials,  
155–156  
*See also* Biomaterials, electroactive  
Titanium dioxide  
electrode material, 114  
*See also* Multi-layer film electrodes  
Triazine, immobilization for sensor  
applications, 8*t*

## V

Voltammetric study, zinc, 136,  
137*f*



**Z****Zinc**

electrochemical surface pretreatment,  
134, 135*f*  
galvanostatic study, 136, 138  
micrographic cut of polypyrrole film  
on, 139*f*

one-step polypyrrole deposition, 134,  
136, 138  
surface pretreatment by immersion,  
133–134  
two-step polypyrrole deposition,  
133–134  
voltammetric study, 136, 137*f*  
*See also* Anticorrosion coatings